FACULTY OF TEXTILE ENGINEERING TUL

Habilitation thesis

ELECTROSPINNING AND MODIFICATION OF FIBROUS MATERIALS WITH BIOMEDICAL POTENTIAL

Ing. DANIELA LUBASOVÁ, Ph.D.

Liberec, 2025

Annotation

This habilitation thesis comprises a collection of published scientific and research works, accompanied by commentary in accordance with §72 paragraph 3 of Act on universities No. 111/1998 Coll. The thesis comprises commentary on 15 peer-reviewed journal articles, 5 conference papers, 2 national patents, 1 international patent, and 1 book chapter, with the 9 most significant publications included in the appendices. The scientific works focus on the development, electrospinning, modification, and biomedical potential of various fibrous materials. The first chapter discusses electrospinning of copolymers and polymer blends into fibrous materials, aiming to optimize their water resistance, biodegradability, mechanical properties, and absorption capacity. The scalability of needle-less electrospinning is particularly highlighted as it allows bridging laboratory research with industrial production. The second chapter explores advanced modification strategies of electrospun fibrous materials to meet specific biomedical requirements, including improving antibacterial properties, enhancing cell-material interactions, and optimizing drug release dynamics. Additionally, a novel predictive numerical model is introduced to optimize fiber morphology based on solvent system properties. The final chapter highlights the biomedical potential of electrospun materials, demonstrating their applicability in bacterial filtration, customised wound care, sublingual drug delivery using mucoadhesive patches, and targeted cancer therapy. This habilitation thesis introduces innovative approaches to scalable production and functional modification of electrospun fibrous materials, underscoring their significance as promising solutions to critical challenges in modern biomedicine.

Keywords: needle-less electrospinning, electrospun fibrous materials, modification strategies, biomedical applications

Contents

Introduction

Traditional textiles have long played a role in biomedical applications, particularly in wound dressings, prosthetics, and implantable materials. While these materials are widely available and mechanically resilient, they often fail to replicate the intricate structural and functional properties of biological tissues. For instance, conventional wound dressings, such as cotton gauze, provide a protective barrier but lack the fine porosity and bioactivity necessary for optimal healing. Similarly, woven or knitted prosthetic textiles offer mechanical support but do not facilitate cell attachment or tissue integration. These limitations stem from their relatively large fiber diameters, restricted surface area, and limited capacity for biofunctionalization. Moreover, their structural features are not easily tunable to meet specific biological requirements, which constrains their efficacy in regenerative medicine, controlled drug delivery, and antimicrobial applications. This growing gap in performance has highlighted the need for innovative materials that can better mimic the properties of biological tissues, providing a compelling rationale for the development of advanced alternatives such as electrospun fibrous materials.

Electrospun fibrous materials have emerged as a highly promising alternative, offering unique advantages such as high porosity for gas exchange and fluid absorption, tunable degradation profiles, and the ability to incorporate bioactive agents. These properties make them particularly suitable for applications in wound healing, tissue engineering, drug delivery, and antimicrobial barriers. Compared to conventional textiles, electrospun fibers exhibit a significantly higher surface-area-to-volume ratio, enhancing their capacity for bioactive agent incorporation and controlled therapeutic release. Additionally, modification strategies—such as antibiotic incorporation, or surface drug immobilization—allow for further optimization of their biomedical functionality. For example, electrospun materials can be engineered for sustained drug release, functionalized with antimicrobial coatings to prevent infections, or integrated with growth factors to promote cellular differentiation and tissue regeneration. By offering a lightweight, flexible, and highly customizable alternative, electrospun fibrous materials address key challenges in biomedical material development, particularly in mimicking the extracellular matrix.

The properties of electrospun fibrous materials are influenced by several factors, including polymer composition, solvent selection, electrospinning parameters, and post-processing modifications. Polymer choice and solvent system are particularly critical in determining fiber morphology, mechanical properties, degradation behavior, and bioactivity. Despite significant advancements, many challenges remain in scaling up electrospinning processes while ensuring consistency, cost-effectiveness, and reproducibility. Key obstacles include optimizing solvent systems, controlling fiber morphology, and advancing biofunctionalization techniques to improve the versatility of electrospun fibrous materials for clinical applications.

This habilitation thesis builds on these advancements by exploring how needle-less electrospun fibrous materials can be tailored through novel design strategies and modifications to meet the unique demands of biomedical applications. The subsequent chapters explore:

1. **Development of electrospun fibrous materials from copolymers and polymer blends** with the desired properties.
2. **Modification strategies** to introduce specific functionalities into electrospun materials.
3. **Biomedical potential** of newly designed electrospun fibrous materials.

This thesis highlights the versatility of electrospinning as a technique for producing fibrous materials with properties required by biomedical applications. A detailed analysis is provided on optimization of polymer solutions and solvent selection, which are critical for successful needle-less electrospinning and large-scale production. By utilizing copolymers and polymer blends, this thesis demonstrates significant advancements in electrospun fibrous material properties, including controlled water resistance, biodegradability, tailored mechanical strength,

and enhanced water absorption. Modification strategies are also explored to improve antibacterial efficacy, drug release dynamics, and cell-material interactions. Potential applications of electrospun fibrous materials discussed in this thesis include bacterial filtration, customizable wound healing, mucoadhesive drug delivery systems, and localized cancer therapies, underscoring their extensive impact in the biomedical field. Anchored in commentary on peer-reviewed scientific publications, this thesis provides a detailed framework on the fabrication, modification, and application of electrospun fibrous materials.

1. Development of electrospun fibrous materials

The designing electrospun fibrous materials for biomedical applications requires careful optimization of their structural, mechanical, and biochemical properties. Unlike conventional textiles, which are typically woven or knitted and offer limited biofunctionality, electrospun fibrous materials can be engineered at the nanoscale to mimic the extracellular matrix, enhancing cell adhesion, moisture retention, and controlled drug release. By tailoring fibrous material characteristics like chemical composition, and biofunctionalization, specialized materials can be developed for advanced biomedical applications such as wound care dressings, tissue engineering scaffolds, antibacterial membranes and drug delivery systems [1]. Electrospinning has revolutionized fabrication of biomedical material by enabling the fabrication of nano- and microfibrous structures from a wide range of polymers. The process involves applying a high voltage to a polymer solution or melt, which generates fine fibers that deposit onto a collector. Depending on the method, electrospinning can be needle-based or needle-less, each offering distinct advantages and limitations. Needle-based electrospinning provides precise control over fiber properties but faces several issues such as clogging, low throughput, and scalability constraints. Needle-less electrospinning has revolutionized the industrial scalability of electrospun materials, enabling high-throughput production while preserving the desired fiber properties. The theoretical foundations and technological advancements of electrospinning are extensively examined in *Physical Principles of Electrospinning: Electrospinning as a Nanoscale Technology of the 21st Century* [2]. This work outlines the evolution of the technique, explores various modifications, and highlights its remarkable potential as a nanoscale fabrication method. As part of this publication [2], the author of this thesis contributed to the chapter *Polymeric Solutions for Electrospinning*, offering key insights into polymer-solvent interactions essential for successful fiber formation.

The choice of polymer-solvent system is a determining factor in electrospinning efficiency. In needle-based electrospinning, the controlled polymer jet formation allows for a broader range of polymers to be processed. Although solvent selection remains crucial, the needle's precision offers greater flexibility in polymer solution concentration and solvent properties. However, in needle-less electrospinning, the absence of a needle requires meticulous polymer-solvent optimization to achieve consistent fiber morphology. *Lubasová's* dissertation thesis [3] highlights the crucial role of solvent selection, emphasizing parameters such as solubility parameters (ensuring proper polymer dissolution), dielectric constant (affecting charge stability), and vapor pressure (influencing fiber solidification). These factors directly impact electrospinnability of a polymer but also play a crucial role in determining fiber diameter, porosity, and surface smoothness, all of which are critical for biomedical applications [4]. Achieving an optimal balance between polymer solution properties and electrospinning parameters is especially challenging when working with polymer blends and copolymers. These materials offer unique advantages, such as adjustable degradation rates, improved mechanical properties, and enhanced bioactivity, but their successful electrospinning—especially in needle-less system—requires careful optimization of polymer-solvent interactions. Overcoming these challenges is essential for translating electrospun fibrous materials from research to commercial biomedical products. Building on these foundational principles, the following sub-chapters explore how copolymer and polymer blend electrospinning can address existing limitations, with a focus on

the author of this habilitation thesis contributions, to further enhance the functionality and clinical applicability of electrospun fibrous materials in biomedical applications.

1.1 Electrospinning of copolymers

In recent years, electrospun fibrous materials composed of copolymers have gained significant attention due to their ability to combine the advantageous properties of different monomers into a single fibrous structure. These materials allow for the fine-tuning of key characteristics such as degradation rate, and biocompatibility, which are essential for biomedical applications. By carefully selecting monomers, the degradation behavior of electrospun fibrous material can be tailored to specific needs [5]. Despite these advantages, the electrospinning of copolymers presents several challenges that must be addressed to achieve optimal fiber properties and reproducibility. One of the critical challenges is **s**olvent compatibility, as identifying a solvent system that effectively dissolves both copolymer components without degradation can be a complex task. Additionally, optimizing spinning parameters is necessary due to the intricate rheological behavior of copolymer solutions. Finally, industrial scalability remains a challenge, as adapting copolymer systems to needle-less electrospinning requires optimizing processing conditions—such as solution viscosity, voltage, humidity, and temperature—to achieve consistent fiber formation at large scales.

To harness the potential of copolymers for biomedical applications, the electrospinability of a novel copolyester composed of polyethylene terephthalate (PET) and lactic acid (LA), derived from recycled PET bottles was explored, as described in patent [6]. Prior to this work, no studies had successfully electrospun PET/LA copolyester or established a viable method for converting PET bottle waste into a biodegradable copolymer. Initial attempts were hindered by the low molecular weight of the synthetized copolymer, compromising its mechanical properties and limiting its practical applicability. However, the work described in patent [6] successfully overcame these limitations, leading to the development of a fibrous material with adjustable degradation properties. By transforming PET—traditionally a non-degradable polymer—into electrospun fibrous materials with controlled biodegradability, a sustainable approach to repurposing PET waste for biomedical applications was introduced. The copolymer synthesis was carried out at the University of Chemistry and Technology in Prague, whereas the author of this thesis developed innovative solvent systems for the newly synthesized copolymer, optimized needle-less electrospinning and melt-blown techniques, and successfully electrospun and characterized the resulting fibrous materials. A set of biodegradable aromatic-aliphatic co-polyesters based on PET was synthesized from disposed beverage PET bottles and LA with various molar ratio of aromatic and aliphatic ester units (from 45 - 55 mol%). Washed PET flakes from disposed colourless bottles were acidolyzed with aqueous solution of LA under inert atmosphere (argon) and catalyzed by zinc acetate. The product of acidolysis–a mixture of low molecular weight aromatic-aliphatic esters–was subsequently polycondensed at 250°C. To utilize the potential of industrial manufacturing, two PET/LA fibrous materials production techniques were employed: (i) needle-less electrospinning and (ii) the melt-blown processing. Given the challenges associated with PET/LA electrospinning and melt-blowing—such as limited solubility in common solvents and a high melting temperature—optimizing the polymer blend composition and electrospinning parameters was essential to achieving successful fiber formation. The PET/LA copolyester was successfully electrospun using a solvent mixture of chloroform/isopropanol/1,1,2,2-tetrachloroethane (4/1/3 vol.). This solvent system was designed based on solvent-polymer solubility parameters, replacing the previously used highly toxic phenol with a less hazardous alternative. The approach leveraged the principle that solvents with similar solubility characteristics and optimal properties, such as permittivity and vapor pressure, can be effectively interchanged in electrospinning, as described in *Lubasová's* dissertation thesis [3]. This solvent system (i) adjusted the copolymer's macromolecular conformation and (ii) enhanced copolymer solution conductivity, enhancing

electrospinning efficiency. Melt-blown fibers were produced using a spinneret temperature of 215°C and an air pressure of 2.5 bar. The resulting fiber diameters were 280 ± 47 nm for electrospun fibers and 4318 ± 317 nm for melt-blown fibers (Figure 1).

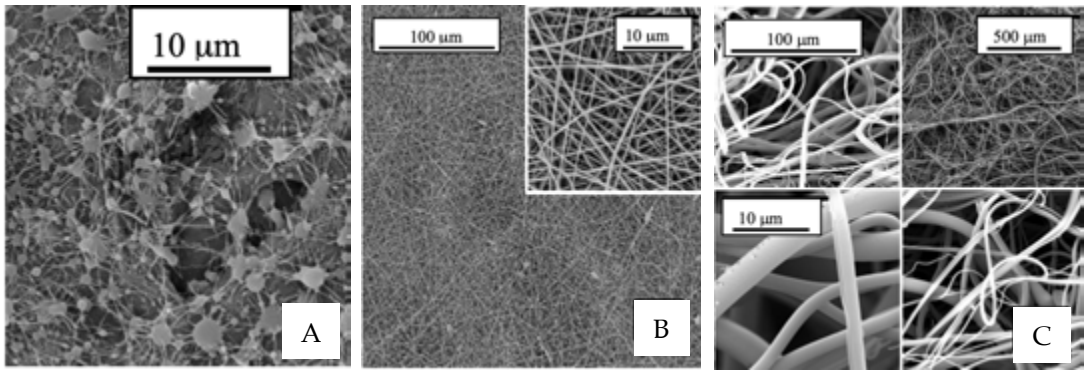

Figure 1. SEM images of PET/LA fibrous materials: (A) example of unsuccessful PET/LA electrospun material, (B) successful needle-less electrospun PET/LA material, and (C) melt-blown PET/LA material [7].

BET isotherm analysis confirmed that electrospun fibers exhibited a significantly higher surface area (9.5 m^2/g) compared to melt-blown fibers (1.95 m^2/g). Furthermore, enzymatic degradation using *Thermonospora fusca* revealed distinct biodegradation behaviors: PET/LA melt-blown fibers degraded primarily within their volume while retaining smooth surfaces, whereas electrospun fibers exhibited surface and volume degradation (Figure 2. (A-B)). Further research aimed to determine why the copolymer PET/LA is biodegradable but becomes less-degradable after melt-blown processing, as described in *Lubasová et al.* [7]. Fourier transform infrared spectroscopy (FTIR) revealed structural differences between the original copolymer and melt-blown fibrous material, particularly around absorbance 1200 cm^{-1}, indicating chemical modifications. Additionally, differential scanning calorimetry (DSC) analysis showed new thermal transitions at 130 and 190 °C in melt-blown fibrous material, absent in the original copolymer and extruded melt, suggesting structural changes during fiber elongation, as shown in Figure 2. (C). These findings suggest that the limitation of degradability is more likely due to chain orientation rather than crosslinking. Further solubility testing in cresol showed that all melt-blown fibrous materials (spun at 9, 25, and 40 cm) remained insoluble after 4 days, unlike the original copolymer and extruded melt.

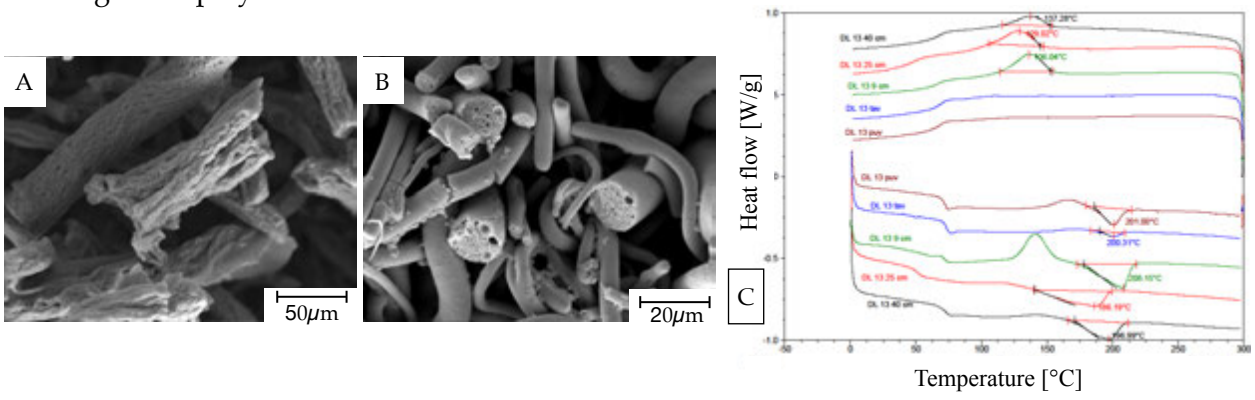

Figure 2. SEM images of PET/LA fibrous materials after enzymatic degradation fabricated by: (A) needle-less electrospinning and (B) melt-blown technology. (C) DSC analysis of melt-blown PET/LA fibrous material [7].

These findings highlight the need for optimizing melt-blown processing conditions to prevent unwanted structural changes in the fibrous material. The significance of this research—focused on needle-less electrospinning and melt-blowing of PET/LA synthesized from PET bottles—was recognized at the AUTEX International Conference by TenCate, *Lubasová et al.* [8], highlighting its potential to advance sustainable biomedical materials.

Another example of harnessing the advantages of electrospun copolymers for biomedical applications is the development of polyesteramide (PEA) fibrous materials. While electrospinning of polyamide 6 (PA6) [9-11] and poly(ε-caprolactone) (PCL) [12, 13] had been widely studied, no prior research was documented the electrospinning of PEAs. These copolymers bridge the properties of PA6 and PCL by copolymerization of ε-caprolactam (CLA) and ε-caprolactone (CLO) structural units, allowing for tailored mechanical and degradation characteristics. Scientific study [14] (Appendix 1) investigated the electrospinning of PEAs with varying CLA and CLO ratios, demonstrating the need for precise solvent selection to optimize fiber formation. The synthesis of the CLA/CLO copolymers was carried at the University of Chemistry and Technology in Prague, whereas the author of this thesis designed, and tested various solvent systems, and further optimized needle-less electrospinning conditions to successfully produce fibrous materials with the desired properties. In this study, PEAs were synthesized through anionic ring-opening copolymerization of CLA and CLO, followed by controlled casting in an inert argon environment. Polymerization, catalyzed by ε-caprolactam magnesium bromide (1.0 mol%), was performed at 150°C for 1 hour, yielding polymer films with precisely defined compositions. Given the role of solvent systems in influencing electrospinning outcomes, various solvents were tested, including 2,2,2-trifluoroethanol, formic acid, and a chloroform/2,2,2-trifluoroethanol (1:1 v/v) mixture. To enhance biocompatibility and reduce environmental concerns associated with fluorinated solvents, an alternative system —formic acid and acetic acid (1:2 v/v)—was explored. This safer approach yielded promising results for the needle-less electrospinning, opening new possibilities for scalable production of PEA-based fibrous biomaterials. The impact of the CLA/CLO ratio, PEA's solution concentration, and molar mass of PEAs on fiber morphology is evident from SEM analysis (Figure 3). Fibers with high CLO content (60–80 mol%) showed aggregation, likely due to their lower polarity, reduced crystallinity, and solvent retention in the amorphous phase. Moreover, the molar mass of the copolymer played a crucial role in determining fiber morphology. Higher molar mass facilitated the transition from beaded structures to uniform fibers (100–160 nm in diameter) due to increased copolymer chain entanglement. This structural change was primarily driven by enhanced molecular interactions, which stabilized the electrospinning process. In contrast, lower molar masses resulted in insufficient chain entanglement, leading to droplet formation—a critical limitation that must be addressed for the successful electrospinning of PEAs.

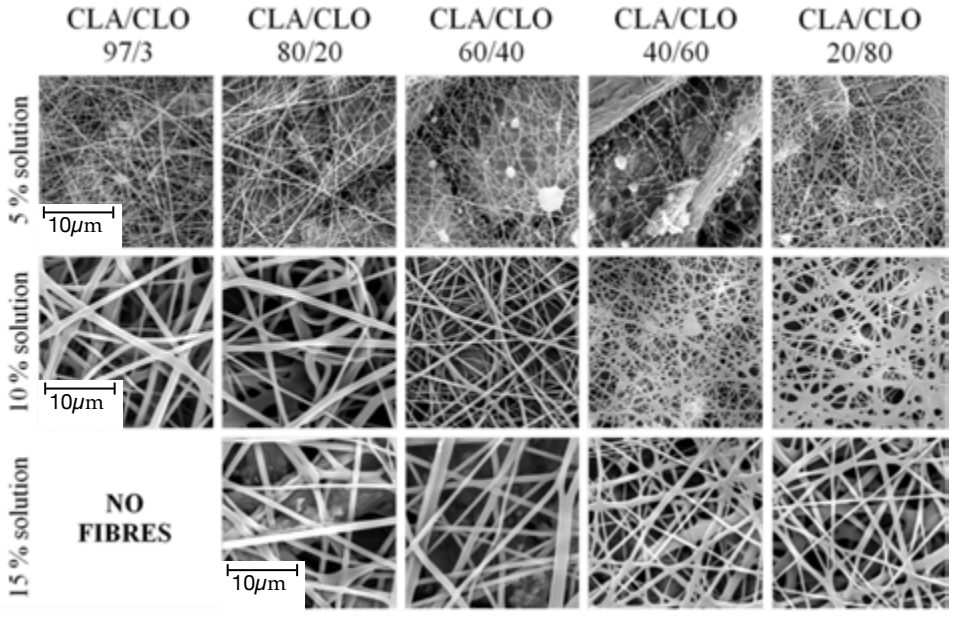

Figure 3. SEM images of needle-less electrospun PEAs fibrous materials containing the CLA and CLO structural units in varying ratio and copolymer concentration 5, 10 and 15 wt% [14].

Table 1 summarizes the composition (^{1}H NMR) and thermal properties of PEAs before and after electrospinning. The composition and melting temperature (Tm) of the fibrous materials remained nearly identical to those of the initial PEAs. Differences in melt enthalpy (ΔHm), observed from the first DSC heating run, reflected variations in the crystallization of the PEA phase between the original copolymer and electrospun fibrous material. These differences arise from distinct crystallization processes: polymer melt cooling versus solvent evaporation during electrospinning. The rapid solvent evaporation and high stretching forces in electrospinning can disrupt or constrain crystallization, resulting in varying degrees of polymer chain alignment and organization, which ultimately affect crystallinity. Such variations influence the mechanical properties, degradation behavior, and stability of the fibers, ultimately affecting their suitability for biomedical applications.

Table 1. Properties of PEA's and electrospun PEA's fibrous materials [14].

CLA/CLO copolymer	Tm (°C)	ΔHm (J/g)	CLA/CLO electrospun material	Tm (°C)	ΔHm (J/g)
80/20	179	51	82/18	178	43
60/40	121	39	60/40	127	13

Moreover, degradation studies further revealed that higher CLO content accelerates ester bond hydrolysis, leading to faster breakdown of the PEAs, as described in study [15]. This faster degradation may be beneficial in applications where the scaffold needs to degrade after fulfilling its purpose, such as in temporary wound healing or drug delivery systems. However, precise optimization is crucial to balance degradation rates and material stability. For instance, in tissue scaffolds, excessively rapid degradation could compromise structural integrity before new tissue has fully developed, potentially hindering the healing process.

1.2 Electrospinning of polymer blends

The electrospinning of polymer blends, similar to copolymers, presents both advantages and significant challenges in the fabrication of fibrous materials. Key challenges include phase separation, where immiscibility between polymers affects fiber uniformity and mechanical properties; solvent compatibility, requiring a solvent that dissolves both polymers without degradation; and the rheological complexity of non-Newtonian behavior of polymer blend solution, which requires careful control of viscosity, and conductivity. Additionally, optimizing electrospinning parameters is crucial to uniform fiber formation, while scalability remains a concern, especially with the needle-less technology. Despite these challenges, polymer blending offers substantial advantages, allowing for the precise tuning of mechanical properties, elasticity, and hydrogel characteristics, which are crucial for enhancing their biomedical potential [16]. Certain polymer combinations also enhance processability and spinability, allowing the optimization of resulting fiber properties for specific applications. These benefits make electrospun polymer blends highly versatile, enabling the creation of customizable fibrous materials.

One example of utilizing electrospun polymer blends for biomedical applications is the electrospinning of soy protein blends with other polymers to produce fibrous material. Plant-derived proteins such as zein, gluten, and soy protein attract attention for their bioactivity, charged surfaces, and hydrophilicity. These characteristics promote cellular interactions and controlled drug release, while their pH-responsive charge and high polar amino acid content enhance targeted drug delivery and cellular adhesion [17]. Several studies have investigated the electrospinning of these proteins with polyvinyl alcohol (PVA), polylactic acid (PLA), zein, or polyethylene oxide (PEO), but the resulting fibrous materials often remained water-soluble or required toxic cross-linking agents to achieve water insolubility [18-20]. Additionally, the need to use needle-based electrospinning limited their scalability for industrial applications. The

challenges were addressed by electrospinning a blend of purified soy flour (PSF) and gluten with PVA, which were cross-linked using a non-toxic alternative, as detailed in *Lubasová et al.* [21] (Appendix 2). This approach enabled the formation of uniform, defect-free fibers, resulting in an eco-friendly, sustainable, protein-based ultrafine fibrous material as a promising alternative to conventional materials. The preparation of soy flour for electrospinning began with an acid-wash process, resulting in PSF with a protein content of approximately 66-70%. The PSF and gluten were then dissolved in deionized (DI) water, adjusted to pH 11 with NaOH, and heated at 60°C for 30 minutes to induce protein denaturation and enhance processability. Early attempts to electrospun pure PSF or gluten were hindered by their complex helical structures in aqueous solutions, preventing continuous fiber formation. To overcome this, PVA was introduced as a helper polymer, facilitating the electrospinning process. By blending PSF or PSF/gluten with PVA in different proportions, uniform electrospun fibrous materials were successfully produced. As confirmed by SEM analysis, defect-free fibrous materials were achieved when the blend contained at least 64% PVA in the case of PSF/PVA and 45% PVA in the case of PSF/gluten/PVA (30/25/45 w/w/w), as shown in Figure 4.

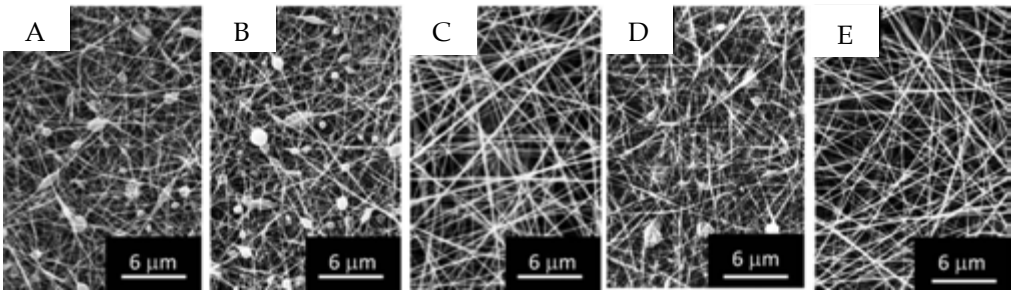

Figure 4. SEM images of electrospun fibrous materials made of: (A) PSF/PVA [46/54 w/w], (B) gluten/PVA [46/54 w/w], (C) PSF/PVA [36/64 w/w], (D) gluten/PSF/PVA [36/26/38 w/w/w] and (E) gluten/PSF/PVA [30/25/45] [21].

Despite the success of electrospinning, the high PVA content compromised the stability of the fibrous material in DI water. To enhance material's water-resistance, a non-toxic crosslinking approach using oxidized sugar (OS), produced by oxidizing sucrose with H_2O_2, was proposed. FTIR analysis confirmed successful crosslinking (Figure 5. (A)), while SEM images revealed that cross-linked fibrous materials swelled in DI water yet maintained their structural integrity (Figure 5. (B-C)).

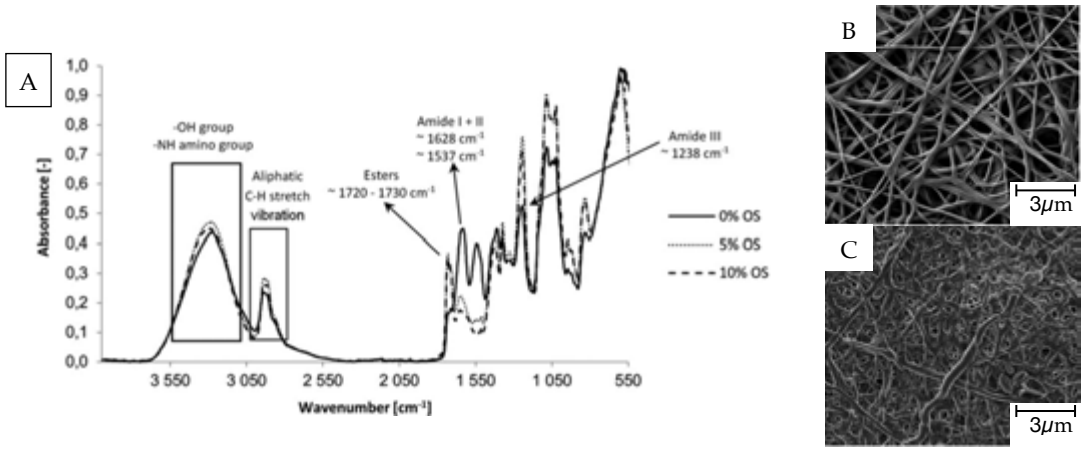

Figure 5. (A) FTIR spectra of electrospun gluten/PSF/PVA fibrous material before and after OS cross-linking. SEM images of OS cross-linked fibrous material after immersion in DI water at room temperature for: (B) 6 hours and (C) 24 hours [21].

The insoluble fraction of PSF/PVA fibrous materials was assessed by measuring their dried weight before and after immersion in DI water at 60°C (3 h), 80°C (6 h), and 21°C (1 month). Figure 6 shows solubility results for materials crosslinked with 0, 5, 10, and 15 wt% glyoxal or

OS. The glyoxal-treated fibers exhibited full stability, whereas fibers crosslinked with 5 wt% OS began to degrade at 80°C after 6 hours but remained intact under lower-temperature conditions. However, fibrous materials crosslinked with 10–15 wt% OS maintained their integrity even after one month in DI water. These findings demonstrate that OS is a promising non-toxic crosslinker for enhancing the stability of PSF/PVA fibrous materials. While OS showed slightly lower crosslinking efficiency compared to glyoxal, it offered a safer alternative, likely due to glyoxal's higher aldehyde content, which facilitates the formation of more crosslinks with protein macromolecules.

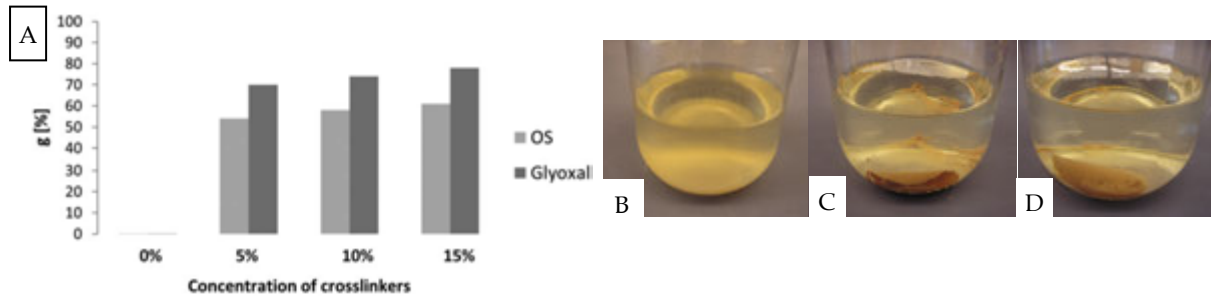

Figure 6. (A) Insoluble content of electrospun gluten/PSF/PVA material cross-linked by OS and glyoxal. OS cross-linked fibrous materials immersed in DI water for 1 month with: (B) 5 wt%, (C) 10 wt%, and (D) 15 wt% [21].

Building on efforts to maximize protein content in electrospun fibrous materials while minimizing structural defects like beading, further needle-less electrospinning experiments were conducted using PSF blended with PEO, as reported in *Lubasová et al.* [22] (Appendix 3). The polymer blend preparation involved dissolving PSF in an alkaline solution (pH 11, adjusted with NaOH) and heating at 60°C to induce protein denaturation. PEO was dissolved separately in DI water before mixing with PSF. As illustrated in Figure 7, needle-less electrospun PSF/PEO blends with PEO content below 20 wt%, particularly the 9/1 w/w blend, exhibited bead formation, whereas increasing PEO to 30 wt% significantly improved fibrous material morphology by enhancing solution viscosity, promoting polymer chain entanglement, and reducing defects. To achieve the highest protein content, PSF was processed into highly purified soy flour (HPSF), and commercially available soy protein isolate (SPI), soy protein concentrate (SPC), and defatted soy flour were obtained. Needle-less electrospinning was successfully applied to blends of PSF/PEO, HPSF/PEO, SPI/PEO, soy flour/PEO, and SPC/PEO (all at a 7:3 w/w ratio). The electrospun fibrous materials had the following protein content per blend, as measured by elemental analysis: HPSF – 1.86 g/m², SPI – 1.8 g/m², PSF – 1.39 g/m², SPC – 1.35 g/m², and soy flour – 1.1 g/m², all at a consistent fibrous material basis weight of 3 g/m². Moreover, electrospun PSF/PEO fibrous materials exhibited enhanced water stability, as the PEO contributes to the formation of continuous fibers, while the PSF remains dispersed within the matrix, providing structural integrity without the need for chemical crosslinking.

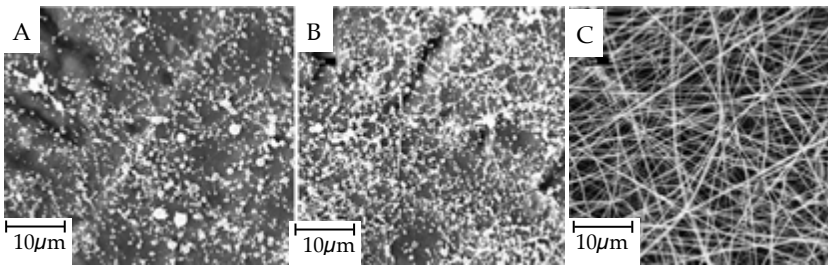

D

Type of protein blend used	Fiber weight (g/m²)	Protein content in the nanofibers (g/m²)
PSF/PEO	**1**	**0.463**
PSF/PEO	3	1.388
HPSF/PEO	**1**	**0.621**
HPSF/PEO	3	1.863
SPI/PEO	**1**	**0.601**
SPI/PEO	3	1.802
SPC/PEO	**1**	**0.451**
SPC/PEO	3	1.352
SF/PEO	**1**	**0.365**
SF/PEO	3	1.096

Figure 7. SEM images of electrospun PSF/PEO fibrous materials: (A) 9/1 w/w, (B) 8/2 w/w, and (C) 7/3 w/w. (D) Protein content in individual electrospun fibrous material [22].

This research, which focused on the electrospinning of PSF, HPSF, SPI, SPC, and gluten blended with PVA and PEO, was carried out at Cornell University. During her postdoctoral position, *Lubasová* was actively involved in developing, optimizing and characterizing those electrospun

fibrous materials, making significant contributions to the fabrication and characterization of these novel fibrous materials. The application of these fibrous materials, particularly in bacterial filtration, will be further explored in Chapter 3.1.

The next research leveraged polymer blends to develop fibrous hydrogels with superior water absorption. Notably, poly(vinylpyrrolidone) (PVP) and poly(acrylic acid) (PAA) exhibit strong hydrogen bonding interactions, where even minor additions (~10%) of one polymer to the aqueous solution of the other induce complex formation. This interaction-driven structuring enhances hydrogel integrity and swelling capacity, providing a tunable platform for tailored biomedical applications [23]. Previous studies have demonstrated the fabrication of electrospun PVP membranes using needle-based electrospinning, followed by crosslinking via UV-C radiation or the Fenton reaction [24]. However, these methods often compromise the fibrous structure, and high-energy radiation techniques remain costly and less accessible. While heat treatment has been explored for PVP stabilization [25, 26], the potential of heat-induced crosslinking to produce insoluble electrospun PVP/PAA hydrogel materials remained unexplored. To address this gap, *Lubasová et al.* [27] (Appendix 4) systematically investigated the electrospinning of PVP/PAA blends, their heat-induced crosslinking, and the resultant material characteristics, presenting a potentially scalable method for the fabricating fibrous hydrogels. This research, carried out at Deakin University, involved the active participation of the author of this thesis in refining the electrospinning process for the polymer blend and characterizing the resulting fibrous hydrogels. The study tested three solvents—acetic acid, trifluoroacetic acid, and DMF—finding that DMF produced the most consistent fiber morphology for the PVP/PAA blend. SEM analysis revealed that the PVP/PAA ratio had a significant impact on fiber formation (Figure 8. (A-C)). A decrease in the ratio from 8/2 to 6/4 led to a reduction in bead formation, likely due to enhanced viscosity resulting from interactions between PVP and PAA. However, further increasing the PAA concentration to 4/6 resulted in the formation of a dense film, likely due to the lower viscosity of the polymer blend solution caused by the reduced molecular weight of PAA. Notably, the addition of PAA reduced the fiber diameter from ~800 nm for pure PVP to ~150 nm for the PVP/PAA blend, suggesting that PAA promotes the production of finer fibers. The study also examined whether heat treatment could render PVP/PAA fibrous materials water-insoluble, enhancing their stability and water uptake. FTIR confirmed hydrogen bonding after heat treatment, particularly at 8/2 and 6/4 PVP/PAA ratios, contributing to hydrogel stability. Heat treatment above 180°C was essential for stability, with swelling ratios ranging from 500% to 3700%, significantly exceeding those of PVP/PAA films (300%–1700%) (Figure 8. (D-E)).

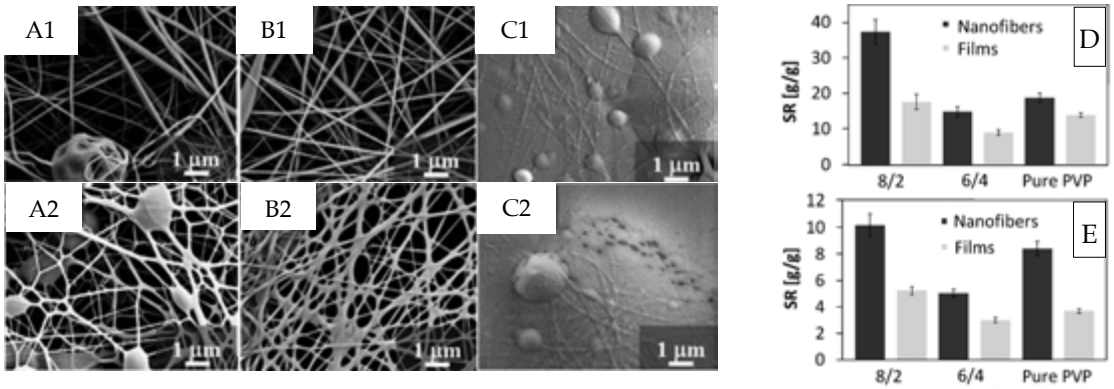

Figure 8. SEM images of electrospun fibrous materials PVP/PAA: (A) (8/2), (B) (6/4), (C) (4/6). 1st line: before heating; 2nd line: after heating at 200°C (1hr). (D-E) Swelling ratios of electrospun PVP/PAA and PVP fibrous materials and films after heat treatment for (D) 180°C and (E) 200°C [27].

Higher PAA content improved water absorption but reduced stability, while pure PVP maintained its structure with lower uptake. Untreated or low-temperature treated fibrous

material disintegrated in water, underscoring the importance of heat treatment. Additionally, the tensile properties of electrospun PVP/PAA fibrous materials were evaluated. Before heat treatment, the tensile strength of pure PVP fibers was 5.5 MPa, whereas PVP/PAA fibers exhibited a lower strength of 1–2.3 MPa, likely due to the low molecular weight of PAA, which weakens PVP inter-chain interactions. After heat treatment, the strain at break decreased for pure PVP fibrous materials, whereas it remained relatively unchanged for PVP/PAA fibers, indicating that a small amount of PAA enhances the plasticity of the fibrous structure. However, after swelling, the strain at break of the PVP/PAA fibrous structure increased to 55.1%, suggesting improved flexibility and water-induced plasticization. The PVP/PAA fibrous hydrogel exhibited consistent swelling ratios over 10 cycles of drying and re-swelling, highlighting its outstanding repeatability and stability, making it a promising candidate for wound dressing applications.

Another example of leveraging electrospun polymer blends for biomedical applications involves incorporating chitosan (CS) into electrospun materials. CS, a natural polymer derived from chitin, has significant potential in drug delivery and wound healing due to its biocompatibility, biodegradability, antimicrobial properties, and amino groups that facilitate bonding with antibiotics and bioactive compounds [28]. Previous studies examined the continuous electrospinning of chitosan/PVA blends, but the maximum CS content in the resulting fibrous materials did not exceed 30 wt% [29]. Building on this, the author of this thesis achieved a major advancement by blending CS with PEO, which not only enhanced the needle-less electrospinability of CS but also enabled the production of highly stable fibrous materials with a CS content of 90–95%, as reported by scientific study [30]. The study further highlighted the crucial role of solvent systems in electrospinning CS/PEO blends. Aqueous citric acid outperformed acetic acid, as it promoted thermal cross-linking, leading to water-resistant CS/PEO (9:1 w/w) fibrous materials. FTIR and SEM analysis (Figure 9) confirmed the successful formation of cross-links, significantly enhancing material's stability and functionality. Moreover, using PEO with a higher molecular weight (900 kDa) improved water-stability of the fibrous materials compared to PEO with a molecular weight of 400 kDa, likely due to the formation of a semi-interpenetrating polymer network supported by interactions between CS hydroxyl groups and PEO oxygen atoms. Additionally, the incorporation of Triton X-100 (a nonionic surfactant) and sodium chloride enhanced the properties of the polymer blend solution, promoted molecular complex formation, and improved fiber morphology.

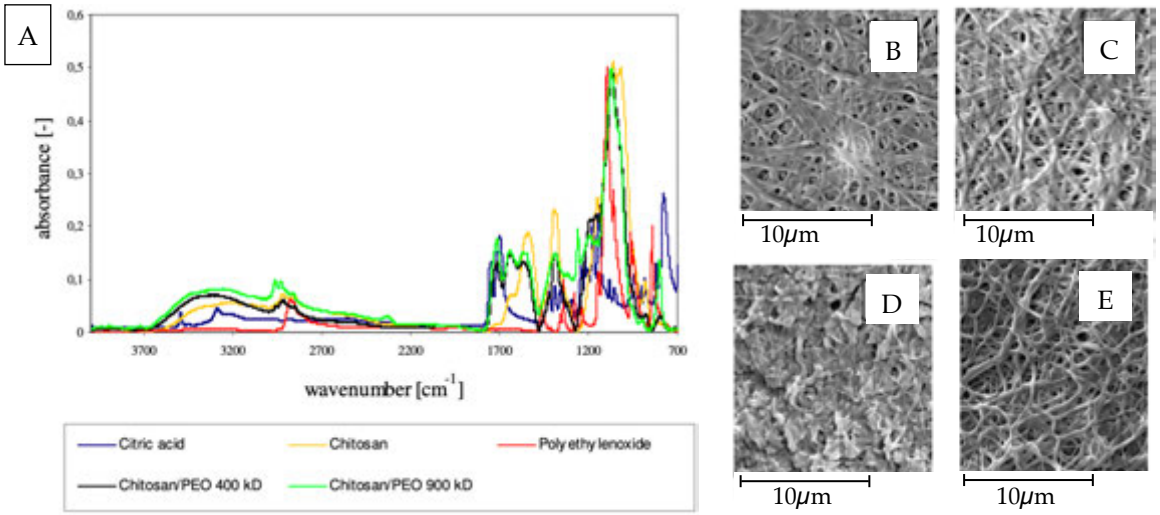

Figure 9. (A) FTIR spectrum of electrospun CS/PEO fibers. SEM images of CS/PEO material (CS dissolved in acetic acid) swelled in DI water for 15 minutes: (B) untreated, (C) heated at 50°C, (D) heated at 145°C, and (E) CS dissolved in citric acid, heated at 145°C [30].

The resulting water-stable electrospun CS/PEO fibrous material, with an average fiber diameter of 169 ± 43 nm and a gram-per-square-meter range of 8 to 40 g/m², demonstrates strong potential for a wide range of biomedical applications. Furthermore, crosslinking through mild Coulombic interactions enhances the material's stability and functionality, increasing its suitability for mucoadhesive drug delivery systems, as discussed in Chapter 3.5.

To enhance the tunability of electrospun CS/PEO fibrous materials—particularly in terms of hydrolytic degradation, mechanical strength, elasticity, and hydrophilicity—the author of this thesis proposed incorporating PCL into the CS/PEO polymer blend. This approach aimed to achieve greater control over these key properties by leveraging the well-known hydrophobicity and mechanical reinforcement of PCL, which had not yet been explored in this specific blend. By systematically varying the PEO/PCL ratio in needle-less electrospun PEO/PCL/CS fibrous materials (mass ratios of 6/2/2, 4/4/2, and 2/6/2), the study evaluated the effects on hydrolytic degradation, mechanical performance, and hydrophilicity, as detailed in *Lubasová et al.* [31] (Appendix 5). To ensure high-quality fibrous materials, two polymer solution preparation methods were compared before needle-less electrospinning. The two-step method, where each polymer was dissolved separately in a 2:1 v/v mixture of acetic and formic acid before mixing the next day, produced more uniform, defect-free fibers. In contrast, the one-step method, in which all polymers were dissolved together in the same solvent mixture, led to more defects. These findings suggest that separate dissolution enhances solution homogeneity, reducing defects in needle-less electrospinning. Additionally, defect-free fibrous materials were consistently produced at a 6 wt% PEO/PCL/CS concentration, while higher concentrations led to macroscopic holes in fibrous materials (Figure 10). The produced fibrous materials exhibited high gram-per-square-meter values ranging from 6.8 to 8.6 g/m², with an average fiber diameter of 134 ± 37 nm.

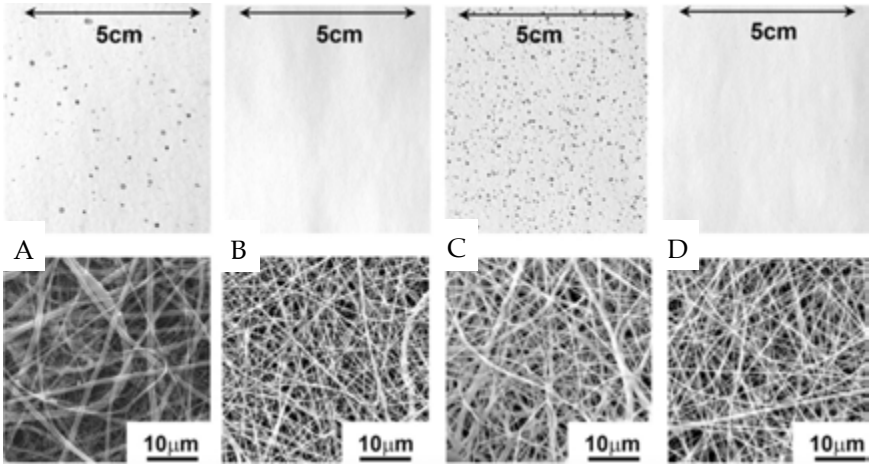

Figure 10. Photographs and SEM images of electrospun PEO/PCL/CS fibrous materials prepared by (A) one-step and (B) two-step method with polymer concentrations of (C) 8 wt% and (D) 6 wt% [31].

FTIR analysis further confirmed the successful incorporation of all three polymers in the fibrous materials, along with hydrogen bonding between PEO and CS. This interaction was evidenced by the increased intensity in the 3200–3600 cm^{-1} range, which became more pronounced with higher PEO content (Figure 11). Moreover, the hydrolytic degradation study of PEO/PCL/CS fibrous materials revealed a wide range of degradation rates (35.8 ± 1% to 73.2 ± 0.8%), directly correlating with the PEO/PCL ratios, where higher PEO content significantly accelerates degradation. Contact angle measurements indicated static contact angles ranging from 42.9 ± 3.8° to 0.7 ± 1.3°, demonstrating enhanced surface wetting due to PEO's pronounced hydrophilicity. Notably, surface-accessible amino groups were consistently detected across all fibrous materials, regardless of PEO/PCL/CS composition. This stability is attributed to the uniform CS content (20 wt.%) across all formulations. Amino group quantification on PEO/

PCL/CS fibrous materials with mass ratios of 2/6/2, 4/4/2, and 6/2/2 yielded values of 86.9 ± 8, 82.6 ± 6, and 83.3 ± 4 nmol NH_2/cm^2, respectively, with no statistically significant differences.

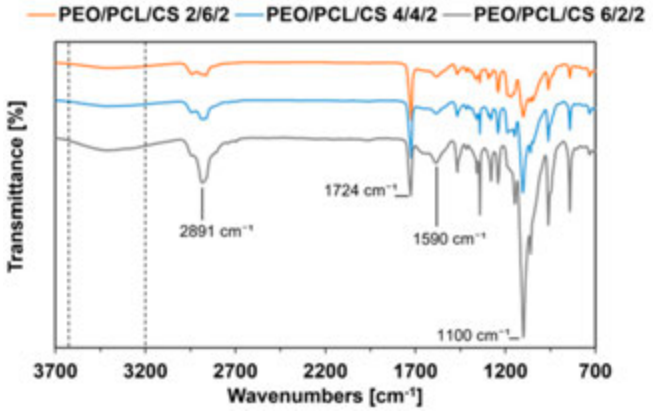

Figure 11. FTIR of electrospun PEO/PCL/CS fibrous materials with varying mass ratios (6/2/2, 4/4/2, 2/6/2) [31].

Mechanical testing revealed a correlation between the PEO/PCL ratio and Young's modulus (Table 2). As the PCL content increased, the material exhibited reduced stiffness due to PCL's inherent flexibility. Conversely, the ultimate tensile strength increased with higher PCL content, suggesting that PCL improves stress distribution and load-bearing capacity. Notably, the elongation at fracture of the 2/6/2 PEO/PCL/CS fibrous material was 26 times higher than that of compositions with lower PCL content. This substantial increase in ductility can be attributed to PCL's ability to enable extensive deformation before failure, highlighting its crucial role in enhancing stretch ability and mechanical resilience.

Table 2. Mechanical properties of electrospun PEO/PCL/CS fibrous materials with different mass ratios [31].

Nanofibrous scaffold	Young's modulus E [MPa]	Ultimate tensile stress UTS [MPa]	Elongation at fracture A [%]
PEO/PCL/CS 2/6/2	106.7 ± 8.5	4.8 ± 0.2	21 ± 2.9
PEO/PCL/CS 4/4/2	128.9 ± 7.2	3.2 ± 0.1	2.1 ± 0.3
PEO/PCL/CS 6/2/2	170.7 ± 11.9	2.3 ± 0.2	0.8 ± 0.1

This compositional strategy effectively balances mechanical strength and hydrolytic stability, distinguishing these materials from previously reported systems [32-34]. Moreover, these findings highlight the enhanced tunability of needle-less electrospun PEO/PCL/CS fibrous materials, reinforcing their potential for advanced wound care applications, which will be further explored in Chapter 3.4.

1.3 Summary

Processability and scalability remain key challenges in electrospinning polymer blends and copolymers. Issues such as poor electrospinability and limited tunability of electrospun fibrous materials have hindered their broader application in biomedical fields. Previous chapters have addressed these limitations by exploring the potential of needle-less electrospinning for polymer blends and copolymers, providing insights into overcoming these challenges and enhancing the functionality of electrospun fibrous materials. This habilitation thesis proposes innovative strategies for fabricating advanced electrospun materials with tunable biodegradability, accessible amino groups, high protein content, and improved mechanical properties. By optimizing solvent systems and incorporating carrier polymers, previously unprocessable polymers were successfully electrospun using needle-less technology, resulting in versatile fibrous materials with significant biomedical potential.

Specifically, newly proposed solvent systems for copolymers such as PET/LA and PEAs facilitated their needle-less electrospinning, enabling the industrial-scale production of biodegradable copolyester fibrous materials with tunable degradation rates—a breakthrough not previously reported. Next notable outcomes include the fabrication of a water-insoluble fibrous material with 88.7% protein content, exhibiting charged surface behavior and a high polar amino acid content. Significant contribution was made in the fabrication of fibrous hydrogels, electrospun from a PVP/PAA polymer blend, demonstrating exceptional water absorption of up to 3700% of its weight. This fibrous hydrogel was solely heat cross-linked eliminating the need for toxic crosslinking agents opening its application for biomedical applications. Another significant achievement was the successful needle-less electrospinning of fibrous material containing over 95% CS, leveraging CS's inherent antimicrobial properties and amino group functionalities to facilitate drug binding and enhance targeted therapeutic potential. Additionally, the successful needle-less electrospinning of PEO/PCL/CS fibrous materials resulted in materials with highly tunable properties, exhibiting elongation from 0.8% to 21%, hydrolytic degradation ranging from 35.8% to 73.2%, and hydrophilicity varying from 42.9° to 0.7°, making them outstanding candidates for various wound care applications.
A fundamental contribution of this research lies in the strategic use of polymer blends and copolymers to enhance the electrospinability of polymer solutions, while simultaneously improving biodegradability and material properties. The integration of non-biodegradable polymers with biodegradable components allowed tuning of degradation kinetics. The incorporation of carrier polymers such as PVA or PEO significantly improved the electrospinability and fiber morphology of otherwise poorly spinnable polymers like CS or PSF. All developed fibrous materials maintained nanoscale fiber diameters between 100–280 nm, ensuring a high surface-area-to-volume ratio. Scalability was a central focus, with needle-less electrospinning (Nanospider™ technology) enabling industrial-scale production while maintaining fibrous material quality and reproducibility. All these fundamental advancements, as demonstrated by the author of this thesis, significantly expand the applicability of electrospun fibrous materials in biomedicine, supporting innovations in wound care, antimicrobial barriers, drug delivery, and cancer therapy, as further described in Chapter 3.

2 Modifications of electrospun fibrous materials

Fabricated electrospun materials, despite their structural versatility, often require modifications to meet specific biomedical demands. While electrospinning of polymer blends or copolymers enables precise control over degradation rate and biocompatibility, it also allows fine-tuning of mechanical properties, elasticity, and hydrogel characteristics. However, their inherent properties may not provide the necessary antibacterial activity, bioactivity, or therapeutic effects required for biomedical applications. Thus, strategic modifications are essential to enhance antibacterial efficacy, regulate therapeutic delivery, and improve cellular interactions, ensuring their suitability for wound healing, tissue engineering, and drug administration. Despite their advantages, these modifications also present several challenges. The modification strategies of electrospun fibrous materials can be categorized into pre-electrospinning (internal) and post-electrospinning (external) approaches, each with distinct benefits and limitations. Pre-electrospinning modifications involve incorporating nanoparticles or bioactive agents into the polymer solution to enhance mechanical properties, bioactivity, and therapeutic release. Morphological adjustments, such as porous or ultrafine structures, optimize cellular adhesion and nutrient exchange. However these strategies may lead to nanoparticle aggregation, altered rheological behavior of polymer solutions, and challenges in achieving uniformity and scalability [35]. Post-electrospinning modifications, such as surface immobilization, and surface coatings, offer precise control over hydrophilicity and drug release but risk structural degradation, cytotoxicity, and increased costs [36]. The choice of modification strategy depends on the intended biomedical application: pre-electrospinning techniques enable scalable

functionalization, while post-electrospinning approaches provide controlled surface modifications, particularly advantageous for wound healing and targeted drug delivery [37].
The following sub-chapters critically examine these approaches, with a focus on the author of this thesis contributions to enhanced antibacterial properties, in optimizing cell-material interactions, and achieving controlled drug release. The balance between functionalization efficiency and processing feasibility is the key factor for the biomedical potential of electrospun fibrous materials therefore being particularly discussed in bellow sub-chapters.

2.1 Internal incorporation of antibacterial nanoparticles

Since most polymers lack inherent antibacterial properties, integrating antimicrobial nanoparticles (NPs), such as metal- and carbon-based materials, enhances microbial resistance and helps to prevent contamination [38]. Electrospinning effectively incorporates NPs by enabling their entrapment or encapsulation within fibrous materials. Several studies have demonstrated that needle-based electrospinning ensures better NP distribution due to stable Taylor cone formation and controlled polymer solution flow, minimizing phase separation and aggregation [39-41]. However, research on NP incorporation via needle-less electrospinning remained limited, and no direct comparison of internal and external NPs incorporation methods had been conducted. Addressing this gap, *Lubasová et al.* [42] investigated NP integration into needle-less electrospun fibrous materials using pre-electrospinning and post-electrospinning methods. Internal incorporation, where NPs were mixed into the polymer solution before electrospinning, resulted in more uniform distribution and enhanced antibacterial properties, particularly against *Escherichia coli*. The addition of Triton X-100 as a surfactant further improved NP dispersion and ensured uniform antimicrobial efficacy (Figure 12. (C-D)). In contrast, external incorporation, where NPs were applied post-electrospinning onto the fibrous structure by blowing them with a dust blower during electrospinning, resulted in uneven distribution, making it less suitable for applications requiring uniformity (Figure 12. (A–B)).

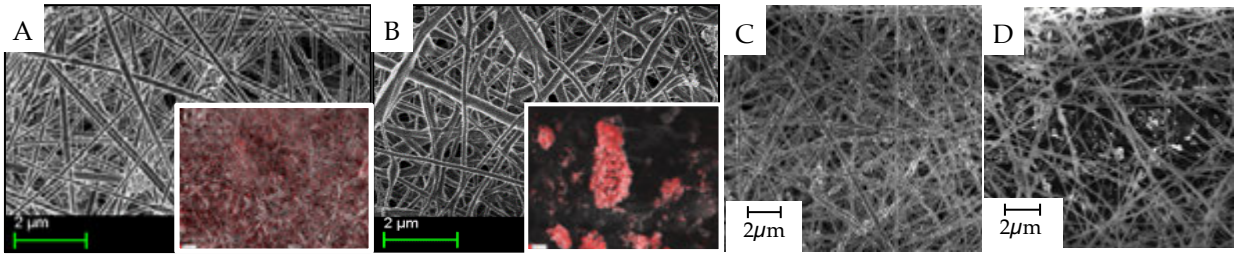

Figure 12. EDX analysis of TiO_2 distribution in electrospun CS/PEO fibrous material: (A) internal incorporation, (B) external incorporation, (C) internal with Triton X-100, and (D) internal without Triton X-100 [42].

The next step focused on investigating the antibacterial activity of needle-less electrospun materials with incorporated NPs. While numerous studies have investigated single NP systems and needle-based electrospinning [43, 44], the incorporation of multiple inorganic NPs into needle-less electrospun fibrous materials had not been extensively explored. Addressing this gap, the study [45] co-authored by *Lubasová* conducted a comparative analysis of the antibacterial properties of needle-less electrospun polyvinyl butyral (PVB) fibrous materials incorporating various NPs. In this study, PVB was dissolved in acetic acid with 0.5% Triton X-100 to reduce NP agglomeration, and various inorganic NPs—including TiO_2, ZnO, ZrO_2, SnO_2, CuO, and $AgNO_3$—were incorporated into the PVB solution and electrospun using the needle-less technology. Fiber diameters varied depending on the NP type: TiO_2 formed the finest fibers (266.5 ± 82.4 nm), while ZnO-TiO_2 produced the thickest (458.5 ± 227 nm), likely due to interactions between the metal oxides and acetic acid affecting solution conductivity. *Escherichia coli* was completely eliminated within 1 hour by PVB fibrous materials containing CuO, ZnO, and ZnO/TiO_2, whereas $AgNO_3$ required 3 hours. SnO_2, TiO_2, and ZrO_2 showed no

significant antibacterial effect after 4 hours. As shown in Figure 13, the antibacterial efficacy followed the order: CuO > ZnO = ZnO/TiO_2 > $AgNO_3$ > ZrO_2 > TiO_2 > SnO_2 ≥ none.

A

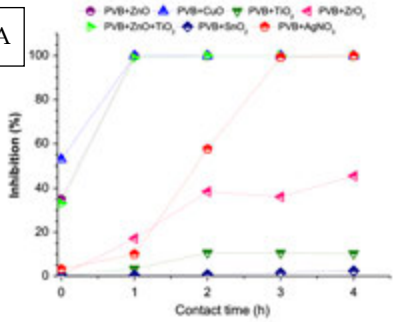

B

Sample	Diameter (nm)	Surface porosity (%)
PVB	368.2 ± 141	63.6
PVB + ZnO	391.4 ± 83.9	62.5
PVB + TiO_2	266.5 ± 82.4	61.1
PVB + ZnO/TiO_2	458.5 ± 227	69.8
PVB + CuO	244.9 ± 80	60.6
PVB + SnO_2	314.6 ± 102.5	61.2
PVB + ZrO_2	356.8 ± 13.9	69.1
PVB + $AgNO_3$	295 ± 72.9	69.5

Figure 13. (A) Reduction of Escherichia coli over the contact time with electrospun PVB fibrous materials with incorporated NPs. (B) Fiber diameters and surface porosity of the PVB fibrous materials with incorporated NPs [45].

This research pioneered the integration of various inorganic nanoparticles into needle-less electrospun materials, identifying CuO as the most effective antibacterial agent when incorporated into PVB fibrous structures. By facilitating the development of cost-effective, high-performance fibrous materials, these findings support large-scale production and real-world applications. The potential of PVB/CuO fibrous materials for protective textiles will be further explored in Chapter 3.2.

2.2 Fiber morphology modifications

In biomedical engineering, the morphology of materials plays a critical role in determining their functionality, particularly when mimicking the natural extracellular matrix. The structural properties of electrospun fibrous materials—such as the fiber diameter, porosity, and interconnectivity—significantly influence cell behavior and tissue regeneration. Morphological modifications, including the development of both porous and non-porous fibers, have profound implications for tissue engineering applications, affecting cell attachment, proliferation, and differentiation [46]. Conventional methods for producing porous fibers, such as bicomponent extraction, thermal degradation, or electrospinning with temperature-controlled collectors [47-49], are technically complex, requiring multi-step processes or specialized equipment. To overcome these challenges, *Lubasová et al.* [50] (Appendix 6) conducted a comprehensive analysis of key parameters influencing fiber morphology and introduced a previously unexplored, single-step needle-less electrospinning technique for the consistent fabrication of porous fibers. In this study, Hansen solubility parameters (HSP) were employed to predict the optimal solvent system for achieving porous fibers via needle-less electrospinning. Hansen's model [51] divides total solubility into polar forces (δ_p [$MPa^{1/2}$]), dispersion forces (δ_d [$MPa^{1/2}$]), and hydrogen bonding forces (δ_h [$MPa^{1/2}$]), providing a more detailed understanding of solvent-polymer compatibility, as expressed in the following equation:

$$\delta^2 = \delta_p^2 + \delta_d^2 + \delta_h^2 \quad (1)$$

For practical applications, model can be simplified to two dimensions, where two of the parameters (typically δ_p and δ_h) are plotted, as shown in Figure 14. In this 2D representation, the "solubility sphere" of the polymer is visualized as a circle with a radius R and center coordinates ($^P\delta_p$,$^P\delta_h$). Solvents, plotted by their respective HSP values ($^S\delta_p$, $^S\delta_h$), are assessed based on their proximity to the centre of solubility sphere. The distance, ($\Delta\delta_{(S-P)2D}$), between a solvent's HSP values and the polymer's solubility sphere center is crucial for quantifying solubility compatibility. A smaller distance indicates closer alignment with the polymer's solubility sphere, suggesting a good solvent, while a larger distance implies limited compatibility, indicating a poor solvent. This distance is calculated using the following equation:

$$\Delta\delta_{(S\text{-}P)2D} = \left[\left({}^{S}\delta_p - {}^{P}\delta_p \right)^2 + \left({}^{S}\delta_h - {}^{P}\delta_h \right)^2 \right]^{1/2} \quad (2)$$

Predicting solvent solubility parameters from chemical structure is inherently complex due to the intricate interactions among structural groups. For a wide range of solvents, HSP components are tabulated [51]. To address HSP of polymers, Van Krevelen introduced a predictive method based on a polymer molecular structure, which provides an estimation of each solubility parameter through individual components: dispersion (*Fd*), polar (*Fp*), and hydrogen bonding (*Eh*), normalized by the polymer's molar volume (*Vm*) [52]. These components help calculate the HSP of polymer using following equations:

$$\delta_d = \frac{\sum F_{di}}{V_m}, \qquad \delta_p = \frac{\sqrt{\sum F_{pi}^2}}{V_m}, \qquad \delta_h = \sqrt{\frac{\sum E_{hi}}{V_m}} \quad (3\text{-}5)$$

In *Lubasová et al.* [50], PVB was used as a model polymer to investigate the effects of solvent selection on fiber morphology. Various solvent combinations—including ethanol/methanol, tetrahydrofuran (THF)/dimethyl sulfoxide (DMSO), and ethanol/DMSO—were tested, encompassing both poor/poor and good/poor solvent systems. The results demonstrated that specific solvent pairings used for PVB dissolving, consistently produced fibers with distinct morphologies, ranging from nonporous to partially or fully porous structures (Figure 14). Precise control over fiber morphology in needle-less electrospinning was achieved through strategic solvent system selection. The $\Delta\delta_{(S-P)2D}$ parameter played a crucial role, as significant differences in $\Delta\delta_{(S-P)2D}$ values of solvent system—such as 2.5 $MPa^{1/2}$ for PVB-THF and 9.9 $MPa^{1/2}$ for PVB-DMSO—promoted porous fiber formation. Conversely, minimal or zero differences in $\Delta\delta_{(S-P)2D}$ of solvent system suppressed porosity. Additionally, differences in solvent system vapor pressure facilitated uniform pore formation, further enabling controlled fiber morphology.

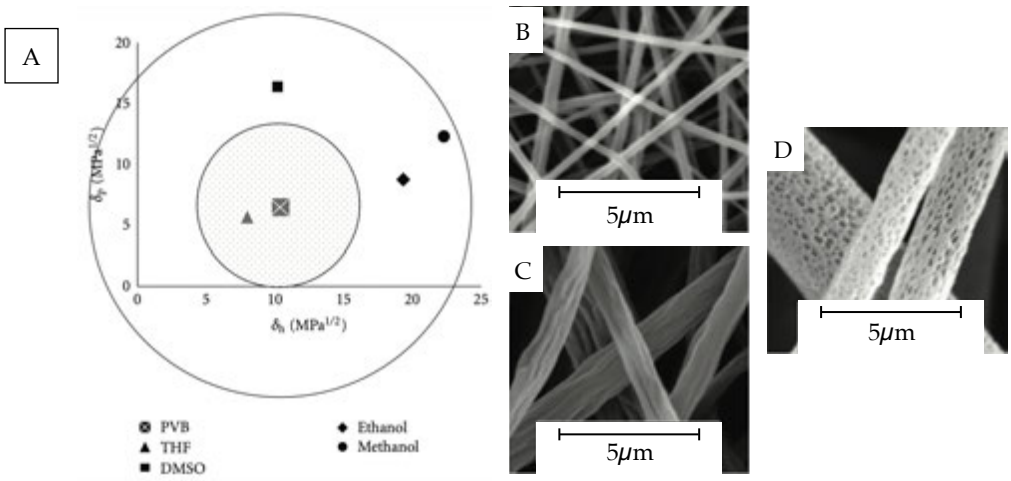

Figure 14. (A) HSP graph for achieving porous PVB fibers: grey area = good solvent, white area = poor solvent. SEM of PVB fibers prepared from: (B) ethanol/methanol (9/1 v/v), (C) ethanol/DMSO (9/1 v/v), (D) THF/ DMSO (9/1 v/v) [50].

Furthermore, the study found that a 9/1 (v/v) good-to-poor solvent ratio significantly enhanced fiber porosity compared to an 8/2 (v/v) ratio, as shown in Figure 15. Additionally, lower polymer solution concentrations resulted in finer fibers while maintaining porosity. Increasing the applied voltage during electrospinning led to smaller fiber diameters but reduced porosity, likely due to accelerated polymer solidification.

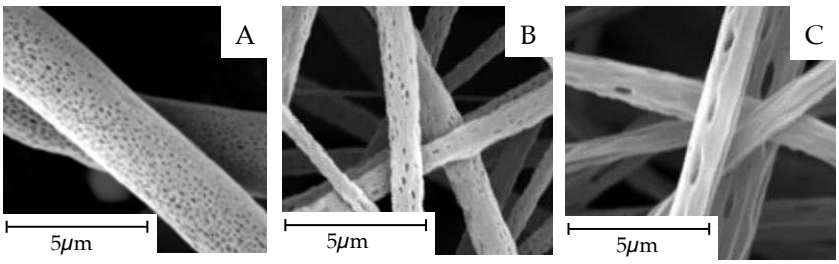

Figure 15. SEM images of electrospun PVB fibers prepared from: (A) 10 wt% THF/DMSO (9/1 v/v), (B) 8 wt% THF/DMSO (9/1 v/v), and (C) 8 wt% THF/DMSO (8/2 v/v) [50].

These findings highlight the role of solvent evaporation in poor-solvent regions as a key factor in pore formation, contributing to a consistently porous fiber structure. Three critical conditions were identified for successful porous fiber formation in needle-less electrospinning: (i) the use of a good/poor solvent system, (ii) significant differences in vapor pressure between the good and poor solvents, and (iii) an optimal good-to-poor solvent ratio for polymer dissolution prior to electrospinning. This approach was further extended to the fabrication of porous PCL fibers, as described by *Lubasová et al.* [53]. Electrospinning solutions were prepared by dissolving PCL in various solvent mixtures, including THF/DMSO and ethyl acetate/DMSO (both 9/1 v/v), chloroform/methanol (9/1 v/v), and acetone/ethanol (7/3 v/v), with polymer concentrations of 16 or 18 wt.%. SEM analysis (Figure 16. (A-D)) revealed that fibers electrospun from THF/DMSO and ethyl acetate/DMSO exhibited a highly porous structure, characterized by elliptical surface pores. In contrast, fibers electrospun from PCL polymer solutions in chloroform/methanol and acetone/ethanol were non-porous, underscoring the importance of solvent system selection in influencing fiber morphology. Porosity formation was primarily observed in good/poor solvent systems with significant differences in solvent vapor pressure, confirming the critical conditions for electrospinning porous fibers identified in previous study. Measured fiber diameters varied significantly among the tested systems, with average values of 830 nm for THF/DMSO, 740 nm for ethyl acetate/DMSO, 1580 nm for chloroform/methanol, and 290 nm for acetone/ethanol. Further characterization using the Barrett-Joyner-Halenda method (Figure 16. (E)) confirmed the presence of pore volumes of 1.3×10^{-4} cm^3/g and 2.9×10^{-4} cm^3/g for THF/DMSO and ethyl acetate/DMSO fibers, respectively, while no detectable porosity was observed in fibers from the other solvent systems. These findings underscore the crucial role of solvent selection. The implications of these morphological characteristics for tissue growth and integration will be further discussed in Chapter 3.3.

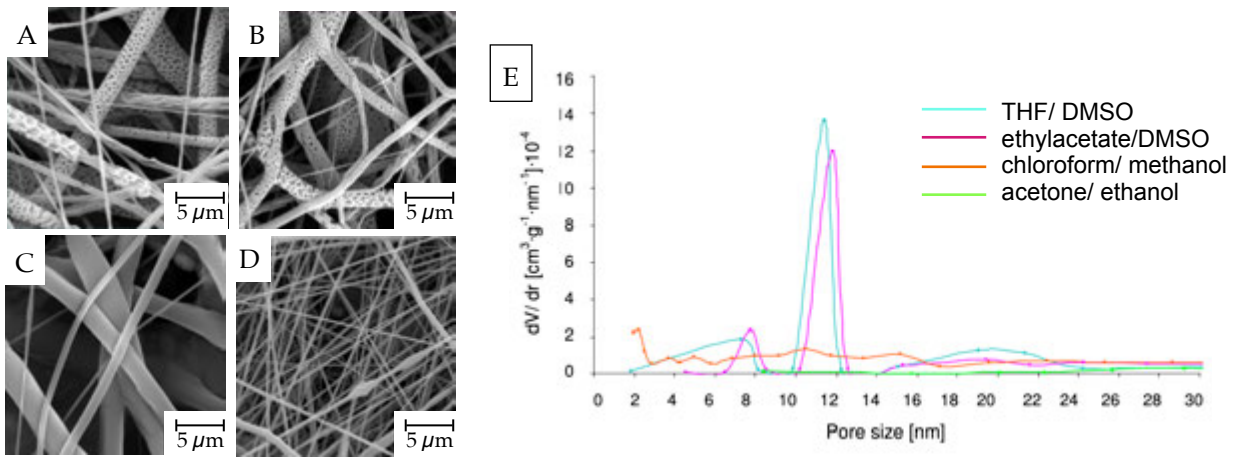

Figure 16. SEM images of needle-less electrospun PCL fibers prepared from solvent system: (A) THF/ DMSO, (B) ethylacetate/ DMSO, (C) chloroform/ methanol and (D) acetone/ ethanol. (E) The pore volume of electrospun PCL materials from various solvent systems [53].

As previous studies have demonstrated that different solvent systems influence fiber morphology, the author of this thesis further explored how solvent properties—$\Delta\delta_{(S-P)}$, permittivity, and vapor pressure—affect electrospinning. A correlation between polymer solution viscosity, electrospinning behavior, and $\Delta\delta_{(S-P)}$ was previously established in *Lubasová's* thesis [3] and in study [54]. At low $\Delta\delta_{(S-P)}$ values, polymer chains remain stretched, leading to high viscosity that remains stable under the applied electric field. In contrast, at higher $\Delta\delta_{(S-P)}$ values, closer to the edge of the polymer's solubility sphere, the chains are coiled. Under the electric field, these chains uncoil, increasing polymer solution viscosity and facilitating electrospinning. Solvent vapor pressure also plays a crucial role during electrospinning: slow evaporation results in the formation of flat fibers, whereas an optimal vapor pressure ensures smooth, defect-free fibers. Additionally, high-permittivity solvents enhance charge distribution, promoting stable fiber formation. Building on these findings, *Lubasová et al.* [55] introduced a predictive numerical model using PVB as a model polymer. This model was proposed, verified, and subsequently implemented as the Nanoestimator software (RIV/46747885:24220/20:00007079). This software employs Raoult's law [56] to calculate the vapor pressure of binary solvent systems and applies Kirkwood theory [57] to determine their permittivity. First, it computes $\Delta\delta_{(S-P)}$, permittivity, and vapor pressure for single solvents and binary solvent systems across a range of volume ratios (1/9 v/v to 9/1 v/v, in 10% increments) using a built-in solvent properties database. Next, the software ranks solvents and binary solvent systems based on hypothetical optimal electrospinning conditions, prioritizing high permittivity, moderate vapor pressure, and high $\Delta\delta_{(S-P)}$ values. Finally, solvents and binary solvent systems ranked on their predicted suitability are provided. Figure 17 presents the predictive model results generated by the software as a graph, using a linear color scale (green for highly suitable solvents, red for the least suitable) and a diameter scale (larger points indicate more suitable solvents). For example, acetone and THF appear as red dots with the smallest diameters, correlating with poor PVB fiber formation during electrospinning, as shown in the SEM images (Figure 17. (C-D)). In contrast, methanol and ethanol are plotted as green points with larger diameters, indicating their suitability for PVB electrospinning. Their effectiveness is confirmed by SEM images (Figure 17. (E-F)), which show defect-free PVB fibrous morphologies, validating the correctness of the solvent ranking. These findings are consistent with study [54], which identified ethanol and methanol as PVB solvents with higher $\Delta\delta_{(S-P)}$ values, a property that enhances electrospinning and improves fiber morphology. Their high permittivity (~22.4, ~32.7) stabilizes the fiber jet, promoting uniform fiber formation while ensuring controlled evaporation and preventing fiber collapse. In contrast, THF and acetone, characterized by low $\Delta\delta_{(S-P)}$ values in PVB, low permittivity (~7.6 and ~20.6), and high vapor pressures (~162 and ~231), lead to rapid solvent evaporation and insufficient charge stabilization. This disrupts the electrospinning process, resulting in film formation or fiber defects instead of continuous fiber generation.

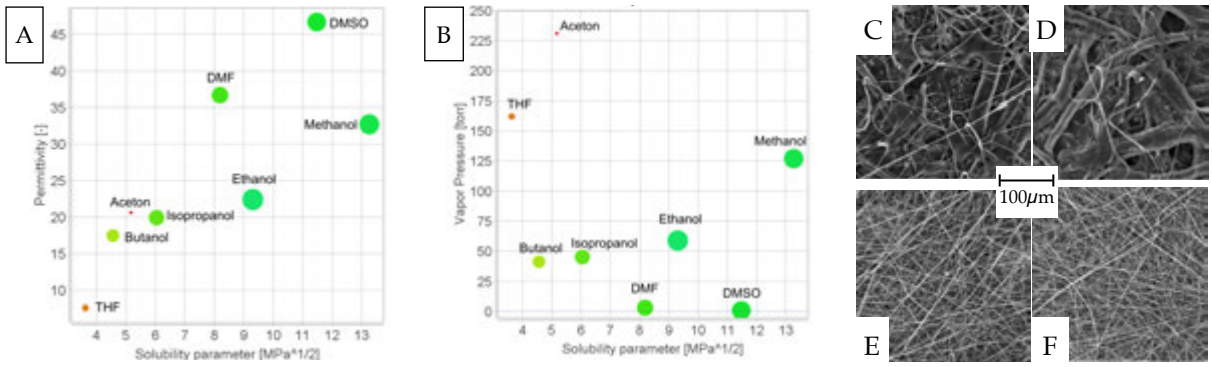

Figure 17. (A-B) Predictive model results for a single solvent system of PVB. SEM of electrospun PVB fibrous materials prepared from polymer solution: (C) acetone, (D) THF, (E) methanol, and (F) ethanol [55].

The predictive model further ranked binary solvent systems to outperform single solvents based on hypothetical optimal electrospinning conditions - a finding later confirmed through experimental validation. For instance, electrospinning with an ethanol/methanol binary system yielded significantly finer fibers compared to ones using ethanol or methanol as single solvents only. As shown in the SEM images (Figure 18. (C-D)), electrospun PVB fibers from ethanol and methanol alone exhibited diameters of 592 ± 34 nm and 663 ± 41 nm, respectively. In contrast, employing a 9/1 v/v ethanol/methanol system reduced fiber diameters to 270 ± 22 nm. This enhancement is likely due to the synergistic effects of optimized polymer solubility and charge distribution, which improve PVB electrospinability and enable finer fiber formation.

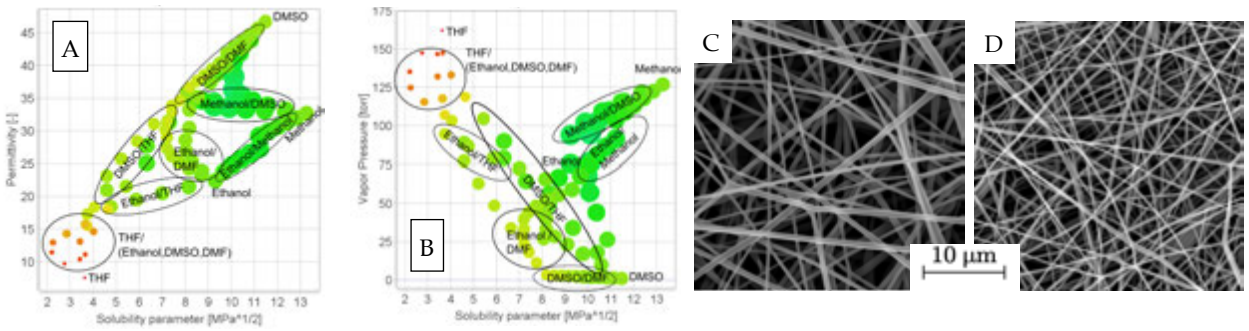

Figure 18. Dependency between HPS distance of polymer/ solvent $\Delta\delta_{(S-P)}$ and: (A) vapor pressure, (B) permittivity. SEM images of PVB dissolved in ethanol/ methanol: (C) 7/3 v/v and (D) 9/1 v/v [55].

Furthermore, the predictive model was successfully validated for PCL, accurately identifying the optimal solvent system for successful electrospinning. By enabling the precise and experiment less selection of optimal solvent systems, the predictive model not only mitigates solvent toxicity risks but also supports the production of fibers with a controlled morphology for biomedical applications. Additionally, it streamlines solvent selection for needle-less electrospinning, minimizing the need for extensive and costly experimental testing, thereby accelerating the development of advanced electrospun materials.

2.3 Surface antibiotic immobilization

Many studies have focused on incorporating antibiotics like tetracycline (TET) into bi-layer electrospun structures, core-shell configurations, or directly within the polymer matrix [58–60]. While these methods offer some benefits, they often incur high costs, exhibit suboptimal drug release profiles, and lack the versatility needed for dynamic wound management, leading to reduced efficacy, batch-to-batch variability in drug concentration, and limited adaptability to diverse wound care needs. In contrast, post-electrospinning surface immobilization of antibiotics represents a significant advancement for biomedical applications, particularly in wound healing and infection control. This approach ensures prolonged antimicrobial activity at lower drug concentrations while maintaining broad applicability across various substrates, including polymers and metals [61]. Since no prior researches had investigated the surface immobilization of TET onto PEO/PCL/CS fibrous materials (Chapter 1.2), with CS serving as the functional site for TET binding through its primary amine groups, *Lubasová et al.* [31] (Appendix 5) explored this strategy to enhance the potential of PEO/PCL/CS fibrous materials for wound care applications. This surface immobilization strategy significantly enhances antibacterial efficacy by preserving TET's activity and enabling post-production customization of the fibrous materials. TET immobilization was achieved by immersing PEO/PCL/CS electrospun fibrous materials in a 0.5 wt% TET solution in ethanol, within a hermetically sealed chamber, for 90 minutes. One set of materials (samples AB) was air-dried after immobilization, while another set (samples B) was washed with ethanol before drying. This experimental setup allowed for a direct comparison of fibrous materials with chemically bound TET (sample B) and those with both chemically bound and physically adsorbed TET (sample AB), enabling the

evaluation of the stability and sustained antibiotic activity provided by chemical binding versus physical adsorption. As shown in Figure 19, microbiological testing using the Kirby-Bauer disk diffusion method on *Escherichia coli* demonstrated that antibacterial activity persisted in fibrous material B after ethanol washing, suggesting stable TET binding and confirming that the activity was not merely due to physical adsorption. However, a reduction in antibacterial efficacy compared to fibrous material AB suggests that approximately 30% of TET may have been physically adsorbed. This reduction can be attributed to the low CS content (20 wt%) in electrospun PEO/PCL/CS fibrous materials, which contain approximately 84 nmol NH_2/cm^2 of surface amino groups. Increasing the CS concentration could enhance TET binding and improve long-term antibacterial efficacy.

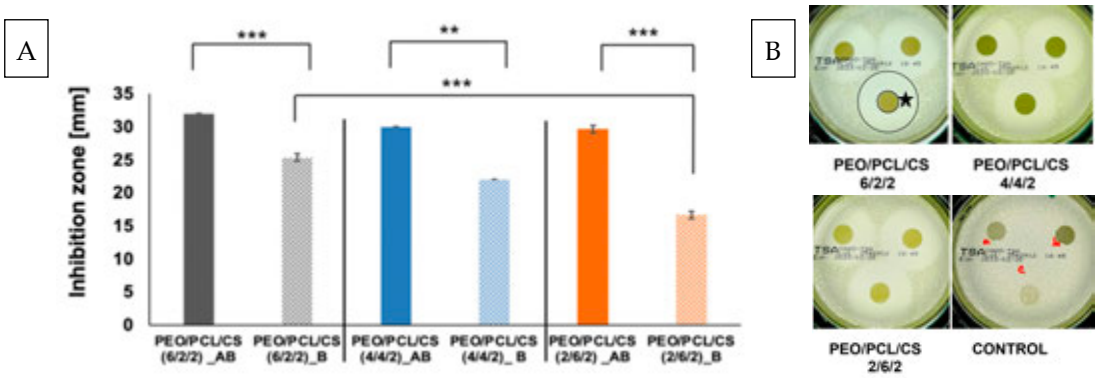

Figure 19. (A) Antibacterial efficacy of electrospun PEO/PCL/CS fibrous materials with different mass ratios against Escherichia coli. (B) Photographs of inhibition zones (asterisks) around electrospun fibrous materials [31].

Furthermore, statistical analysis revealed significant differences in antibacterial efficacy based on the fibrous material composition. Materials with higher PEO content exhibited greater antibacterial activity compared to those with higher PCL content. This enhanced antibacterial effect can be attributed to interactions between TET's multifunctional chemical groups and not only CS but also PEO and PCL. These interactions likely influence antibacterial efficacy by affecting bond stability, strength, and the density of available attachment sites on the surface. Interestingly, fibrous materials without TET did not exhibit any antibacterial efficacy, despite the presence of CS, which is known for its antibacterial properties. This suggests that the CS content in the electrospun fibrous material (limited to 20 wt%) was insufficient to exert a significant antibacterial effect on its own, especially in the presence of a high bacterial load.
The findings highlight the advantages of surface-immobilized TET on needle-less electrospun PEO/PCL/CS fibrous materials, including enhanced antibacterial activity and the ability to customize TET concentration for rapid, patient-specific adjustments prior to use. This enhances the practicality and adaptability of wound care solutions. The potential of these modified materials in wound care applications is further explored in Chapter 3.4.

2.4 Surface absorption of therapeutics

The physicochemical properties of electrospun fibrous materials, particularly their surface hydrophilicity and hydrophobicity, play a pivotal role in determining the adsorption and release kinetics of therapeutics. Numerous studies have shown that the surface characteristics of electrospun fibers significantly influence both drug loading efficiency and release behavior. Hydrophilic surfaces, for instance, tend to enhance drug absorption and facilitate rapid release, whereas hydrophobic surfaces often promote sustained release profiles by restricting the initial dissolution of the drug [62, 63]. This relationship between fibrous materials surface properties and drug delivery performance is particularly crucial in electrospun materials, where both surface chemistry and structural morphology dictate interactions with therapeutic agents. Despite these insights, previous studies primarily focused on individual fiber types, with limited systematic evaluation of various electrospun materials and their effects on drug loading

and release. To address this gap, the author of this thesis studied the absorption and release of poly(lactic-co-glycolic acid)-poly(ethylene glycol) (PLGA-PEG) nanoparticles, liposomes, and paclitaxel (PTX) from fibrous materials with varying hydrophilicity. The study systematically assessed various electrospun materials, including CS/PEO (Chapter 1.2), silk fibroin (SF), SF/PCL, and PCL (Chapter 2.2), with PCL being analyzed in both its untreated and 3M sodium hydroxide (NaOH)-treated forms. By systematically comparing these electrospun materials, this research aimed to establish correlations between fiber hydrophilicity, drug carrier compatibility, and the efficiency of controlled release. The findings contribute to a deeper understanding of the fundamental relationships governing drug delivery performance, offering valuable insights for the design and optimization of electrospun materials in biomedical applications. To fabricate the SF fibrous materials, degummed silk fibers were dissolved in 98% formic acid with 3 wt% $CaCl_2$ at a 12 wt% concentration and electrospun, followed by ethanol treatment to induce crystallization and improve material's water stability. SF/PCL fibrous materials were produced by electrospinning an 8:2 (v/v) mixture of SF and PCL solutions, where PCL (20 wt%) was dissolved in formic acid. SEM analysis revealed fiber diameters of 169 ± 43 nm (CS/PEO), 141 ± 28 nm (PCL), 903 ± 331 nm (SF), and 772 ± 187 nm (SF/PCL). NaOH-treated PCL retained a diameter of 150 ± 31 nm but exhibited increased surface roughness due to nanoscale protrusions (Figure 20). Contact angle measurements further confirmed the hydrophobic nature of untreated PCL (119 ± 4°), whereas CS/PEO, SF, and SF/PCL fibrous materials were hydrophilic (12 ± 3°, 44 ± 5°, and 63 ± 6°, respectively). NaOH treatment significantly enhanced PCL hydrophilicity, reducing the contact angle to 54 ± 6° without altering fiber dimensions. The impact of these surface properties on drug loading and release kinetics was further explored through the incorporation of different therapeutics.

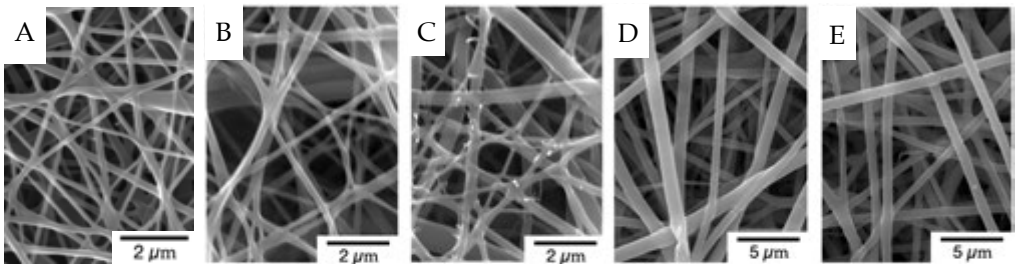

Figure 20. SEM images of electrospun fibrous materials: (A) CS/PEO, (B) PCL, (C) NaOH treated PCL, (D) SF, and (E) SF/PCL [65].

Distinct drug release profiles were observed for each therapeutics formulation, with the surface properties of the fibrous carriers playing a critical role in adsorption and release kinetics. In scientific study [64] (Appendix 7), electrospun fibrous materials were loaded with PLGA-PEG nanoparticles and liposomes in collaboration with Veterinary research institute in Brno. Upon application, these dispersions were uniformly absorbed throughout the electrospun fibrous matrix via capillary action. SEM and confocal microscopy analyses demonstrated a homogeneous distribution of PLGA-PEG nanoparticles and liposomes across the surfaces of the fibrous materials (Figure 21. (A-B)).

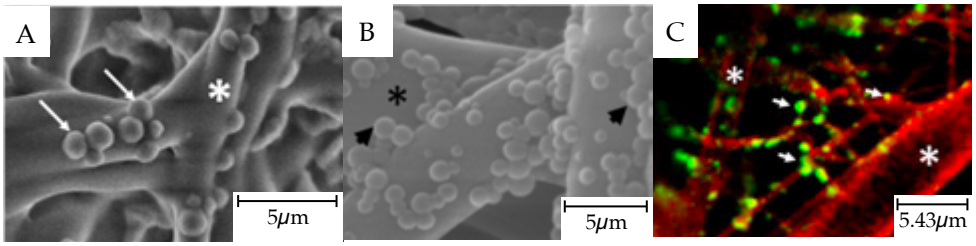

Figure 21. SEM and confocal microscopy details of electrospun SF fibrous material loaded with (A) liposomes, (B) PLGA-PEG nanoparticles, (C) GFP-proteo-liposomes (green) adsorbed to electrospun PCL fibrous layer (red) [64].

Moreover, when using GFP-proteoliposomes as a model for vaccine-oriented nanoparticles, no aggregation or disruption of GFP metallochelation binding was observed (Figure 21. (C)). This suggests that the adsorption process does not compromise the integrity of the nanoparticles. However, the ability of electrospun materials to release nanoparticles varied significantly, highlighting the influence of fiber surface properties on drug release kinetics. SF and CS/PEO fibrous materials exhibited rapid nanoparticle release, with nearly 100% of the loaded nanoparticles released within 30 minutes. In contrast, PCL fibrous material demonstrated significantly lower release levels, likely due to their intrinsic hydrophobicity, which restricted nanoparticle diffusion (Figure 22). Interestingly, NaOH treatment of PCL fibrous materials substantially enhanced nanoparticle release, bringing it close to 100%, a result that strongly correlated with the observed increase in hydrophilicity. This contrast in release behavior underscores the pivotal role of surface chemistry in dictating drug-carrier interactions.

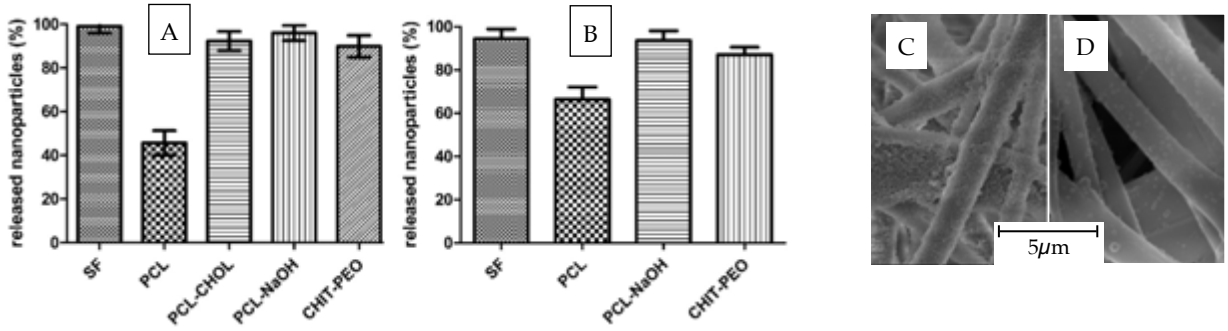

Figure 22. The release quantity of nanoparticles from electrospun fibrous materials: (A) liposome release and (B) PLGA-PEG nanoparticle release. PLGA-PEG loaded onto fibrous material as observed by SEM (C) before and (D) after dissolution test [64].

Hydrophilic fibrous materials promoted the rapid release of PLGA-PEG nanoparticles and liposomes due to enhanced water penetration and diffusion, whereas the release of the hydrophobic drug PTX followed the opposite trend, as described in *Lubasová et al.* [65] (Appendix 8). In this study, a PTX injection solution (6 mg/mL PTX in polyoxyl 35 castor oil and dehydrated alcohol) was loaded onto the electrospun fibrous materials. Unlike hydrophilic carriers, PTX exhibited preferential interactions with the more hydrophobic electrospun materials, particularly untreated PCL. Strong hydrophobic interactions between PTX and PCL fibrous materials resulted in prolonged drug delivery, as reflected by the release behavior confirmed by UV-vis spectrophometry. In contrast, SF fibrous materials, with their higher hydrophilicity, exhibited weaker interactions with PTX, leading to a more rapid release, with the lowest absorbance (0.14), as shown in Figure 23.

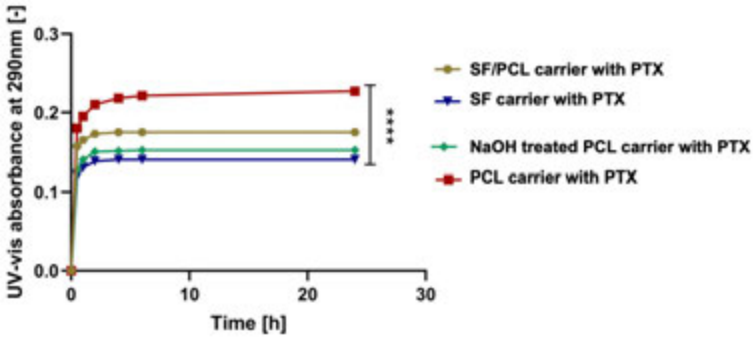

Figure 23. The release behavior of PTX from four types of electrospun fibrous materials: PCL, NaOH-treated PCL, SF, and SF/PCL blend [65].

These observations reinforce the significance of surface hydrophilicity and hydrophobicity to govern drug loading and release behaviors in electrospun materials. Hydrophilic carriers such as PLGA-PEG nanoparticles and liposomes interact favorably with hydrophilic electrospun

fibrous materials through hydrogen bonding and electrostatic interactions, leading to improved adsorption and controlled release profiles. The high porosity of nanofibrous structures further facilitates efficient diffusion, allowing for rapid absorption and release [66]. Conversely, PTX, as a hydrophobic drug, preferentially interacts with hydrophobic fibrous material made of PCL (untreated), where strong hydrophobic interactions lead to lower burst release and prolonged drug retention. In literature, electrospun PCL fibrous materials have been widely employed for targeted and controlled drug delivery, with multiple studies demonstrating their efficacy in sustaining drug release profiles [67-69]. The results of the study [65] further support these findings, confirming the suitability of electrospun PCL fibrous materials for prolonged drug delivery applications. Both release behaviors (immediate vs. prolonged) are crucial for different applications and will be further explored in Chapters 3.5 and 3.6, where the potential of these two systems for sublingual drug delivery and cancer treatment will be evaluated.

2.5 Coatings for controlled drug delivery

Hyaluronic acid (HA) offers significant advantages in drug delivery due to its bioactivity, biocompatibility, and ability to create a hydrophilic environment. As a surface coating on drug carriers, HA enhances drug release profiles and therapeutic efficacy. The molecular weight of HA plays a crucial role in modulating release kinetics, with higher molecular weight HA slowing drug diffusion and lower molecular weight HA facilitating faster release, allowing for tailored drug delivery and optimized therapeutic outcomes. While HA-coated nanoparticles were extensively studied for controlling drug release [70-72], research on HA coatings applied to electrospun PCL fibrous materials was limited, and none had investigated drug release modelling in this context. *Lubasová et al.* [65] (Appendix 8) addressed this gap by examining HA-coated, PTX-loaded electrospun PCL fibrous materials to modulate PTX release. Furthermore, the release profile of PTX from HA-coated electrospun PCL carriers was analyzed using the Hixson-Crowell and Higuchi models, providing valuable insights into the relative contributions of diffusion, erosion, and degradation in PTX release behavior. HA-coated PCL fibrous material were produced by first soaking them in the PTX solution, followed by immersion in the HA (1 wt.% in 0.1 M NaOH) for 1 minute. These HA coated carriers were then dried in oven at 30°C for 24 hours. Coating PTX-loaded electrospun PCL fibrous material with HA led to changes in both morphology and release profiles, as shown in Figure 24. (A). The HA coating formed a continuous film on the fiber surface, increasing the average fiber diameter across three batches from 141 ± 28 nm to 535 ± 115 nm. This result confirms the uniform deposition of HA and highlights the consistency of the fibrous material's morphology. Statistical analysis via ANOVA revealed significant differences in release profiles between HA-coated and uncoated PCL fibrous material, Figure 24. (B).

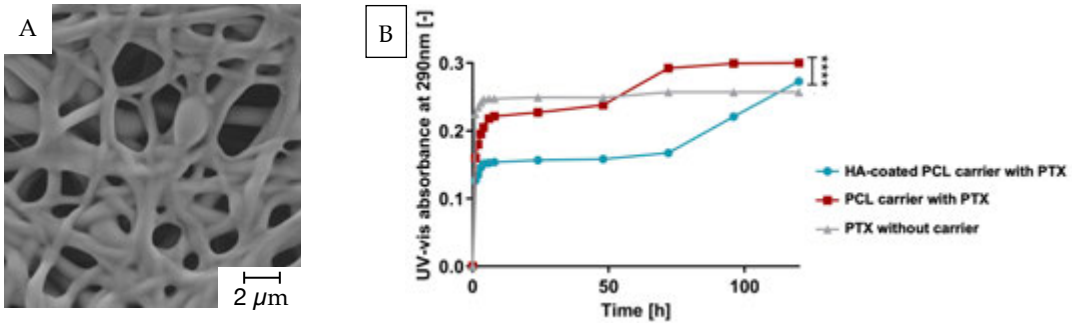

Figure 24. (A) SEM image of detailed fiber structure of HA-coated PTX-loaded electrospun PCL fibrous material. (B) PTX release kinetics from HA-coated and uncoated electrospun PCL fibrous material [65].

The uncoated PCL fibrous material exhibited a rapid initial release, followed by a faster increase after 48 hours, suggesting a diffusion-controlled release. In contrast, the HA-coated PCL material exhibited a sustained release profile for the first three days, followed by a marked increase at 72 hours, which continued up to 120 hours. This prolonged PTX release supports the

hypothesis that HA enhances drug retention, effectively modulating the release kinetics. Additionally, the release profile of PTX from HA-coated electrospun PCL fibrous material was analyzed using the Hixson-Crowell [73] and Higuchi models [74]. Higuchi model, based on Fickian diffusion, assumes that drug release occurs through diffusion from the matrix into the surrounding medium. In contrast, the Hixson-Crowell model is particularly useful for systems where release is governed by matrix erosion or disintegration, assuming that the decreasing surface area available for release controls the process. The Hixson-Crowell model ($R^2 = 0.85$) indicated that HA degradation played a key role in PTX release, with rate constant ($k = 0.001$) reflecting the progressive breakdown of the HA coating, enabling sustained release. Meanwhile, the Higuchi model ($R^2 = 0.74$) suggested that as the HA coating degraded, diffusion became increasingly dominant, supported by a rate constant ($k = 2.9$).
These findings suggest a two-stage PTX release mechanism form HA-coated PCL fibrous material: (i) an initial phase driven primarily by HA degradation and (ii) a later phase dominated by diffusion. The potential of this modified electrospun fibrous material, particularly in cancer treatment, will be further discussed in Chapter 3.6.

2.6 Summary

Modifications of electrospun fibrous materials often face challenges such as nanoparticle aggregation, poor drug retention, low productivity, and inconsistent modification across electrospun materials. Previous chapters explored various strategies to overcome these challenges by optimizing both pre- and post-electrospinning approaches. This habilitation thesis summarizes novel, scalable approaches to modifying needle-less electrospun materials, enhancing therapeutic efficacy and processability, while addressing key challenges in antibacterial properties, bioactivity, and controlled drug release.
A major breakthrough was the development of a novel, single-step method for producing needle-less electrospun porous fibers, overcoming the limitations of traditional multi-step techniques. This method leveraged HSP to precisely control fiber porosity using solvent/non-solvent systems with high evaporation rate differences. Needle-less electrospun porous PVB and PCL fibers exhibited pore volumes ranging from 1.3×10^{-4} to 2.9×10^{-4} cm^3/g. Furthermore, a predictive model integrating HSP, permittivity, and vapor pressure was proposed to streamline solvent selection, reducing experimental trials required for electrospinning of new polymers. Significant advancements was further made in improving NPs distribution within needle-less electrospun fibrous materials by employing Triton X-100, a surfactant that enhanced NP dispersion. By overcoming the challenges of uneven NP distribution and poor dispersion, the incorporation of CuO, ZnO, and ZnO/TiO_2 into electrospun PVB fibrous materials led to the development of materials with enhanced antibacterial activity, effectively eliminating *Escherichia coli* within one hour. A significant improvement was achieved through the surface immobilization of TET, ensuring controlled antibiotic retention. Compared to internal antibiotic incorporation, which is costly, inefficient, and lacks adaptability, this method allowed precise adjustment of antibiotic concentrations in needle-less electrospun CS/PEO/PCL fibrous materials, maintaining 30% TET retention after ethanol washing. Moreover, a systematic evaluation of drug absorption and release from electrospun materials with varying hydrophilicity revealed that wettability, rather than polymer type, primarily governed drug release kinetics. Hydrophilic fibrous materials (CS/PEO, SF) facilitated rapid release of PLGA-PEG nanoparticles (within 30 minutes) and liposomes, while hydrophobic PCL fibrous material exhibited more sustained PTX release (up to 72 hours). Coating PTX-loaded electrospun PCL fibers with HA further optimized drug release kinetics, as HA formed a continuous film on individual fibers, stabilizing PTX release over three days before a marked increase in release extending up to 120 hours. Mathematical modeling provided further insights into the release mechanisms, with the Hixson-Crowell model indicating that HA degradation controlled PTX

release, while the Higuchi model suggested that diffusion became the dominant mechanism over time, ensuring prolonged therapeutic action.
These findings position modifications of needle-less electrospun fibrous materials as a robust platform for tailoring porosity, antimicrobial efficacy, and controlled drug release, thereby notably expanding their biomedical potential. By integrating nanoparticle incorporation, solvent system optimization, and surface functionalization, the author's research presented in this thesis offers a versatile approach to enhancing the clinical applicability of electrospun fibrous materials. These advancements not only demonstrate the feasibility of industrial-scale production but also pave the way for the future development of personalized therapeutic systems and next-generation wound healing materials, as further discussed in Chapter 3.

3 Biomedical potential of electrospun fibrous materials

This chapter delves into the biomedical potential of electrospun fibrous materials, emphasizing recent advancements, ongoing challenges, and their broad applicability in the medical field. Electrospun fibrous materials offer significant promise due to their high surface area-to-volume ratio, and ability to mimic the extracellular matrix, making them ideal for diverse biomedical applications. Despite these advantages, significant challenges remain, particularly in scaling up production while maintaining consistent fiber quality [75-77]. Advances in needle-less electrospinning have successfully addressed scalability challenges, enabling large-scale production without compromising material quality or functionality. This transition from laboratory-scale research to industrial-scale production is pivotal for the clinical adoption of electrospun materials. However, the diverse requirements of biomedical applications make the design of universally adaptable fibrous material impractical and tailored solutions with optimized material properties for specific applications are still a challenge.
The development of plant protein-based electrospun fibrous materials for bacterial filtration, alongside innovations in customizable wound care, localized cancer treatment carriers, and mucoadhesive patches for sublingual drug delivery, demonstrates the significant versatility and clinical relevance of such materials. Moreover, tailored approaches designed to meet specific biomedical demands, along with further investigations into the effectiveness of these materials in animal models, cell cultures, and bacterial studies, are essential. The following sub-chapters address the biomedical potential of needle-less electrospun and modified fibrous materials with a specific focus on the author of this thesis scientific contributions.

3.1 Filters for bacterial filtration

Electrospun fibrous materials are highly effective in filtration applications due to their high surface area and porosity, which enable efficient particle capture. The incorporation of proteins such as soy protein further enhances their performance by introducing electrostatic interactions. Soy protein, composed of both basic (lysine, arginine, histidine) and acidic (glutamate, aspartate) amino acids, can acquire charges under different pH conditions. This property facilitates electrostatic attraction of airborne particles [86]. While electrostatic interactions in particle filtration were well-documented, the potential of protein-based electrospun fibrous materials for bacterial filtration had not been thoroughly investigated. To address this gap, the author of this thesis, during her postdoctoral research stay at Cornel University as part of a project for Axium Nanofibers, investigated whether electrospun fibrous materials made of soy protein could enhance bacterial filtration efficiency (BFE) through surface charge effect, as detailed in *Lubasová et al.* [22] (Appendix 3). Recognizing the limitations of traditional antibacterial assessment methods, such as the agar diffusion test—which provides only qualitative evaluations of bacterial growth inhibition—a laboratory apparatus was designed and constructed to quantitatively assess BFE. This system simulates airborne bacterial exposure by generating bacterial aerosols using a nebulizer to produce particles ranging from 0.3 to 5 microns—sizes representative of many airborne microorganisms. The aerosol is directed

through a chamber containing the fibrous filter, with suction equipment facilitating airflow. Aerosolized bacteria that penetrate the filter are captured on an agar plate positioned beneath it, enabling quantitative BFE measurements after incubation. This innovative system, illustrated schematically and photographically in Figure 25, provides precise and reliable BFE measurements. Following the postdoctoral research, the author of this thesis contributed to the design and validation of a larger operational facility for BFE testing within the antibacterial laboratory at the Technical University of Liberec, where she served as research leader. This facility now supports both research projects and commercial applications, significantly advancing filtration technologies, particularly for respiratory protective equipment and hospital air-conditioning systems.

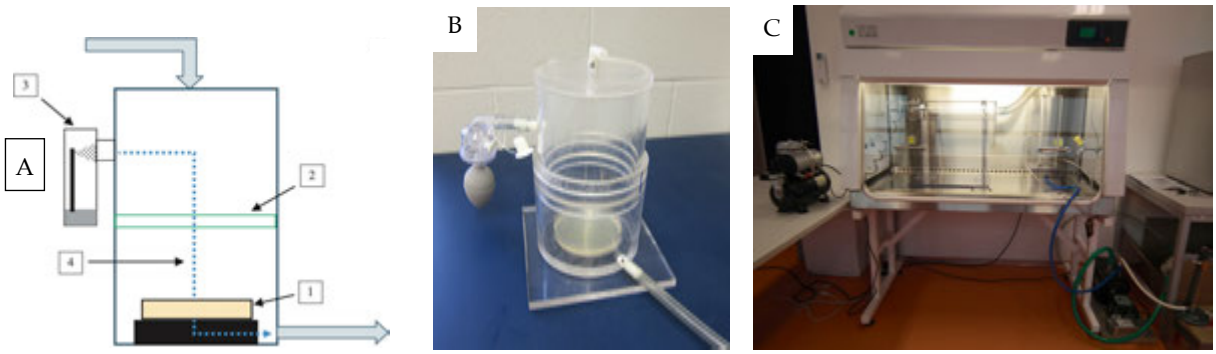

Figure 25. (A) A schematic and (B) photographic representation of BFE testing apparatus: 1 - an agar plate, 2-testing filter, 3 - nebulizer, 4 - aerosolized bacteria [22]. (C) Operational facility for testing BFE.

Following the construction of the apparatus, the BFE of electrospun soy protein-based fibrous materials (Chapter 1.2) was evaluated, achieving 97.7% for soy flour/PEO and 99.6% for SPC/PEO. Remarkably, SPI/PEO, PSF/PEO, and HPSF/PEO electrospun fibrous materials exhibited nearly 100% BFE. The strong correlation between higher protein content in electrospun fibrous materials and BFE underscores the crucial role of protein in improving filtration performance (Figure 26. (C)). These findings demonstrated the outstanding filtration capabilities of soy protein-based electrospun fibrous materials, significantly outperforming electrospun PEO-only materials and the commercial Energy Aire® filter, which lacks electrospun fibers and achieves an average BFE of only 20.8%. Additionally, SEM analysis (Figure 26. (A-B)) revealed the bio-adhesive properties of soy protein-based fibrous materials, which enable them to trap bacteria effectively even when fibrous material pore sizes exceed size of microorganisms such as *Escherichia coli*. This enhanced adhesion likely contributes to improved filtration performance while maintaining excellent breathability.

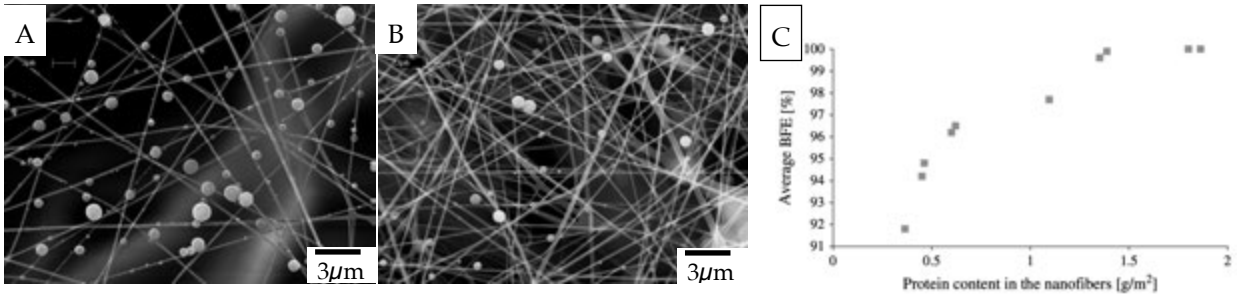

Figure 26. SEM of bacteria Escherichia coli on electrospun PSF/PEO [7/3] fibrous material after filtration with gram-per-square-meter fibers: (A) 1 g/m² and (B) 5 g/m². (C) The efficiency of the protein content on BFE of the filter [22].

Beyond their exceptional filtration performance, protein-based electrospun fibrous materials offer a significant sustainability advantage due to their compostability, thereby reducing landfill waste and contributing to environmental sustainability. In contrast to conventional antibacterial filters, which typically incorporate TiO_2, nano-silver, or other antimicrobial agents—many of

which raise environmental concerns due to their persistence and potential toxicity [87–89]—this approach demonstrates that as little as 3 g/m² of protein-based electrospun fibrous material can achieve nearly 100% BFE. Unlike filters with incorporated nanoparticles, which often involve high material costs and regulatory challenges, this study leverages the intrinsic bacterial capture capabilities of protein-based fibrous structures, eliminating the need for additional chemical agents. As a result, these materials present a cost-effective and environmentally friendly alternative for high-performance filtration. Furthermore, this research highlights the potential of electrospun soy protein-based fibrous materials to enhance filtration efficiency while maintaining breathability, a critical factor in applications such as respiratory protective equipment. These advancements contribute to the development of next-generation sustainable filtration technologies, particularly in healthcare settings where infection control and environmental impact must be carefully balanced.

3.2 Antibacterial composite yarn

To evaluate the potential of needle-less electrospun materials with incorporated NPs for antibacterial textiles, the following research focused on fabricating antibacterial composite yarns coated with electrospun fibers. While previous studies have explored nanofibrous materials incorporating NPs, most have been limited to laboratory-scale experiments [78-80]. Additionally, industrial methods for producing antibacterial textiles, such as melt-blowing, centrifugal spinning, and island-in-the-sea splitting, face challenges including large fiber diameters, broad diameter distributions, and difficulties in fiber separation [81-83]. To address these limitations, the study [84] (Appendix 9) focused on the design and characterization of composite yarns coated with electrospun PVB and polyurethane (PU) fibers containing CuO nanoparticles. The fabrication process involved dissolving PU in DMF and PVB in acetic acid before adding CuO and Triton X-100. A textured polyester base yarn (dtex 167f 36 ×1 ×3) served as the collector in the needle-less electrospinning system. The yarn speed was set to 134 m/min to ensure a uniform nanofiber coating, and a polyamide filament was added to enhance mechanical durability (Figure 27).

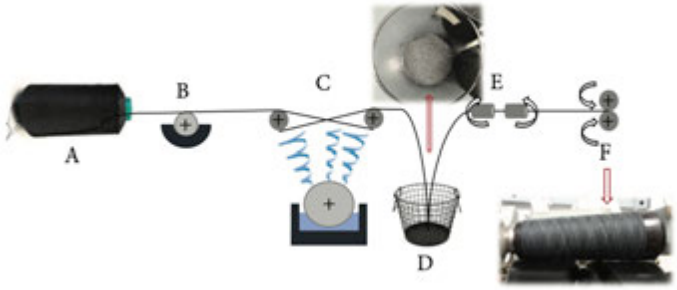

Figure 27. Schematic diagram of a continuous production device: (A) black core yarn, (B) application of a conductive solution, (C) needle-less electrospinning, (D) collector, (E) application of protective yarn, and (F) take-up mechanism [84].

The antibacterial efficacy of the yarns (Figure 28. (B-C)) was tested against *Escherichia coli* and *Staphylococcus gallinarum* using ASTM E2149-01 and a modified AATCC 100-2004 method. Results showed that yarns covered with PVB-CuO electrospun fibers exhibited significantly higher antibacterial efficiency than those covered with PU-CuO (Figure 28. (A)). This increased performance can be attributed to the reaction between CuO and acetic acid, forming copper acetate, which enhances antibacterial activity against both Gram-positive and Gram-negative bacteria. At a 5% CuO concentration, electrospun PVB-CuO fiber-coated yarn achieved 99.99% antibacterial efficiency against *Escherichia coli*, eliminating over 50% of bacteria upon initial contact and achieving complete inhibition within 1 hour. Moreover, the study demonstrated that composite yarn can be plain woven (VÚTS a.s.) into fabric (Figure 28. (D)), confirming its versatility and effectiveness, as described in study [85]. Antimicrobial activity, assessed using

ASTM E2149-01 at 1 min, 1 h, 2 h, 3 h, and 4 h, showed that fabric containing PVB with 10% CuO NPs exhibited strong antibacterial properties, with 60% bacterial reduction immediately and near 100% inhibition after 50 minutes of contact with *Escherichia coli*.

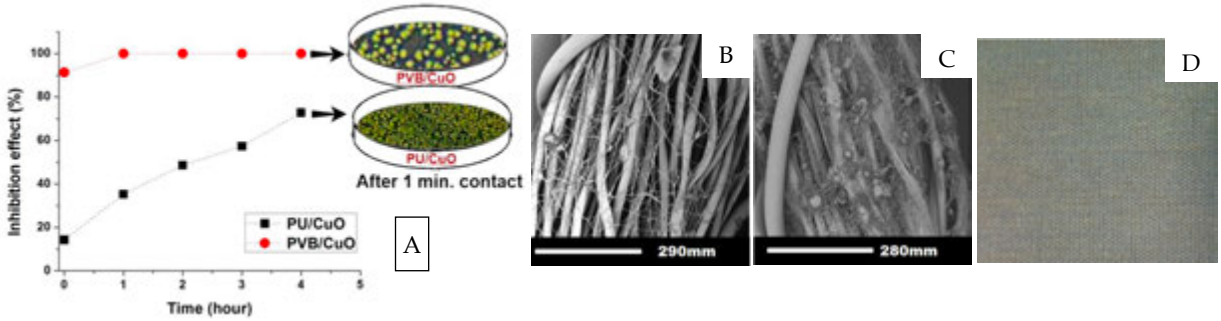

Figure 28. (A) Antibacterial efficiency of electrospun PVB-CuO and PU-CuO fibres covered yarn. SEM images of yarns covered by electrospun fibers made of: (B) PU/CuO, and (C) PVB/CuO [84]. (D) Woven fabric with electrospun fiber-covered yarn [85].

These findings underscore the potential of electrospun PVB-CuO fiber-coated yarn as a promising antibacterial material, offering a strong antibacterial performance even at low CuO concentrations, making it suitable for protective textiles.

3.3 Scaffold supporting cells growth

The morphology of electrospun fibers is crucial in tissue engineering, as it significantly impacts cell adhesion, proliferation, and overall scaffold functionality. While much attention had been given to the general properties of electrospun scaffolds, no study specifically compared the effects of porous and non-porous electrospun fibers on hepatocyte behavior. To explore this, *Lubasová et al.* [53] focused on exploring this under-investigated aspect of scaffold design. This study, conducted in collaboration with the Institute of Experimental Medicine at the Academy of Sciences of the Czech Republic, assessed the potential of electrospun PCL fibrous scaffolds for liver tissue engineering applications. To evaluate hepatocyte adhesion and proliferation, liver cells isolated from male Wistar rats were cultured on sterilized electrospun PCL fibrous materials consisting of both porous and non-porous fibers (Chapter 2.2). Immunohistochemical staining using phalloidin and 4′,6-diamidino-2-phenylindole (DAPI) provided insights into cell morphology, cytoskeletal organization, and attachment patterns over six days. The result demonstrated that porous electrospun PCL fibers significantly enhanced hepatocyte adhesion and proliferation compared to non-porous fibers. This improvement is likely due to porous surface area, enhanced permeability, and biomimetic architecture of the porous fibers (Figure 29. (A-C)).

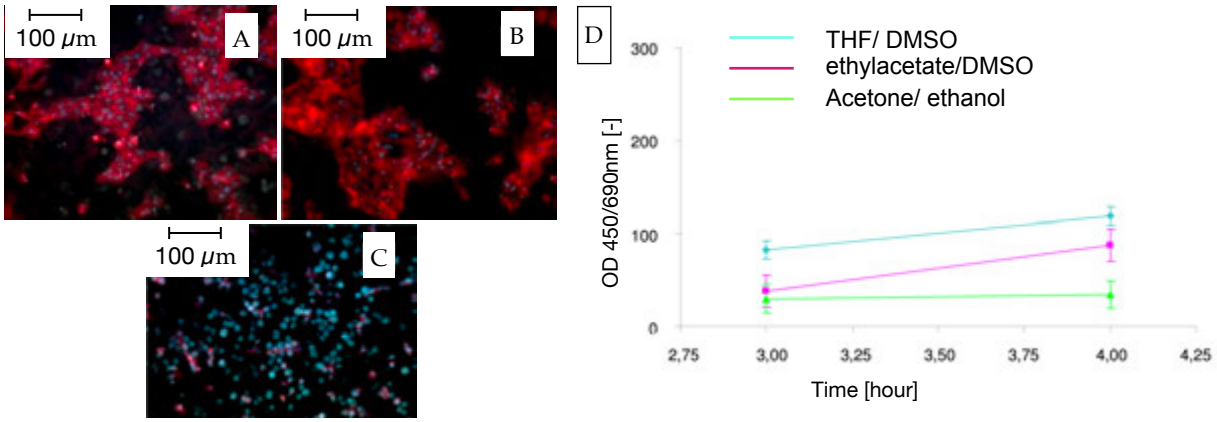

Figure 29. Hepatocytes stained with phalloidin (red) and DAPI (blue) on electrospun PCL fibers after 3 days made of polymer solution containing: (A) THF/ DMSO (9/1 v/v), (B) ethylacetate/ DMSO (9/1 v/v), (C) acetone/ ethanol (7/3 v/v). (D) Cell proliferation assay of hepatocytes on PCL fibrous materials after 6 days [53].

Moreover, cell viability was assessed using WST-1 assay, a colorimetric method based on the cleavage of tetrazolium salt into soluble formazan dye by the succinate-tetrazolium reductase system within the number of mitochondrial respiratory chain. Since formazan dye formation correlates directly with the number of metabolically active cells, this assay allowed for precise evaluation of scaffold biocompatibility. The results revealed that hepatocytes on porous PCL fibers exhibited higher metabolic activity and proliferation rates than those on non-porous fibers (Figure 29. (D)). This superior performance suggest that porous fibers more effectively mimic the extracellular matrix, enhance nutrient diffusion, and promote cellular interactions.
These findings underscore the critical role of fiber porosity in scaffold design for hepatic tissue engineering. By creating more supportive microenvironment for hepatocytes, porous electrospun PCL scaffolds hold promise for bioreactor systems, *in vitro* drug metabolism studies, and bio-artificial liver support devices.

3.4 Customizable wound dressing

Electrospun fibrous materials offer significant advantages for wound dressings due to their high surface area, porosity, and extracellular matrix-mimicking properties, which promote cell adhesion, nutrient transport, and moisture retention—key factors in wound healing. However, challenges remain in controlling drug release, optimizing breathability, enhancing surface activity, tailoring materials for different wound types, and achieving scalable production with consistent quality [90]. To address these challenges, needle-less electrospun fibrous materials composed of CS/PEO/PCL in various ratios were fabricated (Chapter 1.2), enabling tunable hydrolytic degradation, hydrophilicity, mechanical strength and elasticity. Additionally, post-surface immobilization of TET (Chapter 2.3) enhances antibacterial stability with adjustable TET concentrations, providing greater control over therapeutic efficacy. One of the critical properties of electrospun fibrous materials is their porous structure, which directly influences moisture management in wound environments. The moisture vapor transmission rate (MVTR) serves as a vital parameter for assessing wound dressings performance. Research suggests that MVTR values below 1000 g/m²/day may lead to excessive moisture retention, increasing the risk of exudate accumulation and bacterial growth, while values above 2000 g/m²/day are optimal for highly exuding wounds, ensuring proper moisture balance without excessive dehydration [91].
To evaluate the suitability of PEO/PCL/CS fibrous materials for wound care, MVTR and cytotoxicity assessments were conducted, as described in *Lubasová et al.* [31] (Appendix 5). These tests provided valuable insights into the suitability of these materials for various wound types. MVTR of electrospun fibrous materials was measured following the EN 13726-2:2002 standard for vapor-permeable dressings, with measurements taken over seven days. Initially, the MVTR of electrospun fibrous materials was comparable to commercial polypropylene/viscose-based dressings. However, after seven days, electrospun materials transmitted 55–63% moisture, compared to only 13% for the commercial dressing (Figure 30). This indicates superior moisture permeability of electrospun fibrous materials, whereas the commercial dressing retains moisture, potentially creating an over hydrated environment that may hinder healing.

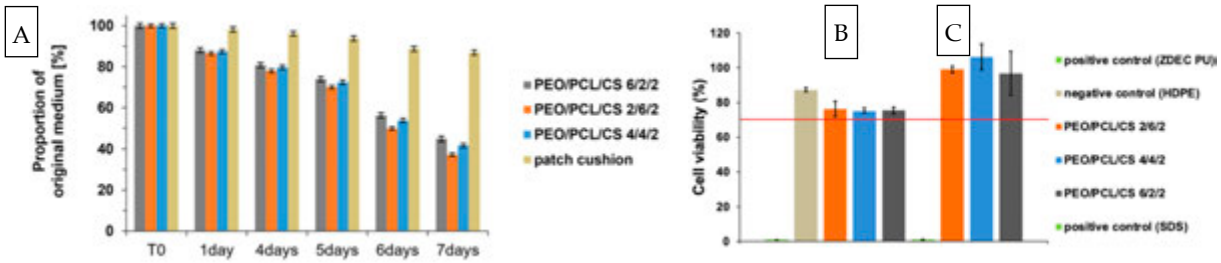

Figure 30. (A) Monitoring of moisture vapor leakage from the Paddington cup system through fibrous materials composed of PEO/PCL/CS with different mass ratios, and a commercially available patch cushion. (B) In vitro cytotoxicity assessed by the MTT assay of 3T3 cells seeded in: (B) direct and (C) indirect contact with electrospun PEO/PCL/CS fibrous materials after 1 day of culture [31].

The MVTR of PEO/PCL/CS electrospun fibrous materials ranged from 1904.3 ±28.6 to 2005.7 ± 42.9 g/m²/day, confirming their suitability for wound care applications. Cytotoxicity tests on 3T3 fibroblasts further validated their biocompatibility (Figure 30. (B-C)), with cell viability exceeding the 70% threshold recommended by ISO 10993-5 [92]. MTT assay results demonstrated high fibroblast survival, supporting the potential of these fibrous materials for wound healing.

These findings demonstrate that the developed materials offer tunable hydrolytic degradation, mechanical strength, and hydrophilicity—where PCL-rich fibrous materials provide durability suitable for acute wounds, while PEO-rich materials enhance hydrophilicity for chronic wound applications. Unlike previous studies [93,94], which reported weak mechanical strength, poor vapor permeability, use of toxic solvents, and limited scaleability, the PEO/PCL/CS fibrous materials ensure superior moisture control, enhanced antibacterial properties, and customizable degradation rates. Crucially, they are fabricated via needle-less electrospinning, enabling industrial scalability. Additionally, post-fabrication TET immobilization further improves antibacterial efficacy, allowing tailored wound care. This study introduces a versatile strategy for needle-less electrospun PEO/PCL/CS materials, advancing personalized wound dressings with optimized moisture management, mechanical adaptability, and antibacterial functionality.

3.5 Mucoadhesive patches for sublingual drug delivery

Mucoadhesion, defined as the interaction between biomaterials and mucosal surfaces, has emerged as a key strategy for enhancing non-invasive drug and vaccine delivery. The book chapter *Nanofibers in the Mucosal Administration of Drugs and Vaccines* [95] provides a comprehensive analysis of mucoadhesive systems, emphasizing their potential for optimizing therapeutic outcomes via oral, nasal, and vaginal routes. It systematically addresses critical factors influencing mucoadhesion, including mucosal histology, barrier properties, and the fundamental principles of transmucosal drug and vaccine delivery. Mucosal administration offers distinct advantages over conventional delivery methods, such as reduced reliance on syringes, elimination of sterility concerns, and improved patient compliance. Additionally, mucosal vaccination presents a cost-effective alternative by simplifying logistics and reducing sterility requirements, thereby facilitating large-scale distribution. However, challenges remain, including antigen variability, limited therapeutic absorption, and enzymatic degradation in the gastrointestinal tract. Addressing these obstacles necessitates the development of advanced delivery platforms, such as intranasal sprays and oral capsules. Among these, sublingual vaccine delivery has gained prominence due to its ability to achieve direct systemic absorption via the highly vascularized sublingual mucosa. By bypassing the gastrointestinal tract and first-pass hepatic metabolism, this route enhances bioavailability and ensures a rapid onset of action. Its non-invasive nature is particularly beneficial for paediatric and geriatric populations, as well as individuals with dysphagia or needle phobia. The sections of the book chapter [95], authored by *Lubasová*, explore the potential of electrospun fibrous materials in mucosal drug delivery, detailing their advantages, preparation, and characterization. Electrospun fibrous materials present a promising approach in sublingual drug administration due to their exceptionally high surface area, unique surface topology, and high porosity—key factors that enhance mucoadhesion. Their architecture enables prolonged and intimate contact with the mucosal surface, ensuring a high local drug concentration at the site of administration (Figure 31). This positions electrospun fibrous materials as a highly effective platform for mucosal drug delivery, marking a significant advancement in the field.

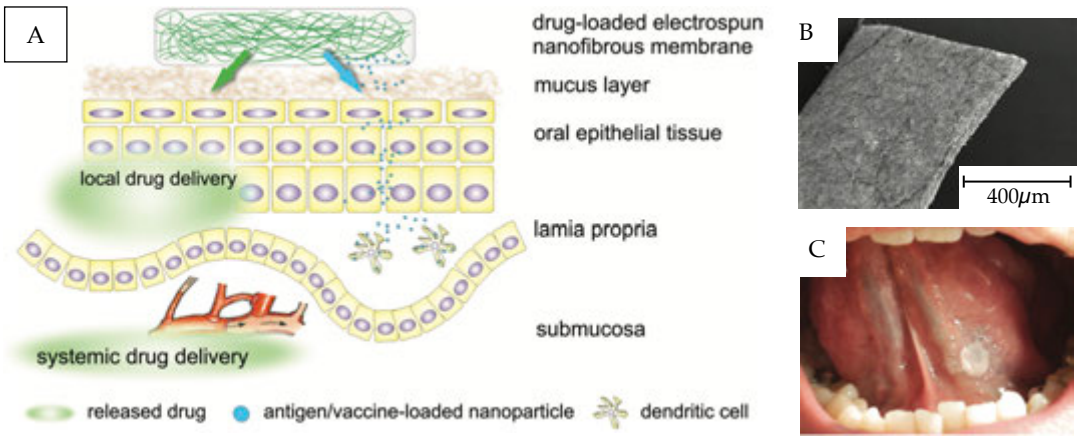

Figure 31. (A) Schematic of drug and vaccine delivery via electrospun fibrous material-based system after mucosal administration. (B) SEM image of fibrous layer produced by needle-less electrospinning. (C) Application of a mucoadhesive patch with an electrospun fibrous layer to the sublingual mucosa [95].

Building on these advantages, and as part of a collaborative effort with the Veterinary Research Institute in Brno, the author of this thesis contributed to the design, fabrication, and evaluation of an innovative electrospun mucoadhesive fiber-based patch for sublingual vaccine delivery, as detailed in [64] (Appendix 7). This multi-layered system, optimized for adhesion, integrity, and sustained release, overcoming key challenges in mucosal drug delivery. It consists of three distinct layers: (i) an electrospun fibrous reservoir layer, (ii) a mucoadhesive layer, and (iii) a protective backing layer (Figure 32).

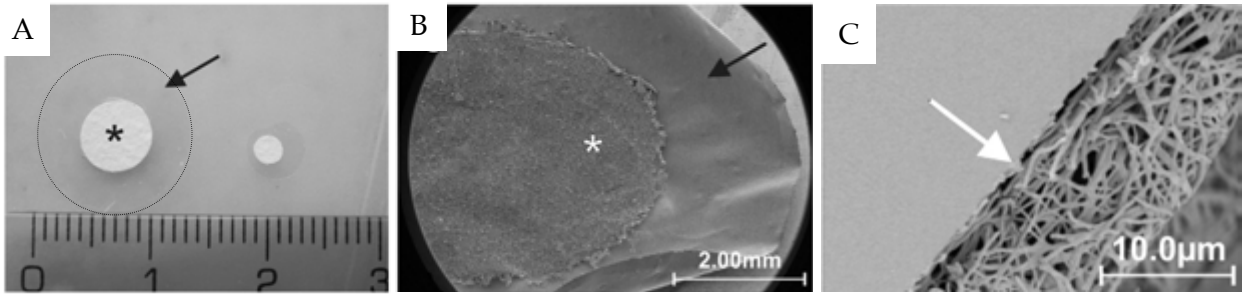

Figure 32. Mucoadhesive patch: (A) photograph showing patches for large (pig) and small (mouse) animal experiments, (B) SEM images of individual layers, with the electrospun fibrous reservoir layer (*) and mucoadhesive layer (arrow), (C) cross-sectional view highlighting the interface (arrow) between the mucoadhesive and reservoir layers [64].

The reservoir layer, fabricated via needle-less electrospinning using polymers such as CS/PEO, or SF (Chapters 1.2, and 2.4), serves as a depot for nanoparticles that are either surface-adsorbed or embedded within its porous matrix. The mucoadhesive layer ensures prolonged adhesion at the application site, while the backing layer prevents premature drug diffusion and minimizes interference form saliva and mucosal secretions. This structural optimization enhances the practical application of sublingual patches, ensuring controlled drug release and improved bioavailability. Preclinical evaluations in animal models demonstrated the adhesive efficacy and biocompatibility of the mucoadhesive patches. In mice models, the patches maintained adherence to the sublingual mucosa for at least two hours without inducing local irritation (Figure 33). The flexible nature of the electrospun patch facilitated optimal contact with the mucosal surface, preventing premature detachment or clearance by salivary flow.

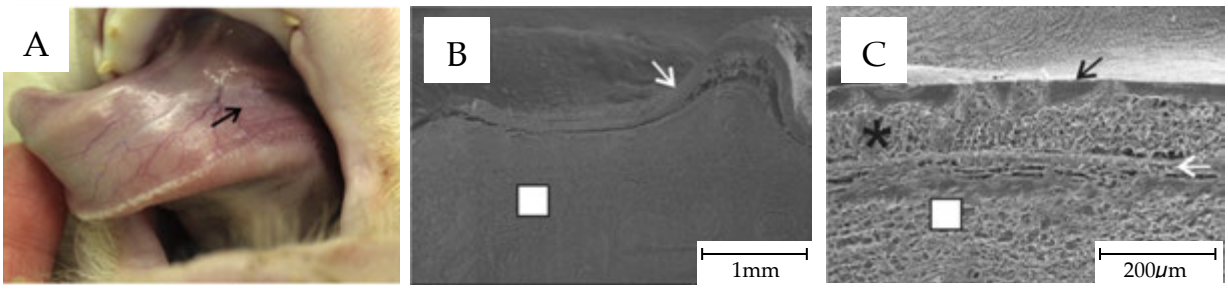

Figure 33. Tight adhesion of the mucoadhesive patch to mouse sublingual mucosa: (A) photograph showing the patch (black arrow) 2 hours post-application. (B, C) Cryo-SEM images of adhesion, with (B) showing attachment and (C) a detailed view (electrospun layer, □ mucosal surface, → a protective backing layer) [64].*

Given the anatomical and physiological differences between mice and human sublingual mucosa, piglet models were utilized for translational studies. Before application, the PLGA-PEG nanoparticle dispersion was uniformly absorbed throughout the electrospun fibrous layer via capillary action (Chapter 2.4). Histological analysis of excised tissue samples, collected two hours post-application, confirmed PLGA-PEG nanoparticle penetration through the mucosa and subsequent transport to regional lymph nodes (Figure 34). These findings align with the antigen and nanoparticle transport mechanisms described by Dukhin and Labib [96], where passive diffusion across the mucus layer, epithelium, and submucosa is followed by convective transport through lymphatic capillaries. The passive diffusion mechanism of the first three steps, combined with convective diffusion through lymphatic pathways, accounts for the rapid appearance of nanoparticles in lymph nodes after 2 hours of mucosal administration. The high adsorption capacity of electrospun fibrous layers enhances this transport by ensuring rapid release and creating a concentration gradient that facilitates effective diffusion into the submucosa.

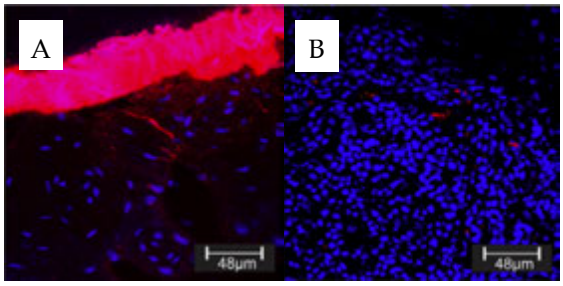

Figure 34. Lymph node delivery of PLGA-PEG nanoparticle applied onto sublingual mucosa via mucoadhesive patch: (A) cross-section of porcine sublingual mucosa after 2h in vivo incubation, showing nanoparticle penetration, (B) nanoparticles in a regional lymph node (red dots: PLGA-PEG nanoparticles, red layer: PLGA-PEG loaded mucoadhesive patch, blue: epithelial cell nuclei) [64].

The research confirmed that electrospun mucoadhesive patches represents a significant advancement in controlled nanoparticle delivery, enabling fast drug release, targeted deposition in submucosal tissues, and efficient transport to draining lymph nodes. Unlike conventional mucoadhesive films, where swelling can hinder nanoparticle diffusion [97], this approach leverages an electrospun reservoir layer to ensure controlled release, independent of the swelling properties of the mucoadhesive film. The patch design minimizes premature clearance while maintaining a stable nanoparticle concentration gradient at the mucosal surface., ensuring prolonged retention and enhanced bioavailability. A key advantages of these patches is their superior flexibility and adhesion, effectively addressing challenges associated with tongue movement and saliva production. These mechanical factors are particularly pronounced in the sublingual region, where conventional mucoadhesive films often struggle to maintain stability. *Ex vivo* and *in vivo* studies in porcine models confirmed the effectiveness of electrospun patches for delivering PLGA-PEG and liposomal nanoparticles, showcasing prolonged retention times and enhanced drug absorption. The innovative nature of this technology is further underscored

by its protection through domestic and international patents granted [98, 99], and its recognition with the *2018 Novartis Discovery Award*. Ongoing research efforts are focused on optimizing industrial-scale production and integrating printed vaccine technologies with electrospun fibrous materials to enhance manufacturing feasibility. This study, currently under preparation for submission to *Advanced Healthcare Materials*, highlights the growing relevance of electrospun mucoadhesive platforms in modern therapeutic delivery, offering a scalable and effective strategy for mucosal drug administration.

Beyond vaccine applications, electrospun mucoadhesive patches hold significant potential for allergen immunotherapy, particularly in sublingual immunotherapy (SLIT). Conventional SLIT protocols require daily administration over 3–5 years, leading to poor patient adherence, with over 70% of patients discontinuing treatment within the first year [100]. To address this challenge, the author of this thesis contributed to the development and evaluation of an electrospun mucoadhesive patch for allergen delivery in collaboration with the Veterinary Research Institute in Brno, as detailed in study [101]. This platform integrates allergens, such as ovalbumin (OVA), co-formulated with tolerogenic bacterial particles (TBPs) within a mucoadhesive patch to enhance immune tolerance and mitigate hypersensitivity responses. A pig model was chosen due to its physiological similarities to humans, particularly in oral mucosa and immune response. The experimental protocol involved an initial sensitization phase, followed by desensitization starting on day 55, during which piglets received five weekly sublingual treatments using two mucoadhesive patches per administration (Figure 35. (A)). To asses therapeutic efficacy, intradermal tests for immediate allergic reactions to OVA were performed before (day 48) and after treatment (day 95), with flare wheal size serving as an indicator of allergic response. The results demonstrated a substantial reduction in allergic reactivity, with 45% of the OVA + TBP-treated group (Group 2) achieving complete desensitization, compared to only 8% in the OVA-alone group (Group 1), underscoring the strong synergistic effect of TBPs (Figure 35. (B)). The treatment was well tolerated, with no signs of local irritation at the application site.

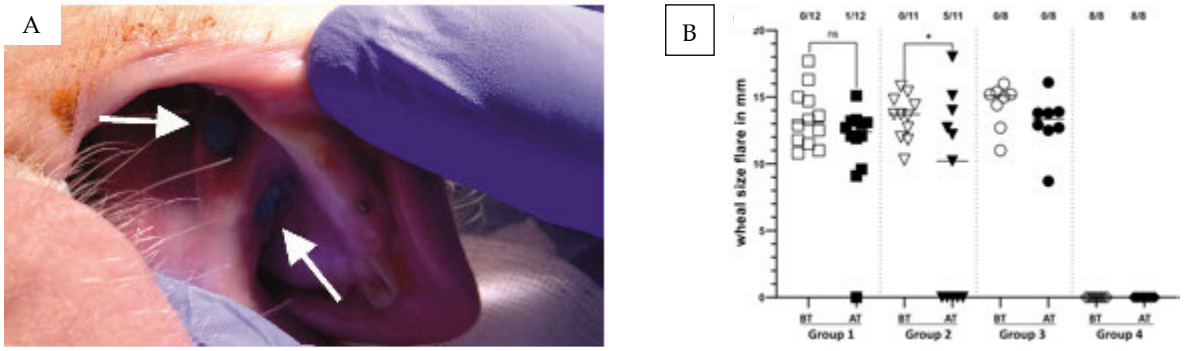

Figure 35. (A) Placement of mucoadhesive patches on pig sublingual mucosa (indicated by white arrows). (B) Intradermal test results for immediate allergic reactions to OVA, measured as flare wheal size (mm) at the injection site. Group 1: OVA- only patches (n=12), Group 2: OVA+TBP patches (n=11), Group 3: PBS- infused patches (control), Group 4: non- sensitized (negative control) [101].

This approach suggests that combining mucoadhesive patches with tolerogenic particles could simplify SLIT method by (i) reducing the number of required doses, (ii) achieving effective desensitization with fewer sessions, and (iii) enabling the use of smaller allergen doses compared to conventional SLIT, which often requires milligram-range doses. These findings underscore the potential of mucoadhesive patches combined with tolerogenic particles to enhance allergen presentation and prolong exposure, offering a safer, more effective, and patient-friendly alternative for allergy treatment. This approach not only improves patient adherence and therapeutic outcomes but also addresses the critical need for next-generation SLIT strategies. The results further validate electrospun mucoadhesive patches as a promising platform for allergen immunotherapy.

3.6 Carriers for localized cancer therapy

Localized chemotherapeutic delivery systems offer a promising alternative to systemic chemotherapy, addressing critical limitations such as severe side effects, rapid drug clearance, and poor tumor penetration [102]. However, pancreatic tumors presents additional challenges due to their dense stromal microenvironment, which significantly impedes efficient drug diffusion. To overcome these barriers, the author of this thesis developed an HA-coated PTX-loaded electrospun PCL carrier designed for enhance tumor-specific targeting, as detailed in study [65] (Appendix 8). Previous studies have established that HA selectively binds to CD44 receptors, which are over-expressed on pancreatic cancer cells, thereby facilitating targeted drug accumulation and improved cellular uptake. This interaction is governed by a catch-bond mechanism, which strengthens under mechanical stress, enhancing drug retention at the tumor side [103]. Additionally, HA-coated nanoparticles loaded with chemotherapeutic agents such as gemcitabine or quercetin have demonstrated the ability to overcome chemoresistance while minimizing systemic toxicity [104, 105]. However, prior to this study, the potential of HA-coated electrospun PCL fibrous material as a localized drug delivery system for pancreatic cancer had not been investigated. As demonstrated in Chapter 2.5, HA plays a crucial role in regulating PTX release, preventing premature depletion, and ensuring sustained therapeutic exposure. The effectiveness of this carrier was further evaluate through an *in vitro* cytotoxicity assay following ISO 10993-5.40 standards, using MiaPaCa pancreatic cancer cells. The results confirmed the superior efficacy of HA-coated PTX-loaded PCL carrier compared to both uncoated carrier and free PTX. While free PTX moderately reduced MiaPaCa cell viability (from 58% to 40% over 96 hours), HA-coated PTX-loaded carrier significantly enhanced this effect, reducing cell viability from 44% at 72 hours to just 13% at 96 hours (Figure 36).

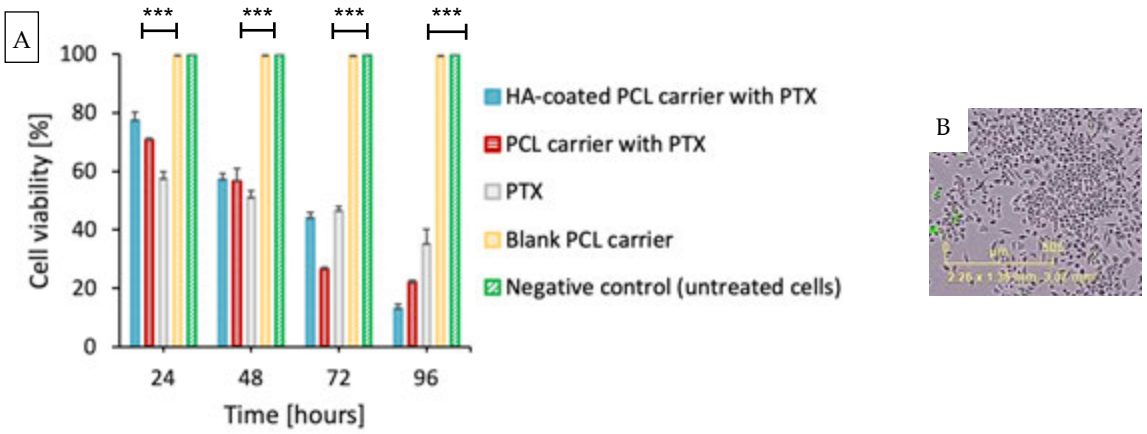

Figure 36. Cytotoxicity of PTX-loaded PCL fibrous carriers against MiaPaCa pancreatic cancer cell monolayers. (A) cell viability at varying exposure times, showing significant differences between HA-coated and uncoated PTX-loaded carriers, as well as in comparison to free PTX. (B) representative optical microscope image of the MiaPaCa cell monolayer [65].

These findings, achieved in collaboration with the University of Bergen and Haukeland University Hospital, highlight the pivotal role of HA in enabling selective tumor targeting and controlled drug release. While electrospun carriers had been extensively studied for various cancers, their application in pancreatic cancer therapy remained relatively underexplored. Previous studies have demonstrated that electrospun fibrous materials, such as gemcitabine-loaded core-shell fibers and PCL fibers encapsulating chemotherapeutic agents like 5-fluorouracil and methotrexate, can enable sustained drug release. However, challenges remain, including slow degradation rates, limited drug release, and scalability and reproducibility issues associated with conventional needle-based electrospinning [106, 107]. In contrast, HA-coated needle-less electrospun PCL carriers offer a more favorable degradation profile,

improved drug release kinetics, and enhanced scalability for industrial production. These advantages make them a promising platform for pancreatic cancer therapy. Looking ahead, the author of this thesis aims to conduct comprehensive *in vivo* studies to further investigate the pharmacokinetics, tumor penetration, and therapeutic efficacy of HA-coated electrospun PCL carriers. These studies will focus on evaluating tumor growth inhibition and recurrence prevention, while also proving the carrier's safety and effectiveness. Furthermore, advanced imaging techniques will be employed to monitor carrier distribution and assess their ability to maintain sustained drug concentrations at the tumor site. These investigations will provide critical insights necessary for bridging the gap between preclinical development and clinical application. Ultimately, this research reinforces the feasibility of a scalable and translational strategy for pancreatic cancer therapy, with the potential to significantly improve treatment outcomes.

3.7 Summary

Electrospun fibrous materials offer significant potential for a broad range of biomedical applications. However, challenges related to scalability and functional customization hinder their widespread clinical adoption. Previous chapters examined the potential of electrospun materials in bacterial filtration, wound healing, antibacterial textiles, and drug delivery systems, with a particular focus on overcoming these critical limitations. This habilitation thesis systematically evaluated innovative electrospun materials, including antibacterial fiber-coated yarns, bacterial filters, three-layer mucoadhesive patches, customizable wound dressings, and localized cancer treatment patches. The application of these materials in specific biomedical contexts demonstrated their potential to address existing constraints and advance clinical practice.

In the development of antibacterial textiles, PVB-CuO electrospun fiber-coated yarns were investigated as a scalable alternative to nanoparticle-loaded materials produced via melt-blown or centrifugal spinning. By incorporating 5% CuO into electrospun fibers, these yarns achieved 99.99% antibacterial efficacy against *Escherichia coli* within 50 minutes (ASTM E2149-01) and were successfully integrated into plain-weave protective textile. This innovation addressed key limitations of previous studies, such as large fiber diameter, broad diameter distribution, and fiber separation, which necessitate higher nanoparticle content to achieve comparable antibacterial performance. For bacterial filtration, soy protein-based electrospun filters were explored as a sustainable alternative to conventional filters containing TiO_2, nano-silver, or other antibacterial agents, which pose environmental concerns due to their persistence and toxicity. These soy protein-based filters achieved nearly 100% BFE at just 3 g/m^2, leveraging the bioadhesive properties of soy protein and the sieving effects of nanofiber structure. This approach provides an eco-friendly, cost-effective solution for infection control in healthcare settings. In the filed of wound healing, needle-less electrospun CS/PEO/PCL fibrous materials were engineered to offer tunable degradation rates and mechanical adaptability, addressing common limitations such as poor mechanical strength, suboptimal vapor permeability, and limited scalability. By adjusting the PCL/PEO ratios, these materials can be optimized for acute and chronic wounds, while post-fabrication TET immobilization enables customizable antibacterial properties. With a moisture vapor transmission rate of approximately 2000 $g/m^2/$ day, these materials demonstrated excellent suitability for wound care. Furthermore, cytotoxicity tests on 3T3 fibroblasts confirmed cell viability above 70% (ISO 10993-5), proving material's biocompatibility. Unlike previous studies that reported material's weak mechanical properties, inadequate vapor permeability, and the use of toxic solvents, these fibrous materials provide superior moisture regulation, enhanced antibacterial efficiency, and customizable degradation, all while being scalable via needle-less electrospinning. For mucoadhesive vaccine delivery, a three-layer electrospun patch was designed to enhance sublingual administration. Unlike conventional mucoadhesive films, which hinder nanoparticle diffusion due to swelling,

this design incorporates an electrospun reservoir layer for fast nanoparticles release. The patch prevented premature clearance while maintaining a stable nanoparticle concentration gradient at the mucosal surface. In porcine models, the electrospun patch improved drug retention and bioavailability, with nanoparticles detected in lymph nodes within two hours. Beyond vaccine delivery, these mucoadhesive patches show promise for allergen immunotherapy, with e*x vivo* and *in vivo* studies demonstrating reduced dosing frequency and effective desensitization, potentially improving patient adherence in sublingual immunotherapy. In localized cancer therapy, HA-coated PTX-loaded electrospun carriers were developed to enhance tumor targeting. The HA coating facilitated selective drug delivery to MiaPaCa pancreatic cancer cells, significantly reducing cell viability compared to free PTX. While free PTX resulted in a 40% reduction in cell viability after 96 hours, HA-coated PCL carriers exhibited enhanced efficacy, achieving 13% reduction, highlighting HA's role in targeted therapy. Unlike previously reported PCL matrices, which struggled with limited drug release and scalability, these HA-coated, needle-less electrospun carriers ensured sustained PTX release, enhancing therapeutic efficacy, reproducibility and industrial scalability.

Results presented in this habilitation thesis show significant contributions to the development of scalable biomedical solutions. By leveraging needle-less electrospinning of polymer blends and copolymers, alongside targeted modifications to electrospun materials, the author's research enhances industrial scalability, functional adaptability, and clinical feasibility. The versatility of these tailored electrospun fibrous materials underscores their potential for widespread biomedical applications, including infection control, personalized wound care, sublingual therapy, and localized cancer treatment.

4 Conclusion

This habilitation thesis summarizes significant contributions of author to textile technology, particularly in the design, electrospinning, modification, and biomedical applications of fibrous materials. Through the body of works—including peer-reviewed journal articles, conference contributions, patents, a book chapter, and awards—this research has driven advancements in the customisation of electrospun materials for biomedical use. The nine most significant, highly cited scientific works included in the appendices highlight the transformative impact of these findings, while citations from other key studies further underscore their novelty and relevance. By integrating electrospinning of copolymers and polymer blends with targeted modification techniques, this research addresses complex biomedical challenges. Innovations in electrospinning have led to improved material properties, including enhanced water resistance, mechanical strength, biodegradability, water uptake, and hydrolytic degradation. The successful implementation of needle-less electrospinning bridged the gap between laboratory-scale research and industrial production, ensuring scalability, material consistency, and customization for diverse biomedical applications. Modification strategies—including surface immobilization of tetracycline, incorporation of antibacterial nanoparticles, therapeutics absorption, and morphological optimization—have significantly enhanced the functionality of electrospun fibrous materials, particularly in drug release dynamics, antibacterial efficacy, and cell-material interactions. Furthermore, the newly developed predictive numerical model that integrates Hansen solubility parameters, permittivity, and vapor pressure enables the design of solvent systems without the need for experimental trials, reducing costs and facilitating the production of fibers with the desired morphology. This approach optimizes solvent selection for electrospinning, streamlining the development of clinically relevant fibrous materials and accelerating their translation into medical applications.

In conclusion, this research has not only advanced material development but also established a strong foundation for clinical implementations. The findings demonstrate the potential of electrospun fibrous materials in bacterial filtration, customizable wound care, drug delivery, and cancer therapy, laying the groundwork for future applications in gene therapy and other

specialized therapeutic approaches. The development of electrospun mucoadhesive patches has notably improved sublingual vaccine delivery and immunotherapy. Additionally, *in vivo* testing of electrospun fibrous carriers for localized pancreatic cancer therapy has showcased their potential for precise and effective treatment.
Future research will focus on exploring the potential of electrospun fibrous materials for glioblastoma therapies using gene therapy, in collaboration with Regional Hospital Liberec. Additionally, an innovative industrial approach will be submitted to a high-impact journal, detailing the modification of mucoadhesive patches by directly printing vaccine-containing liposomes onto electrospun fibrous materials. While this body of work contributes significantly to the broader research field, it also establishes a solid platform for continued advancements and industrial-scale applications, ensuring that electrospun fibrous materials will play a pivotal role in the next generation of biomedical solutions.

Declaration

I would like to express my sincere gratitude to all the co-authors who contributed to the scientific works included in this habilitation thesis. I affirm that my involvement in the preparation, execution, and interpretation of the results was at least on par with, if not greater than, that of the other co-authors in all instances.

References

[1] Yan, B., Zhang, Y., Li, Z., Zhou, P., Mao, Y. Electrospun nanofibrous membrane for biomedical application. *SN Appl Sci* 2024;4(172).

[2] Lukas, D., Sarkar, A., Martinova, L., Vodsedalkova, K., LUBASOVA, D., Chaloupek, J., Pokorny, P., Mikes, P., Chvojka, J. and Komarek, M. Physical principles of electrospinning (Electrospinning as a nano-scale technology of the 21st century). *Text Prog* 2009;41(2):59-140. (https://doi.org/10.1080/00405160902904641)

[3] LUBASOVA, D. Effect of solvent on the electrospinning system. Ph.D. thesis, Technical university of Liberec, Czech republic, 2011.

[4] Xue, J., Wu, T., Dai, Y., Xia, Y. Electrospinning and electrospun nanofibers: methods, materials, and applications. *Chem Rev* 2019;1198:5298–5415.

[5] Alaswad, S.O., Mahmoud, A.S., Arunachalam P. Recent advances in biodegradable polymers and their biological applications: A brief review. *Polymers (Basel)* 2022;14(22):4924.

[6] A method of chemical recycling of polyethylene terephthalate (PET) and a method of producing nanofibers from aromatic-aliphatic copolyesters obtained in this way. Originators: Prokopova, I., LUBASOVA, D., Martinova, L., Tureckova, J. and Vlčková, E. NP2012-47, CZ201247A3, 2012. (https://isdv.upv.gov.cz/webapp/resdb.print_detail.det?pspis=PT/2012-47&plang=CS)

[7] LUBASOVA, D., Tureckova, J., Martinova, L., Prokopova, I. (2010). *Properties of biodegradable meltblown textiles*. Research report, Research Centre TEXTIL II, project 1M0553. Ministry of Education, Youth and Sports (MSM).

[8] LUBASOVA, D., Tureckova, J., Martinova, L and Prokopova, I. Biodegradable non-woven textiles prepared from disposed PET bottles. In: Proceedings of the AUTEX 2009 World Textile Conference, 2009:1-7.

[9] De Vrieze, S., De Schoenmaker, B., Ceylan, Ö., Depuydt, J., Van Landuyt, L., Rahier, H., Van Assche, G., De Clerck. K. Morphologic study of steady state electrospun polyamide 6 nanofibres. *J Appl Polym Sci* 2011;119(5):2984–90.

[10] Heikkilä, P., Harlin, A. Parameter study of electrospinning ofpolyamide-6. *Eur Polym J* 2008;44(10):3067–79.

[11] Marsano, E., Francis, L., Giunco, F. Polyamide 6 nanofibrous nonwovens via electrospinning. *J Appl Polym Sci* 2010;117(3):1754–65.

[12] Lowery, J.L., Datta, N., Rutledge, G.C. Effect of fiber diameter, pore size and seeding method on growth of human dermal fibroblasts in electrospun poly(e-caprolactone) fibrous mats. *Biomaterials* 2010;31(3):491–504.

[13] Van der Schueren, L., De Schoenmaker, B., Kalaoglu, ÖI., De Clerck, K. An alternative solvent system for the steady state electrospinning of polycaprolactone. *Eur Polym J* 2011;47(6):1256–63.

[14] Malinova, L., Stolinova, M., LUBASOVA, D., Martinova, L. and Brozek J. Electrospinning of polyesteramides based on ε-caprolactam and ε-caprolactone from solution. *Eur Polym J* 2013;49 (10):3135-3143. (https://doi.org/10.1016/j.eurpolymj.2013.07.015)

[15] Malinova, L., Benesova, V., LUBASOVA, D., Martinova, L., Roda J. and Brozek J. Polyamide/ polyesteramide based nanofibers. *Funct Mater Let* 2011;4(4):365-368. (https://doi.org/10.1142/S1793604711002159)

[16] Nyamweya, N.N. Applications of polymer blends in drug delivery. *Futur J Pharm Sci* 2021;7:18.

[17] Reddy, N., Yang, Y. Potential of plant proteins for medical applications. *Trends Biotechnol* 2011;29(10):490-8.

[18] Vega-Lugo, A.C., Lim, L.T. Controlled release of allyl isothiocyanate using soy protein and poly(lactic acid) electrospun fibers. *Food Res Int* 2009;42(8): 933-940.

[19] Yao, C.; Li, X.S.; Song, T.Y. Electrospinning and crosslinking of zein nanofiber mats. Appl. Polym. Sci. 2007;130:380-385.

[20] Phiriyawirut, M., Rodchanacheewa, N., Nensiri, N., Supaphol, P. Morphology of electrospun mats of soy protein isolate and its blend. *Adv Mater Res* 2008;55-57:733-736.

[21] LUBASOVA, D., Mullerova, J. and Netravali, A. N. Water-resistant plant protein-based nanofiber membranes. *J Appl Polym Sci* 2015;132(16):1-9. (https://doi.org/10.1002/app.41852)

[22] LUBASOVA, D., Netravali, A. Parker, J. and Ingel, B. Bacterial filtration efficiency of green soy protein based nanofiber air filter. *J Nanosci Nanotechnol* 2014;14(7):4891–4898. (https://doi.org/10.1166/jnn.2014.8729)

[23] Kadłubowski, S., Henke, A., Ulański, P., Rosiak, J.M. Hydrogels of polyvinylpyrrolidone (PVP) and poly(acrylic acid) (PAA) synthesized by radiation-induced crosslinking of homopolymers. *Radiat Phys Chem* 2010;79(3):261-266.

[24] Fogaça, R., Catalani, L.H. PVP hydrogel membranes produced by electrospinning for protein release devices. *Soft Mater* 2013;11:61–68.

[25] Niu, H.T., Zhang, J., Xie, Z.L., Wang, X.G., Lin, T. Preparation, structure and supercapacitance of bonded carbon nanofiber electrode materials. *Carbon* 2011;49:2380-2388.

[26] Wang, P.Q., Zhang, D. , Ma, F.Y. ,Ou, Y., Chen, Q.N., Xie, S.H., Li, J.Y. Mesoporous carbon nanofibers with a high surface area electrospun from thermoplastic polyvinylpyrrolidone. *Nanoscale* 2012;4:7199–7204.

[27] LUBASOVA, D., Niu, H.T., Zhao, X.T., Lin, T. Hydrogel properties of electrospun polyvinylpyrrolidone and polyvinylpyrrolidone/poly(acrylic acid) blend nanofibers. *RSC Adv* 2015;5(67):54481-54487. (https://doi.org/10.1039/C5RA07514A)

[28] Tien, N., Lyngstadaas, S., Mano, J., Blaker, J., and Haugen, H. Recent developments in chitosan-based micro/nanofibers for sustainable food packaging, smart textiles, cosmeceuticals, and biomedical applications. *Molecules* 2021;26(9):2683.

[29] Ruzickova, J., Martinova, L., Rehakova, M., Jirsak, J. Electrospinning of chitosan nanofibers. In: AMBIENCE 05, 2005.

[30] Martinova, L. and LUBASOVA, D. Electrospun chitosan based nanofibers. *Res J Text Appar* 2008;12(2):72-79. (https://www.emerald.com/insight/content/doi/10.1108/rjta-12-02-2008-b009/full/html)

[31] LUBASOVA, D., Tomankova, H., and Polakova, D. Industrial-scale needle-less electrospinning of tetracycline-immobilized nanofibrous scaffolds using a polycaprolactone/polyethylene oxide/chitosan blend for wound healing. *J Ind Text* 2024;54:1-32. (https://doi.org/10.1177/15280837241291215)

[32] Andrade del Olmo, J., Mikes, P., Asatiani, N., Alonso, J.M., Sáez Martínez, V., Pérez González, R. Alternating current electrospinning of polycaprolactone/chitosan nanofibers for wound healing applications. *Polymers* 2024;16:1333.

[33] Miguel, S.P., Ribeiro, M.P., Coutinho, P., Correia, I.J. Electrospun polycaprolactone/aloe vera_chitosan nanofibrous asymmetric membranes aimed for wound healing applications. *Polymers* 2017;9:183.

[34] Abdollahimajd, F., Pourani, M.R., Mahdavi, H., Mirzadeh, H., Younespour, S., Moravvej, H. Efficacy and safety of chitosan-based biocompatible dressing versus nanosilver (Acticoat™) dressing in treatment of recalcitrant diabetic wounds: a randomized clinical trial. *Dermatol Ther* 2022; 35(9).

[35] Elsherbini, A.E. and Sabra, S.A. Nanoparticles-in-nanofibers composites: Emphasis on some recent biomedical applications. *J Control Release* 2022;348:57-83.

[36] Sagitha, P., Reshmi, C.R., Sundaran, S.P., Sujith, A. Recent advances in post-modification strategies of polymeric electrospun membranes. *Eur Polym J* 2018;105:227-249.

[37] Mohammadalizadeh, Z., Bahremandi-Toloue, E., Karbasi, S. Recent advances in modification strategies of pre- and post-electrospinning of nanofiber scaffolds in tissue engineering. *React Funct Polym* 2022;172:105202.

[38] Chen, S., Xie, Y., Ma, K., Wei, Z., Ran, X., Fu, X., Zhang, C. and Zhao, C. Electrospun nanofibrous membranes meet antibacterial nanomaterials: From preparation strategies to biomedical applications. *Bioact Mater* 2024;42:478-518.

[39] Kong, H. and Jang, J. Antibacterial properties of novel poly(methylmethacrylate) nanofiber containing silver nanoparticle. *Langmuir* 2008;24:2051-2056.

[40] Song, J., Kang, H., Lee, Ch., Hwang, S.H., Jang, *J.* Aqueous synthesis of silver nanoparticle embedded cationic polymer nanofibers and their antibacterial activity. *ACS Appl Mater Interfaces* 2012;4:460-465, 2012.

[41] Panta, H.R., Pandeyac, D.R., Namd, K.T., Baekd, W., Hongc, S.T., Kim, *H.Y.* Photocatalytic and antibacterial properties of a TiO2/nylon-6 electrospun nanocomposite mat containing silver nanoparticles. *J Hazard Mater* 2011;189:465-471.

[42] LUBASOVA, D. and Smykalova, B. Antibacterial efficiency of nanofiber membranes with biologically active nanoparticles. In: Proceedings of the International Conference on Agriculture, Biology and Environmental Sciences, 2014:1-4.

[43] Joo Kim, H., Raj Pant, H., Hee Kim, J., Jung Choi, N., Sang Kim, C. Fabrication of multifunctional TiO2– fly ash/polyurethane nanocomposite membrane via electrospinning. *Ceram. Int.* 2014;40(2):3023–3029.

[44] Narendiran, V., Quan, S., Joshua, N., Kathryn, K., Jane, M.C., Frederick, B., Mohamed, B., Marian, M., Xiangwu, Z. Multifunctional ZnO/Nylon 6 nanofiber mats by an electrospinning-electrospraying hybrid process for use in protective applications. *Sci Technol Adv Mat* 2011;12 (5):055004.

[45] Yalcinkaya, F. and LUBASOVA, D. Quantitative evaluation of antibacterial activities of nanoparticles (ZnO, TiO2, ZnO/TiO2, SnO2, CuO, ZrO2, and AgNO3) incorporated into polyvinyl butyral nanofibers. *Polym Advan Technol* 2017;28(1):137-140. (https://doi.org/10.1002/pat.3883)

[46] Flores-Jiménez, M.S., Garcia-Gonzalez, A., and Fuentes-Aguilar, R.Q. Review on porous scaffolds generation process: A tissue engineering approach. *ACS Appl Bio Mater* 2023;6 (1):1–23.

[47] Kim, C.H., Jung, Y.H., Kim, H.Y., Lee, D.R., Dharmaraj, N., Choi, K. E. Effect of collector temperature on the porous structure of electrospun fibers. *Macromol Res* 2006;14(1):59–65.

[48] You, Y., Youk, J.H., Lee, S.W., Min, B.M., Lee, S.J., Park, W. H. Preparation of porous ultrafine PGA fibers via selective dissolution of electrospun PGA/PLA blend fibers. *Mater Lett* 2006;60(6):757–760.

[49] Han, S.O., Son, W.K., Cho, D., Youk, J.H., Park, W.H. Preparation of porous ultra-fine fibres via selective thermal degradation of electrospun polyetherimide/poly(3- hydroxybutyrate-co-3-hydroxyvalerate) fibres. *Polym Degrad Stab* 2004;86(2):257–262.

[50] LUBASOVA, D. and Martinova, L. Controlled morphology of porous polyvinyl butyral nanofibers. *J Nanomater* 2011. (https://doi.org/10.1155/2011/292516)

[51] Hansen, C.M. Hansen Solubility Parameters: A User's Handbook, 2 edn., CRC Press, NY, USA (2007).

[52] van Krevelen D.W. and Nijenhuis, K. Properties of polymers. Their correlation with chemical structure; their numerical estimation and prediction from additive group contributions, 4 edn., Elsevier, Amsterdam, Netherlands (2009).

[53] LUBASOVA, D., Martinova, L., Marekova, D., Kostecka, P. Cell growth on porous and non-porous polycaprolactone nanofibers, in: Proceedings of the International Conference on Nano Technology (NANOCON'10), 2009:1-6.

[54] Svrcinova, P., Filip, P., LUBASOVA, D., Martinova, L. Impact of electrorheological behaviour of PVB solutions on the process of electrospinning. In: Electro-rheological fluids and magneto-rheological suspensions. 2011:311-317.

[55] LUBASOVA, D. and Spanek, R. Study of relationships between morphology of polyvinylbutyral nanofibers and solvents properties using a predictive numerical model. *J Comput Theor Nanosci* 2017;14 (6):2802-2811. (https://doi.org/10.1166/jctn.2017.6578)

[56] Tzias, P., Treiner, C. and Chemla, M. Applicability of Raoult's law in nonideal mixed solvents. *J Solution Chem* 1977;6:393.

[57] Kirkwood, J.G. The dielectric polarization of polar liquids. *J Chem Phys* 1939;7:911.

[58] Rezk, A.I., Lee, J.Y., Son, B.C., Park, C.H., Kim, C.S. Bi-layered nanofibers membrane loaded with titanium oxide and tetracycline as controlled drug delivery system for wound dressing applications. *Polym* 2019; 11: 1602.

[59] Leyva-Verduzco, A.A., Quiroz Castillo, J.M., Chan-Chan, L.H., Ramirez-Mendoza, C.G., Castillo Ortega, M.M., Plascencia-Martínez, D.F., López-Peña, I.Y., García-Sifuentes, C.O. Study of electrospun membranes composed of PCL and Tilapia-skin collagen with tetracycline or chloramphenicol in contact with human skin fibroblasts for wound dressing treatment. *ACS Omega* 2024; 9(5):5361–5370.

[60] Lin, M., Liu, Y., Gao, J., Wang, D., Xia, D., Liang, C., Li, N., Xu, R. Synergistic effect of co-delivering ciprofloxacin and tetracycline hydrochloride for promoted wound healing by utilizing coaxial PCL/ gelatin nanofiber membrane. *Int J Mol Sci* 2022; 23(3): 1895.

[61] Hassan, M.E., Yang, Q., Xiao, Z., Liu, L., Wang, N., Cui, X., Yang, L. Impact of immobilization technology in industrial and pharmaceutical applications. *Biotech* 2019;9(12):440.

[62] Wu, A., Wu, J., Yue, J., To, M.K.T., Pan, H., Lu, W.W., Zhao, X. Poly (d,l-lactic acid) electrospun fibers with tunable surface nanotopography for modulating drug release profiles. *Mater Lett* 2015;161:716-719.

[63] Faglie, A., Emerine, R., Chou, S.F. Effects of poloxamers as excipients on the physicomechanical properties, cellular biocompatibility, and in vitro drug release of electrospun polycaprolactone (PCL) fibers. *Polymers* 2023;15:2997.

[64] Masek, J., LUBASOVA, D., Lukac, R., Turanek-Knotigova, P., Kulich, P., Plockova, J., Maskova, E., Prochazka, L., Koudelka, S., Sasithorn, N., Gombos, J., Bartheldyova, E., Hubatka, F., Raska, M., Miller, A.D., Turanek, J. Multi-layered nanofibrous mucoadhesive films for buccal and sublingual administration of drug-delivery and vaccination nanoparticles - important step towards effective mucosal vaccines, *J Control Release 2018;*249:183-195. (https://doi.org/10.1016/j.jconrel.2016.07.036)

[65] LUBASOVA, D., Safont, M.M., and Mc Cormack, E. Localized paclitaxel delivery using a novel hyaluronic acid-coated fibrous carrier produced via needle-less electrospinning. *J Ind Text* 2025;55. (https://journals.sagepub.com/doi/10.1177/15280837251322712)

[66] Huo, P., Han, X., Zhang, W., Zhang, J., Kumar, P., Liu, B. Electrospun nanofibers of polycaprolactone/ collagen as a sustained-release drug delivery system for artemisinin. *Pharmaceutics* 2021;13(8):1228.

[67] Hadjianfar, M., Semnani, D., Varshosaz, J., Mohammadi, S., Rezazadeh Tehrani, S.P. 5FU-loaded PCL/chitosan/Fe3O4 core-shell nanofibers structure: An approach to multi-mode anticancer system. *Adv Pharm Bull* 2022;12(3):568-582.

[68] Kamath, S.M., Sridhar, K., Jaison, D., Gopinath, V., Ibrahim, B.K.M., Gupta, N., Sundaram, A., Sivaperumal, P., Padmapriya, S., Patil, S.S. Fabrication of tri-layered electrospun polycaprolactone mats with improved sustained drug release profile. *Sci Rep* 2020;10(1):18179.

[69] Karuppuswamy, P., Reddy Venugopal, J., Navaneethan, B., Luwang Laiva, A., Ramakrishna, S. Polycaprolactone nanofibers for the controlled release of tetracycline hydrochloride. *Mater Lett* 2015;141:180-186.

[70] Ravar, F., Saadat, E., Gholami, M., Dehghankelishadi, P., Mahdavi, M., Azami, S., Dorkoosh, F.A.. Hyaluronic acid-coated liposomes for targeted delivery of paclitaxel, in-vitro characterization and in-vivo evaluation. *J Control Release* 2016;229:10-22.

[71] Kim, K., Choi, H., Choi, E.S., Park, M.H., Ryu, J.H. Hyaluronic acid-coated nanomedicine for targeted cancer therapy. *Pharmaceutics* 2019;11(7):301.

[72] Espinosa-Cano, E., Huerta-Madroñal, M., Cámara-Sánchez, P., Seras-Franzoso, J., Schwartz, S., Abasolo, I., Román, J.S., Aguilar, M.R. Hyaluronic acid (HA)-coated naproxen-nanoparticles selectively target breast cancer stem cells through COX-independent pathways. *Mater Sci Eng: C*;124:2021.

[73] Hixson, A. W., Crowell, J. H. Dependence of reaction velocity upon surface and agitation. *Ind Eng Chem* 1931;23:1002-1009.

[74] Higuchi, T. Theoretical analysis of rate of release of solid drugs dispersed in solid matrices. J. Pharm. Sci. 1963;52:1145-1149.

[75] Rasouli, R., Barhoum, A., Bechelany, M., and Dufresne, A. Nanofibers for biomedical and healthcare applications. *Macromol Biosci* 2018;19(2).

[76] Anup, N., Chavan, T., Chavan, S., Polaka, S., Kalyane, D., Abed, S., Venugopala, K.N., Kalia, K., Tekade, R.K. Reinforced electrospun nanofiber composites for drug delivery applications. *J Biomed Mater Res A* 2021;109(10):2036-2064.

[77] Mamidi, N., García, R.G., Martínez, J.D.H., Briones, C.M., Martínez Ramos, A.M., Tamez, M.F.L., Del Valle, B.G., Segura, F.J.M. Recent advances in designing fibrous biomaterials for the domain of biomedical, clinical, and environmental applications. *ACS Biomater Sci Eng* 2022;8(9):3690-3716.

[78] Saquing, C.D., Manasco, J.L., Khan, S.A. Electrospun nanoparticle-nanofiber composites via a one-step synthesis. *Small* 2009;5(8):944–951.

[79] Tseng, R.J.,Huang, J., Ouyang, J., Kaner, R.B., Yang, Y. Polyaniline nanofiber/gold nanoparticle nonvolatile memory. *Nano Lett* 2005;5(6):1077–1080.

[80] Wang, H., Wang, T., Ye, Y.-X., Zhang, Y., Yang, P., Cai, H.H., Cai. J. Construction of an electrochemical cytosensor based on polyaniline nanofiber/gold nanoparticle interface and application to detection of cancer cells. *Chinese J Anal Chem* 2012;40(2):184–190.

[81] Melt-blowing die for producing nonwoven mats. Originators: Harding, J., Keller, J., Buntin, R. US3825380A,1974.

[82] Sarkar, K., Gomez, C., Zambrano, S., Ramirez, M., de Hoyos, E., Vasquez, H., Lozano, K. Electrospinning to forcespinning. *Mater Today* 2010;13(11):12–14.

[83] Liu, R., Cai, N., Yang, W., Chen, W., Liu, H. Sea-island polyurethane/polycarbonate composite nanofiber fabricated through electrospinning. *J Appl Polym Sci* 2010;116(3):1313–1321.

[84] Yalcinkaya, F., Komarek, M., LUBASOVA, D., Sanetrnik, F. and Maryska, J. Preparation of antibacterial nanofibre/nanoparticle covered composite yarns. *J Nanomater* 2016. (https://doi.org/10.1155/2016/7565972)

[85] Yalcinkaya, F., Komarek, M., LUBASOVA, D., Sanetrnik, F. and Maryska, J. Producing antibacterial textile material by weaving PVB/CuO nanocomposite fiber covered yarn, in: Proceedings of the International Conference on Nano Technology (NANOCON'14), 2014:1-6.

[86] Dumetz, A.C., Chockla, A.M. Kaler, E.W. Lenhoff, A.M. Effects of pH on protein–protein interactions and implications for protein phase behavior. *Biochimi Biophys Acta-Proteins Proteom* 2008;1784 (4):600-610.

[87] Greiner, A., Wendorff, J.H. Electrospinning: a fascinating method for the preparation of ultrathin fibers. *Angew Chem Int Ed Engl* 2007;46(30):5670-703.

[88] Kong, H., Jang, J. Antibacterial properties of novel poly(methyl methacrylate) nanofiber containing silver nanoparticles. *Langmuir* 2008;24(5):2051-2056.

[89] Song, J., Kang, H., Lee, C., Hwang, S.H., Jang, J. Aqueous synthesis of silver nanoparticle embedded cationic polymer nanofibers and their antibacterial activity. *ACS Appl Mater Interfaces* 2012;4(1):460–465.

[90] Gürtler, A.L., Rades, T. and Heinz, A. Electrospun fibers for the treatment of skin diseases, *J Control Release* 2023;363:621-640.

[91] Zehrer, C.L., Holm, D., Solfest, S.E., Walters, S.A. A comparison of the in vitro moisture vapour transmission rate and in vivo fluid-handling capacity of six adhesive foam dressings to a newly reformulated adhesive foam dressing. *Int Wound J* 2014;11(6):681-90.

[92] Sharma, A. and Luthra, G. Significance of ISO 10993 standards in ensuring biocompatibility of medical devices: a review. *J Pharm Res Int* 2023;35(8):23–34.

[93] Asghari, F., Rabiei Faradonbeh, D., Malekshahi, Z.V., Malekshahi, Z.V., Nekounam, H., Ghaemi, B., Yousefpoor, Y., Ghanbari, H., Faridi-Majidi, R. Hybrid PCL/chitosan-PEO nano-fibrous scaffolds incorporated with A. euchroma extract for skin tissue engineering application. *Carbohydr Polym* 2022;278: 118926.

[94] Dubsky, M., Kubinova, S., Sirc, J., Voska, L., Zajicek, R., Zajicova, A., Lesny, P., Jirkovska, A., Michalek, J., Munzarova, M., Holan, V., Sykova E. Nanofibers prepared by needleless electrospinning technology as scaffolds for wound healing. *J Mater Sci Mater Med* 2012;23:931–941.

[95] Masek, J., Maskova, E., LUBASOVA, D., Spanek, R., Raska, M., and Turanek, J. (2020) Nanofibers in mucosal drug and vaccine delivery. Nanomaterials - Toxicity, human health and environment. IntechOpen. (https://www.intechopen.com/chapters/64646)

[96] Dukhin, S.S, Labib, M.E. Convective Diffusion of Nanoparticles from the Epithelial Barrier toward Regional Lymph Nodes. *Adv Colloid Interf Sci* 2013;199-200:23–43.

[97] Chunbai, H., Fuying, C., Lichen, Y., Feng, Q., Cui, T., Chunhua, V. A polymeric composite carrier for oral delivery of peptide drugs: Bilaminated hydrogel film loaded with nanoparticles. *Eur Polym J* 2009; 45:368–376.

[98] Mucoadhesive carriers of particles, method of preparation and uses therefor. Originators: Masek, J., LUBASOVA, D., Lukac, R., Raska, M., Knotigova Turanek, P. and Turanek, J. PV 2014-665, 2014. (https://isdv.upv.gov.cz/webapp/resdb.print_detail.det?pspis=PT/2014-665&plang=CS)

[99] Carrier. Originators: Mašek, J., Lukáč, R., Raška, M., Knoetigová Turánek, P., Turánek, J. , LUBASOVA, D. and Miller, D. A. WO2018033744A1, 2018. (https://worldwide.espacenet.com/patent/search?q=pn%3DWO2018033744A1)

[100] Hoffmann, H.J., Valovirta, E., Pfaar, O., Moingeon, P., Schmid, J.M., Skaarup, S.H., Cardell, L.O., Simonsen, K., Larché, M., Durham, S.R., Sørensen P. Novel approaches and perspectives in allergen immunotherapy. *Allergy* 2017;72(7):1022-1034.

[101] Sørensen, P., Turanek-Knotigova, P., Masek, J., Kotoucek, J., Hubatka, F., Maskova, E., Kulich, P., LUBASOVA, D., Raska, M., Leenhouts, K., Turanek, J. Short-course sublingual immunotherapy by mucoadhesive patch and tolerogenic particle enhanced allergen presentation. *Clin Exp Allergy* 2021;51(6):853-857. (https://doi.org/10.1111/cea.13862)

[102] Borandeh, S., van Bochove, B., Teotia, A., Seppälä, J. Polymeric drug delivery systems by additive manufacturing. *Adv Drug Deliv Rev* 2021;173:349–373.

[103] Guan, X., Bian, Y., Guo, Z., Zhang, J., Cao, Y., Li, W., Wang, W. Bidirectional allostery mechanism in catch-bond formation of CD44 mediated cell adhesion. *J Phys Chem Lett* 2024;15(43):10786–10794.

[104] Serri, C., Quagliariello, V., Iaffaioli, R.V., Fusco, S., Botti, G., Mayol, L., Biondi, M. Combination therapy for the treatment of pancreatic cancer through hyaluronic acid-decorated nanoparticles loaded with quercetin and gemcitabine: a preliminary in vitro study. *J Cell Physiol* 2019;234:4959–4969.

[105] Tarannum, M., Vivero-Escoto, J.L. Nanoparticle-based therapeutic strategies targeting major clinical challenges in pancreatic cancer treatment. *Adv Drug Deliv Rev* 2022;187:114357.

[106] Bartkowski, M., Bincoletto, V., Salaroglio, I.C., Ceccone, G., Arenal, R., Nervo, S., Rolando, B., Riganti, C., Arpicco, S., Giordani, S. Enhancing pancreatic ductal adenocarcinoma (PDAC) therapy with targeted carbon nano-onion (CNO)-mediated delivery of gemcitabine (GEM)-derived prodrugs. J *Colloid Interface Sci* 2024;659:339-354.

[107] Xia, G., Zhang, H., Cheng, R., Wang, H., Song, Z., Deng, L., Huang, X., Santos, H.A., Chi, W. Localized controlled delivery of gemcitabine via microsol electrospun fibers to prevent pancreatic cancer recurrence. *AdvHealthc Mater 2018;*7(18):e1800593.

List of attached scientific works

Table 3 summarizes *Lubasová's* most significant scientific works (9 peer-reviewed journal articles) relevant to this habilitation thesis. The table includes the journal impact factors and citation counts, as indexed in Web of Science, as of January 11, 2025.

Table 3: Summary of Lubasová's key publications related to this habilitation thesis.

Journal paper	Journal IF	Times cited
[14] Malinova, L., Stolinova, M., **LUBASOVA, D.**, Martinova, L., Brozek, J. Electrospinning of polyesteramides based on ε-caprolactam and ε-caprolactone from solution. *Eur Polym J* 2013;49(10):3135-3143.	5.3	16
[21] **LUBASOVA, D.,** Mullerova, J., Netravali, A.N. Water-resistant plant protein-based nanofiber membranes. *J Appl Polym Sci* 2015;132(16):1-9.	2.8	16
[22] **LUBASOVA, D.**, Netravali, A.N., Parker, J., Ingel, B. Bacterial filtration efficiency of green soy protein based nanofiber air filter. *J Nanosci Nanotechnol* 2014;14(7):4891–4898.	1	43
[27] **LUBASOVA, D.**, Niu, H.T., Zhao, X.T., Lin, T. Hydrogel properties of electrospun polyvinylpyrrolidone and polyvinylpyrrolidone/poly(acrylic acid) blend nanofibers. *RSC Adv* 2015;5(67):54481-54487.	3.9	35
[31] **LUBASOVA, D.**, Tomankova, H., Polakova, D. Industrial-scale needle-less electrospinning of tetracycline-immobilized nanofibrous scaffolds using a polycaprolactone/polyethylene oxide/chitosan blend for wound healing. *J Ind Text* 2024;54.	2.7	-
[50] **LUBASOVA, D.** and Martinova, L. Controlled morphology of porous polyvinyl butyral nanofibers. *J Nanomater* 2011:1-6.	3.5	50
[64] Masek, J., **LUBASOVA, D.**, Lukac, R., Turanek-Knotigova, P., Kulich, P., Plockova, J., Maskova, E., Prochazka, L., Koudelka, S., Sasithorn, N., Gombos, J., Bartheldyova, E., Hubatka, F., Raska, M., Miller, A.D., Turanek, J. Multi-layered nanofibrous mucoadhesive films for buccal and sublingual administration of drug-delivery and vaccination nanoparticles - important step towards effective mucosal vaccines. *J Control Release* 2017;249:183-195.	10,6	95
[65] **LUBASOVA, D.**, Safont, M.M., and Mc Cormack, E. Localized paclitaxel delivery using a novel hyaluronic acid-coated fibrous carrier produced via needle-less electrospinning. *J Ind Text* 2025;55.	2.7	-
[84] Yalcinkaya, F., Komarek, M., **LUBASOVA, D.,** Sanetrnik, F., Maryska, J. Preparation of antibacterial nanofibre/nanoparticle covered composite yarns. *J Nanomater* 2016:1-7.	3.5	32

Appendix 1

Malinova, L., Stolinova, M., LUBASOVA, D., Martinova, L. and Brozek J. Electrospinning of polyesteramides based on ε-caprolactam and ε-caprolactone from solution. European polymer journal 2013;49(10):3135-3143.

European Polymer Journal 49 (2013) 3135–3143

Contents lists available at ScienceDirect

European Polymer Journal

journal homepage: www.elsevier.com/locate/europolj

Macromolecular Nanotechnology

Electrospinning of polyesteramides based on ε-caprolactam and ε-caprolactone from solution

Lenka Malinová [a], Michaela Stolínová [a], Daniela Lubasová [b], Lenka Martinová [b], Jiří Brožek [a,*]

[a] Department of Polymers, Institute of Chemical Technology, Prague, Technická 5, 166 28 Prague 6, Czech Republic
[b] Department of Nonwovens, Technical University of Liberec, Studentská 2, 461 17 Liberec 1, Czech Republic

ARTICLE INFO

Article history:
Received 14 December 2012
Received in revised form 1 July 2013
Accepted 9 July 2013
Available online 26 July 2013

Keywords:
Polyesteramide
Fiber morphology
System parameters
Electrospinning

ABSTRACT

The paper is focused on the preparation of nanofiber layers of polyesteramides with various ratios of ε-caprolactam/ε-caprolactone structural units. We have studied the effect of the system parameters, i.e., the composition of the copolymer, its molar mass and the concentration of the solution on morphology of fiber layers being formed during the electrostatic wet spinning. The process parameters were constant during the processing. Morphology of the fiber layers is given by the composition of the copolymer, i.e., by its polarity, the content of the crystalline phase and thus its separation in the process of evaporating the solvent. Fibers with diameters ranging from 100 to 160 nm were obtained for polyesteramides containing 20 or 40 mol% lactone units during optimizing the system parameters, i.e., the concentration of the solution and molar mass of polyesteramide.

1. Introduction

Thanks to their interesting properties, such as large specific surface with respect to their mass or volume, or the possibility to prepare porous structures, polymeric nanofibers have recently increased their popularity. Nanofiber layers are already in use in a range of applications such as filters for purification of fuels, water and air, membranes, sensors etc. Research is also focused on biomedical applications of nanofibers, based mainly on biologically degradable polymers, such as tissue substitute, materials for scarless wound healing or drug carriers with gradual drug releasing [1].

Conventional techniques of the fiber preparation (wet spinning, dry spinning, melt spinning) yield polymeric fibers with dimensions in the order of magnitude of micrometers. Nanofiber structures are prepared by electrostatic spinning or, for short, electrospinning. In spite of the fact that the process of electrospinning has been known for almost 80 years (the first patent was granted to Formhals in 1934 [2]), only for the recent 10 years this technique has increasingly been used to prepare nanofiber layers from various types of materials. The Nanospider™ [3] electrospinning method is an efficient technique enabling one to produce polymeric nanofiber layers (fiber polymer mats), the fibers being formed using an electrostatic field from a thin layer of a polymer solution and put on a collector in the form of a fiber layer. The ability of a polymer to form fibers is influenced by a number of parameters which can be divided into the process and the system ones. The process parameters are, e.g., the intensity of the electric field, the distance between the electrode and the collector, temperature and humidity of the ambient air, the type of the electrode or the flow speed of the cooling air during the melt spinning. The system parameters, such as chemical structure and molar mass of the polymer, rheological behavior of the melt, thermodynamics of the polymer interactions, concentration of the polymer in the solution, viscosity or the dielectric properties of the solution [4], play a fundamental role. The speed of forming the nanofiber layer is determined also by the type of the electrode, on which the polymer solution is deposited. Most frequently,

* Corresponding author. Tel.: +420 22044 3190; fax: +420 22044 3175.
E-mail address: jiri.brozek@vscht.cz (J. Brožek).

0014-3057/$ - see front matter © 2013 Elsevier Ltd. All rights reserved.
http://dx.doi.org/10.1016/j.eurpolymj.2013.07.015

the electrostatic wet spinning is performed in the way illustrated in Fig. 1: needle, flat electrode, a small roller.

Much attention is paid in the literature to the preparation of nanofibers from polyamide 6 (PA6) [5–7] and poly(ε-caprolactone) (PCLO) [8–10]. These polymers differ in their physico-chemical properties (glass transition temperature, melting temperature, solubility or tendency to degrade). Continuous change of properties between PA6 and PCLO can be realized by polyesteramides (PEAs) containing structural units derived from ε-caprolactam (CLA) and ε-caprolactone (CLO). The preparation of fiber layers from PEA's by the technique of electrostatic spinning from a PEA solution was mentioned for the first time in [11].

PEAs can be prepared by hydrolytic [12,13] or anionic [14–16] copolymerization of CLA and CLO. Hydrolytic mechanism was used to prepare polyether–polyesteramide block copolymers [12]. Indisputable benefit of the anionic copolymerization of CLA and CLO relies in its high rate and low content of unreacted monomers in the product. In this case, especially ε-caprolactam magnesium bromide (CLAMgBr) proved itself as an initiator of the copolymerization [15]. At the beginning of the process, PCLO is formed first, while the CLA units are incorporated at higher temperatures and the product of the polymerization process is a statistical copolymer [14,15]. The same type of the statistical PEA was prepared also by the anionic polymerization of CLA in the presence of dissolved PCLO [17].

Biological degradability of PEAs was studied by a model abiotic hydrolysis, composting the samples and testing the effect of ligninolytic fungi on the degradation rate. It was found that it is especially chemical hydrolysis of ester bonds which is responsible for the splitting the PEAs chains. The rate of the degradation of the PEA matrix increases with increasing content of the CLO units in the copolymer and thus with decreasing content of the crystalline phase [18–20].

Thanks to their biological degradability, the fiber layers made from PEAs could find their application as, e.g., filter for a bioremediation of water polluted by organic compounds. The present paper is focused on the effect of the system parameters, i.e., the composition of PEA, molar mass and concentration of the solution, on the morphology of the fiber layers prepared by electrostatic wet spinning.

2. Experimental

2.1. Chemicals

ε-Caprolactam (CLA) (DSM) was used without further purification and stored in a dessicator over P_2O_5, water content 65 ppm. ε-Caprolactone (CLO) (Sigma-Aldrich) was purified by distillation under reduced pressure over powdered calcium hydride, water content 40 ppm. δ-Valerolactone (VLO) (Fluka) was distilled (prior to polymerization) under reduced pressure (b.p. 71–76 °C, 70 Pa); water content was 50 ppm. ε-Caprolactam magnesium bromide (CLAMgBr) concentrate in CLA (Brügemann) was stored in a round-bottom flask under the protective argon atmosphere. The content of Mg^{2+} was 1.02 mol/kg (determined by chelatometric titration). Formic acid (Penta) and acetic acid (Penta) were used with concentration 99%.

2.2. Preparation of polyesteramides

The reference PEAs have been synthesized by the anionic ring-opening copolymerization of CLA and CLO using reaction casting of thin slabs (4 mm) of material in a closed Teflon-covered aluminum mould under protective atmosphere of argon according to procedure described in Ref. [15]. CLAMgBr (1.0 mol%) was used as an initiator and the polymerizations were carried out at 150 °C (1 h).

PEAs with lower molar mass were obtained by the anionic copolymerization of CLA, CLO initiated by CLAMgBr (1.0 mol%), where a part of CLO was substituted by VLO. CLA and initiator were placed into a test-tube and equilibrated under dry argon at 90 °C until a clear liquid was obtained. After complete dissolution, a mixture of CLO and VLO (at 20 °C) was introduced using a syringe and the mixture was thoroughly stirred. Polymerizations proceeded at 150 °C for 1 h.

A part of prepared PEAs was rasped and used for the gravimetrically determination of polymer yield by cold-water extraction at laboratory temperature (three times for 24 h). Extracted samples were dried at laboratory temperature under reduced pressure (30 Pa) over P_2O_5 to constant weight.

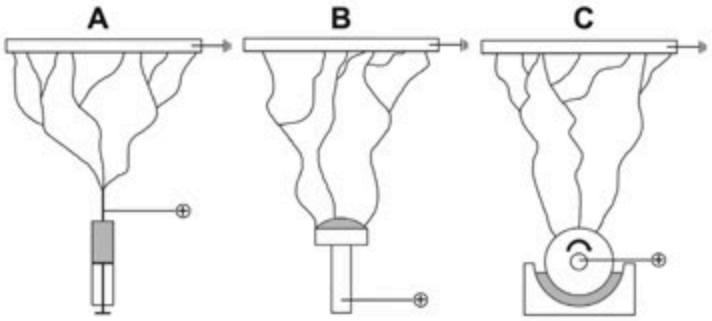

Fig. 1. Possibilities of electrostatic spinning – the types of the electrodes: A – needle, B – flat electrode, C – roller.

2.3. Differential scanning calorimetry

DSC measurements were performed with Q 100 DSC (TA Instruments) at a constant heating rate of 10 °C/min; nitrogen purge flow rate of 50 cm^3/min: 1st run – heating from 40 °C to 240 °C, isothermal at 240 °C (3 min), quenching in liquid nitrogen; 2nd run – heating from −80 °C to 240 °C.

2.4. Viscosity measurements

Reduced viscosities (η_{red}) were determined by using Ubbelohde viscometer at 25 °C. Copolymers were dissolved in tri-cresol (concentration of polymer in solution was approx. 1.9–2.1 × 10^{-3} g/cm^3).

$\eta_{red} = \eta_i/c$ [cm^3/g], where η_i is relative viscosity increment (specific viscosity) ($\eta_i = \eta_r - 1$) and c is polymer concentration in g/cm^3.

Intrinsic viscosity (limiting viscosity number) [η] and apparent viscosity-average molar mass $(M_v)_{app}$ were calculated from the following equations [21,22]:

$$[\eta] = [(1 + 1.6 \cdot \eta_i)^{0.5} - 1]/0.8 \cdot c$$

$$(M_v)_{app} = 113 \cdot 119 \cdot (0.01 \cdot \eta])^{1.35}$$

2.5. Nuclear magnetic resonance

Nuclear magnetic resonance (^{1}H NMR) analysis of PEAs dissolved in deuterated formic acid was performed using a Bruker 600 Avance^{III}. The measured data were transformed by the Fourier transform. The ratios of lactam and lactone units in PEAs were evaluated from the integrated intensities.

2.6. Electrospinnig process

The electrospinning setup from polymer solution is schematically illustrated in Fig. 1(B). PEAs were dissolved in mixed solvent formic/acetic acid 1/2 v/v and placed on the top of a special flat metal electrode with a diameter of 3.5 cm, which is at same time positive electrode. The high-voltage power supply (Glassman High Voltage, Inc., USA) allows control of voltage in the range of 0–55 kV. The electric field is switched on and slowly increased to 30 kV. The so-called Taylor cones were then formed due to the effect of high voltage from the thin layer of polymer solution on the flat electrode. The cones cleave into (nano)-fibers which are carried onto the negative electrode and collected on the polypropylene non-woven fabric (fiber diameter 20–30 μm). During this process, the solvent evaporates and the fibers are fixed. All fiber spinning was performed at laboratory temperature, 40–60% relative humidity and the electrode-to-collector distance 10 cm. Traces of solvent after electrospinning process were removed by drying at laboratory temperature under reduced pressure (30 Pa). Fiber layers were kept over P_2O_5 to minimized water content.

2.7. Scanning electron microscope

The morphology of the electrospun fiber layers was observed using the scanning electron microscope (SEM) VEGA-TECSAN TS 5130.

3. Results and discussion

3.1. Preparation of polyesteramides

PEAs having various content of the lactone units and molar masses were prepared by the time-proven way

Table 1
Properties of PEAs prepared by anionic polymerization of CLA and a mixture of lactones CLO/VLO (1 mol% CLAMgBr, polymerization temperature 150 °C, polymerization time 1 h).

CLA/CLO/VLO[a]	CLA/(CLO + VLO)[b]	y_w[c] (%)	η_{red}[d] (cm^3/g)	$(M_v)_{app}$[e] (g/mol)	T_m[f] (°C)	ΔH_m[g] (J/g)	T_g[h] (°C)
97/3/0	nd	93	330	52,000	212	83	42
80/20/0	81/19	98	370	59,000	179	51	22
80/17.5/2.5	*83/17*	*98*	*319*	*50,000*	*184*	*58*	*25*
80/15/5	*82/18*	*97*	*130*	*17,000*	*181*	*52*	*24*
80/10/10	*80/20*	*93*	*96*	*12,000*	*173*	*58*	*21*
60/40/0	60/40	95	259	39,000	121	39	−4
60/35/5	*60/40*	*95*	*94*	*11,000*	*123*	*53*	*2*
60/30/10	*58/42*	*92*	*92*	*11,000*	*107*	*37*	*−6*
60/25/15	*60/40*	*85*	*87*	*10,000*	*112*	*41*	*−2*
60/20/20	*55/45*	*73*	*65*	*7000*	*100*	*31*	*−9*
40/60/0	nd	94	220	32,000	75	54	−24
20/80/0	nd	96	245	37,000	59	37	−45

nd – not determined.
[a] Molar ratio of monomers in copolymerization feed.
[b] Molar ratio of lactam and lactone units in extracted PEA calculated from ^{1}H NMR.
[c] Gravimetric conversion obtained by extraction with water.
[d] Reduced viscosity in tri-cresol at 25 °C (concentration 1.9–2.1 × 10^{-3} g/cm^3).
[e] Apparent viscosity-average molar mass.
[f] Melting temperature evaluated from the 1st run in DSC measurement.
[g] Melt enthalpy evaluated from the 1st run in DSC measurement.
[h] Glass transition temperature evaluated from the 2nd run in DSC measurement.

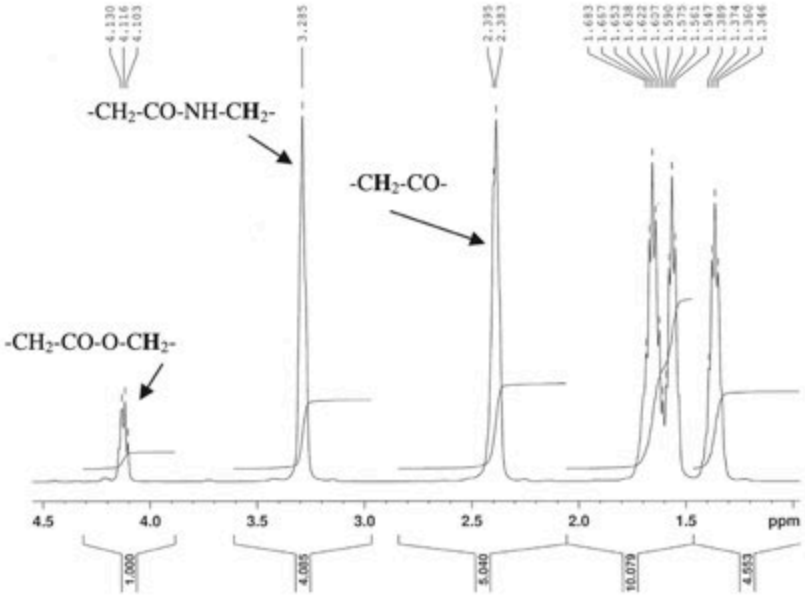

Fig. 2. Scheme of evaluation of ^{1}H NMR spectra of PEA prepared.

[15], i.e., by anionic copolymerization of CLA and CLO/VLO mixture initiated by CLAMgBr. The composition and basic properties of PEA's thus prepared are given in Table 1.

Reference PEAs (i.e. without VLO) were prepared in high yield (not less than 93%); consequently, the composition of the copolymer is virtually identical to that of the feed. Melting temperature (T_m) of PEAs decreases with increasing content of the CLO structural units. Melt enthalpy (ΔH_m) attains its maximum for the homopolymer (i.e., PA6 with CLA/CLO 97/3) and decreases with increasing CLO content. Prepared PEAs are statistical copolymers, as manifested by a single T_g value, continuously decreasing with increasing content of the CLO units from 42 °C (CLA/CLO 97/3) to −45 °C (CLA/CLO 20/80). Reliable T_g values were read from the 2nd heating of the sample, preceded by quenching its melt in liquid nitrogen.

Determination of molar masses of PEAs is complicated due to their solubility mostly in polar solvents and absence of the Mark-Houwink constants *a* and *K* for various compositions. PEAs were therefore characterized by reduced viscosities (η_{red}) measured in tri-cresol, from which the so called apparent viscosity-average molar masses $(M_v)_{app}$ were calculated using the relations for PA6, see experimental part. Values thus obtained do not represent the true ones for PEAs because the hydrodynamic behavior of PA6 and PEAs differ in dependence on the content of the lactone units.

In the present paper we focused on the regulation of PEAs molar masses, with starting molar ratios CLA/CLO in the feed being 80/20 and 60/40. A part of CLO was substituted by VLO so that the overall content of lactones in the feed was 20 and 40 mol%, respectively. We assumed that incorporating the VLO units in addition to the CLO ones we will not affect the physico-chemical properties of PEAs, including their tendency to undergo biodegradation.

In Table 1, basic properties of PEAs containing the CLA, CLO and VLO structural units are presented and compared with those of PEAs containing only CLA and CLO. For the ratio CLA/(CLO + VLO) 80/20, increasing content of VLO causes a decrease of the copolymer content to about 93%. In contrast, when the content of the lactone units is 40 mol%, the copolymer content drops quickly to as low value as 73% for 20 mol% VLO.

The CLA/lactone units molar ratio in extracted copolymer was calculated from ^{1}H NMR spectra (Table 1). A spectrum of PEA as well as the procedure of evaluating the ratio of CLA and the mixture of lactone units incorporated in the copolymer is presented in Fig. 2. Since VLO differs from CLO in the number of the ring members (the difference being one CH_2 group), it was impossible to evaluate the CLO/VLO units ratio in the copolymer from ^{1}H NMR spectra. Even though the content of copolymers decreased with increasing content of the regulators, the ratios of incorporated CLA and lactone units in extracted PEAs are close to the monomer ratios in the feed. On the basis of the measurements performed it is impossible to confirm that the CLO/VLO ratios in extracted PEA and in the feed are the same.

For PEAs thus prepared, η_{red} were measured in tri-cresol and $(M_v)_{app}$ were calculated therefrom (Table 1). Even for the content of the VLO regulator in the feed being as low as 5 mol%, η_{red} decreases three times as much as compared to PEA without regulator. The drop of η_{red} a $(M_v)_{app}$ values on addition of more VLO units is slower.

For the CLA/lactone ratio equal to 80/20, the T_g values read from the second heating (see above) range between

21 and 25 °C. This range is broader for the ratio being 60/40 (2 to −9 °C), reflecting thus the fact that the content of lactones in the isolated samples is higher than in the polymerization feed.

Certain differences were observed for melting temperatures and enthalpies, mainly for the CLA/lactone ratio 60/40, where the melt endotherms are relatively broad and the areas beneath the curves are small.

(5)

tion of the CLA units into the polymer structure can also proceed through the reaction in the following equation:

The following neutralization reaction leads to an equilibrium between the anions of the amide groups of the polyamide segments and the CLA anions.

Afterwards, a series of reactions proceed in the system, determining the structure of the resulting polymer, that is, statistical copolymer. The end oxyanion of the (co)polyester is acylated by amide (Eq. (6)) or by *N*-acyllactam (Eq. (7)).

(6)

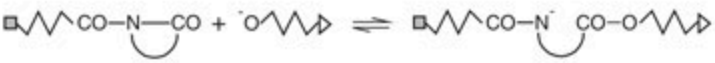

(7)

3.2. Mechanism of polyesteramide formation

In analogy to the suggested mechanism of CLA/CLO copolymerization [14], reaction of CLO or VLO with the lactam anion yields an oxyanion which represents an initiation center for the growth of the polyester chain.

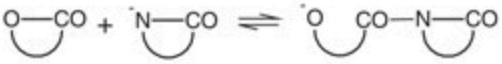

(1)

Lactones convert into a copolyester already in the first stage of the polymerization process, i.e., during the preparation of the polymerization feed [15]. Formation of the (co)polyester soluble in the CLA melt (within 5 min at 90 °C) increase substantially the polymerization feed viscosity.

The CLA polymerization proceeds at higher temperatures (above 130 °C) [17] through a repeated addition of the lactam anion on the *N*-acyllactam end group (Eq. (2)) formed according Eq. (1).

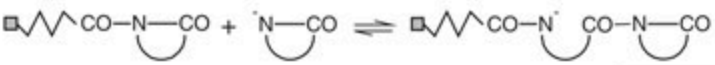

(2)

Further *N*-acyllactam growth centers are formed at higher temperatures through an acylation of the lactam anion by the ester group of the polyester chain.Incorporater is acylated by amide (Eq. (6)) or by *N*-acyllactam (Eq. (7)).

The VLO structural units, incorporated in the polyester or polyesteramide chains being formed, affect above all the formation of the *N*-acyllactam structures (Eq. (3)) and thus (fundamentally) also molar mass of PEA.

(3)

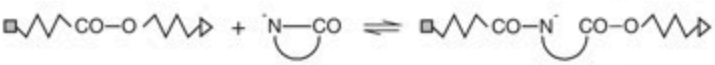

(4)

3.3. Electrostatic spinning of polyesteramides

A number of studies deal with electrostatic spinning of a single type of polymer or copolymer, and with the effect of system and process parameters on the course of the process and morphology of the fiber layers. The prepared PEAs differ in the lactam/lactone units ratio, that is, in the polarity of chains, content of the crystalline phase and the rate of the polymer separation from the solution. These properties govern the morphology of the fiber layers formed. In order to decrease the number of variables decisive for the spinning process, the process parameters were kept fixed (cf. Experimental part). Electrospinning proceeded from the PEAs solutions in a mixed solvent. The composition of PEA, its molar mass and the concentration of the solution represented adjustable parameters.

As the ratio of CLO decreased, the polarity of the copolymer increased, thereby reducing the choice of suitable solvents. Apart from PCLO which undergoes acidolysis in formic acid; 2,2,2-trifluoroethanol (TFE), formic acid and the $CHCl_3$:TFE 1:1 mixture were the only solvents suitable for all prepared PEAs [23]. However, PEAs with 3, 20 and 30 mol% CLO units are insoluble in acetic acid [11]. Very toxic and expensive fluorinated solvents are, however, rarely used for PA6 electrospining. Formic acid and acetic acid are the least toxic solvents from this group.

Formic acid is often used for electrospinning of various polymers [24–31], most frequently polyamides [24–29]. It was found that a solution of PA6 in highly polar solvent, such as formic acid (dielectric constant $\varepsilon_0 = 57.2$ at 298 K [32]), can be electrospun, but not under steady state conditions. Electric field applied during electrospinning causes reorientation of solvent molecules. However, this rearrangement of solvent molecules is position dependent during electrospinning of polyamide 6.6 because of each position the electrical field intensity and formic acid concentration are different [33].

A combination of formic and acetic acid is less exploited but showed to be very promising for PA6 [34]. The presence of acetic acid which has much lower dielectric constant ($\varepsilon_0 = 6.6$ at 298 K [32]) can reduce the interactions between formic acid and PA6. Depending on the composition, this mixed solvent has a lower polarity. This results in a better stability of the system and enables one to achieve steady state conditions. Thus, the formic/acetic acid mixed solvent (1/2 v/v) was successfully used in the electrospinning of both PA6 and PCLO from a solution under steady state conditions. This mixture dissolved all PEAs prepared.

The most important parameters governing the fiber morphology and diameter were concentration of polymer solution and the structure of PEA determining the viscosity. In the polymer–solvent binary systems, viscosity is proportional to the polymer concentration and depends on all intermolecular interactions in the system. With decreasing CLO structural units in PEA, the polarity of the copolymer increased, thereby promoting solvent-amide bond interactions. As a result of these interactions, polymer coils became more expanded and the viscosity of the solution increased. It is well known that, for a given PEA, the entanglement density increases with concentration, i.e. an increase in viscosity. Density of chain entanglements is one of many parameters that can significantly influence fiber formation during electrospinning.

The ability of PEAs with varying composition to form fibers was tested on 5, 10 and 15 wt% solutions, see Fig. 3. For 5 wt%, the fibers are in diameter close to nanofibers (i.e. diameter ~100 nm). Certain amount of beaded fibers occurred in some experiments where the content of the CLO structural units in PEAs exceeded 40 mol%.

For PEAs with CLA and CLO structural units, fibers become thicker when the PEA concentration increases. This is due to the growth of viscosity when the concentration of PEA increases, which is distinct especially for ratio CLA/CLO 97/3, i.e., material close to PA6. Higher viscosity causes higher amount of entanglements and thus thicker

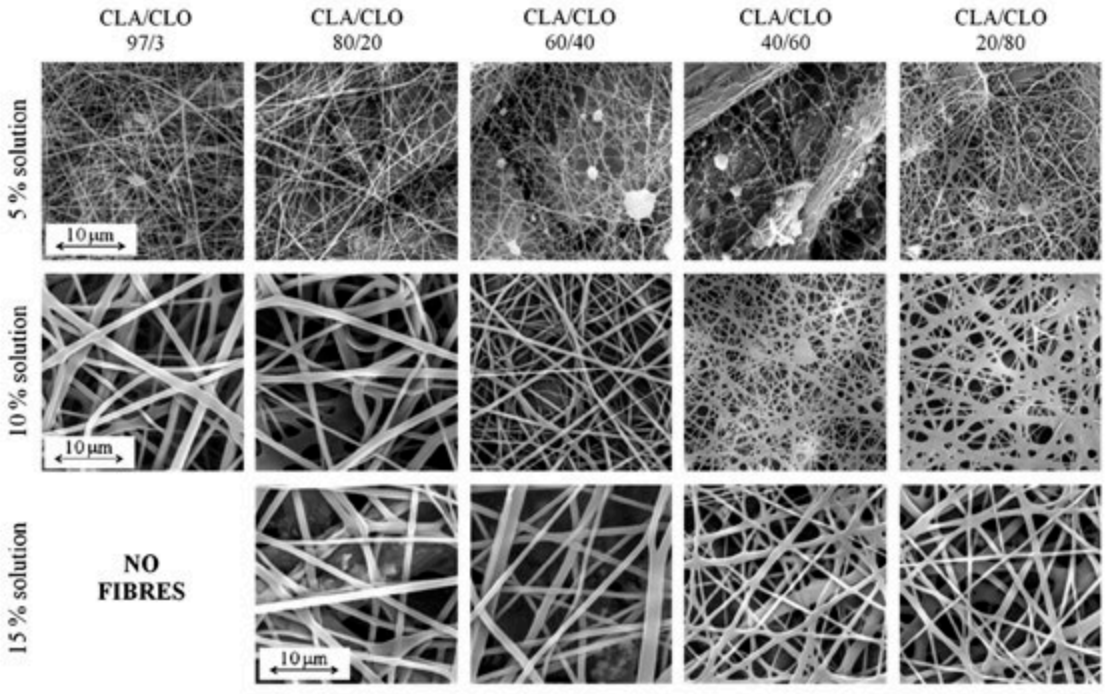

Fig. 3. SEM images of the PEAs fiber layers containing the CLA and CLO structural units in varying ratio and obtained by electrostatic wet spinning (5, 10 and 15 wt% solutions).

Table 2
Properties of PEA's fiber layers prepared by electrospinning process.

CLA/CLO[a]	CLA/CLO fiber layer[b]	T_m[c] (°C)	ΔH_m[d] (J/g)
80/20	82/18	178	43
60/40	60/40	127	13

[a] Molar ratio of monomers in copolymerization feed.
[b] Molar ratio of lactam and lactone units in electrospun fiber layer from ^{1}H NMR.
[c] Melting temperature.
[d] Melt enthalpy evaluated from the 1st run in DSC measurement.

fibers. Moreover, at higher concentrations, a faster solidification of the jet occurs, mainly for materials with a higher content of crystalline portion (i.e. PEA with a low content of the CLO units). Formic acid evaporates faster from a solution than acetic acid due to its higher vapor pressure. When the content of the CLA units in PEA is high, more formic acid is needed to keep the PEA dissolved. This will occur at higher concentration of the solution much faster.

When 15 wt% solution of PEA CLA/CLO 97/3 ratio is used, no fibers are formed (Fig. 3). The reason is that, due to such as high PEA concentration, relatively high molar mass (Table 1) and a given electric field intensity, charge repulsion does not exceed surface tension and a jet of solution is not ejected from Taylor cone towards the grounded target substrate.

The morphology of fiber layers changed with the polarity of PEA. Very fine fiber layers are shown in Fig. 3 for PEA with 20 mol% CLO units. Further, average size of fibers decreases with increasing content of the CLO units (samples with 20 and 40 mol% CLO units). Aggregation of fibers is evident in PEA with 60 mol% CLO units. It can be explained by (i) low polarity of PEAs as compared to the reference PEA 97/3 and (ii) low crystallinity of the copolymer (see

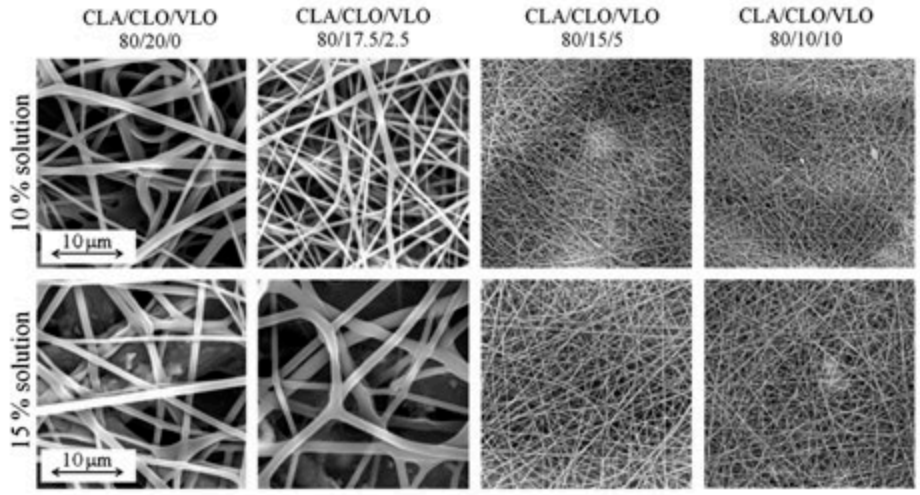

Fig. 4. SEM images of the PEAs fiber layers with the CLA/(CLO + VLO) molar ratio of 80/20, obtained by electrostatic wet spinning (10 and 15 wt% solutions).

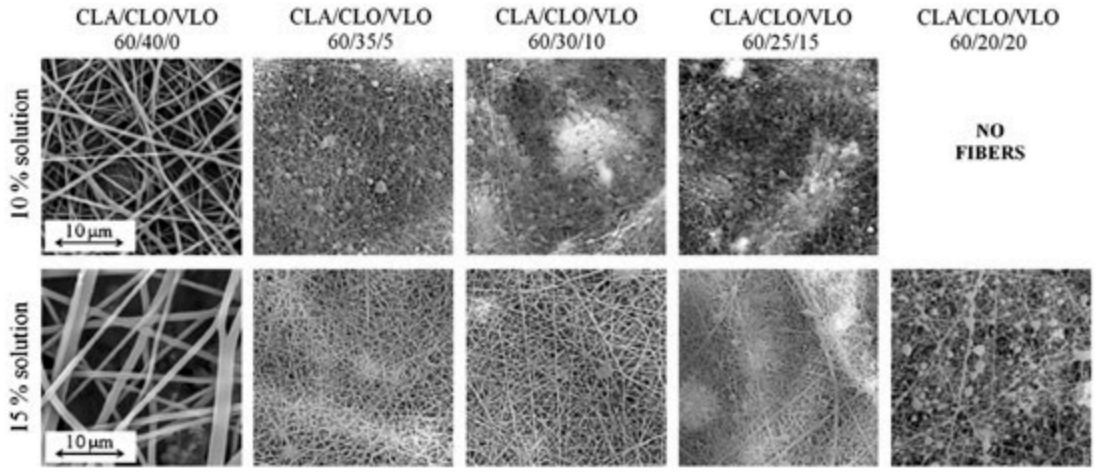

Fig. 5. SEM images of the PEAs fiber layers with the CLA/(CLO + VLO) molar ratio of 60/40, obtained by electrostatic wet spinning (10 and 15 wt% solutions).

Table 1) and (iii) binding the solvent in an amorphous phase of fibers being formed which prevents their fixation.

Table 2 summarizes composition (^{1}H NMR) and thermal properties of selected PEA after electrospinning. Composition of fiber layers and T_m are practically the same as initial material (cf. Table 1). There are differences in ΔH_m, it reflects different crystallization of PEA phase (from melt and polymer solution).

Our attention has been focused on PEAs containing 20 and 40 mol% of lactone structure units and having various molar mass. It is evident from Fig. 4 that, at a given concentration of the solution, fiber morphology is determined by molar mass. With PEAs containing 20 mol% of lactone units and molar mass 17,000 and 12,000 g/mol, fibers in nanoscale range were obtained.

A miscellaneous morphology of fibers was obtained when PEAs contained 40 mol% of lactone units and varying molar mass (Fig. 5). When the concentration of the solution was 10 wt% and molar mass dropped to 11,000 g/mol, beaded fibers occurred. The solution of PEA with molar mass of 7000 g/mol gave no stream of polymer solution from a flat electrode. At the concentration of 15 wt%, it was observed that an increase of PEA molar mass changed gradually the fiber morphology in the following order: beaded fibers, nanofibers and submicron fibers morphologies. The growing chain entanglement has been recognized as the main cause of this progression, as reported in [35]. Therefore, at low concentration of the solution (10 wt%) and low molar mass of PEA (10,000 g/mol), the entanglements between the polymer chains were not sufficiently dense to provide a stable jet and droplets were formed.

4. Conclusion

Polyesteramides having a statistical arrangement of structural units were obtained by anionic copolymerization of ε-caprolactam and ε-caprolactone. The copolymers were used to prepare fiber layers by the technique of electrostatic spinning from their solutions in a mixed solvent formic/acetic acid 1/2. At fixed process parameters, morphology of the fiber layers depended on the polarity of polyesteramides and thus on the content of ε-caprolactone units in the copolymer. The SEM method revealed a crucial effect of the concentration of the copolymer solution and the copolymer composition, especially the content of the polyesteramide amorphous phase, on the values of the fiber diameter. At higher content of the ε-caprolactone units, the fiber layers contained more point junctions.

To study the effect of the system parameters on the morphology of fiber layers in more detail, solutions of polyesteramides containing 20 and 40 mol% lactone units and varying molar mass were tested. The control of polyesteramide molar mass consisted in substituting a part of ε-caprolactone units by δ-valerolactone in the polymerization feed. The ε-caprolactam/lactones units ratio in the extracted polyesteramide was the same as that in the polymerization feed. The statistical nature of the polyesteramides prepared originates from the acylation of the lactam anions and oxianions by the cyclic ester or polyester.

In addition to the copolymer composition and copolymer molar mass, also the concentration of the solution played an important role in determining its spinnability and the morphology of the layers being formed. Quality nanofiber layers were obtained from solutions of polyesteramide containing 20 mol% lactone units and having molar masses of 17,000 and 12,000 g/mol (10 and 15 wt% solution) and that containing 40 mol% lactone units having a molar mass of 11,000 g/mol (15 wt% solution).

Acknowledgement

The research was supported by the Czech Science Foundation (Grant No. 106/09/1378).

References

[1] Fang J, Niu H, Lin T, Wang X. Applications of electrospun nanofibers. Chin Sci Bull 2008;53(15):2265–86.
[2] Formhals A. Process and apparatus for preparing artificial threads. US Patent No. 1 975 504; 1934.
[3] Jirsák O, Sanetrník F, Lukáš D, Kotek V, Martinová L, Chaloupek J. A method of nanofibers production from polymer solution using electrostatic spinning and a device for carrying out the method. CZ Patent 294274 (B6), WO 2005024101; 2005.
[4] Sill TJ, von Recum HA. Electrospinning: applications in drug delivery and tissue engineering. Biomaterials 2008;29(13):1989–2006.
[5] De Vrieze S, De Schoenmaker B, Ceylan Ö, Depuydt J, Van Landuyt L, Rahier H, et al. Morphologic study of steady state electrospun polyamide 6 nanofibres. J Appl Polym Sci 2011;119(5):2984–90.
[6] Heikkilä P, Harlin A. Parameter study of electrospinning of polyamide-6. Eur Polym J 2008;44(10):3067–79.
[7] Marsano E, Francis L, Giunco F. Polyamide 6 nanofibrous nonwovens via electrospinning. J Appl Polym Sci 2010;117(3):1754–65.
[8] Lowery JL, Datta N, Rutledge GC. Effect of fiber diameter, pore size and seeding method on growth of human dermal fibroblasts in electrospun poly(ε-caprolactone) fibrous mats. Biomaterials 2010;31(3):491–504.
[9] Van der Schueren L, De Schoenmaker B, Kalaoglu Öl, De Clerck K. An alternative solvent system for the steady state electrospinning of polycaprolactone. Eur Polym J 2011;47(6):1256–63.
[10] Wang Y, Wang B, Wang G, Yin T, Yu Q. A novel method for preparing electrospun fibers with nano-/micro-scale porous structures. Polym Bull 2009;63(2):259–65.
[11] Malinová L, Benešová V, Lubasová D, Martinová L, Roda J, Brožek J. Polyamide/polyesteramide based nanofibers. Funct Mater Lett 2011;4:365–8.
[12] Michell RM, Müller AJ, Deshayes G, Dubois P. Effect of sequence distribution on the isothermal crystallization kinetics and successive self-nucleation and annealing (SSA) behavior of poly(ε-caprolactone-co-ε-caprolactam) copolymers. Eur Polym J 2010;46(6):1334–44.
[13] Liu S, Li C, Zhao J, Zhang Z, Yang W. Synthesis and characterization of polyesteramides having short Nylon-6 segments in the main chains through polycondensation and chain extension. Polymer 2011;52(26):6046–55.
[14] Goodman I, Vachon RN. Copolyesteramides—II. Anionic copolymers of ε-caprolactam with ε-caprolactone. Preparation and general properties. Eur Polym J 1984;20(6):529–37.
[15] Chromcová D, Baslerová L, Roda J, Brožek J. Polymerization of lactams. 99 Preparation of polyesteramides by the anionic copolymerization of ε-caprolactam and ε-caprolactone. Eur Polym J 2008;44(6):1733–42.
[16] Toncheva N, Jerome R, Mateva R. Anionically prepared poly(ε-caprolactam-co-ε-caprolactone) and poly(ε-caprolactam-co-δ-valerolactone) copolymers: thermal and mechanical properties. Eur Polym J 2011;47(2):238–47.
[17] Bernášková A, Chromcová D, Brožek J, Roda J. Polymerization of lactams, 95 Preparation of polyesteramides by the anionic polymerization of ε-caprolactam in the presence of poly(ε-caprolactone). Polymer 2004;45(7):2141–8.
[18] Brožek J, Šašek V, Prokopová I, Chromcová D, Náhlík J, Erbanová P. Degradation of polyesteramides during composting under standard and isothermal conditions. Folia Microbiol 2009;54(5):451–6.

[19] Chromcová D, Bernášková A, Brožek J, Prokopová I, Roda J, Náhlík J, et al. Degradation of polyesteramides prepared by the anionic polymerisation of ε-caprolactam in the presence of poly(ε-caprolactone). Polym Degrad Stab 2005;90(3):546–54.
[20] Šašek V, Vitásek J, Chromcová D, Prokopová I, Brožek J, Náhlík J. Biodegradation of synthetic polymers by composting and fungal treatment. Folia Microbiol 2006;51(5):425–30.
[21] Goebel CV, Čefelín P, Stehlíček J, Šebenda J. Anionic polymerization of caprolactam. XLIII. Relationship between osmometric molecular weight, viscosity, and endgroups of a polymer. J Polym Sci Part A-1: Polym Chem 1972;10(5):1411–27.
[22] Rybníkář F. Viscometry of polyamides. Chem Listy 1955;49:1442–7.
[23] Kredatusová J, Brožek J. Preparation of clay mineral polymer nanocomposites by adsorption in solution. Appl Clay Sci 2012;62–63:94–100.
[24] Behler K, Havel M, Gogotsi Y. New solvent for polyamides and its application to the electrospinning of polyamides 11 and 12. Polymer 2007;48(22):6617–21.
[25] Dersch R, Liu T, Schaper AK, Greiner A, Wendorff JH. Electrospun nanofibers: internal structure and intrinsic orientation. J Polym Sci Part A: Polym Chem 2003;41(4):545–53.
[26] Jeong JS, Jeon SY, Lee TY, Park JH, Shin JH, Alegaonkar PS, et al. Fabrication of MWNTs/nylon conductive composite nanofibers by electrospinning. Diamond Relat Mater 2006;15(11–12):1839–43.
[27] Li L, Frey MW, Green TB. Modification of air filter media with nylon-6 nanofibers. J Eng Fibers Fabrics 2006;1(1):1–22.
[28] Ryu YJ, Kim HY, Lee KH, Park HC, Lee DR. Transport properties of electrospun nylon 6 nonwoven mats. Eur Polym J 2003;39(9):1883–9.
[29] Tan K, Obendorf SK. Fabrication and evaluation of electrospun nanofibrous antimicrobial nylon 6 membranes. J Membr Sci 2007;305(1–2):287–98.
[30] Ki CS, Baek DH, Gang KD, Lee KH, Um IC, Park YH. Characterization of gelatin nanofiber prepared from gelatin-formic acid solution. Polymer 2005;46(14):5094–102.
[31] Wongsasulak S, Kit KM, McClements DJ, Yoovidhya T, Weiss J. The effect of solution properties on the morphology of ultrafine electrospun egg albumen-PEO composite fibers. Polymer 2007;48(2):448–57.
[32] Dean J. Lange's handbook of chemistry and physics. 15th ed. New York: McGraw-Hill; 1998.
[33] De Vrieze S, Westbroek P, Van Camp T, De Clerck K. Solvent system for steady state electrospinning of polyamide 6.6. J Appl Polym Sci 2010;115(2):837–42.
[34] Daels N, De Vrieze S, Decostere B, Dejans P, Dumoulin A, De Clerck K, et al. The use of electrospun flat sheet nanofibre membranes in MBR applications. Desalination 2010;257(1–3):170–6.
[35] Shenoy SL, Bates WD, Frisch HL, Wnek GE. Role of chain entanglements on fiber formation during electrospinning of polymer solutions: good solvent, non-specific polymer–polymer interaction limit. Polymer 2005;46(10):3372–84.

Appendix 2

LUBASOVA, D., Mullerova J. and Netravali, A. N. Water-resistant plant protein-based nanofiber membranes. Journal of applied polymer sciences 2015;132 (16):1-9.

Journal of Applied Polymer Science

Water-resistant plant protein-based nanofiber membranes

Daniela Lubasova,[1] Jana Mullerova,[1] Anil N. Netravali[2]

[1]Institute for Nanomaterials, Advanced Technologies and Innovation, Technical University of Liberec, Studentska 2, Liberec, 461 17, Czech Republic

[2]Department of Fiber Science and Apparel Design, Cornell University, Ithaca, New York 14853-4401

Correspondence to: A. N. Netravali (E-mail: ann2@cornell.edu)

ABSTRACT: Developing green and sustainable alternative materials to replace petroleum based ones is the need of the day. Such green materials are becoming popular because they can be composted once their useful life is over. In the current research, protein-based nanofibers were fabricated without the use of any toxic cross-linking agent. Defatted soy flour was purified using an acid-wash process to obtain material with higher protein content, blended with gluten, and successfully electrospun into nanofibers with the help of polyvinyl alcohol. Oxidation of sucrose with hydrogen peroxide (H_2O_2) was carried out to synthesize oxidized sugar-containing aldehyde (—CHO) groups and used as green cross-linker. The cross-linking quality of protein-based nanofibers modified by oxidized sugar was found to be similar to nanofibers cross-linked using toxic glyoxal and show good resistance to water. These novel green protein-based nanofibers can be useful in fabricating inexpensive products with very high specific surface area and highly porous structure. © 2015 The Authors Journal of Applied Polymer Science Published by Wiley Periodicals, Inc. J. Appl. Polym. Sci. **2015**, *132*, 41852.

KEYWORDS: biodegradable; biopolymers and renewable polymers; cross-linking; proteins; thermosets

Received 24 October 2014; accepted 8 December 2014

DOI: 10.1002/app.41852

INTRODUCTION

Nanofiber-based membranes have been used in myriad of applications.[1–3] Nearly, all currently used membranes are made using nonbiodegradable polymers derived from petroleum.[4–6] For such nonbiodegradable materials, there are no environmentally acceptable end-of-life solutions as of now. Most of them, unfortunately, end up in landfills. Availability of environment-friendly, biodegradable, and fully sustainable plant-derived polymers such as proteins, starches, and cellulose have slowly begun to change this scenario. Plant-derived proteins and starches also tend to be inexpensive compared to petroleum-based polymers. Other factors contributing to the current "Green Movement" are the abundant availability of the biomass and the possibilities of water-based "green" processing. These advantages have also resulted in developing "green" nanofiber-based membranes as replacement for petroleum-derived nondegradable ones that are being used at present.[7–10] In contrast to the materials derived from petroleum, most plant-based materials can be easily composted after their intended life without harming the nature.

Electrospinning is a simple, low-cost, efficient technique to produce nanofibers.[11,12] It utilizes a high electrostatic field to generate nanofibers from a polymer fluid. Electrospun nanofibers often show large surface-to-weight (volume) ratio, high porosity, and excellent pore interconnectivity. These unique features together with the functionality from the material have opened up enormous potential to use nanofibers in diverse fields such as filtration, tissue engineering, sound absorption, or medicine.[13–16] In most of these cases, the nanofibers can be made using green polymers as well. Several reviews on electrospun biobased materials have been published in the past few years.[17–19] Most of the reported studies, however, are based on polypeptide-based materials such as silk fibroin, collagen, and chitosan. Most of these materials are expensive, and hence, they are used only in niche biomedical applications rather than mass-scale commodity-type applications.[20] Substituting these materials with inexpensive plant-based proteins can provide the means for overcoming some of the cost challenges and can also expand their applications. For example, soybean is one of the most abundant crops grown in the world and the protein derived from it is available commercially in

three different forms, namely defatted soy flour (SF), soy protein concentrate (SPC), and soy protein isolate (SPI). The SF obtained after extracting oil from soybeans contains about 52% protein, the SPC is the next purified version which contains 65–70% protein, and the most purified version, SPI, contains about 90% protein. The rest consists of carbohydrates, minerals, ash, and moisture. Of all these forms, SF is the least expensive (about \$0.50 kg^{-1}) variety. Further, a simple acid-wash process can be used to increase the protein content of SF to the level of about 70% found in SPC.[21] This method is based on precipitating the protein at its isoelectric point (pH 4.5) in water and removing most of the soluble nonprotein constituents, mostly low-molecular-weight carbohydrates. These constituents commonly include water-soluble and some low-molecular-weight nitrogenous substances and minerals. Gluten is another plant-derived material that contains high percentage of protein and is relatively inexpensive (about \$0.90 kg^{-1}). Gluten is composed of various proteins and is mostly obtained from wheat, barley, or rye. When wheat dough is washed to remove starch granules and water-soluble constituents, the rubbery mass that remains is termed as gluten. Depending on the thoroughness of washing, the dry solid gluten contains 75–85% protein and 5–10% lipids. The remaining 5–20% is nonstarch carbohydrates and starch. Gluten is unique in terms of the amino acid composition and contains high amounts of glutamic acid, proline, and low amounts of amino acids with charged side groups, including lysine and histidine.[22]

As mentioned earlier, there is great interest in developing green nanofiber membranes. Several studies have described production of nanofibers prepared by electrospinning of soy protein blends with polyvinyl alcohol (PVA), polylactic acid (PLA), zein or polyethylene oxide (PEO).[23–26] Despite the fact that protein-blend nanofibers have been reported recently, most of them are either water-soluble due to insufficient cross-linking or made insoluble in water by cross-linking using toxic agents. Cross-linking of polymers is one of the most common techniques to obtain enhanced resistance to water and to improve their physical and mechanical properties. Cross-linking is carried out using multifunctional cross-linking agents (cross-linkers) that are capable of chemically reacting with the functional groups present on proteins or other molecules. Protein structure is complex and contains several different amino acids with reactive groups. However, only a small number of functional groups can be targeted for cross-linking. In fact, only four protein functional groups account for most of the cross-linking modifications. These include the following: (a) primary amines (—NH_2) in lysine and arginine residues, (b) carboxyls (—COOH) in aspartic acid and glutamic acid, (c) hydroxyls (-OH) in serine, threonine tyrosine, and (d) sulfhydryls (—SH) in cysteine. For each of these functional or reactive groups present in proteins, there exist many reactive groups that can react with them and form a three-dimensional cross-linked structure.[27] Most commonly used cross-linkers for amine groups are bi-functional compounds, such as glutaraldehyde or glyoxal.[28,29] Both of these cross-linkers, however, are toxic and inappropriate from the environmentally-friendly point of view, and hence, green cross-linkers are preferred. The oxidized sugars (OS) have been found to be useful in such cases and are regarded as green cross-linkers for soy and other protein-based resins.[30–32]

Oxidized sugars are carbohydrates that are oxidized by weak oxidizing agents to generate compounds containing reactive aldehyde or carboxyl groups. The aldehyde groups in OS can cross-link the nucleophilic amino groups in protein-based resins utilizing the Maillard reaction and form bonds responsible for nondisintegration of soy protein-based resin in water.[33] Since OS can have multiple aldehyde groups, they can react with different protein molecules forming a cross-linked system. One of the major advantages of this reaction is that it can be carried out in an aqueous medium.

In this study, we report on the preparation and green cross-linking of very inexpensive protein-based nanofibers focusing on the use of SF. Being the least expensive source of the soy protein with the lowest content of protein, SF was used in this study. However, an acid-wash process was used to increase the protein content of SF to the level of about 70% found in commercial SPC. This "purified soy flour" (PSF) was used as the major constituent for fabrication of nanofiber membrane. The important key factors are as follows: (i) play significant role in electrospinning process of protein-based polymer solution and (ii) influence the morphology of resulted nanofiber membrane are summarized. Part of this study was to cross-link protein nanofibers by green cross-linkers to increase its moisture resistance and, thus, increase the durability. Sucrose was oxidized with H_2O_2 to synthesize OS which has been confirmed as a good cross-linker for protein-based nanofibers using Fourier transform infrared spectroscopy (FTIR) and solubility test. Finally, cross-linking quality of OS was compared with the properties of glyoxal cross-linked nanofibers. Such "green" nanofiber membranes may be used for filtration of dust, bacteria, or viruses and also in biotechnology applications.[34]

EXPERIMENTAL

Materials

Powdered PVA with molecular weight of 130,000 $g \cdot mol^{-1}$ was purchased from Sigma Aldrich, (St. Louis, MO), and gluten was purchased from MGP Ingredients, (Atchison, KS).

SF obtained from Archer Daniels Midland Company (Decatur, IL) was purified using an acid-wash process to obtain PSF with

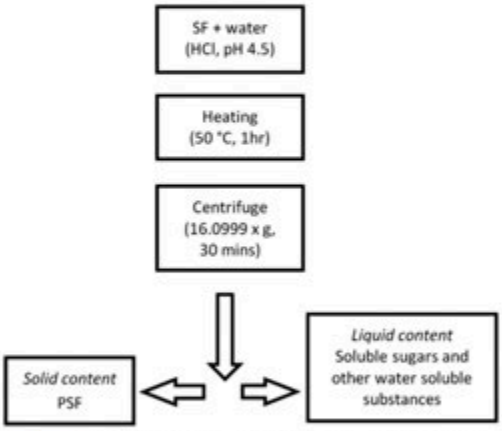

Figure 1. Scheme for purification of soy flour to obtain PSF.

higher protein content. About 10 g of soy flour was dissolved in 100 mL deionized (DI) water, and the solution pH was lowered to 4.5 using HCl. The acidified SF solution was afterward heated to 50°C for 1 hr. Soy protein becomes insoluble in water at its isoelectric point (pH 4.5) and the molecules precipitate, while the sugars remain soluble. As a result, sugars can be filtered out easily from the SF solution increasing its protein content. Centrifuging was found to be useful to separate most of the soluble sugars leaving a PSF residue with a high protein concentration. For this reason, the SF solution was centrifuged for 30 min at 16.099 × g, when the precipitated protein was obtained in solid form. The scheme for the SF purification process to obtain PSF is shown in Figure 1.

Synthesis of cross-linker OS was performed by oxidation of sucrose. The oxidation reaction was carried out for 30 min at 45°C with occasional shaking. Finally, the solution was heated in an oven for two days at 45°C to complete oxidation.

Electrospinning of Nanofibers

Polymer solutions with different compositions of PSF, PVA, and gluten were blended to obtain different protein contents. To obtain the highest possible protein content in nanofibers which contained minimum number or no polymer beads or other defects was one of the main aims of this study. PVA was initially dissolved in DI water at room temperature overnight to obtain a polymer concentration of 14% (by wt.). Gluten and PSF were individually dissolved in water, and the solution pH was adjusted to 11 using NaOH while being heated at 60°C for 30 min. This step was performed to denature the protein and open up the molecules. Solution concentrations for gluten and PSF were kept at 10 and 12% (by wt.), respectively. Thereafter, the individually prepared solutions were mixed together at room temperature in different volume composition to obtain the desired blend proportions of proteins/PVA and stirred for 2 hrs. Various combinations of polymer solutions used in the study are presented in Table I. Triton X-100 (0.5 wt %) was added to all solutions as a nonionic surfactant to obtain uniform dispersion of the protein molecules. Nanofiber membranes were prepared by needle electrospinning for all polymer compositions. All electrospinning experiments were carried out at an applied voltage of 25 kV, polymer solution flow rate of 0.015 mL·min^{-1} and an electrode-collector distance 15 cm. Electrospun nanofibers were deposited on a polypropylene spun-bonded substrate.

Cross-Linking of Protein Nanofibers

Two different cross-linkers, glyoxal and OS, were used to obtain gluten/PSF/PVA resin with higher stability in water. Glyoxal is commercially available but more toxic option, in contrast, the laboratory synthesized OS was used as the green option. Glyoxal is known to cross-link proteins[35] and was used as a benchmark for comparing the quality of the cross-linking of gluten/PSF/PVA nanofibers by OS.

Table I. Polymer Blends Used for the Preparation of Nanofiber Membranes

Polymer blend	Dry basis composition
PSF/PVA	[36/64]
PSF/PVA	[46/54]
Gluten/PVA	[46/54]
Gluten/PSF/PVA	[36/26/38]
Gluten/PSF/PVA	[30/25/45]

Aqueous solution of glyoxal (40%) and 85% phosphoric acid (H_3PO_4), used as catalyst, were purchased from VWR International. As mentioned earlier, PVA was dissolved in DI water to obtain 14% concentration. Glyoxal with H_3PO_4 were added to PVA solutions in three different concentrations 2 hrs before blending with gluten/PSF polymer solution. PVA with gluten/PSF polymer solution was stirred for 2 hrs at room temperature thereafter. Dry basis composition of the final polymer blend was gluten/PSF/PVA [30/25/45], and the amount of glyoxal used was 5, 10, and 15% (by wt.). The surfactant, Triton X-100, was added in the amount of 0.5% (by wt.) to all solution mixtures, as the final step.

As stated earlier, OS was tested as the green cross-linker. Firstly, OS was added to gluten/PSF solutions in different amounts, separately, and stirred for 1 hr at 70°C. PVA solution in required proportion was added to gluten/PSF polymer solution afterward and stirred for 2 hrs at room temperature. The final polymer-blend composition on dry weight basis of gluten/PSF/PVA was [30/25/45] with OS in varying amounts of 5, 10, and 15% (by wt.). As in the case of glyoxal, Triton X-100 as surfactant, 0.5% (by wt. of total solids), was added to all solution mixtures.

The cross-linking reaction was completed to the maximum extent possible under the experimental conditions by heating the nanofiber membranes in an oven at 100°C for 30 min.

Solubility of Protein-Based Nanofibers

Nanofiber membranes prepared from gluten/PSF/PVA with 0, 5, 10, and 15% (by wt.) of glyoxal and OS were fully dried at 60°C for 24 hrs prior to any characterization. The unreacted protein extractions (solubles) were carried out in DI water using Erlenmeyer flasks that were placed on a shaker table (MAXQ 4450, Thermo Scientific) at 175 rpm for: (i) 3 hrs at 60°C, (ii) 6 hrs at 80°C, and (iii) 1 month at room temperature (21°C). The solid residual after extraction was collected using a Whatman filter paper (no. 4, QTY) and dried to constant weight (60°C for 24 hrs). The content of insoluble part (gel), g (%), was calculated according to the following eq. (1):

$$g(\%) = \left(\frac{w_e}{w_d}\right) \times 100 \quad (1)$$

where w_d and w_e are the weights of dry samples before and after extraction, respectively.[36–38]

Other Characterization of Protein-Based Nanofibers

The surface morphologies of nanofibers were characterized using a scanning electron microscope (SEM), LEO 1550 FE-SEM, Zeiss, at an accelerating voltage of 15 kV.

FTIR in attenuated total reflectance (ATR-FTIR) was recorded by Nicolet Magna-IR 560 (Thermo Scientific spectrophotometer). ATR-FTIR spectra were taken in the range of 4000–550 cm^{-1} wave numbers using a split peak accessory. Each scan was an average of 64 scans obtained at a resolution of 4 cm^{-1}

Table II. Protein Content in SPC, SF, PSF, and Gluten Analyzed by Elemental Analysis Technique

Type of protein source	Protein content [%]
SPC	64.4
SF	52.2
PSF	66.1
Gluten	77.7

wave number. Reproducibility was confirmed by repeating the ATR-FTIR analysis three times for each specimen prepared at different times. The spectra of sucrose and OS as well as nanofiber membranes made of gluten/PSF/PVA with 0, 5, and 10% OS before and after cross-linking were compared.

RESULTS AND DISCUSSION

Purification of SF

The protein contents in the SF, gluten, and laboratory prepared PSF were measured by elemental analysis. The average protein content values obtained from three separate tests are presented in Table II. From the results, it is clear that the purification of SF carried out in the laboratory was successful as the protein content in PSF reached 66.1%, up from 52% in SF and was comparable to the protein content of 65–70% found in commercial SPC. The repeatability of the purification process was confirmed by measuring the protein content of three independent purification tests. The standard deviation for the protein content for PSF was 1% of the average protein content value. Based on these results, it was concluded that it is possible to prepare PSF of consistent quality and comparable to the commercially available SPC, from SF using the acid-wash process. The lost material during the purification of SF amounted to about 44%. Commercial gluten was used without modification, since it contained high protein content of over 77%.

Morphology of Protein-Based Nanofibers

The electrospinning was performed to investigate the ability of nanofiber formation from polymer solutions that contained different amounts of proteins. As mentioned earlier, one of the main goals of this paper was to obtain the highest possible protein content in the nanofiber membranes with the least amount of beads and/or other defects. Pure PSF polymer solution heated to 60°C for 30 min and alkali-treated (pH 11) could not be spun into nanofibers. The continuous and uniform fiber formation of pure PSF by electrospinning process was seen as difficult, perhaps due to the complex helical conformations of soy protein in the aqueous solution.[40,41] However, when PVA, a linear polymer, was added, as a "helper polymer," to form PSF/PVA or gluten/PSF/PVA solutions, they were readily electrospun into nanofibers. Figures 2(a–e) show SEM images of nanofibers formed by PSF/PVA [46/54], [36/64], gluten/PVA [46/54], and gluten/PSF/PVA [36/26/38], or [30/25/45] compositions, respectively. As can be seen from Figure 2, electrospinning of PSF/PVA [46/54] or gluten/PVA [46/54] solutions led to nanofiber structure that contained a few polymer beads. The best nanofiber structure without polymer beads, however, was formed in the case of PSF/PVA [36/64] blend. To reach the maximum protein content in the nanofiber membrane, gluten/PSF/PVA compositions were electrospun. Nanofiber structure without any defect was obtained for gluten/PSF/PVA composition with dry basis close to [30/25/45]. Unfortunately, a decrease in PVA content in the polymer-blend gluten/PSF/PVA to [36/26/38] led to fiber structure with beads. The introduction of PVA in the mixed solution gluten/PSF/PVA increased the solution viscosity because of the ionic interactions between polymer molecules, which increased charge density of solution and led to uniform nanofibers without any bead formation.[42] These observations indicate that help from PVA is required to produce protein-based nanofibers, perhaps because of the helical nature of the protein. Nevertheless, protein content of up to 55% could be elctrospun into good nanofibers as shown in Figure 2(e).

Electrospinnable blend of gluten/PSF/PVA [30/25/45] was chosen for the cross-linking study because of its highest content of protein in the nanofibers and their good morphology. Two different cross-linkers (i) glyoxal and (ii) OS were used as mentioned earlier.

Electrospinning of gluten/PSF/PVA composition with 5, 10, and 15% of glyoxal led to very similar fiber structure and contained only a few polymer beads as can be seen in Figure 3. The beads formed during electrospinning process are possibly due to partially cross-linked polymer that is unable to straighten out. Electrospinning of gluten/PSF/PVA solution with 5, 10, and 15% of

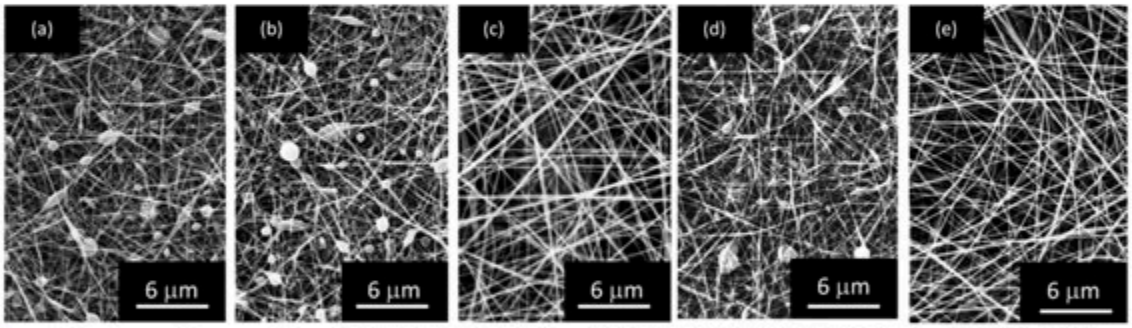

Figure 2. Nanofiber membranes consisting of (a) PSF/PVA [46/54], (b) gluten/PVA [46/54], (c) PSF/PVA [36/64], (d) gluten/PSF/PVA [36/26/38], and (e) gluten/PSF/PVA [30/25/45].

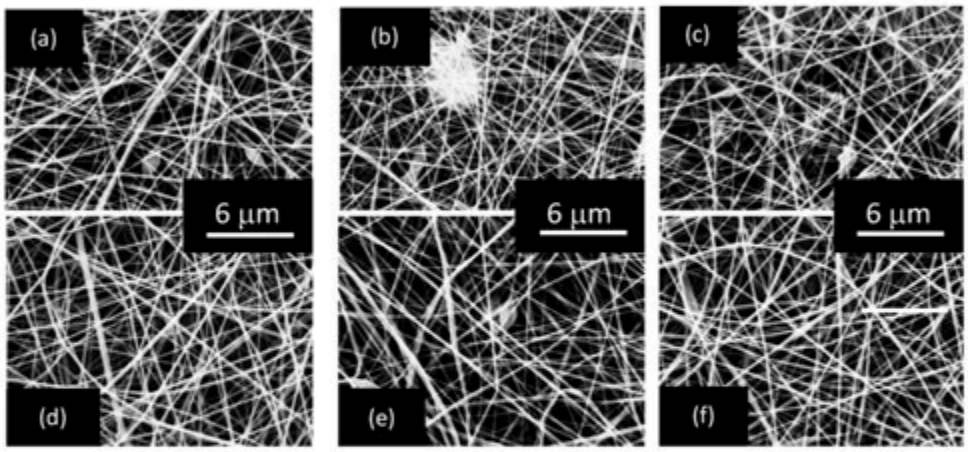

Figure 3. Nanofiber membranes gluten/PSF/PVA [30/25/45] cross-linked by glyoxal: (a) 5 wt %, (b) 10 wt %, and (c) 15 wt % and by OS: (d) 5 wt %, (e) 10 wt %, and (f) 15 wt %.

OS, however, led to the most uniform nanofiber structure with no polymer beads. It is clear from Figures 3(d–e) that the fibers are uniform, cylindrical shaped, and exhibit a narrow range of fiber diameters. This is perhaps because of the lower cross-linking density obtained with OS compared to that obtained by glyoxal.

ATR-FTIR Characterization of OS

Aldehydes (—CHO) are reactive varieties of more general functional group, carbonyl (C═O). The polarity of this bond (especially in the context of aldehydes) makes the carbon atom electrophilic and reactive to nucleophiles such as primary amines. Aldehydes are often used to cross-link proteins that contain amine groups as is the case in the present study.

Aldehyde groups can be created from oxidizable sugar groups.[39] In this study, oxidation of sucrose was carried out by H_2O_2 to generate dialdehyde molecules, which was used as the green cross-linker for gluten/PSF/PVA nanofibers. ATR-FTIR spectra of sucrose before and after the H_2O_2 oxidation are shown in Figure 4. The spectrum clearly shows the absorption peak at 1720 cm^{-1} which corresponds to carbonyl peaks from the oxidation of the primary alcohols to aldehydes. This peak is absent in the unreacted sugar which do not have carbonyl groups. It is also possible that OS contains some carboxyl (—COOH) groups which also results in absorption at 1720–1725 cm^{-1}. The aqueous process along with the use of H_2O_2 as a green and harmless oxidizing reagent for converting sucrose into a cross-linker can be considered as a "green" process as noted by earlier researchers.[30]

Chemical Characterization of Cross-Linked Protein-Based Nanofibers

Figure 5 shows ATR-FTIR spectra of gluten/PSF/PVA nanofiber membranes without cross-linker and after cross-linking reaction with 5 and 10 wt % of OS. The ATR-FTIR analysis of the nanofiber membranes was based on the identification of absorption bands related to the functional groups present in gluten, PSF, PVA, and OS.

A broad band at 3050–3550 cm^{-1} corresponds to hydroxyl (—OH) stretching vibration resulting from the presence of amino acids containing —OH and —COOH groups in proteins as well as the —OH groups in PVA and OS. These groups are

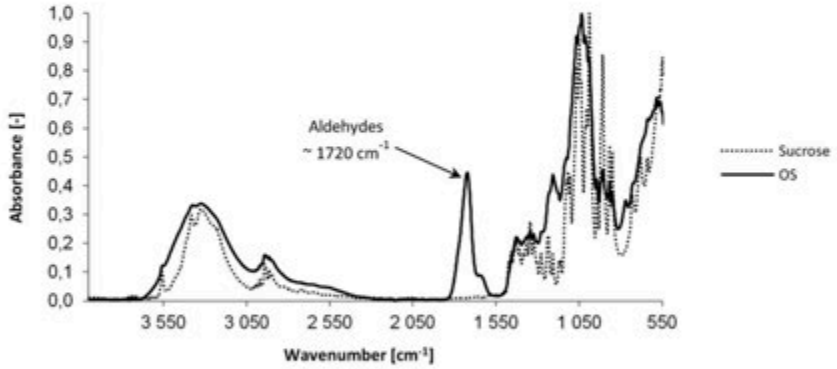

Figure 4. ATR-FTIR spectra of sucrose and OS.

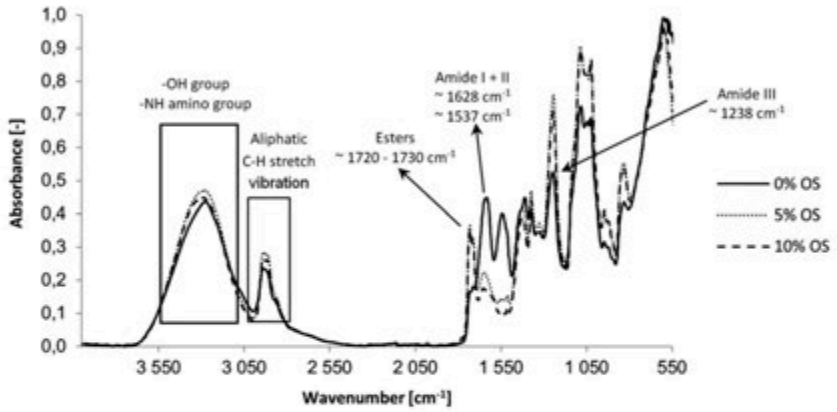

Figure 5. ATR-FTIR spectra of gluten/PSF/PVA nanofiber membranes before and after cross-linking with 5 and 10 wt % of OS.

capable of forming strong intra- and intermolecular hydrogen bonds, in PVA and soy protein as well as with the amino (—NH) groups in protein.[43,44] The absorption band observed between 2820 and 3000 cm^{-1} corresponds to the aliphatic C—H bond (stretching) in PVA as well as protein.[45,46] A typical soy protein spectrum consists of three major peaks, 1628 cm^{-1} corresponding to amide I band (associated with the C—O stretching vibration), 1537 cm^{-1} corresponding to amide II band (N—H deformation) and 1238 cm^{-1} assigned to amide III band (C—N stretching and N—H vibration). ATR-FTIR spectrum of the gluten/PSF/PVA nanofiber membranes without cross-linker in Figure 5 confirms these peaks and agrees well with earlier observations by others.[47,48]

The carboxylic acids formed during sucrose oxidation can also cross-link proteins via formation of anhydride, ester, or amide linkages.[49,50] As can be seen from the spectra shown in Figure 5, absorptions in the range of 1630 and 1530 cm^{-1} shifted down after cross-linking the nanofibers. These strong amide bands present in soy protein disappeared and a new absorption band at about 1720 cm^{-1} appeared after cross-linking assigned to ester peak. These spectral changes indicate cross-linking reaction between the amine groups in the protein and the aldehyde groups in the OS via formation of ester linkages. Because of the large number of amide linkages already present in the PSF, it is not possible to detect the formation of any additional amide bonds. Other formation of imine linkages by the reaction of amine groups with aldehyde is known as Maillard reaction.[30,51] In fact, nucleophilic varieties of primary amines ($—NH_2$) are the main class of compounds that react with aldehydes. Unfortunately, due to the overlap of several peaks in the fingerprint region, it is hard to detect this peak in the ATR-FTIR spectrum. However, the Maillard reaction can be easily confirmed using other characterization techniques including the color change. The Maillard reaction is also known as the nonenzymatic browning reaction and is responsible for the color changes in processed food such as bread, baguette, and most of the bakery products. It is also associated with the color changes that occur during food degradation.[51] The color of the gluten/PSF/PVA nanofiber membranes intensified from pale yellow to brown, as shown in Figure 6, with increasing concentration of OS in gluten/PSF/PVA. Thus, the change in color also indicates, qualitatively, the extent of Maillard reaction. Since this reaction is strongly dependent on reaction conditions such as duration and temperature of reaction, pH and type of sugar present, heating and addition of NaOH to gluten/PSF/PVA solution were carried out to stabilize the conjugation.[33] Addition of NaOH also denatures the protein, that is, opens up the molecules making the Maillard reaction easier.

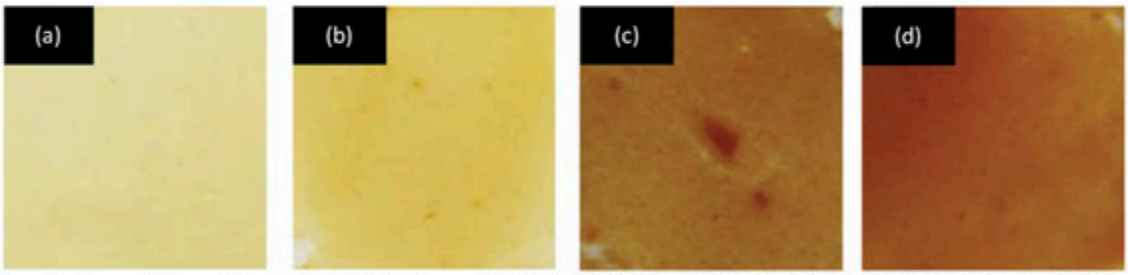

Figure 6. Photographs of nanofiber membranes obtained from gluten/PSF/PVA [30/25/45] with OS: (a) 0 wt %, (b) 5 wt %, (c) 10 wt %, and (d) 15 wt % after cross-linking. [Color figure can be viewed in the online issue, which is available at wileyonlinelibrary.com.]

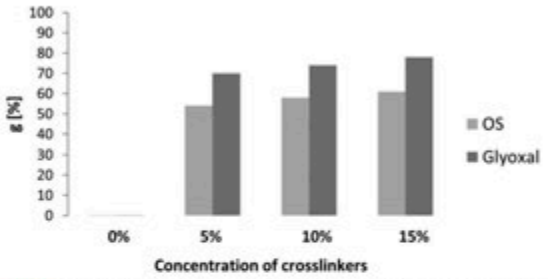

Figure 7. Insoluble content (g) % obtained by the solubility test of gluten/PSF/PVA nanofibers cross-linked by OS and glyoxal.

Solubility of Cross-Linked Protein-Based Nanofibers

The insoluble (cross-linked) content of a given nanofiber membrane was estimated by measuring its insoluble part in dried state after immersion in DI water for, 3 hrs at 60°C, 6 hrs at 80°C, and 1 month at room temperature (21°C). Figure 7 presents the solubility (g [%]) results for nanofibers cross-linked by different cross-linkers: 0, 5, 10, and 15 wt % of glyoxal and OS.

Nanofiber membranes prepared from gluten/PSF/PVA polymer composition without any cross-linkers disintegrated completely within 3 hrs when kept in water at the elevated temperature of 60°C. The results in Figure 7 show that the percentage of insoluble content, g (%), of the cross-linked gluten/PSF/PVA by 5, 10, or 15 wt % of glyoxal reached 70 to 78% depending on the glyoxal concentration. As can be expected, g (%) increased with higher glyoxal content. Since the main reaction occurs between the amine groups in protein and aldehyde groups in glyoxal and that the reaction with the hydroxyl groups in PVA is minimal, the g (%) of 70–78% is considered reasonable. As compared to glyoxal, approximately 54 to 61% of insoluble content was obtained for gluten/PSF/PVA using 5, 10, or 15 wt % of cross-linker OS. Nevertheless, the results of this test demonstrate that the OS did work as a good cross-linker, but the level of cross-linking was slightly lower in comparison to glyoxal. This is believed to be because of the higher number of aldehyde groups present in glyoxal offering more possibilities to link protein macromolecules. All tested nanofiber membranes (cross-linked) did swell when immersed in water, although they remained intact and unbroken as can be seen in Figure 8.

None of the nanofibers prepared from gluten/PSF/PVA composition cross-linked with glyoxal dissolved after any of the testing conditions of 3 hrs at 60°C, 6 hrs at 80°C or 1 month at room temperature. Nanofibers prepared from gluten/PSF/PVA composition with 5 wt % of OS did not dissolve in water after 3 hrs at the temperature 60°C as well. However, after 6 hrs at 80°C, they seem to begin to disintegrate. In contrast, nanofibers cross-linked by 10 and 15 wt % of OS did not dissolve when treated under the same conditions or after 1 month of water immersion at room temperature. Structures of nanofiber membranes immersed in water after 1 month at the room temperature are shown in Figure 8.

Typical SEM images presented in Figure 9 show changes in the nanofiber membrane morphology of gluten/PSF/PVA after cross-linking with 15 wt % of OS and water treatment for 6 hrs and 1 day at room temperature, respectively. Nanofibers can be clearly seen to have swollen after water immersion for 6 hrs compared to unsoaked nanofibers shown in Figures 2 and 3. However, the nanofiber membranes retained the fiber structure even after 1 day of water immersion test, although the pores almost disappared due to swelling.

To compare the water resistance of the plant protein-based green nanofiber membranes with the petroleum-based ones, it is important to realize that both water-resistant and water-soluble polymers made of petroleum are available and that the nanofiber membranes could be fabricated using both of them. This fact plays an important role for final applications. For example, water-resistant nanofibers are desirable in water filtration, whereas water-soluble nanofibers could play an important role in drug delivery systems.

Water-resistant petroleum-based nanofiber membranes with high mechanical properties and good water permeability have contributed in a major way in the water treatment.[52,53] In the past decade, numerous journal articles have documented nanofiber membranes for water treatment applications made from poly(vinyldifluoride),[54] poly(amide),[55] poly(ethersulfone),[56,57] poly(acrylonitrile),[58] etc. In these cases, petroleum-based polymers

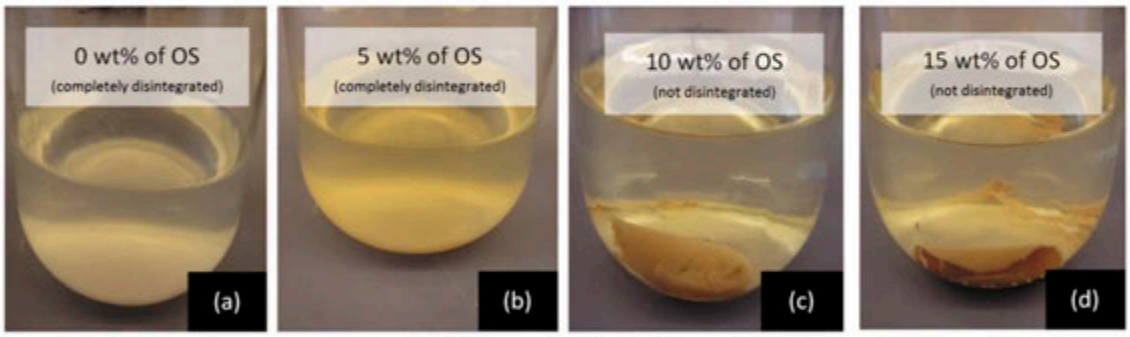

Figure 8. Cross-linked nanofiber membranes of gluten/PSF/PVA immersed in DI water for 1 month: (a) without cross-linker (control), (b) with 5 wt %, (c) with 10 wt %, and (d) with 15 wt % of OS. [Color figure can be viewed in the online issue, which is available at wileyonlinelibrary.com.]

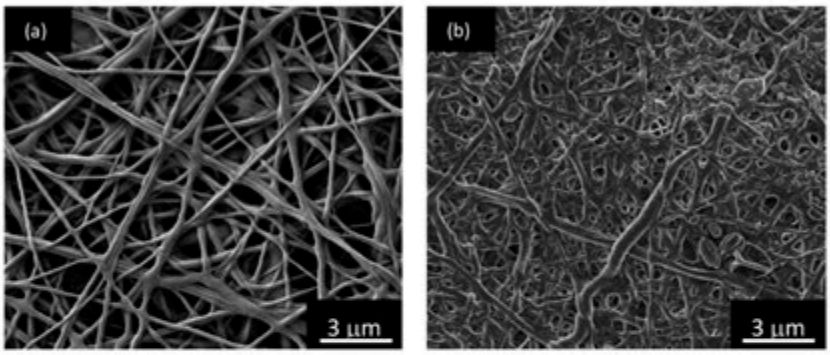

Figure 9. Cross-linked nanofiber membranes of gluten/PSF/PVA with 15 wt % of OS after: (a) 6 hrs of water immersion test and (b) 1-day water immersion test at room temperature.

are water-resistant and do not need any cross-linking. The nanofiber membranes made of these polymers did not change their morphology after immersion in DI water as can be expected.

On the other hand, there are hydrogels or water-soluble nanofiber membranes made from poly(ethylene-glycol), poly(vinyl-pyrrolidone), poly(vinyl-alcohol), poly(ester), poly(acrylic acid) which have been reported as well.[59–62] These polymers are not water-resistant. In these cases, the large surface area of nanofibers can be effective for controlled release of antibiotics or growth factors into wound while the high porosity of nanofiber mats allows rapid diffusion and absorption of body fluids and waste. Such types of petroleum-based nanofiber membranes are not or partially water-resistant which is desirable for this type of application.

In the present study, water-resistant inexpensive plant protein-based nanofiber membranes were prepared by cross-linking them with green cross-linker (OS). By controlling the cross-link density, it should be possible to control either the release rate and/or the nanofiber membrane degradation rate in water.

CONCLUSIONS

The present research discusses fabrication of novel and inexpensive plant protein-based nanofiber membranes prepared by electrospinning process. The SF was successfully purified using an acid-wash process to increase the protein content and used as the major constituent material along with gluten for electrospinning process and successfully spun into nanofiber membranes with no polymer beads or other defects. PVA, a linear polymer, was used as the "helper material" for easier electrospinning. The higher stability of nanofiber membrane in water was achieved by cross-linking reaction without the use of any toxic cross-linkers. OS, prepared by a benign H_2O_2 oxidizing process, was confirmed as a green cross-linker for protein-based nanofiber membranes by ATR-FTIR analysis and solubility test. The stability of protein-based nanofiber membranes in water was confirmed by water immersion test. However, if kept away from water, such nanofiber structures can last for a long time. Also, while the cross-linking achieved by OS was slightly lower than that achieved by glyoxal, the nanofibers do show good resistance to water.

The use of such nanofiber-based membranes for filtering fine dust, bacteria, and possibly, viruses is very promising.[34] These protein-based nanofiber membranes may also be used with other natural resins to develop composite materials with higher value-added products. Finally, some biotechnology applications also seem to be very interesting and promising. To outline future prospects, products based on this type of nanofiber membranes could be promising for tissue engineering, wound healing, or biosensors as well.

ACKNOWLEDGMENTS

This study was financially supported by the Axium Nanofibers, LLC. We would like to thank Dr. Trina Ghosh Dastidar for her help with sugar oxidation experiments. Daniela Lubasova would like to thank the Ministry of Education, Youth and Sports in the framework of National Program for Sustainability I, the OPR and DI project LO1201, Centre for Nanomaterials, Advanced Technologies and Innovation (CZ.1.05/2.1.00/01.0005), the Project Development of Research Teams of R and D Projects at the Technical University of Liberec (CZ.1.07/2.3.00/30.0024) for the support to prepare and complete the manuscript.

REFERENCES

1. Feng, C.; Khulbe, K. C.; Matsuura, T. *J. Appl. Polym. Sci.* **2010**, *115*, 756.
2. Im, J. S.; Kang, S.; Lee, S.; Lee, Y. *Carbon* **2010**, *48*, 2573.
3. Lee, J. Y.; Bashur, C. A.; Goldstein, A. S.; Schmidt, C. E. *Biomaterials* **2009**, *30*, 4325.
4. Ji, L.; Zhang, X. *Nanotechnology* **2009**, *20*, 1.
5. Niu, H.; Zhang, J.; Xie, Z.; Wang, X.; Lin, T. *Carbon* **2011**, *49*, 2380.
6. Asran, A. S.; Seydewitz, V.; Michler, G. H. *J. Appl. Polym. Sci.* **2012**, *125*, 1663.
7. Malinova, L.; Stolinova, M.; Lubasova, D.; Martinova, L.; Brozek, J. *Eur. Polym. J.* **2013**, *49*, 3135.
8. Gui, B. Y.; You, Z. Z.; Shu, D. W.; De Bing, S.; Zhi, H. D.; Wei, G. F. *J. Biomed. Mater. Res. A* **2010**, *93*, 158.

9. Agarwal, S.; Wendorff, J.; Greiner, A. *Polymers* **2008**, *49*, 5603.
10. Malinova, L.; Benesova, V.; Lubasova, D.; Martinova, L.; Roda, J.; Brozek, J. *Funct. Mater. Lett.* **2011**, *4*, 365.
11. Reneker, D. H.; Chun, I. *Nanotechnology* **1996**, *7*, 216.
12. Greiner, A.; Wendorff, J. H. *Angew. Chem. Int. Edn. Engl.* **2007**, *46*, 5670.
13. Cui, W.; Zhou, Y.; Chang, J. *Sci. Technol. Adv. Mater.* **2010**, *11*, 1.
14. Thien, D. V. H.; Hsiao, S. W.; Ho, M. H.; Li, Ch. H.; Shih, J. L. *J. Mater. Sci.* **2013**, *48*, 1640.
15. Mirzaei, E.; Amani, A.; Sarkar, S.; Saber, R.; Mohammadyani, D.; Faridi-Majidi, R. *J. Appl. Polym. Sci.* **2012**, *125*, 1910.
16. Liu, X.; Lin, T.; Fang, J.; Yao, G.; Wang, X. *Adv. Sci. Technol.* **2008**, *57*, 125.
17. Cao, H.; Chen, X.; Yao, J.; Shao, Z. *J. Mater. Sci.* **2013**, *48*, 150.
18. Chen, Z. G.; Wang, P. W.; Wei, B.; Mo, X. M.; Cui, F. Z. *Acta Biomater.* **2010**, *6*, 372.
19. Hassan, M. L.; Fadel, S. M.; El-Wakil, N. A.; Oksman, K. *J. Appl. Polym. Sci.* **2012**, *125*, E216.
20. Khadka, D. B.; Haynie, D. T. *Nanomedicine* **2012**, *8*, 1242.
21. Wang, H.; Johnson, L. A.; Wang, T. *J. Am. Oil Soc.* **2004**, *81*, 713.
22. Wieser, H. *Food Microbiol.* **2004**, *24*, 115.
23. Yao, C.; Li, X. S.; Song, T. Y. *Appl. Polym. Sci.* **2007**, *30*, 380.
24. Phiriyawirut, M.; Rodchanacheewa, N.; Nensiri, N.; Supaphol, P. *Adv. Mater. Res.* **2008**, *55*, 733.
25. Vega-Lugo, A. C.; Lim, L. T. *Food Res. Int.* **2009**, *42*, 933.
26. Cho, D.; Netravali, A. N.; Joo, Y. L. *Polym. Degrad. Stabil.* **2012**, *97*, 747.
27. Wong, S. S. Chemistry of Protein Conjugation and Cross-Linking: National Institutes of Health; CRC Press: USA, **1991**.
28. Park, S. K.; Bae, D. H.; Rhee, K. C. *J. Am. Oil Soc.* **2000**, *77*, 879.
29. Chabba, S.; Netravali, A. N. *J. Mater. Sci.* **2005**, *40*, 6275.
30. Ghosh-Dastidar, T.; Netravali, A. N. *Green Chem.* **2013**, *15*, 3243.
31. Velarde, A. M.; Bartl, P.; Nießen, T. E. W.; Hoelderich, W. F. *J. Mol. Catal. A: Chem.* **2000**, *157*, 225.
32. Comotti, M.; Pina, C. D.; Falletta, E.; Rossi, M. *Adv. Synth. Catal.* **2005**, *348*, 313.
33. Ikan, R. The Maillard Reaction, Consequences for the Chemical and Life Sciences; John Wiley and Sons Ltd.: United Kingdom, **1996**.
34. Lubasova, D.; Netravali, A.; Parker, J.; Ingel, B. *J. Nanosci. Nanotechnol.* **2014**, *14*, 4891.
35. Glomb, M. A.; Monnier, V. M. *J. Biol. Chem.* **1995**, *270*, 10017.
36. Hoffman, A. S. *Adv. Drug Delivery Rev.* **2002**, *43*, 3.
37. Peppas, N. A.; Huang, Y.; Torres-Lugo, M.; Ward, J. H.; Zhang, J. *Annu. Rev. Biomed. Eng.* **2000**, *02*, 9.
38. Wichterle, O.; Lim, D. *Nature* **1960**, *185*, 117.
39. Cho, D.; Nnadi, O.; Netravali, A. N.; Joo, Y. L. *Macromol. Mater. Eng.* **2010**, *295*, 763.
40. Wolf, W. J.; Peterson, R. E.; Schaer, M. L. *J. Agric. Food Chem.* **1992**, *40*, 1809.
41. Renkema, J. M. S. Formation, Structure and Rheological Properties of Soy Protein Gels. PhD Thesis, Wageningen University: The Netherlands, **2011**.
42. Lin, T.; Wang, H.; Wang, H.; Wang, X. *Nanotechnology* **2004**, *15*, 1375.
43. Gohil, J. M.; Bhattacharya, A.; Ray, J. *J. Polym. Res.* **2006**, *13*, 161.
44. Mansur, H. S.; Sadahira, C. M.; Souza, A. N.; Mansur, A. A. P. *Mater. Sci. Eng. C.* **2008**, *28*, 539.
45. Qiu, K.; Netravali, A. N. *Polym. Composite.* **2013**, *34*, 799.
46. Qiu, K.; Netravali, A. N. *J. Mater. Sci.* **2012**, *47*, 6066.
47. Chittur, K. K. *Biomaterials* **2006**, *19*, 357.
48. Lu, C. F.; Nadarajah, A.; Chittur, K. K. *J. Colloid. Interf. Sci.* **1994**, *168*, 152.
49. Nakamura, R.; Netravali, A. N.; Morgan, A. B.; Nyden, M. R.; Gilman, J. W. *Fire Mater.* **2012**, *37*, 75.
50. Huang, X.; Netravali, A. N. *J. Macromol. Sci., A.* **2008**, *45*, 899.
51. George, P. R. *Food Rev. Int.* **1997**, *13*, 1.
52. Balamurugan, R.; Sundarrajan, S.; Ramakrishna, S. *Membranes* **2011**, *1*, 232.
53. Feng, C.; Khulbe, K. C.; Matsuura, T.; Tabe, S.; Ismail, A. F. *Sep. Purif. Technol.* **2013**, *102*, 118.
54. Gopal, R.; Kaur, S.; Ma, Z.; Chan, C.; Ramakrishna, S.; Matsuura, T. *J. Membr. Sci.* **2006**, *281*, 581.
55. Aussawasathien, D.; Teerawattananon, C.; Vongachariya, A. *J. Membr. Sci.* **2006**, *315*, 11.
56. Homaeigohar, S.Sh.; Buhr, K.; Ebert, K. *J. Membr. Sci.* **2010**, *365*, 68.
57. Tang, Z.; Qiu, C.; McCutcheon, J. R.; Yoon, K.; Ma, H.; Fang, D.; Lee, E.; Kopp, C.; Hsiao, B. S.; Chu, B. *J. Polym. Sci. Polym. Phys.* **2009**, *47*, 2288.
58. Kaur, S.; Barhate, R.; Sundarrajan, S.; Matsuura, T.; Ramakrishna, S. *Desalination* **2011**, *279*, 201.
59. Zhu, J.; Marchant, R. *Expert Rev. Med. Devic.* **2011**, *8*, 607.
60. Yu, D.; Shen, X.; Zhang, X.; Branford-White, C.; Zhu, L. *Acta Polym. Sini.* **2009**, *11*, 1171.
61. Dai, M.; Jin, S.; Nugen, S. R. *Biosensors* **2012**, *2*, 388.
62. Mollá, S.; Compañ, V. *J. Membr. Sci.* **2011**, *372*, 191.

Appendix 3

LUBASOVA, D., Netravali, A.N., Parker, J. and Ingel, B. Bacterial filtration efficiency of green soy protein based nanofiber air filter. Journal of nanoscience and nanotechnology 2014;14 (7):4891–4898.

Journal of
Nanoscience and Nanotechnology
Vol. 14, 1–8, 2014

Bacterial Filtration Efficiency of Green Soy Protein Based Nanofiber Air Filter

D. Lubasova[1,2], A. Netravali[2,*], J. Parker[3], and B. Ingel[3]

[1] *Technical University of Liberec, The Institute for Nanomaterials, Advanced Technologies and Innovation, Liberec, Studentska 2, 461 17, Liberec 1, Czech Republic*
[2] *Cornell University, Fiber Science and Apparel Design, 233 Human Ecology Building (HEB), 148 50, Ithaca, NY*
[3] *Cornell University, Baker Institute for Animal Health, College of Veterinary Medicine, Hungerford Hill Road, 148 53, Ithaca, NY*

High bacterial filtration efficiency (BFE) filters, based on nanofibers derived from blends of grain proteins and poly-ethylene-oxide (PEO), were produced by an electrospinning process. Specifically, polymer blends consisting of purified soy flour/PEO with a ratio of 7/3 were spun into nanofibers and characterized. A new laboratory based experimental apparatus for testing BFE was designed and used to test BFE of bacterial aerosols consisting of Escherichia coli (*E. coli*). Performances of soy protein based nanofiber filters with nanofiber mass varying from 1 to 5 g/m^2 as well as a nanofiber filters prepared from pure PEO were compared. The results showed that BFE values for filters containing 5 g/m^2 protein based nanofibers and PEO nanofiber filter were 100 and 81.5%, respectively. The results also indicated that the BFE increased as the protein content in the nanofiber filter increased. These novel protein based nanofiber filters have demonstrated a clear potential for effective removal and retention of *E. coli* bacteria during air-filtration. These filters can be effectively deployed in environments such as hospitals and senior residential areas to reduce bacterial infections.

Keywords: Electro-Spinning, Soy Protein, Nanofibers, E. Coli, Air Filtration.

RESEARCH ARTICLE

1. INTRODUCTION

Soybean is one of the most abundant crops grown in the world and the protein derived from it is available commercially in three different forms: soy protein isolate (SPI), soy protein concentrate (SPC) and defatted soy flour (SF) which contain ~90, 70 and 52% protein, respectively. An acid-wash process has been commonly used to increase the protein content of SF to the level (70%) found in SPC.[1] This method is based on precipitating the protein at its isoelectric point (pH 4.5), in water, and then removing most of the soluble non-protein constituents. These constituents commonly include water, soluble carbohydrates (sucrose, glucose, fructose, raffinose and stachyose) and some low molecular weight nitrogenous substances and minerals. Soy proteins are globulins, carry no net charge and become insoluble in water in the regions of their isoelectric point (pH 4.5). On the other hand, the sugars and other water soluble substances remain in solution under this condition and can then be separated from the SF protein precipitate by filtration or centrifugation.

The charge on a protein molecule affects its behavior and can play an important role in applications such as filters where the charge can be used to attract particles as shown in previous researches.[2–4] Proteins contain many ionizable groups on their amino acid side chains. These include the basic side chains of lysine, arginine and histidine, the acidic side chains of glutamate and aspartate and the hydroxyl groups found on the side chains of serine, threonine and tyrosine. In general terms, as the pH of a protein-containing solution increases, deprotonation of the acidic and basic groups occurs, such that carboxyl groups are converted to carboxylate anions (R-COOH to R-COO$^-$) and amine groups are converted to amino groups (R-NH$_3^+$ to R-NH$_2$).[5]

Bacterial attachment to a surface is influenced by surface charges on the bacterial cell and on the substrate. Gram-negative bacterial cells have a net negative charge on their cell walls;[6] the magnitude of this charge is strain-dependent. The surface charge of bacterial cells has been measured by electrostatic interaction chromatography.[7,8] Dickson and Koohmaraie studied the relationship between cell surface charge and bacterial attachment to the surface of meat. They found out that some of the tested bacterial

*Author to whom correspondence should be addressed.

strains exhibited either negative or positive charges. For example, *E. coli* have an outer membrane composed of phospholipids and lipopolysaccharides that impart a strong negative charge to the surface of these gram-negative bacterial cells.[9]

From then until today, nanofibers technology has benefited numerous industries including filtration, transportation, construction, agriculture, etc.[10–16] The filter technology developed in the present study consists of soy protein based nanofibers produced by an electrospinning process. Electrospinning process is a simple low-cost method that can produce nanofibers and nanofiber based membranes with very high specific surface areas and a porous structure.[17,18] Many papers have discussed the antibacterial properties of nanofibers prepared using electrospinning method.[19–21] In most cases silver and TiO_2 nanoparticles or other antibacterial agents are incorporated into nanofibers during electrospinning. Some of the toxic and non-biodegradable agents will not decompose through natural processes and can have long-lasting damage to the soils. When put in landfills, these toxic pollutants can also contaminate ground water. On the other hand, natural products such as soy protein break down easily when they are disposed as waste and are environmentally friendly. Also, adding TiO_2, nanosilver, or other additives into nanofibers can increase the cost of final filter. Our goal was to understand and characterize the capabilities of the protein based nanofiber filters in capturing bacteria by themselves.

Commercially available bacterial and viral filters do provide effective protection against various types of particles including bacteria, viruses and moisture droplets. These filters help protect the patient, the equipment, and the breathing circuit or apparatus from getting contaminated. Several types of bacterial filter are available and currently being used. These primarily include glass and ceramic filters. Glass filters mostly consist of porous glass, sealed into funnels while the ceramic filters are made of kaolin or kieselguhr. These bacteria filters are available in specific configurations depending upon the nature of their use. However, these filters are mainly used for sterilization and cleaning fluids of bacteria.

While different testing methods to characterize the antibacterial properties have been used, the nanofiber layers have been commonly tested by agar diffusion tests.[22,23] In these tests a small piece of the specimen to be characterized is placed on an agar plate, inoculated with a test microorganism and then incubated for a specific period. After incubation the agar plates are inspected for the growth of bacteria and the antibacterial effect is estimated from the size and number of bacterial colonies surrounding the specimen. This method, however, only provides a qualitative measure of the efficiency of the antibacterial additive. In addition, the agar diffusion test is not useful for testing the bacterial filtration efficiency (BFE) of airborne microorganisms. In the present study nanofiber based filters were prepared and characterized for their BFE by drawing aerosolized *E. coli* through the filters in placed in the testing apparatus specially built for the study. The filtered aerosol passed over an agar gel where any bacteria present could be deposited. The bacterial colonies were counted after incubation to obtain a quantitative measurement of the filter BFE.

2. EXPERIMENTAL DETAILS

2.1. Purified Soy Flour, Highly Purified Soy Flour and Other Materials Used for Production of Nanofibers

Soy flour was obtained from Archer Daniels Midland Company (Decatur, IN, USA). Soy flour with 53% nominal protein content was purified using an acid-wash process to obtain purified soy flour (PSF) with ∼66% protein content. Soy flour was purified by dissolving 10 g in 100 mL deionized (DI) water and then lowering the pH to 4 by addition of HCl. The acidified soy flour solution was then heated at 50 °C for 1 hour and the precipitated protein filtered using a water aspirator as a vacuum source for 10 minutes to obtain PSF. Soy protein is insoluble at its isolectric point (pH 4) and is precipitated while sugars remain soluble. Filtering thus removes most of the soluble sugars leaving a PSF residue with a higher protein concentration.

To obtain highly purified soy flour (HPSF), 10 g of soy flour was dissolved in 100 mL of DI water, adjusted to pH 8.5 by the addition of NaOH, and heated at 60 °C for 30 minutes. The solution was then centrifuged for 30 minutes at 16,099 × g. The protein-containing supernatant was removed and adjusted to pH 4.5 by the addition of HCl. Protein was then precipitated by incubating the acidified supernatant to 4 °C for 1 hr and the HPSF was pelleted by centrifugation.

Powdered polyethylene-oxide (PEO) with molecular weight of 6×10^5 g/mol was purchased from Sigma Aldrich, (St. Louis, MO).

2.2. Electrospinning Setup and Polymer Compositions

In the electrospinning method the spinning jets originate from the surface of the polymer solution and thus the process does not need any nozzles or needles (the nozzleless or needle-less free liquid surface technology).[24] The method is based on creating multiple Taylor cones that create multiple jets from a thin layer of polymer solution placed on a flat circular electrode. The fluid jets ejected from the Taylor cones form the nanofibers which are carried onto a collector. Since multiple jet streams are formed simultaneously over the entire surface of the flat electrode, this process results in much higher production capacity in comparison to single-needle electrospinning process.

Polymer solutions with different compositions were prepared to obtain different protein contents in the resulting

solutions. There were prepared polymer blends PSF/PEO with dry basis ratios [9/1], [8/2] and [7/3], HPSF/PEO, SPI/PEO and SPC/PEO with dry basis ratio [7/3]. PEO was dissolved in DI water at room temperature overnight to achieve a polymer concentration of 5% (by wt%). SPI, SPC, PSF and HPSF were individually dissolved in water and the solution pH was adjusted to 11 using NaOH while being heated at 60 °C for 30 min. Under these pH and heat conditions, SPI, SPC, PSF and HPSF dissolved easily and formed transparent solutions. Solution concentrations for SPI, SPC, PSF and HPSF were kept at 12% (by wt%). Thereafter, the individually prepared solutions were mixed together at room temperature with different volume ratios and stirred for 2 hours. Triton X-100 (1 wt%) was added to all solutions as a non-ionic surfactant. Electrospinning of polymer solutions was carried out at a voltage of 30 kV and an electrode-collector distance of 15 cm. Electrospun nanofibers were deposited onto different substrates as described below.

2.3. Tested Filters

Polymer solutions with different compositions (SPI/PEO, SPC/PEO, SF/PEO, PSF/PEO,HPSF/PEO and pure PEO) were electrospun onto grade no. 1 cellulose based filter paper or non-woven fabric 2006 purchased from Fiberweb® (Figs. 1(a) and (b)). The resulting nanofiber filter consisted of a single nanofiber layer placed (bonded) onto the filter paper or the non-woven fabric substrate. The weight of the nanofiber layer was varied between 1 and 5 g/m.^{2} For comparison, nanofiber filter made from pure PEO and commercially available air filter Energy Aire® (Flanders Corp., Washington, NC) with a MERV rating of 6 and filter thickness of about 4 mm were also characterized in this study (Fig. 1(c)). A MERV rating of 6 means that the filter has 35 to 50% minimum efficiency at capturing particles sized 3–10 μm. This is a general purpose filter for household dust and lint and did not contain any nanofibers. It is also not meant to be used for bacterial filtration.

2.4. Test Agent

A non-pathogenic BSL-1 laboratory strain of *E. coli* K-12 was chosen as the biological test agent. Bacterial stocks were grown in Luria-Bertani medium at 37 °C until the optical density at 600 nm of the solution was equivalent to 0.5–0.6 (OD_{600}).[25] This led to a stock bacterial solution that had a concentration of 4–4.8 $\times$ 10^8 bacterial cells per mL that was used for bacterial aerosolization. An optical image of the bacterial stock suspension prepared from single colony from a freshly grown agar plate of *E. coli* strain is shown in Figure 2. It is clearly seen that the bacteria used in all experiments are round shaped with typical size of 2 μm.

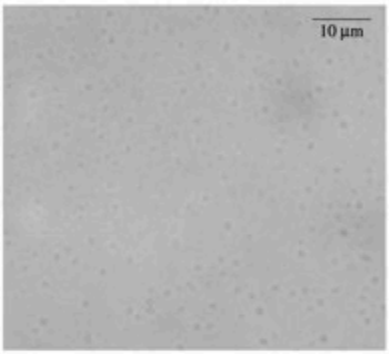

Fig. 2. Bacterial suspension of E. coli under the optical microscope.

2.5. Bacterial Filtration Efficiency Testing

A schematic drawing of the bacterial filtration efficiency testing apparatus that was built and used in this study is shown in Figure 3(a). A bacterial aerosol was generated using a nebulizer (model no. 45) obtained from DeVilbiss Healthcare, LLC (Somerset, PA). The hand-held spray nebulizer generated an aerosol with particle sizes between 0.3 and 5 microns of uniformly consistent density. The aerosol was introduced into the upper chamber of the testing apparatus and the bottom outlet was connected to the vacuum such that the aerosol was drawn through the filter; the filtered air then passed over the agar plate depositing any bacteria that had passed through the filter. The assembled version of the apparatus is shown in Figure 3(b). The top and bottom chambers of the apparatus were made

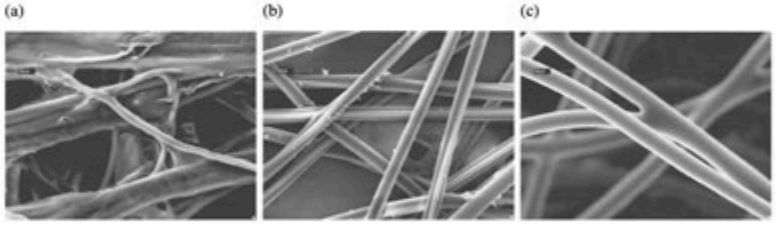

Fig. 1. SEM of: (a) grade no. 1 filter paper, (b) non-woven fabric 2006 and (c) commercially available air filter energy aire® (Flanders Corp., Washington, NC).

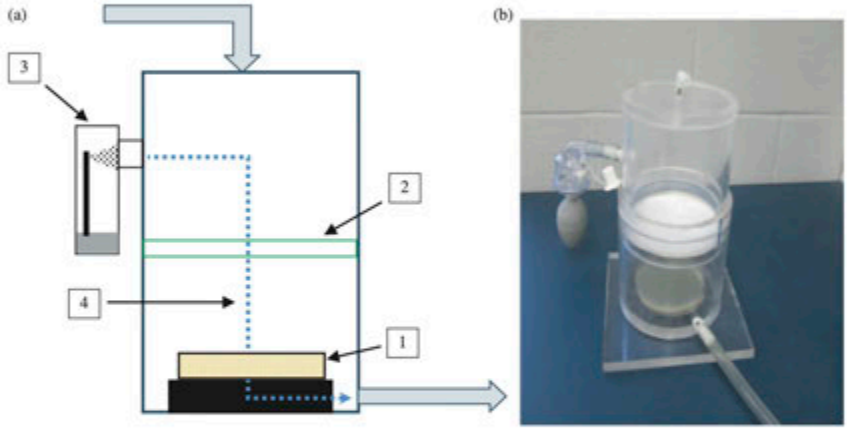

Fig. 3. (a) A schematic drawing and (b) photograph of the bacterial testing apparatus: 1—an agar plate, 2—testing filter, 3—nebulizer, 4—aerosolized bacteria.

separable to allow introduction of an agar plate and to allow filters to be mounted and removed.

The BFE test was conducted by introducing the aerosolized bacteria (*E. coli*) into the top chamber of the testing apparatus. A vacuum was then applied across the filter for 5 minutes. This allowed the aerosol to flow from the top chamber to the bottom chamber by passing through the filter and any bacteria that passed through the filter were then deposited onto the agar plate. The vacuum was maintained for 5 minutes to ensure that all bacteria were cleared from the testing chamber. The agar plates with bacteria, if any, were incubated overnight at 37 °C. After 24 hours the numbers of bacterial colonies present on each agar plate were counted. Four independent tests were performed for each condition.

3. RESULTS AND DISCUSSION

3.1. Purification of PSF and HPSF

The protein content in the commercially obtained SPI, SPC, SF and laboratory prepared PSF, HPSF specimens was measured by elemental analysis. It was found out that purification of SF was successful in both cases. Protein content in HPSF and SPI were comparable (88.7 and 85.8%, respectively). Similarly, the protein content in PSF and SPC were comparable (66.1 and 64.4%, respectively). The protein content in PSF and HPSF, increased from 52 (in SF) to about 66 and 89%, respectively, after the SF purification. The repeatability of the purification process was confirmed by measuring the protein content on three independent purification tests. The standard deviation in protein content for both PSF and HPSF was 1% of the average protein content. Based on this finding it was concluded that it is possible to prepare products very similar to SPC and SPI in the laboratory from SF using an acid wash process for PSF and a two-step sequential alkali and acid wash process for HPSF.

3.2. Electrospinning of Polymer Mixtures Consisting of SPI, SPC, PSF or HPSF

A pure SPI, SPC, PSF or HPSF heated to 60 °C for 30 min and alkaline-treated could not be spun into nanofibers. However, when PEO was added, a SPI/PEO, SPC/PEO, PSF/PEO or HPSF/PEO solution could be readily electrospun into nanofibers. Figure 4 shows SEM images of nanofibers formed by (a) PSF/PEO [9/1], (b) PSF/PEO [8/2], (c) PSF/PEO [7/3], (d) HPSF/PEO [7/3], (e) SPC/PEO [7/3] and (f) SPI/PEO [7/3]. Nanofiber structures were obtained for all PSF/PEO, HPSF/PEO, SPI/PEO and SPC/PEO blends with dry basis ratio close to 7/3. PEO content of lower than 30% led to fiber structure with polymer beads. The most polymer beads were formed in the PSF/PEO [9/1] blend (Fig. 4(b)). It was noted that increasing the PEO content in the PSF/PEO or HPSF/PEO polymer blend led to a fibrous structure. This effect can be attributed partially to the increase in viscosity with increased PEO content that results in enhanced polymer chain entanglement which reduces the surface tension of the polymer and prevents bead formation.[26–30] These observations confirm earlier results that PEO is required to produce protein based nanofibers and aids in electrospinning of protein blends.

3.3. Bacterial Filtration Efficiency of Filter Paper, Nanofiber Based Filter and Commercial Filter

The BFE of filter paper covered with nanofibers prepared using a PSF/PEO [7/3] blend with a fiber weight of 5 g/m^2,

RESEARCH ARTICLE

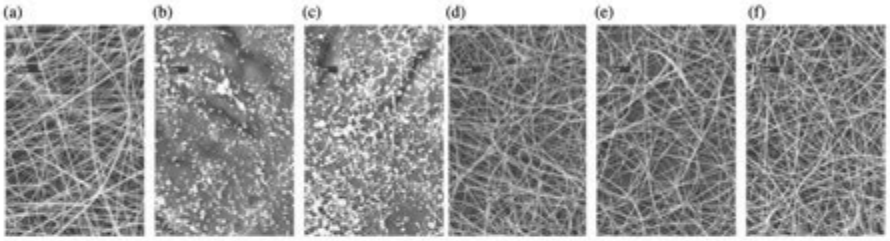

Fig. 4. Nanofiber layers consisting of: (a) PSF/PEO [9/1], (b) PSF/PEO [8/2], (c) PSF/PEO [7/3], (d) HPSF/PEO [7/3], (e) SPC/PEO [7/3] and (f) SPI/PEO [7/3].

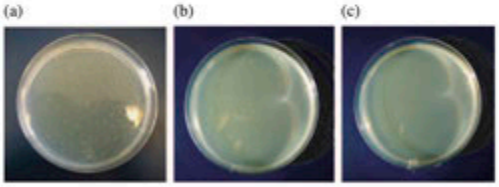

Fig. 5. Photographs of agar plates with bacterial colonies following BFE testing of: (a) no filter, (b) filter paper alone (c) and filter paper coated with nanofibers (5 g/m^2) prepared using a PSF/PEO [7/3] blend.

was compared with that of filter paper without nanofibers, filter paper with pure PEO and a commercial filter (Energy Aire®) using the bacterial testing apparatus shown in Figure 3. Typical results obtained on agar plates showing bacterial colonies after the BFE tests and overnight incubation are shown in Figure 5.

The numbers of colonies on agar plates without the use of a filter (control), with filter paper alone, with filter paper coated with nanofibers, with a commercial filter (Energy Aire®) for four independent experiments are presented in Table I. Average BFE values were calculated using Eq. (1) and are compared in Figure 6. Average BFE values of 100, 81.5% and 58.5% were obtained for filter paper with 5 g/m^2 nanofibers prepared using a PSF/PEO [7/3] blend, pure PEO and filter paper without nanofibers, respectively. These data clearly indicate that protein nanofibers are highly effective in filtering bacteria in comparison to filters prepared using pure PEO nanofibers with equal wt of fibers. The commercial Energy Aire® filter which did not contain any nanofibers had the lowest BFE (20.8%).

$$\begin{aligned}\text{Efficiency} = {} & ((\text{number of colonies without filter}) \\ & -(\text{number of colonies with filter})) \\ & \cdot(\text{number of colonies without filter})^{-1} \\ & \times 100 \end{aligned} \quad (1)$$

To understand the bacteria trapping mechanism, the filters were examined by SEM after the BFE tests (Fig. 7). The SEM images show that the protein based nanofibers have bio-adhesive properties as all of the bacteria were attached to the nanofibers even when the pore sizes were many times larger than the size of the bacteria. This is believed to be because of the positive electrical charge on the protein based nanofibers that attracts and attaches the electronegative particles such as the aerosolized *E. coli*. In addition, as expected, the nanofiber based filters have much smaller pore sizes, though significantly larger compared to the size of *E. coli* bacteria, than the other tested filters. The common mechanisms by which filter media can capture particles include inertial impaction, interception, diffusion, electrostatics and sieving.[31] Sieving is the most common mechanism in filtration and occurs when particles are too large to pass between the fiber spaces or pores. Electrostatic filters are based on their capacity to attract and bind charged particles of the opposite charge as they traverse the media. The results of this study strongly suggest that electrostatic attraction is the predominant mechanism while sieving mechanism may also exist. The small

Table I. Bacterial colony counts on agar plates in the absence of a filter or when aerosolized bacteria were passed through a paper filter, a paper filter coated with nanofibers, or a commercial filter.

	Number of colonies without a filter	Number of colonies with paper filter	Number of colonies with a paper filter PSF/PEO [7/3] nanofibers (5 g/m^2)	Number of colonies with a paper filter with PEO nanofibers (5 g/m^2)	Number of colonies with a commercial filter energy aire®
	174	72	0	32	137
	179	76	0	33	142
	177	74	0	34	141
	172	69	0	31	136
AVG	175.5	72.8	0	32.5	139.0
BFE (%)		58.5	100.0	81.5	20.8

RESEARCH ARTICLE

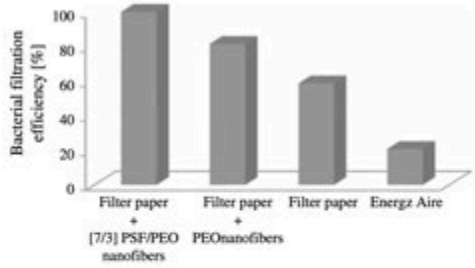

Fig. 6. Bacterial filtration efficiency of tested substrates.

diameters of the fibers provide ample surface area to attract bacterial particles and thus result in high BFE for the protein nanofiber based filter. In addition, the bio-adhesive properties of the protein keep the *E. coli* bound to the nanofibers. These properties along with small pore sizes of the nanofiber membrane make this material promising for bacterial filtration.

The net charge on the protein is determined by the sum of the positively and negatively charged amino acid residues.[16] For example, if a protein has aspartic and glutamic acid residues, it carries a negative charge at pH 7 and is termed an acidic protein. If it has lysine and arginine residues, it is considered to be a basic protein and carries a positive charge at pH 7. The equilibrium between charged and uncharged groups and hence the net charge of a protein is determined by the pH of the solution. The charge of the ionizable groups found on unmodified proteins as a function of pH is shown in Table II.

The unique biochemical properties of amino acids are defined by the type of side chains they possess. Amino acid residues that can possess an electric charge depending on their protonation include lysine (+), arginine (+), histidine (+), aspartic acid (−) and glutamic acid (−). There are 18 amino acids that are commonly present in soy protein.[20] In general, soy protein contains numbers of amino acids with negative charge (aspartic acid and glutamic acid) 34.7% and amino acid residue with positive charge (Histidine, Lysine, Arginine) 17.3%. Hence it is believed that soy protein may be the main constituent in attracting gram negative *E. coli* bacteria.

3.4. Effect of Nanofiber Mass on BFE

The effect of fiber weight of nanofibers spun onto non-woven fabric 2006 was studied in the second set of experiments. PSF/PEO blend with a dry basis ratio of [7/3] was prepared as before. Nanofibers were electrospun onto non-woven fabric 2006 with various deposition times to obtain filters with nanofiber weights of 0, 1, 3 and 5 g/m.^{2} BFE was then characterized using the testing apparatus as in the previous experiment. Three independent experiments were performed to obtain average BFE. These results are presented in Table III. The results clearly show that the BFE increased from 89.0 to 100% as the fiber weight of the nanofibers deposited on non-woven fabric increased from 1 to 5 g/m.^{2}

It is common sense that filters with lower pressure gradients across them are preferable, as they need smaller fans to draw or push air across them and, as a result, they consume less energy. For this reason non-woven fabric 2006 which has a lower pressure gradient across it than the filter paper was investigated in this study. The BFE of non-woven fabric was slightly higher than that of the filter paper (69.5 vs. 58.5%; compare Figure 6 with Table III). The BFE of non-woven fabric was further increased significantly (from 69.5 to 96.8%) by the addition of 3 g/m^2 nanofiber wt. Further increase in the nanofiber wt. to 5 g/m^2 increased the BFE only slightly, but to maximum possible of 100%. These results clearly indicate that the BFE is strongly correlated to the nanofiber mass, which in turn, is related to higher protein content, higher surface area of nanofibers and lower pore size.

3.5. Effect of Protein Content on BFE

To assess the effect of nanofiber protein content on BFE, non-woven fabric 2006 containing nanofibers spun from SPI/PEO, SPC/PEO, SF/PEO, PSF/PEO and HPSF/PEO blends with dry basis ratio [7/3] were prepared. The protein content in the commercial SPI, SPC, SF was 85.8, 64.4, 52.2%, respectively and laboratory prepared PSF and HPSF was 66.1 and 88.7% respectively. Nanofibers were spun onto non-woven fabric with fiber weights of 1 or 3 g/m^2 and their BFE tested. The protein content in nanofibers and average BFE are presented in Table IV.

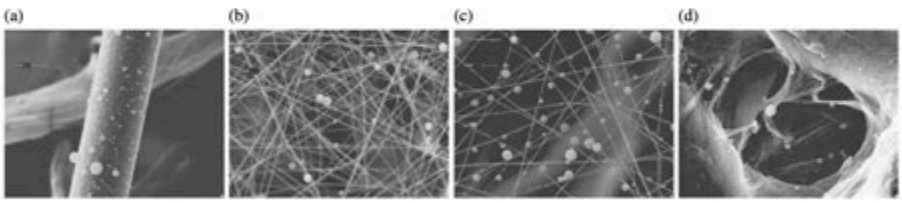

Fig. 7. SEM of bacteria after filtration on: (a) commercial filter, (b) nanofiber filter PSF/PEO [7/3] with fiber weight of 1 g/m^2, (c) nanofiber filter PSF/PEO [7/3] with fiber weight of 5 g/m^2 and (d) filter paper with pore size 11 μm.

RESEARCH ARTICLE

Table II. The charge of the ionizable groups found on proteins as a function of pH.[25]

Ionizable group	pH 2	pH 7	pH 12
Histidine	+ + + + + + + + + + + + + + + + + + + +	0000000000	
Lysine	+ +	000000	
Arginine	+ +	000	
Aspartic acid	0000000	– –	
Glutamic acid	0000000	– –	

Table III. Effect of nanofiber mass on BFE.

Number of bacterial colonies on agar plate without filter	Number of bacterial colonies on agar plate with non-woven fabric (0 g/m^2)	Number of bacterial colonies on agar plate with non-woven fabric (1 g/m^2)	Number of bacterial colonies on agar plate with non-woven fabric (3 g/m^2)	Number of bacterial colonies on agar plate with non-woven fabric (5 g/m^2)	Fiber weight [g/m^2]	BFE [%]
154	48	18	4	0	0	69.5
151	45	15	6	0	1	94.8
156	49	18	5	0	3	99.9
					5	100.0

The BFE for non-woven baric without any nanofibers was 69.5% (Table III). There was a modest increase in BFE as the protein content of nanofibers deposited on non-woven fabric was increased at fiber weights of 1 and 3 g/m.[2] The data in Table IV clearly show that the lowest BFE of 91.8% was obtained for SF/PEO blend which contained the least amount of nanofibers (1 g/m^2) and soy protein of only 0.365 g/m^2. Even when the fiber weight increased to 3 g/m^2 which resulted in 1.096 g/m^2 of protein, the SF/PEO blend could achieve only 97.7% BFE. For SPC/PEO blend, at 1 g/m^2 fiber weight (0.451 g/m^2 of protein), the BFE was 94.2%. When the fiber weight rose to 3 g/m^2 (1.352 g/m^2 of protein) the BFE reached value 99.6%. For SPI/PEO blend, even 1 g/m^2 of nanofibers (0.601 g/m^2 of protein) was sufficient to achieve 96.2% BFE and increased to 100% for fiber weight of 3 g/m^2. Similar to the findings with SPI, SPC and SF nanofibers, average BFE increased for nanofibers prepared from PSF/PEO or HPSF/PEO blends when the fiber weight increased from 1 to 3 g/m^2. Comparing the results obtained for SPI/PEO and SPC/PEO with those for PSF/PEO and HPSF/PEO (Table IV), it may be noted that both protein content and nanofiber weights correlate positively with BFE, as can be expected. The standard deviation of BFE measurements was low, in the range of 0.3 to 0.6% indicating excellent reproducibility. These data confirm a good correlation between the protein content in nanofibers and BFE (Fig. 8).

Table IV. Effect of protein content on BFE.

Type of protein blend used	Fiber weight (g/m^2)	Protein content in the nanofibers (g/m^2)	Average BFE [%; $n = 4$]
PSF/PEO	**1**	**0.463**	**94.8**
PSF/PEO	3	1.388	99.9
HPSF/PEO	**1**	**0.621**	**96.5**
HPSF/PEO	3	1.863	100.0
SPI/PEO	**1**	**0.601**	**96.2**
SPI/PEO	3	1.802	100.0
SPC/PEO	**1**	**0.451**	**94.2**
SPC/PEO	3	1.352	99.6
SF/PEO	**1**	**0.365**	**91.8**
SF/PEO	3	1.096	97.7

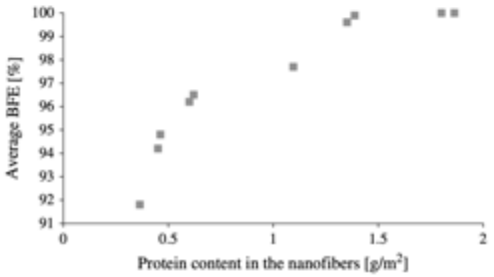

Fig. 8. The efficiency of the protein on BFE of the filter.

4. CONCLUSIONS

Soy flour was successfully purified to PSF and HPSF using acid and alkali wash processes that resulted in protein contents very close to commercially available SPC and SPI, respectively. While pure HPSF or PSF mixtures treated by thermal and alkaline conditions could not be spun into nanofibers, their blends with PEO were easily electrospun.

The bacterial filtration tests and SEM images of tested filters indicate that soy protein based nanofibers can capture gram-negative *E. coli* bacteria most likely as a consequence of the positive charge present on these nanofibers. The nanofibers also possess unusual bio-adhesive properties by which the captured bacteria remain attached to the nanofibers. The results indicate that just 3 g/m^2 of the

RESEARCH ARTICLE

protein based nanofibers deposited on a base filter can be sufficient to capture 100% of the air borne bacteria. The results also indicate that protein content in the nanofibers is an important factor in their BFE performance.

The novel protein based nanofiber filters prepared in this study have demonstrated a clear potential for effective removal and capture of *E. coli* bacteria during air-filtration. These filters can be effectively deployed in environments such as hospitals and senior residential areas to reduce bacterial infections. Further, these filters at the end of their life may be easily disposed of or composted rather than putting in landfills.

Acknowledgments: This work was financially supported by the Axium Nanofibers, LLC. Daniela Lubasova would like to thank the project OP VaVpI Centre for Nanomaterials, Advanced Technologies and Innovation CZ.1.05/2.1.00/01.0005 and the project Development of Research Teams of R&D Projects at the Technical University of Liberec CZ.1.07/2.3.00/30.0024 for the support to complete the manuscript.

References and Notes

1. H. Wang, L. A. Johnson, and T. Wang, *J. Am. Oil Chem. Soc.* 81, 713 (**2004**).
2. D. A. Lundgren and K. T. Whitby, *Ind. Eng. Chem. Process Des. Dev.* 4, 345 (**1965**).
3. C. H. Kanaoka, H. Emi, Y. Otani, and T. Iiyama, *Aerosol Sci. Technol.* 7, 1 (**1987**).
4. H. L. Schreuder-Gibson, P. Gibson, P. Tsai, P. Gupta, and G. Wilkes, *International Nonwovens Journal* 13 (**2005**).
5. D. R. Marshak, J. T. Kadonaga, R. R. Burgess, M. W. Knuth, W. A. Brennan, and S. H. Lin, Strategies for Protein Purification and Characterization: A Laboratory Course Manual, Cold Spring Harbor Laboratory (**1996**).
6. W. A. Corpe and B. Coll, Mechanism of Attachment of Marine Bacteria to Solid Surfaces, Academic Press, Inc., New York (**1972**).
7. M. Hermansson, S. Kjelleberg, T. K. Korhonen, and T. A. Stenstrom, *Arch. Microbiol.* 131, 308 (**1982**).
8. K. Pedersen, *Microbiol. Lett.* 12, 365 (**1980**).
9. J. S. Dickson and M. Koohmaraie, *Appl. Environ. Microbiol.* 55, 832 (**1989**).
10. D. H. Reneker and I. Chun, *Nanotechnology* 7, 216 (**1996**).
11. D. Rodoplu, Y. Sen, and M. Mutlu, *Nanosci. Nanotechnol. Lett.* 5, 444 (**2013**).
12. L. Heng, B. Wang, Y. Zhang, L. Zhang, B. Z. Tang, and L. Jiang, *J. Nanosci. Nanotechnol.* 12, 8443 (**2012**).
13. H. Jiang, Y. Jiao, M. R. Aluru, and L. Dong, *J. Nanosci. Nanotechnol.* 12, 6333 (**2012**).
14. J.-H. Jung, M.-S. Cha, and J.-B. K., *J. Nanosci. Nanotechnol.* 12, 5412 (**2012**).
15. R. Shabani and H. J. Cho, *Rev. Nanosci. Nanotechnol.* 1, 85 (**2012**).
16. S. Ameen, H.-K. Seo, M. S. Akhtar, and H. S. Shin, *Sci. Adv. Mater.* 5, 21 (**2013**).
17. G. Panthi, A. M. Barakat, A. M. Hamza, A. R. Unnithan, M. Motlak, K. A. Khalil, Y.-S. Shin, and H. Y. Kim, *Sci. Adv. Mater.* 4, 1118 (**2012**).
18. D. H. Reneker and I. Chun, *Nanotechnology* 7, 216 (**1996**).
19. A. Greiner and J. H. Wendorff, *Angew. Chem. Int. Ed. Engl.* 46, 5670 (**2007**).
20. H. Kong and J. Jang, *Langmuir* 24, 2051 (**2008**).
21. J. Song, H. Kang, C. Lee, S. H. Hwang, and J. Jang, *Appl. Mater. Interfaces* 4, 460 (**2012**).
22. A. M. Azad, S. L. McKelvey, and Z. Al-Firdaus, *The AM MTIAC Qaerterly* 3, 1 (**2008**).
23. G. Vedel, *Journal of Antimicrobial Chemotherapy* 56, 657 (**2005**).
24. H. R. Panta, D. R. Pandeyac, K. T. Namd, W. Baekd, S. T. Hongc, and H. Y. Kim, *J. Hazard. Mater.* 89, 465 (**2011**)
25. O. Jirsak, F. Sanetrnik, D. Lukas, V. Kotek, L. Martinova, J. Chaloupek, A Method of nanofibers production from polymer solution using electrostatic spinning and a device for carrying out the method, CZ Patent, 294274 (B6). WO 2005024101 (**2005**).
26. R. Rapley and J. M. Walker, Molecular Biomethods Handbook, Humana Press, New Jersey (**1998**).
27. A. C. Vega-Lugo and L. T. Lim, *J. Biobased Mater. Bio.* 2, 223 (**2008**).
28. J. E. Bergsma, F. R. Rozema, R. R. M. Bos, W. C. de Bruijn, G. Boering, and A. J. Pennings, *Biomaterials* 16, 267 (**1995**).
29. W. K. Son, J. H. Youk, T. S. Lee, and W. H. Park, *Polymer* 45, 2959 (**2004**).
30. S. A. Theron, E. Zussman, and A. L. Yarin, *Polymer* 45, 2017 (**2004**).
31. N. P. Desai and J. A. Hubbel, *Biomaterials* 12, 144 (**1991**).
32. D. B. Purchas and K. Sutherland, Handbook of Filter Media, 2nd edn., Elsevier, Advanced Technology, Oxford (**2002**).

Received: 6 October 2013. Accepted: 8 June 2013.

RESEARCH ARTICLE

Appendix 4

LUBASOVA, D., Niu H.T., Zhao, X.T. and Lin, T. Hydrogel properties of electrospun polyvinylpyrrolidone and polyvinylpyrrolidone/poly(acrylic acid) blend nanofibers. RSC Advances 2015;5 (67):54481-54487.

RSC Advances

PAPER

Cite this: *RSC Adv.*, 2015, **5**, 54481

Hydrogel properties of electrospun polyvinylpyrrolidone and polyvinylpyrrolidone/poly(acrylic acid) blend nanofibers

Daniela Lubasova,[ab] Haitao Niu,[b] Xueting Zhao[b] and Tong Lin*[b]

Received 25th April 2015
Accepted 15th June 2015

DOI: 10.1039/c5ra07514a

www.rsc.org/advances

Hydrogel nanofibers with high water-absorption capacity and excellent biocompatibility offer wide use in biomedical areas. In this study, hydrogel nanofibers from polyvinylpyrrolidone (PVP) and PVP/poly(acrylic acid) (PAA) blend were prepared by electrospinning and by subsequent heat treatment. The effects of post-electrospinning heat treatment and PVP/PAA ratio on hydrogel properties of the nanofibers were examined. Heat treatment at a temperature above 180 °C was found to play a key role in forming insoluble and water-absorbent nanofibers. Both PVP and PVP/PAA nanofibers showed high morphology stability in water and excellent water retention capacity. The swelling ratio of PVP/PAA nanofibers declined with increasing heating temperature and decreasing PVP/PAA unit ratio. In comparison with dense casting films, these nanofiber membranes showed nearly doubled swelling ratio.

Introduction

Hydrogels can absorb a significant amount of water and retain their structure integration owing to their hydrophilic three-dimensional polymer network structure. Hydrogels with high water-absorption capacity and good biocompatibility offer wide applications in areas such as wound healing, drug delivery systems, and scaffolds for tissue engineering.[1–4] Nevertheless, most hydrogels are prepared in the form of dense films or powders. The former are often impermeable to air and liquid, and have lower surface area than porous materials, while the latter are inapplicable to many applications due to the lack of structure integration. Recently, fibrous hydrogels have received considerable attention for their high air/liquid permeability and fast access of water to the internal surface. Hydrogel nanofibers, which are prepared mostly by electrospinning, are of particular interest because of the large surface area and highly porous feature.[5,6]

Electrospinning is a simple and efficient technique to produce nanofibers.[7,8] It utilizes a high electrostatic field to generate nanofibers from a fluid. Electrospun nanofibers often show large surface-to-weight (volume) ratio, high porosity, and excellent pore interconnectivity.[9] These unique features allow electrospun nanofibers have extensive applications in diverse areas including filtration, wound healing, cosmetic, energy conversion/storage, and medicine.[10–14]

Hydrogel nanofibers can combine the advantages of both nanofibers and hydrogels. The large surface area of nanofibers enables fast release of antibiotics or growth factors into wound whereas the high porosity of nanofiber mats ensures fast absorption of body fluids and diffusion of waste.[15] Despite the fact that several hydrogel nanofibers, *e.g.* poly(vinyl alcohol) (PVA),[16] protein,[17] collagen,[18] and poly(*N*-isopropylacrylamide),[19] have been reported recently, most of the hydrogel nanofibers either are water-soluble due to the lack of sufficient crosslinking[20] or use toxic chemicals as crosslinking agents.[21]

Poly-(*N*-vinyl-2-pyrrolidone) (PVP) is a water-soluble polymer with excellent biocompatibility. It has high ability to absorb and retain water. Although PVP nanofibers have been reported by a few papers,[22–24] they did not exhibit hydrogel feature due to their high solubility in water. PVP hydrogel membranes have been produced by electrospinning and further crosslinking through UV-C radiation and Fenton reaction.[25] However, fibrous structure was hardly maintained and only a porous membrane was obtained instead after the crosslinking reaction. Moreover, the high energy radiation is often expensive and unavailable readily.

It was reported that PVP and poly(acrylic acid) (PAA) can form strong hydrogen bond interaction.[26] The addition of a small amount of the one mentioned polymer (~10%) to the aqueous solution of the other is sufficient to induce interactions between them to form a complex. There are ion-dipol and ion–ion interactions between PVA and PAA as well, especially in a partially neutral condition. It was also reported that PVP can be stabilized through heat treatment.[27,28] However, whether PVP and PVP/PAA blend can form insoluble hydrogel nanofibers through a heat treatment has not been proved in the research literature yet.

Herein, we report on the preparation of PVP and PVP/PAA blend hydrogel nanofibers simply by heat treatment of the

[a]*Institute for Nanomaterials, Advanced Technologies and Innovation, Technical University of Liberec, Liberec 461 17, Czech Republic*

[b]*Institute for Frontier Materials, Deakin University, Geelong, VIC3216, Australia. E-mail: tong.lin@deakin.edu.au; Tel: +61 3 522 71245*

electrospun nanofibers. Without using any toxic agent for crosslinking, the nanofiber membranes showed twice larger water-swelling ratio in comparison to their film counterparts. The effects of heat-treatment temperature and PVP/PAA ratio on swelling behavior and water solubility were examined. This work may provide a simple method to prepare non-toxic hydrogel nanofibers from two widely available polymers, PVP and PAA. The hydrogel nanofibers developed are expected to find applications in the areas where bio-safety has high priority, such as biomedical, cosmetic and food industry.

Experimental

Materials

PVP (M_w ~1 300 000), PAA (M_w ~2000), and *N*,*N*-dimethylformamide (DMF) were purchased from Sigma-Aldrich and used as received. PVP and PAA solutions were prepared separately by dissolving PVP or PAA powder in DMF under magnetic stirring at room temperature. The concentration of PVP and PAA solutions is 20 wt%. PVP/PAA solutions with unit ratio 8/2, 6/4 and 4/6 were produced by mixing a PVP solution with a PAA solution at room temperature, respectively. The ratio of base unit number between PVP and PAA, *i.e.* (number of base units for PVP)/(number of base units for PAA), in the solution was used to express the molar ratio of the two polymers.

Preparation of nanofiber membranes and films

The polymer solution was placed to a plastic syringe and then charged with a high voltage of 20 kV (ES30P, Gamma High Voltage Research) through a metal syringe needle (21 gauges). Nanofibers were electrospun at the needle tip and collected on an aluminum foil mounted onto the rotating metal drum (100 rpm). The drum was electrically ground and placed 15 cm away from the tip of the needle. The flow rate of the polymer solution was controlled at 0.8 ml h^{-1} by a syringe pump (KD Scientific, Holliston, MA, USA). The nanofiber membranes used for further analysis were removed from aluminum foil and were about 300 μm in thickness. Finally, the as-spun nanofiber membranes were heated at temperatures of 140, 180 and 200 °C, for 1 hour each. After heating, the samples were stored in a desiccator for further characterizations.

Polymer films were prepared by casting the solution PVP and PVP/PAA to a glass Petri dish. The samples were placed in an air circulating oven at 60 °C overnight to remove DMF solvent residue and stored in a desiccator for further experiments, their thickness was about 300 μm. The polymer films were used as a control to examine the effect of nanofibrous structure on swelling and solubility properties.

Swelling behavior of nanofiber membranes

The swelling behavior was evaluated according to Japanese Industrial Standard (K8150 method). Briefly, dry nanofiber membranes (0.05–0.1 g) were immersed in DI water (30 ml) at room temperature for 30 minutes. After swelling, nanofiber membranes were filtered with a filter (0.45 μm, QTY 90 mm). Swelling ratio (SR) was calculated according to eqn (1):

$$\mathrm{SR(g/g)} = \left(\frac{w_s - w_0}{w_0}\right) \quad (1)$$

where w_s is the weight of the nanofiber membrane after immersing in water and w_0 is the weight of the nanofiber membrane in dry state.

Solubility behavior of nanofiber membranes

Nanofiber membranes were fully dried at 60 °C for 24 hours prior to test. The extraction with DI water was performed in glass bottles which were placed on a roller mixer at room temperature overnight. The solid residual after extraction was collected using a nylon filter (0.45 μm, QTY 90 mm), which was dried to constant weight (60 °C for 24 h).[29,30] The insoluble part of nanofiber membranes (gel content), g (%), was calculated according to eqn (2):

$$g(\%) = \left(\frac{w_e}{w_d}\right) \times 100 \quad (2)$$

where w_d and w_e are the weight of the dry nanofiber membrane before and after extraction, respectively.

Other characterizations of nanofiber membranes

Surface morphology of nanofiber membranes before and after swelling was observed using a scanning electron microscope (SEM, Supra 55VP, Zeiss) at an accelerating voltage of 5 kV and distance of 10 mm. Hydrogel nanofibers were dried in a vacuum oven overnight, and they are then mounted onto an Al sample holder with a conducting tape specific for SEM use. The sample surface was then sputter-coated with a thin layer of gold. Fourier transform infrared spectroscopy (FTIR) spectra were recorded on Bruker Vertex 70 spectrophotometer in ATR mode. Each spectrum with an average of 100 scans was obtained at a resolution of 4 cm^{-1} wavenumber. All tests were carried out in a controlled environment 20 ± 2 °C and 65 ± 2% relative humidity. Differential scanning calorimetry (DSC) analysis was performed on TA instruments (Q100 DSC). All nanofiber membranes were dried in an oven at 60 °C for 12 hours before testing. The test was conducted in a temperature range of 40–150 °C (ramp 10 °C min^{-1}) under a nitrogen atmosphere (flow rate, 5 ml min^{-1}). The tensile property of nanofiber membranes was tested on an Instron tensile tester at controlled environment, 20 ± 2 °C and 65 ± 2% relative humidity. The specimens were 30 mm in length and 10 mm in width. The membrane thickness was measured using a thicknesses tester (Digimatic Indicator, Mitutoyo).

Results and discussion

Nanofiber morphology

Fig. 1 shows the SEM images of as-electrospun nanofibers. Pure PVP nanofibers appeared to be coarser than PVP/PAA nanofibers. The PAA content in PVP/PAA mixture noticeably affected the fiber uniformity. When the PVP/PAA unit ratio in the electrospinning solution changed from 8/2 to 6/4, beaded fibers were considerably reduced. The introduction of PAA in the

mixed solution increased solution viscosity because of the interaction between PVP and PAA molecules, which led to the formation of uniform nanofibers. A further increase in PAA content (PVP/PAA 4/6) declined the electrospinning ability. As a result, only dense film was collected. This result could be attributed to low molecular weight of PAA which in predominance decreased final solution viscosity.

The 2nd and the 3rd lines images of Fig. 1 show nanofibers after heat treatment at 180 and 200 °C, respectively. No significant morphology change was observed when the heat treatment was at 180 °C. When the heat treatment was around 200 °C, interconnections formed among nanofibers because nanofibers began to melt at this temperature. PVP nanofibers have an average fiber diameter over 800 nm, while the diameter of PVP/PAA nanofibers was less than 120 nm (Fig. 1e). The heat treatment increased the PVP fiber diameter, but had a little influence on the diameter of PVP/PAA fibers.

FTIR spectra of nanofiber membranes

The FTIR spectra of pure PVP and PVP/PAA nanofibers are shown in Fig. 2a. The band at 1710 cm^{-1} corresponded to carbonyl stretching of carboxylic acid in PAA. The absorption band at 1660 cm^{-1} was assigned to a combined contribution from C=O and C–N stretching of PVP.[31] The peak at 1495 cm^{-1} came from the vibration of CH_2 in PVP. The spectra of the PVP/PAA fibers showed the combination of both polymers. The higher ratio of PAA led to higher intensity of carbonyl stretching band.

To better describe the composition of PVP/PAA blends, the carbonyl band in FTIR was curving fitted (Fig. 2b). The shape of the carbonyl absorption bands for PVP/PAA blends depended on the unit ratio of individual components. Little difference in the carbonyl region was observed between PVP and PVP/PAA (unit ratio 8/2). By increasing the PAA content, red shift of band at around 1640 cm^{-1} appeared which was attributed to the formation of hydrogen-bonds between the carbonyl groups in PVP and the carboxyl groups of PAA. This absorption band-shift to the lower wavenumber has been explained previously.[26,32]

Fig. 2c and d show the FTIR spectra of the nanofibers before and after heat treatment. In the case of PVP/PAA nanofibers (unit ratio 6/4), the small peak appeared at 1760 cm^{-1} and side peak at 1710 cm^{-1} (in Fig. 2c). This was probably due to the crosslinking of PVP, which has been reported before.[27,28] The

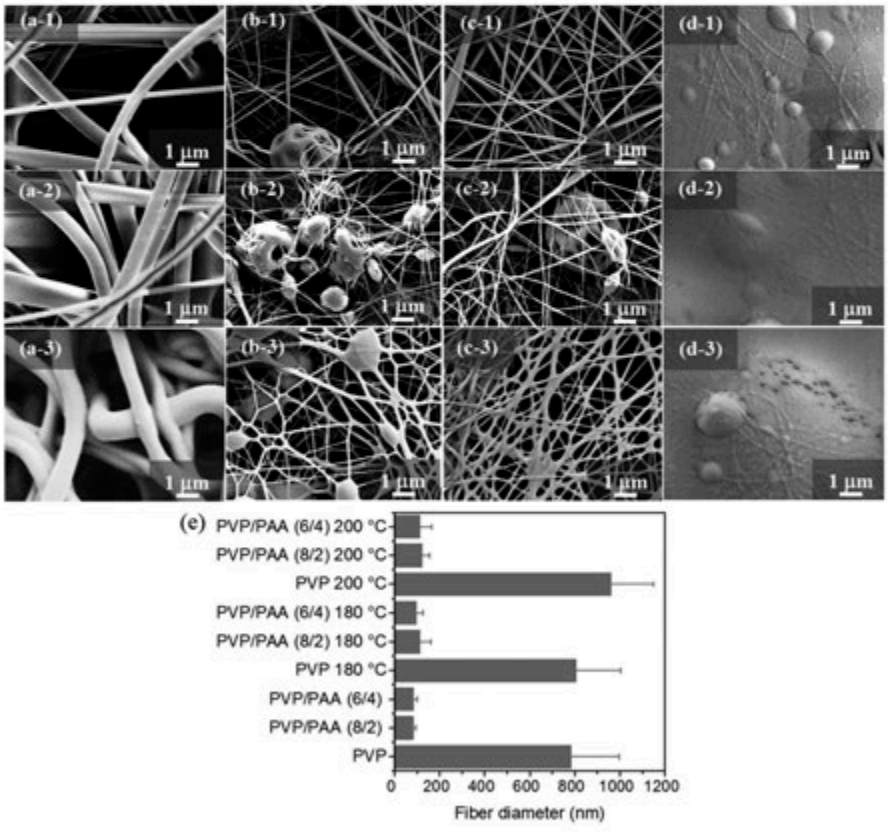

Fig. 1 SEM images of nanofibers prepared from: (a) pure PVP, (b) PVP/PAA (unit ratio 8/2), (c) PVP/PAA (unit ratio 6/4), (d) PVP/PAA (unit ratio 4/6). 1st line: as-spun; 2nd line: after heating at 180 °C (1 hour); 3rd line, after heating at 200 °C (1 hour), (e) average diameter of PVP and PVP/PAA nanofibers.

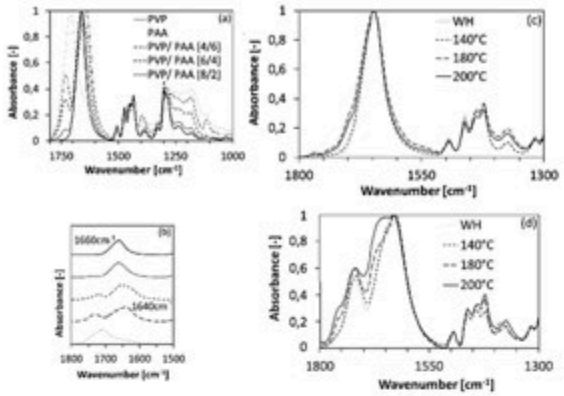

Fig. 2 FTIR spectra of (a) nanofibers with different PVP/PAA unit ratios, (b) enlarged carbonyl band of PVP, PAA and their blends, (c) pure PVP nanofibers without heat (WH) and after heat treatment, and (d) PVP/PAA (unit ratio 6/4) nanofibers WH and after heat treatment (from 140 to 200 °C).

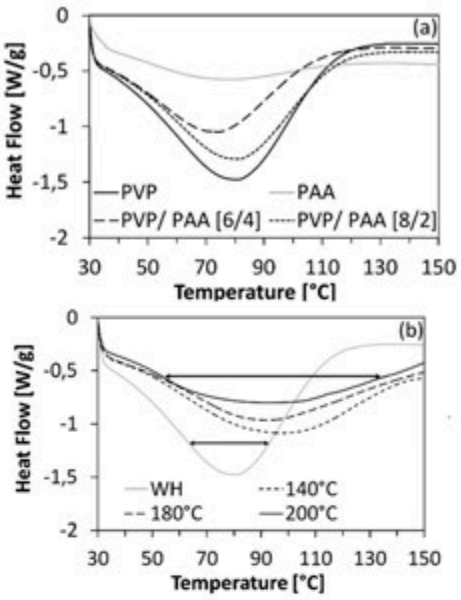

Fig. 3 DSC curves of nanofibers (a) with different PVP/PAA unit ratio, (b) PVP/PAA (unit ratio 6/4) WH and after heat treatment (from 140 to 200 °C).

presence of PAA showed a little influence on the heat crosslinking reaction. In the case of PVP/PAA (unit ratio 6/4) nanofibers, the absolute absorbance of carbonyl absorption peak at 1710 cm^{-1} increased with increasing the temperature.

Thermal analysis of nanofiber membranes

Fig. 3a shows DSC curves of PVP and PVP/PAA nanofibers with different unit ratios. No peaks were found to be associated with fusion or phase transition. A broad endothermic peak was observed in the temperature range between 60 °C and 100 °C, corresponding to the dehydration of PVP. In the presence of PAA, the intensity of these endothermic peaks declined. Fig. 3b shows DSC curves of PVP/PAA nanofibers (unit ratio 6/4) before and after heat treatment. Weaker endothermic peak resulted when they were treated at higher temperature. The reduced endothermic peak was attributed to the removal of certain water from the nanofiber samples after the heat treatment.

Hydrogel behavior of nanofiber membranes

Before immersing in water, the heat treated PVP/PAA nanofiber membranes were white and opaque. The can be explained by the randomly orientated electrospun nanofiber structure, which forms a porous structure with strong reflection to light. In contrast, casting film looked more transparent because it has a dense structure without trapping air inside. They became transparent and swollen after being immersed in DI water (Fig. 4). However, they remained insoluble even after immersing in water for 24 hours. Similar phenomenon was also found on PVP nanofiber membranes and films. This indicates that PVP undergoes crosslinking after heat treatment.

Heat treatment temperature had an effect on the morphology of PVP/PAA nanofibers after immersing in water. Both PVP/PAA and PVP nanofibers after heat treatment at a temperature lower than 180 °C dissolved in water immediately due to insufficient crosslinking. For PVP/PAA nanofibers treated at 180 °C, they did not dissolve in water after 24 hours, however they failed to retain the fiber structure after immersing in water (Fig. 5a-1–c-1). The fibers merged together to form a film. This is presumably due to insufficient crosslink. When nanofibers were treated at 200 °C, they maintained the fibrous structure after immersing in water, although they had swollen. PVP nanofibers can also retain their fiber shape after heating treatment at 200 °C (Fig. 5a-2–c-2).

The unit ratio affected the morphology of PVP/PAA nanofibers after immersing in water as well. From the Fig. 5b-2 and c-2, it is clearly seen that PVP/PAA nanofibers with unit ratio 6/4 maintained the best nanofiber structure without any bead or defect. This should come from the formation of crosslinked structure, making the PVP/PAA nanofibers retain fiber morphology (Fig. 1c-3).

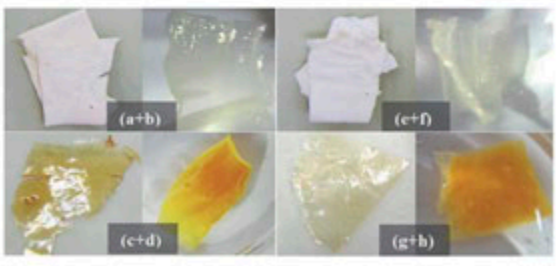

Fig. 4 Photos of PVP nanofibers (a) in dried state and (b) after swelling in water; PVP/PAA film (c) in dried state and (d) after swelling in DI water for 24 hours. Photos of PVP/PAA nanofibers (e) in dried state and (f) after swelling in water; PVP film (g) in dried state and (h) after swelling in DI water for 24 hours.

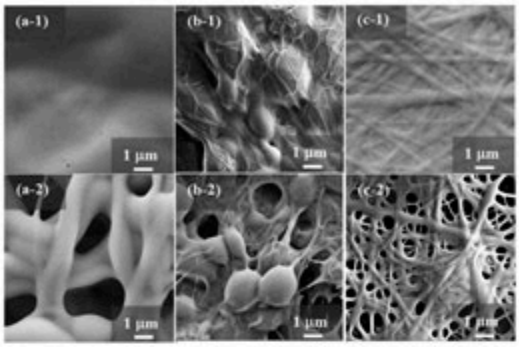

Fig. 5 SEM images of nanofibers after immersing in water. 1st line treated at 180 °C. 2nd line treated at 200 °C: (a) PVP, (b) PVP/PAA (unit ratio 8/2) and (c) PVP/PAA (unit ratio 6/4).

The swelling ratio is an important characteristic for hydrogels. Fig. 6 shows the swelling test results. The PVP/PAA nanofibers after heat treatment reached a swelling ratio in the range between 500% and 3700%, which was higher than that of PVP/PAA films (300%–1700%). The swelling ratio did not change significantly after 30 minutes immersing in water. The swelling ratio of PVP/PAA nanofibers decreased with rising the heat temperature from 180 °C to 200 °C, because more crosslinks formed at higher temperature, which impeded the swelling of nanofibers.

The unit ratio of PVP/PAA hydrogel nanofibers affected the swelling ratio. For the pure PVP nanofibers, their swelling ratio was lower than that of nanofibers with a PVP/PAA unit ratio of 8/2, but larger than those with PVP/PAA ratio of 6/4. The film PVP/PAA samples showed a similar trend. This is because PAA in the nanofibers increases the water absorption ability. As a result, PVP absorbed less water and retained better fiber morphology. It is worth to notice that higher PAA content in nanofibers could lead to instability of the hydrogels.

The hydrogel content was estimated by immersing nanofiber membranes in DI water at room temperature for 24 hour and then measuring their dried insoluble part. When hydrogel nanofiber samples were immersed in deionized water for over 1 day, the weight of insoluble part was almost unchanged. For PVP and PVP/PAA nanofiber membranes after heat treatment at 180 °C, they exhibited considerable swelling in DI water, but remained insoluble after 24 hours. In contrast, for the untreated nanofiber membranes and those treated at lower temperature, disintegration happened when they were placed to water. Apparently, the non-solubility resulted from heat treatment at a temperature above 180 °C. The heat treatment also made our PVP and PVP/PAA nanofibers distinct to the conventional electrospun PVP nanofibers[22–24] in water solubility and swelling feature.

Fig. 7 shows the solubility result of nanofibers and films. After immersing in DI water, the insoluble part for the heat treated PVP/PAA nanofibers reached 63–85% (g [%]), which increased with increasing the treatment temperature. The insoluble part decreased with increasing the PAA content in the PVP/PAA nanofibers. The insoluble part of pure PVP nanofibers reached approximately 69.5%–75%, which was slightly higher than that of the PVP/PAA nanofibers with unit ratio of 6/4 but lower than PVP/PAA nanofibers with the unit ratio of 8/2. These results suggest that the heat induced crosslinking reaction mainly takes place within PVP, and the

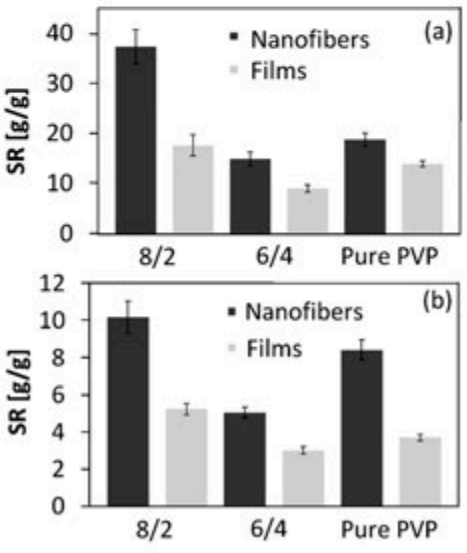

Fig. 6 Swelling ratio of PVP/PAA and PVP crosslinked nanofiber membranes and films after heat treatment for: (a) 180 °C and (b) 200 °C.

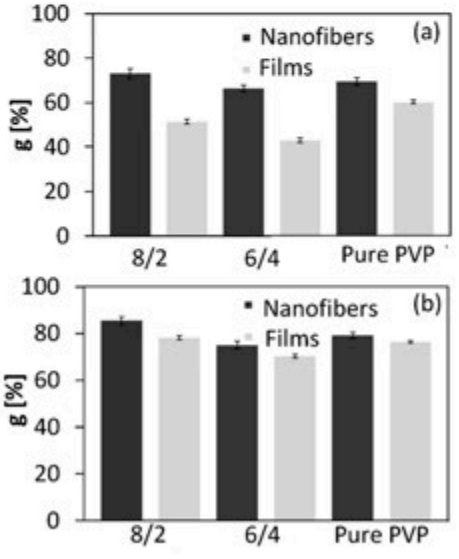

Fig. 7 The insoluble part of heat treated PVP/PAA nanofibers (g [%]) and films after immersing into water for 24 h. Heat treatment temperature: (a) 180 °C and (b) 200 °C.

Table 1 Tensile property of nanofiber membranes

Nanofiber membranes	States	Strain at break (%)	Strength (MPa)
PVP	As-spun	15.3	5.5
	After heat[a]	18.9	8.9
	Water swollen[b]	9.6	0.005
PVP/PAA (8/2)	As-spun	16.6	2.3
	After heat[a]	29.9	7.6
	Water swollen[b]	29.1	0.13
PVP/PAA (6/4)	As-spun	10.1	1.0
	After heat[a]	10.2	1.2
	Water swollen[b]	55.1	0.089

[a] Heat treatment at 200 °C. [b] Fully swollen in water.

addition of a small amount of PAA to PVP improves the stability of the hydrogel nanofiber membranes in water. PVP was reported to open the pyrrolidone ring to generate amine and –COOH groups at high temperature.[32] This leads to PVP chains crosslinking with each other. When PAA is present, the reaction may be extended to the –COOH groups of PAA, allowing the PAA link up with PVP.

The insoluble part of PVP/PAA films showed a similar trend to PVP/PAA nanofibers. However, the weight ratio of insoluble part for the PVP/PAA films was lower when compared to their nanofiber counterparts at the same PVP/PAA unit ratio. This is presumably because of the highly porous feature of nanofiber membranes which facilitates water up taking.

Table 1 lists the tensile property of the nanofiber membranes. Before heat treatment, the PVP nanofiber membrane had a tensile strength of 5.5 MPa. For the PVP/PAA nanofibers, the membrane tensile strength was lower than that of the pure PVP. This could come from the low molecular weight of PAA, which weakens the PVP inter-chain interaction. The heat treatment showed an effect on the tensile strength. After heat treatment at 200 °C, these nanofibers in dry state showed improved tensile strength. The tensile strength for the PVP/PAA nanofiber membrane was 7.6 MPa and 1.1 MPa when their unit ratio was 8/2 and 6/4, respectively.

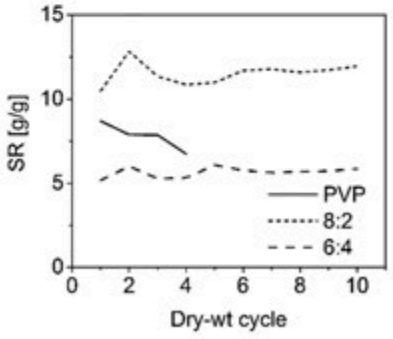

Fig. 8 Swelling ratio of PVP and PVP/PAA nanofiber membranes changing with dry- & swelling cycles. (All nanofiber were heat treated at 200 °C.)

After heating treatment, the strain at break decreased for the pure PVP and the PVP/PAA (8/2) nanofiber membranes, whereas the break strain for the PVP/PAA was not changed much. This indicates that small amount of PAA in PVP increases the plasticity of the polymer blend.

Upon fully swollen with water, the heat-treated nanofiber membranes decreased the tensile strength dramatically due to the absorption of a large quantity of water. The PVP/PAA (8/2) had the tensile strength of 0.13 MPa, while PVP/PAA (6/4) and PVP nanofiber membranes had smaller tensile strength, presumably due to the low crosslinking structure.

The swelling repeatability of the hydrogel nanofibers was tested. As shown in Fig. 8, PVP/PAA hydrogel nanofiber membranes (*e.g.* unit ratio 8/2 and 6/4, treated at 200 °C) show constant swelling ratio after 10 cycles of drying and re-swelling. For the pure PVP nanofiber membrane after heating treatment, the result of swelling repeatability cannot be obtained due to the low mechanical strength of the fiber membrane in swelling state.

Conclusions

PVP and PVP/PAA hydrogel nanofibers have been prepared by an electrospinning method followed by a thermal treatment. Heat treatment at a temperature above 180 °C plays a key role in forming insoluble nanofiber membranes in water. PVP/PAA unit ratio in the nanofibers affects swelling ratio and solubility. The PVP/PAA nanofibers containing a small amount of PAA show higher swelling ratio and stability in water than pure PVP nanofibers. Both pure PVP and PVP/PAA blend nanofibers have higher swelling ratio and better stability in water than their film counterparts. Since no toxic agent is used for crosslinking, PVP and PVP/PAA blend hydrogel nanofibers may find applications in the areas of cosmetic, pharmacy or wound dressings where bio-safety is pre-request to the materials.

Acknowledgements

Financial support from the Ministry of Education, Youth and Sports in the framework of National Program for Sustainability I, the OPR & DI project LO1201, Centre for Nanomaterials, Advanced Technologies and Innovation (CZ.1.05/2.1.00/

01.0005), the Project Development of Research Teams of R & D Projects at the Technical University of Liberec (CZ.1.07/2.3.00/30.0024) and Deakin University for visiting scholar is acknowledged.

Notes and references

1 A. Hoffman, *Adv. Drug Delivery Rev.*, 2002, **54**, 3–12.
2 J. L. Drury and D. J. Mooney, *Biomaterials*, 2003, **24**, 4337–4351.
3 C. Liu, Z. Zhang, X. Liu, X. Ni and J. Li, *RSC Adv.*, 2013, **3**, 25041–25049.
4 J. S. Boateng, K. H. Matthews, H. N. E. Stevens and G. M. Eccleston, *J. Pharm. Sci.*, 2008, **97**, 2892–2923.
5 B. V. Slaughter, S. S. Khurshid, O. Z. Fisher, A. Khademhosseini and N. A. Peppas, *Adv. Mater.*, 2009, **21**, 3307–3329.
6 M. Goldberg, R. Langer and X. Q. Jia, *J. Biomater. Sci., Polym. Ed.*, 2007, **18**, 241–268.
7 A. Greiner and J. Wendorff, *Angew. Chem., Int. Ed.*, 2007, **46**, 5670–5703.
8 D. Li and Y. Xia, *Adv. Mater.*, 2004, **16**, 1151–1170.
9 S. Ramakrishna, K. Fujihara, W. Teo, T. Yong, Z. Ma and R. Ramaseshan, *Mater. Today*, 2006, **9**, 40–50.
10 D. Lubasova, A. Netravali, J. Parker and B. Ingel, *J. Nanosci. Nanotechnol.*, 2014, **14**, 4891–4898.
11 F. Jian, W. Xungai and L. Tong, *Nanofibers - Production, Properties and Functional Applications*, InTech, Shanghai, China, 2011.
12 L. Malinova, V. Benesova, D. Lubasova, L. Martinova, J. Roda and J. Brozek, *Funct. Mater. Lett.*, 2011, **4**, 365–368.
13 Z. M. Huang, Y. Z. Zhang, M. Kotaki and S. Ramakrishna, *Compos. Sci. Technol.*, 2003, **63**, 2223–2253.
14 L. Malinova, M. Stolinova, D. Lubasova, L. Martinova and J. Brozek, *Eur. Polym. J.*, 2013, **49**, 3135–3143.
15 J. Zhu and R. Marchant, *Expert Rev. Med. Devices*, 2011, **8**, 607–626.
16 A. Cay and M. Miraftab, *J. Appl. Polym. Sci.*, 2013, **129**, 3140–3149.
17 D. Lee, J. Park, E. Lee, H. Kim and J. Lee, *Analyst*, 2013, **138**, 4786–4794.
18 K. S. Rho, L. Jeong, G. Lee, B. M. Seo, Y. J. Park, S. D. Hong, S. Roh, J. J. Cho, W. H. Park and B. M. Min, *Biomaterials*, 2006, **27**, 1452–1461.
19 J. Wang, A. Sutti, X. Wang and T. Lin, *Soft Matter*, 2011, **7**, 4364–4369.
20 P. Taepaiboon, U. Rungsardthong and P. Supaphol, *Nanotechnology*, 2006, **17**, 2317–2329.
21 L. Yang, C. F. C. Fitie, K. O. van der Werf, M. L. Bennink, P. J. Dijkstra and J. Feijen, *Biomaterials*, 2008, **29**, 955–962.
22 D. Yu, X. Shen, X. Zhang, C. Branford-White and L. Zhu, *Acta Polym. Sin.*, 2009, 1170–1174.
23 M. Dai, A. Senecal and S. Nugen, *Nanotechnology*, 2014, **25**, 225101.
24 X. Q. Li, L. Lin, Y. N. Zhu, W. W. Liu, T. S. Yu and M. Q. Ge, *Polym. Compos.*, 2013, **34**, 282–287.
25 R. Fogaca and L. Catalani, *Soft Mater.*, 2013, **11**, 61–68.
26 H. Kaczmarek, A. Szalla and A. Kaminska, *Polymer*, 2001, **42**, 6057–6069.
27 H. T. Niu, J. Zhang, Z. L. Xie, X. G. Wang and T. Lin, *Carbon*, 2011, **49**, 2380–2388.
28 P. Q. Wang, D. Zhang, F. Y. Ma, Y. Ou, Q. N. Chen, S. H. Xie and J. Y. Li, *Nanoscale*, 2012, **4**, 7199–7204.
29 N. Peppas, Y. Huang, M. Torres-Lugo, J. Ward and J. Zhang, *Annu. Rev. Biomed. Eng.*, 2000, **2**, 9–29.
30 R. K. Gangwar, V. A. Dhumale, D. Kumari, U. T. Nakate, S. W. Gosavi, R. B. Sharma, S. N. Kale and S. Datar, *Mater. Sci. Eng., C*, 2012, **32**, 2659–2663.
31 Y. Tan, K. Peh and O. Al-Hanbali, *J. Pharm. Pharm. Sci.*, 2001, **4**, 7–14.
32 M. Yin, Y. Ye, M. Sun, N. Kang and W. Yang, *Macromol. Rapid Commun.*, 2013, **34**, 616–620.

Appendix 5

LUBASOVA, D., Tomankova, H., and Polakova, D. Industrial-scale needle-less electrospinning of tetracycline-immobilized nanofibrous scaffolds using a polycaprolactone/polyethylene oxide/chitosan blend for wound healing. Journal of Industrial Textiles 2024;54:1-32.

Original Research Article

Journal of Industrial Textiles

Volume 54: 1–32

DOI: 10.1177/15280837241291215
journals.sagepub.com/home/jit
Sage

Industrial-scale needle-less electrospinning of tetracycline-immobilized nanofibrous scaffolds using a polycaprolactone/polyethylene oxide/chitosan blend for wound healing

Daniela Lubasova[1], Hana Tomankova[2] and Dagmar Polakova[2,3]

Abstract

Nanofibrous scaffolds offer significant promise for wound healing due to their ability to absorb exudates, prevent microbial contamination, and enhance oxygen diffusion. However, challenges remain in fully realizing their clinical potential, as previous research has primarily focused on scaffolds made of two polymers or those encapsulating therapeutic agents within nanofibers. Additionally, scaling up fabrication while maintaining functionality presents a significant challenge. This study introduces a novel type of nanofibrous scaffold, combining poly (ethylene oxide) (PEO), poly (caprolactone) (PCL), and chitosan (CS) in various mass ratios, electrospun using Nanospider™ technology. The scaffolds featured fiber diameters ranging from 134 ± 37 to 148 ± 38 nm and exhibit

[1]Faculty of Textile Egineering, Technical University of Liberec, Liberec, Czech Republic
[2]Institute for Nanomaterials, Advanced Technologies and Innovation, Technical University of Liberec, Liberec, Czech Republic
[3]Regional Hospital Liberec, a.s., Liberec, Czech Republic

Corresponding author:
Daniela Lubasova, Faculty of Textile Egineering, Technical University of Liberec, Studentska 2, Liberec 46117, Czech Republic.
Email: daniela.lubasova@tul.cz

high gram-per-square-meter values between 6.8 and 8.6 g/m^2. An optimal balance of hydrophilicity was achieved, and the scaffolds demonstrated superior breathability with moisture vapor transmission rates ranging from 1904.3 ± 28.6 to 2005.7 ± 42.9 g/m^2/day, outperforming commercial wound dressings. Additionally, a wide range of hydrolytic degradation rates (3.8 ± 1% to 73.2 ± 0.8%), elongation at fracture (21% to 0.8%), and Young's modulus (106.7 ± 8.5 MPa to 170.7 ± 11.9 MPa) were observed. Surface-immobilized tetracycline (TET) significantly enhanced antibacterial efficacy, with inhibition zones exceeding 20 mm against *Escherichia coli*. Our findings confirm that scaffold properties can be effectively tailored by adjusting the PEO/PCL ratio, advancing customization for wound care. Post-fabrication soaking in TET solutions further boosts antibacterial performance and allows for tailored post-production adjustments. Compared to existing studies, this approach simplifies customization and improves the practicality of wound care solutions.

Keywords
Nanofibers, needle-less electrospinning, wound healing, chitosan, polycaprolactone, polyethylene oxide

Introduction

Wound healing is a complex and dynamic process crucial for restoring the skin's barrier function and ensuring complete coverage of injuries. Factors such as infections, chronic conditions like diabetes, and the nature of the wound itself can significantly complicate this process, all of which require advanced therapeutic interventions. The management of extensive wounds, in particular, presents a medical challenge, requiring effective strategies to restore barrier function and achieve complete skin coverage.[1] Depending on the nature of the wound, a range of dressings may be considered, with conventional options such as gauze, bandages, and cotton wool being modified to provide protection against microbial contaminants. However, these traditional options often have limitations, such as adherence to the wound site, causing pain and further injury upon removal, and are generally suitable only for uninfected wounds with moderate exudate levels.[2] On the other hand, advanced wound dressings like hydrogels offer distinct advantages over traditional gauze. They are absorbent, non-stick, and capable of creating a moist microenvironment that promotes wound healing by keeping the wound bed hydrated, facilitating cell migration, and supporting tissue regeneration. Hydrogel dressings are designed to prevent wounds from drying out and to aid in the healing process.[3,4] Despite these benefits, traditional hydrogel dressings in the form of films often lack sufficient breathability, leading to issues like wound infections and poor adaptability to wounds of varying shapes.[5,6] Recent advancements in skin regeneration have led to the development of functional scaffolds that act as physical barriers against microbial infections, are non-stick, breathable, and maintain structural integrity while creating and sustaining a moist healing environment.[7,8] Various fabrication techniques such as phase separation,

freeze-drying, self-assembly, and 3D bioprinting are employed to create functional scaffolds, each of which requires specific parameters to achieve the desired characteristics and topographies.[9–11] Among these fabrication techniques, electrospinning stands out for producing nanofibrous scaffolds with nanoscale fiber diameters. This method offers several advantages, including a high surface area-to-volume ratio, significant porosity, and the ability to incorporate various therapeutic agents, making it particularly well suited for wound healing applications.[12–14]

The electrospinning process involves applying an electric force to draw charged polymer fluids or melts into nanofibers. Different types of electrospinning processes are categorized based on the spinneret used, such as the traditional mono-tube needle, a tri-layer needle, an eccentric needle, or a concentric needle.[15] Needle electrospinning techniques offer precise control over fiber formation; however, they have significant drawbacks, such as the potential for needle clogging, cleaning challenges, and interference between jets, leading to operational complexities and frequent maintenance. Additionally, the layout of multiple needles in these setups can be intricate, requiring large operating spaces and making the process more cumbersome.[16,17] In contrast, needle-less electrospinning techniques, such as free-liquid electrospinning, have been developed to address some of these limitations. Needle-less electrospinning systems can offer higher production rates and circumvent issues like needle clogging and the low manufacturing capability inherent in traditional needle-based processes.[18,19] By eliminating the need for needles, these techniques can enhance the uniformity of fiber diameter and scaffold formation, which is often challenging in needle-based electrospinning due to the localized charge concentration at the needle tip.[20] The production of nanofibers via needle-less, high-voltage, free-liquid surface electrospinning processes, such as Nanospider™ technology, holds considerable promise for industrial applications owing to its distinctive attributes. This technology facilitates the fabrication of high-quality nanofibers characterized by minimal solvent consumption, continuous manufacturing capabilities, and compatibility with a diverse array of polymers.[21] Renowned for its adaptability, Nanospider™ technology offers ease of adjustment to optimize specific properties through the manipulation of various process parameters.[22]

Nanofibrous scaffolds with interconnected porous networks not only support the overall wound healing process but also enhance tissue regeneration by providing structural support, promoting cell adhesion, and facilitating the exchange of vital molecules involved in the healing cascade.[23–25] Studies have demonstrated that nanofibrous scaffolds can improve wound closure, reduce scar formation, and enhance overall wound healing outcomes.[26] By leveraging the unique properties of nanofibers, such as their biocompatibility and high drug absorption capabilities, these scaffolds hold immense potential for advancing wound care practices and addressing the challenges of chronic wounds.[27–29] The selection of appropriate biomaterials is critical to the effectiveness of nanofibrous scaffolds in wound healing.[30]

Chitosan (CS), a natural biopolymer, has garnered considerable interest due to its distinctive properties, such as its hemostatic, antimicrobial activity, and biocompatibility, making it a valuable material for creating advanced wound dressings. CS-based wound dressings have been shown to effectively manage exudates, prevent infections, and

accelerate the healing process in various wound types, including diabetic ulcers and burns.[31–33] Additionally, nanofibrous CS scaffolds have been observed to positively influence re-epithelialization and the regeneration of the granular layer of wounds, thereby enhancing the wound healing process.[34,35] While CS-based nanofibrous scaffolds show promise in various applications, including wound dressings, they often encounter limitations due to their fragility. Furthermore, challenges persist in achieving spinability and reproducibility of CS to yield stable nanofibrous scaffolds using Nanospider™ technology. To overcome these challenges, CS is often blended with other synthetic polymers. Polyvinyl alcohol (PVA), polyethylene oxide (PEO), and polycaprolactone (PCL) have gained widespread adoption to facilitate CS electrospinning and reduce its fragility.[36–39] These blends not only facilitate the electrospinning process but also enhance the biological performance of the resulting nanofibers, making them more effective in wound healing applications.[40–42] Additionally, the incorporation of antibacterial, antimicrobial, or antioxidant agents into nanofibrous scaffolds has proven to be a key strategy in wound healing. These agents can include metallic nanoparticles, carbon-based composites, and herbal medicines, which offer unique pharmacological effects that combat inflammation and microbial infections in wound areas.[43–50] Nanofibers loaded with antibacterial agents play a vital role in inhibiting bacterial growth and promoting wound healing.[51] The development of nanofibrous scaffolds loaded with antibiotics or other medical agents, such as tetracycline (TET), a broad-spectrum antibiotic, has garnered attention for their potential in rapid wound healing, encompassing infection control, inflammation reduction, and accelerating wound closure.[52–58]

Despite significant advancements in nanofibrous scaffolds, critical challenges persist in fully realizing their clinical potential. Previous research has often focused on binary polymer systems and encapsulation of therapeutic agents, leading to suboptimal drug release and reduced surface activity. Additionally, scaling up production while preserving scaffold functionality remains inadequately addressed. Our research aims to design, fabricate, and characterize nanofibrous scaffolds composed of three polymers, specifically examining how varying PEO and PCL compositions influence scaffold properties. We successfully electrospun a polymer blend of CS, PCL, and PEO into nanofibrous scaffolds using Nanospider™ technology, enabling large-scale production while maintaining desired functional properties. The scaffolds were characterized through SEM, FTIR, contact angle measurements, hydrolytic degradation, water vapor permeability tests, mechanical tests, and antibacterial activity assays, with cytotoxicity assessed using 3T3 fibroblasts. This approach advances beyond previous studies constrained by binary systems,[38,39,41,59] complex multi-step processes,[48] or traditional needle electrospinning.[60] Additionally, our approach enhances antibacterial efficacy through surface immobilization of TET, preserving its activity and allowing for post-production customization. This innovative approach: (i) demonstrates the feasibility of industrial-scale production for wound healing, (ii) enables surface immobilization of TET for personalized care, and (iii) offers tunable hydrophilicity, hydrolytic degradation and mechanical properties by adjusting the PEO/PCL ratio.

Materials and methods

As mentioned in the introduction, CS is a well-known natural biopolymer with great potential for wound dressing due to its biocompatibility, biodegradability, low immunogenicity, and antimicrobial properties, which help prevent infections and promote cell growth.[61] Its reactive amino groups further enhance wound healing by facilitating drug bonding and delivery. However, CS has drawbacks, including fragility and difficulties with spinnability during electrospinning.[62] To address these challenges, literature suggests that blending CS with PCL or PEO improves the mechanical strength, spinnability, and biocompatibility of the scaffolds, creating an optimal environment for wound healing.[38,39,41,59] PCL, with its flexibility, durability, and slow biodegradation, provides long-term structural support and enables controlled drug release.[63] However, PCL is highly hydrophobic and lacks cell-binding sites.[64] On the other hand, PEO enhances spinnability in needle-less electrospinning, aids in moisture retention, and promotes the formation of uniform nanofibers, though it has lower mechanical strength and is water soluble.[65] Our nanofibrous scaffold was designed to be easy to handle, non-toxic, and breathable, with the additional capability of drug bonding through its amino groups while effectively managing moisture. We hypothesize that adjusting the PEO/PCL ratio can tailor the scaffold's properties, leveraging the distinct characteristics of PEO and PCL for various wound healing applications. The selected mass ratios (6/2/2, 4/4/2, 2/6/2) were chosen to systematically examine how variations in PEO and PCL quantity affect scaffold properties, while maintaining a constant CS content. This approach enabled us to isolate the impact of different polymer ratios on critical factors such as antibacterial efficacy, breathability, moisture management, and mechanical strength.

Fabrication of nanofibrous scaffolds

Nanofibrous scaffolds were electrospun from polymer mixture solutions using needle-less electrospinning technology (Nanospider™ NS-Lab 1WS500U, Elmarco, Czech Republic). This standalone electrospinning system integrates industrial production technology with the precision of a high-end laboratory instrument (see Figure 1). The Nanospider™ technology employs a spinning electrode in the form of a thin wire, along with a head that applies the polymer solution across the entire length of this wire. When subjected to a strong electric field, nanofibers are generated from a thin layer of polymer solution deposited on the underlying material at the opposite electrode. Numerous studies have reported that the morphology of electrospun fibers is significantly influenced by factors such as polymer concentration, collector-wire distance, spinning speed, applied voltage, temperature, and air humidity. By carefully controlling these parameters, the morphology of the fibers can be precisely engineered.[66] In this study, we optimized both the polymer solution preparation and the electrospinning process to successfully produce defect-free nanofibrous scaffolds with consistent nanofiber morphology and high productivity using Nanospider™ technology. We specifically compared polymer blend concentrations of 8 wt% and 6 wt% for PEO/PCL/CS. At 4 wt%, bead formation occurred instead of nanofibers, while concentrations above 8 wt% hindered the initiation of needle-

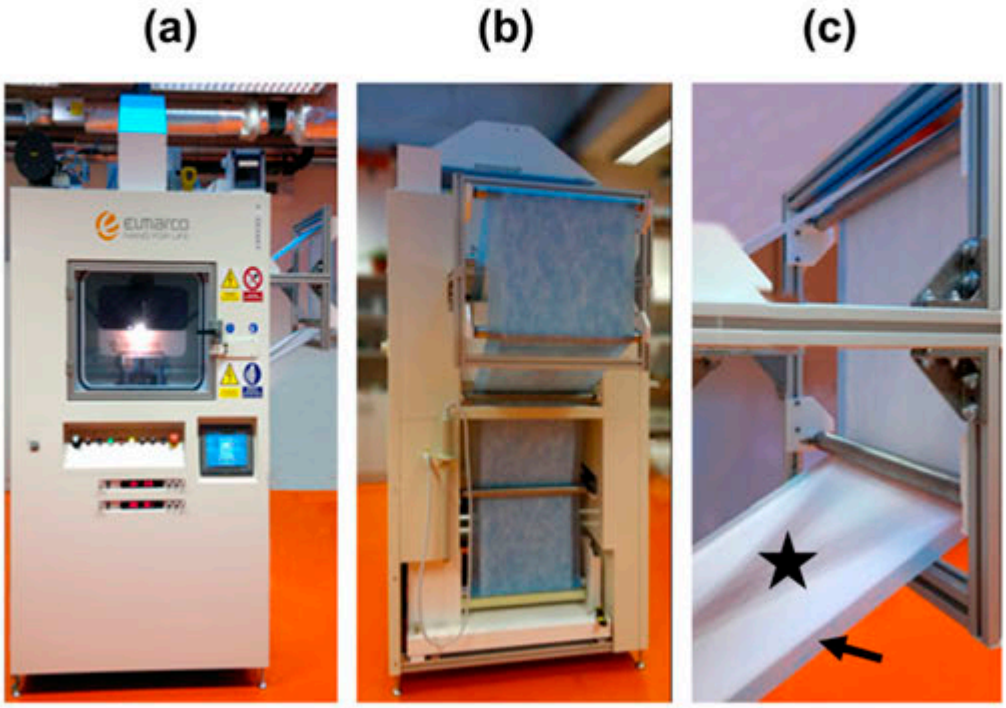

Figure 1. Photographs of the Nanospider™ NS-Lab 1WS500U: (a) front view, (b) side view, and (c) the resulting nanofibrous scaffold (asterisk) deposited onto the underlying spun-bond (arrow).

less electrospinning. The viscosities of polymer solutions prior to electrospinning were measured using a HAAKE RotoVisco 1 (Thermo Scientific) at 24°C, with a RV1 spindle operating from 10 r/min to 4000 r/min for 90 s.

For polymer solution preparation, two methods were compared. In the one-step method, solid polymers—PEO (Mn 100,000 g/mol, Sigma-Aldrich, USA), PCL (Mw 80,000 g/mol, Sigma-Aldrich, USA), and CS (Mw 30,000 g/mol, Glentham, UK)—were weighed in the ratios of 6/2/2, 4/4/2, and 2/6/2. The solvent mixture, consisting of acetic acid (AA, 99.98%, Sigma Aldrich) and formic acid (FA, 99%, Sigma Aldrich) in a 2/1 vol ratio, was added to dissolve the solid polymers. The polymer solutions were stirred at 200 r/min at room temperature for 24 h using a magnetic stirrer.

In the two-step method, each polymer was dissolved separately in the AA/FA solvent mixture (2/1, v/v) and stirred at 200 r/min for 24 h using a magnetic stirrer. The following day, the individual polymer solutions of PEO, PCL, and CS were mixed in the respective mass ratios (6/2/2, 4/4/2, 2/6/2). The combined solutions were stirred overnight using a magnetic stirrer for proper homogenization. The polymeric solutions PEO/PCL/CS were then transferred into a 500 mL reservoir connected to the head of the electrospinning apparatus. A voltage of either 40 or 65 kV was applied between the wire and the collector, with a distance of 150 or 180 mm, at a controlled temperature of 22°C and humidity of 10%. The resulting nanofibers were deposited onto a backing paper along a negative collector electrode at a velocity of 15 mm/min (see Figure 2).

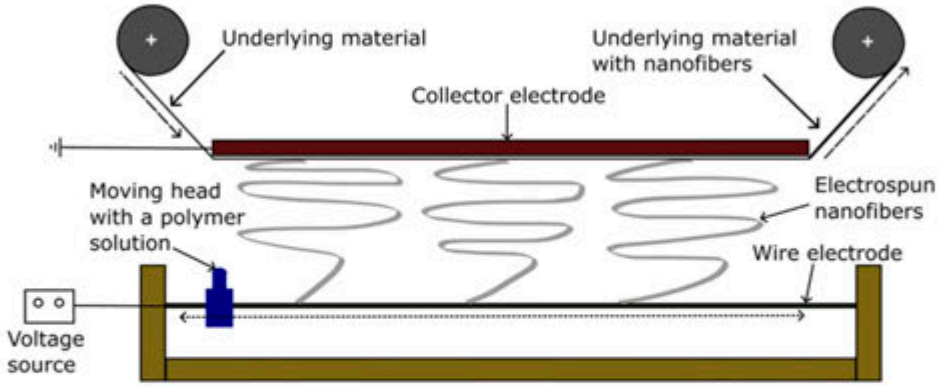

Figure 2. Schematic of needle-less electrospinning.

The resulting nanofibrous scaffolds were sheet-shaped, with dimensions of 50 × 600 cm. After electrospinning, the scaffolds were cut into A4-sized sheets and subjected to a stabilization process. This process involved heating the sheets overnight at 60°C, followed by removal of the scaffolds from the backing paper. The purpose of this step was to stabilize the scaffolds through cross-linking. After stabilization, the scaffolds were stored in a desiccator for further characterization.

Immobilization of tetracycline onto the nanofibrous scaffolds

The immobilization of TET (98.0%–102.0% HPLC, Sigma-Aldrich, USA) onto the PEO/PCL/CS nanofibrous scaffolds was carried out by immersing the scaffolds in a 0.5 wt% TET solution dissolved in ethanol. This process was conducted in a hermetically sealed chamber, where the scaffolds were placed in glassware containing the TET solution and shaken at 50 r/min using a laboratory shaker at room temperature. After 90 min, the scaffolds labeled as AB were removed from the TET solution and laid out on a silicone sheet to air dry at room temperature for 24 h. In contrast, scaffolds labeled as B underwent the same removal process but were thoroughly washed with ethanol before drying. These distinct treatments were designed to evaluate the antibacterial efficacy of the nanofibrous scaffolds, comparing those with the surface-bound TET component (sample_B) to those where TET was merely adsorbed onto the nanofibers (sample_AB).

Morphological characterization

Scanning electron microscopy (SEM) using the VEGA TS 5130 instrument was employed to characterize the surface morphology of the nanofibrous scaffolds and to measure the diameters of the nanofibers. SEM images were acquired with an accelerating voltage of 30 kV. Prior to imaging, each nanofibrous scaffold was coated with gold via sputtering. SEM micrographs were then analyzed using the image analysis software VegaTC to measure the average diameter of approximately 100 fibers from each scaffold type. The

gram per square meter (GSM) of the nanofibrous scaffolds was measured according to ISO 3801:1977.

Chemical analysis

Fourier transform infrared spectroscopy (FTIR) analysis was performed using attenuated total reflectance (ATR) with a Nicolet Magna-IR 560 spectrophotometer (Thermo Scientific). ATR-FTIR spectra were recorded over the wavenumber range of 3700–700 cm^{-1} using a split peak accessory. Each spectrum was the average of 64 scans, with a resolution of 4 cm^{-1}. The FTIR spectra of PEO/PCL/CS nanofibrous scaffolds, with mass ratios of 2/6/2, 4/4/2, and 6/2/2, were analyzed before and after immersion in deionized (DI) water for 1 and 7 days.

The content of functional amino groups on the surface of the scaffolds was determined spectrophotometrically through a specific reaction with methyl orange (MO, Sigma-Aldrich, USA), which binds to primary amino groups.[67] Nanofibrous scaffolds were incubated in a 0.05% MO solution and 0.01 M phosphate buffer (Sigma-Aldrich, USA) at pH 4.7 for 1 h. After incubation, unbound dye was washed away, and MO bound to the amino groups was released by rinsing with a 0.1 M sodium carbonate solution (anhydrous, ≥99.5%, Sigma-Aldrich, USA). The concentration of bound MO, which indicates the available functional groups, was measured spectroscopically at 465 nm using Lambert-Beer's law:

$$A = \varepsilon_\lambda * c * d \tag{1}$$

where ε_λ is the molar extinction coefficient of the substance with molar concentration c [mol.L^{-1}] at wavelength λ [nm], and A is the absorbance of the solution, which depends on the thickness of the measured solution layer d [cm].

Hydrolytic degradation test

A hydrolytic degradation test was conducted to evaluate the stability and degradability of the nanofibrous scaffolds. The scaffolds were initially dried at 60°C for 24 h. Subsequently, they were immersed in DI water and incubated at 37°C for 7 days. During this period, the solid material was collected using a nylon filter (9 cm diameter) at 1, 2, and 7 days, and then dried to a constant weight at 60°C for an additional 24 h.[68] The percentage of remaining nanofiber mass g, representing the insoluble portion of the scaffolds, was calculated using the following equation:

$$g(\%) = \left(\frac{w_e}{w_d}\right) * 100 \tag{2}$$

where w_d and w_e are the weights of the dry nanofibrous scaffold [g] before and after hydrolytic degradation, respectively.

Structural and morphological changes in the nanofibrous scaffolds were assessed through SEM imaging before and after hydrolytic degradation.

Contact angle measurement

Optical tensiometry, also known as contact angle goniometry, is a widely used technique for determining the contact angle of a liquid droplet on a solid surface, thereby characterizing its surface properties.[69] To assess the hydrophilicity of the nanofibrous scaffolds, contact angle measurements were performed at three different positions using a Kruss Drop Shape Analyzer DS4 at room temperature. A 2 μL droplet of DI water was placed onto the dry scaffold surface, and the average contact angle values were calculated from these measurements.

Characterization of mechanical properties

The mechanical properties of the nanofibrous scaffolds were evaluated using a uniaxial tensile test performed with a LabTest 2.010 system (LabControl, Czech Republic) at room temperature. Nanofiber scaffolds, sized 20 × 60 mm, were placed within a window frame and mounted onto the tensile test grips. Prior to initiating the test, the vertical ribs of the frame were cut. The scaffolds were stretched at a strain rate of 10 mm/min until failure. Stress-strain curves were recorded, and Young's modulus was calculated from the slope of these curves within the strain range of 5%–10%.

Moisture vapor transmission rate measurement

Moisture vapor transmission rate (MVTR) of the nanofibrous scaffolds was measured according to the European Standard EN13726-2:2002, which outlines test methods for vapor-permeable film dressings.[70] Each scaffold was affixed to a Paddington cup with a 10 cm^2 opening, containing 25 mL of water. The cup, along with its contents, was weighed and placed in an incubator at 37°C. To maintain low relative humidity within the chamber, a tray filled with 1 kg of freshly dried silica gel was placed at the bottom of the incubator. At predetermined intervals (ranging from 1 to 7 days), the entire cup system was reweighed, and the weight of moisture vapor loss through the nanofibrous scaffold was recorded. MVTR [g/m^2/day] was calculated using the formula:

$$MVTR = \frac{weight\ loss}{area * time} \tag{3}$$

where *weight loss* is the difference in weight [grams] before and after the test, *area* is the exposed surface area of the sample [m^2] and *time* is the duration of the test [days].

In vitro cytotoxicity evaluation

In vitro cytotoxicity of the nanofiber scaffolds was evaluated using two methods in accordance with ISO 10993-5.[71] Prior to testing, the nanofibrous scaffolds were rinsed three times in DI water for 10 min and dried overnight at room temperature to remove any residual solvents. The dried scaffolds were then sterilized on both sides using UV light for 20 min.

For the direct cytotoxicity assay, 3T3 fibroblasts (American Type Culture Collection, Manassas, USA) were seeded at a concentration of 6×10^4 cells per well in sterile 24-well tissue culture plates. The cells were cultured in Dulbecco's Modified Eagle Medium (DMEM, StableCell™, Sigma-Aldrich, USA) supplemented with 5% fetal bovine serum (FBS, non-USA origin, Sigma-Aldrich, USA), 5% newborn calf serum (NBCS, USA origin, Sigma-Aldrich, USA), and 1% penicillin-streptomycin (P/S, suitable for cell culture, Sigma-Aldrich, USA) at 37°C in a 5% CO_2 environment for 24 h. After confirming cell layer consistency under a microscope, the supplemented DMEM was removed, and the scaffolds with controls (6 mm diameter circle-shaped) were carefully placed on the cell layer. Fresh supplemented DMEM was added, and the scaffolds were incubated in direct contact with the cells at 37°C in a 5% CO_2 environment for the next 24 h. Polyethylene high-density film (HDPE film, Sigma-Aldrich, USA) served as the negative control, while a 0.1% ZDEC-polyurethane (PU) film (ZDEC-PU film, Hatano Research Institute, Food and Drug Safety Center, Japan) was used as the positive control.

For the indirect cytotoxicity assay, 3T3 fibroblasts were seeded at a concentration of 1×10^4 cells per well in sterile 96-well tissue culture plates. The cells were cultured in DMEM supplemented with 5% FBS, 5% NBCS, and 1% P/S at 37°C in a 5% CO_2 environment for 24 h. Eluates of the tested materials were prepared in supplemented DMEM at a concentration of 5 mg/mL and were incubated at 37°C in a 5% CO_2 environment for 24 h. After confirming cell layer consistency, the supplemented DMEM was removed, and the eluates from the tested scaffolds and controls were carefully added to the cell layer. The cells were then incubated with the eluates at 37°C in a 5% CO_2 environment for the next 24 h. Sodium dodecyl sulfate (SDS, ≥98.5% (GC), Sigma-Aldrich, USA) at a concentration of 0.2 mg/mL in supplemented DMEM served as the positive control.

Both direct and indirect cytotoxicity assays of the nanofibrous scaffolds were evaluated using the 3-(4,5-dimethylthiazol-2-yl)-2,5-diphenyl tetrazolium bromide (MTT, Duchefa Biochemie, Netherlands) assay. Sample aliquots (10 per each time point) of 100 µL were transferred to a 96-well plate, and the absorbance was measured at 570 nm against 650 nm using a microplate reader. Viability of nanofibrous scaffolds was calculated based on the absorbance values obtained from wells containing cells incubated with the scaffold/eluate (A_{SAMPLE}), the mean absorbance of wells containing only DMEM (A_{DMEM}), and the absorbance of wells containing non-affected cells (incubated with no material) (A_{CELLS}):

$$Viability(\%) = \left(\frac{A_{SAMPLE} - A_{DMEM}}{A_{CELLS} - A_{DMEM}}\right) * 100 \quad (4)$$

Antimicrobial activity

The antibacterial activity of the nanofibrous scaffolds was evaluated using the Kirby-Bauer disk diffusion method against two bacterial strains: *Escherichia coli* (ATCC 25922) and *Staphylococcus gallinarum* (ATCC 35539), obtained from the Czech Collection of

Microorganisms at Masaryk University. Both strains were prepared at a concentration of 1×10^6 CFU/mL, cultured in a shaker incubator at 200 r/min and 37°C, and adjusted to an OD_{600} of 0.5. The bacterial suspension was then evenly spread on sterile agar plates using a sterile swab. Nanofibrous scaffolds with TET, cut into 1 cm diameter circles, and controls (scaffolds without TET) were placed on the agar surfaces. After a 24-h incubation at 37°C, the presence of a clear zone of inhibition around the scaffolds was measured. The zone of inhibition, indicative of antibacterial activity, reflects the diffusion of TET from the scaffold and its effectiveness in preventing bacterial growth. The size of this zone correlates with the level of antimicrobial activity, with larger zones indicating greater effectiveness.

Statistical analysis

All experiments were performed in triplicate (at a minimum) to ensure accuracy and reproducibility. Results are expressed as the mean ± standard deviation (SD). Statistical analysis was conducted using the *t* test to compare data between scaffolds. Significance levels are indicated: $p < 0{,}05$ (*), $p < 0{,}01$ (**), *and* $p < 0{,}001$ (***).

Results and discussion

Morphology of PEO/PCL/CS nanofibrous scaffolds

Structural factors such as fiber diameter, porosity, and homogeneity are crucial in designing wound healing patches to optimize therapeutic outcomes. Finer nanofibers, with a higher surface area-to-volume ratio, enhance cell attachment and drug absorption, making them effective for wound care.[72,73] A porous structure facilitates moisture retention, gas exchange, and nutrient transport, creating an ideal healing environment.[74,75] Homogeneous nanofibers ensure consistent drug distribution and scaffold integrity, leading to reliable healing.[76] Conversely, larger fibers, non-porous structures, and non-homogeneous scaffolds can impair these processes and reduce wound healing efficacy.[77] Therefore, incorporating these structural features through electrospinning is essential for advancing wound care solutions. While needle-less electrospinning offers advantages such as scalability, it also presents several challenges. In this method, the polymer solution is exposed to a large surface area, causing multiple jets to form spontaneously due to surface tension. Controlling the number and uniformity of these jets is difficult, often resulting to non-uniform fiber diameters and inconsistent fiber structures. Additionally, not all polymers are compatible with needle-less electrospinning, as some require specific solvents or conditions that are not feasible in this system. The viscosity and conductivity of the polymer solution are crucial, as they must fall within a specific range to initiate and sustain multiple jets. If these parameters are not met, stable jet formation may fail, leading to interrupted fiber production or the formation of beads.[66]

SEM images revealed that nanofibrous scaffolds electrospun under our proposed and repeatedly tested conditions (both process and materials) exhibited a homogeneous structure, providing a porous texture with no apparent beads or significant defects

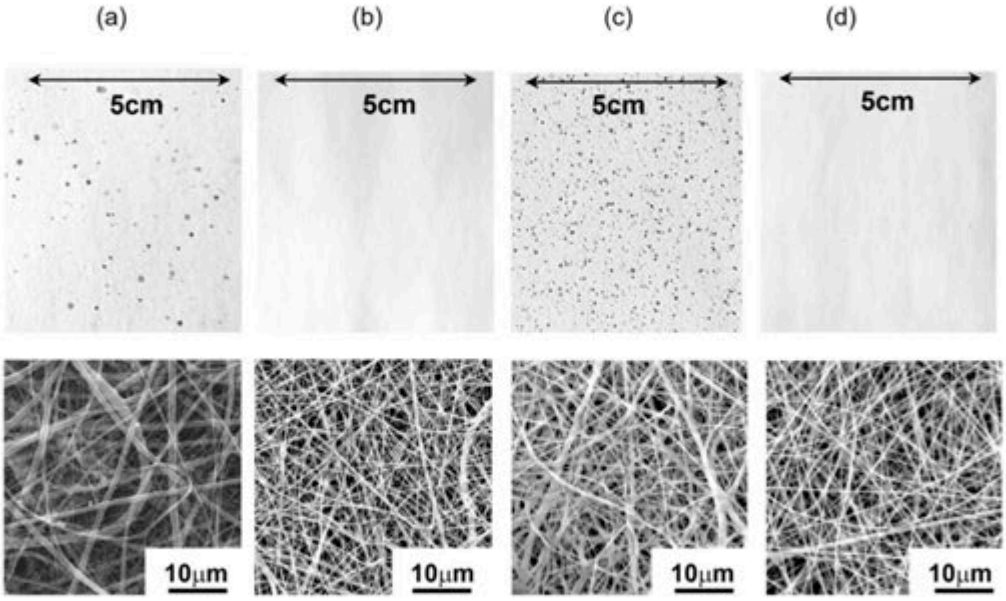

Figure 3. Photographs and SEM images of electrospun nanofibrous scaffold PEO/PCL/CS from polymer solutions prepared by (a) one-step and (b) two-steps method. Polymer solution concentrations are shown in (c) 8 wt% and (d) 6 wt%.

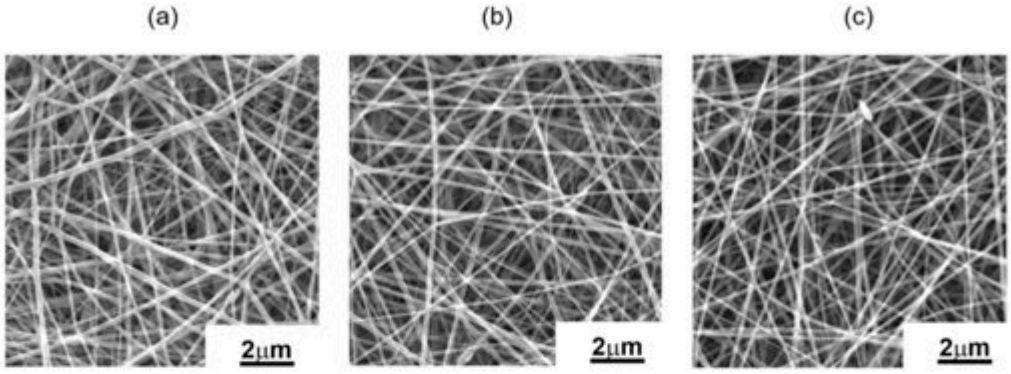

Figure 4. SEM images of nanofibrous scaffolds prepared from PEO/PCL/CS polymer mixtures with mass ratios of (a) 6/2/2, (b) 4/4/2, and (c) 2/6/2. The scaffolds were produced using the two-step preparation method at a polymer concentration of 6 wt% by needle-less electrospinning with a 150 mm electrode distance and a voltage of 65 kV.

(see Figures 3 and 4). To produce defect-free nanofibrous scaffolds, the two-step method for polymer solution preparation proved to be more effective, resulting in higher-quality nanofibers compared to the one-step method (see Figure 3(a) versus (b)). In terms of polymer solution concentration, a consistent production of defect-free nanofibers was observed at a concentration of 6 wt%. At higher concentrations, macroscopic holes began to appear in the scaffolds (see Figure 3(c) versus (d)). For electrospinning with an

electrode distance of 150 mm and a voltage of 40 kV, all scaffolds exhibited macroscopic holes (photographs not shown). When the voltage was adjusted to 65 kV at the same electrode distance, no macroscopic holes were observed in the nanofibrous scaffolds. Moreover, all nanofibrous scaffolds produced under these conditions achieved a higher GSM than those produced at 40 kV. When electrospinning was performed with an electrode distance of 180 mm and a voltage of 65 kV, all nanofibrous layers showed a lower GSM (see Table 1).

Literature suggests that the ideal GSM for wound healing patches depends on their application and desired properties. Higher GSM patches provide robust protection, better absorption, and greater structural integrity, making them suitable for high-exudate wounds that require cushioning.[78] Conversely, lower GSM patches are lighter, thinner, more breathable, and flexible, making them ideal for wounds where mobility and comfort are prioritized.[79] The selection should balance the wound's needs with patient comfort to achieve optimal healing outcomes.

Upon comparing fiber diameters, the highest value of 185 ± 53 nm was observed in scaffolds produced with an electrode distance of 150 mm and a voltage of 40 kV. In contrast, the lowest fiber diameter of 129 ± 40 nm was observed in scaffolds produced with an electrode distance of 180 mm and a voltage of 65 kV (see Table 1). Statistical analysis using the *t* test revealed no significant differences in fiber diameters between scaffolds with varying mass ratios of PEO/PCL/CS.

For further characterization and TET immobilization, nanofibrous scaffolds prepared using (i) the two-step method, (ii) a polymer concentration of 6 wt%, and (iii) an electrode distance of 150 mm with a voltage of 65 kV were selected. The viscosities of the polymer solutions for the 6/2/2, 4/4/2, and 2/6/2 compositions were 309 ± 6, 487 ± 9, and 546 ± 8 MPa·s, respectively. The structural morphologies of these scaffolds are shown in Figure 4 and Table 1.

In a previous study,[80] needle-less electrospinning was employed to produce wound healing patches from a single-component PCL system, resulting in a maximum GSM of 3.4 g/m^2 and an average fiber diameter of 160 nm. In contrast, this study successfully fabricated nanofibrous scaffolds composed of three polymers (PEO/PCL/CS) using needle-less electrospinning, without the need for toxic solvents or cross-linking agents.

Table 1. GSM and fiber diameters (fd) of nanofibrous scaffolds prepared by needle-less electrospinning under different electrode distance and voltage conditions. Results are expressed as mean ± SD.

Electrospinning parameters	PEO/PCL/CS 6/2/2	PEO/PCL/CS 4/4/2	PEO/PCL/CS 2/6/2
Distance 150 mm/ voltage 40 kV	GSM: 2.6 ± 0.1 g/m^2, fd: 185 ± 53 nm	GSM: 2.1 ± 0.2 g/m^2, fd: 159 ± 35 nm	GSM: 1.9 ± 0.1 g/m^2, fd: 153 ± 41 nm
Distance 150 mm/ voltage 65 kV	GSM: 8.6 ± 0.2 g/m^2, fd: 148 ± 38 nm	GSM: 7.4 ± 0.2 g/m^2, fd: 138 ± 40 nm>	GSM 6.8 ± 0.1 g/m^2, fd: 134 ± 37 nm
Distance 180 mm/ voltage 65 kV	GSM: 6 ± 0.2 g/m^2, fd: 146 ± 35 nm	GSM: 4.8 ± 0.1 g/m^2, fd: 135 ± 37 nm	GSM: 4.3 ± 0.1 g/m^2, fd: 129 ± 40 nm

Our scaffolds achieved finer fiber diameters, ranging from 134 to 148 nm, and demonstrated superior structural integrity and ease of manipulation, with GSM values between 6.8 and 8.6 g/m^2. These results suggest that our multi-component system offers enhanced structural properties, making it more suitable for wound healing applications.

Chemical characterization of PEO/PCL/CS nanofibrous scaffolds

FTIR analysis was employed to characterize the structure and interactions within the PEO/PCL/CS nanofibrous scaffolds, focusing on identifying the presence of individual polymers. The FTIR spectrum was anticipated to show characteristic peaks corresponding to the functional groups of PEO, PCL, and CS.

PEO typically exhibits C–O–C stretching around 1100 cm^{-1}, CH_2 wagging and twisting near 1342–1240 cm^{-1}, and C–H stretching at 2891 cm^{-1}.[81] PCL is known for its strong C = O stretching peak around 1720–1735 cm^{-1}.[82] CS typically shows a broad O–H and N–H stretching between 3200 and 3600 cm^{-1}, N–H bending (amide II) around 1550–1650 cm^{-1}, and C–N stretching (amide III) near 1250–1310 cm^{-1}.[83,84] In polymer blends, these peaks may overlap, with potential shifts or changes in intensity due to interactions such as hydrogen bonding between the polymers.[85] The ATR–FTIR spectra of the PEO/PCL/CS nanofibrous scaffolds with different mass ratios are shown in Graph 1.

The FTIR analysis of nanofibrous scaffolds composed of PEO, PCL, and CS revealed characteristic peaks confirming the successful incorporation of these polymers. A prominent peak at 1724 cm^{-1} corresponds to the C = O stretching of PCL, confirming its presence. Notably, there was no significant increase in the intensity of this C = O stretching vibration band across the different scaffold compositions, indicating that the chemical environment of PCL remains relatively consistent regardless of the PEO or CS

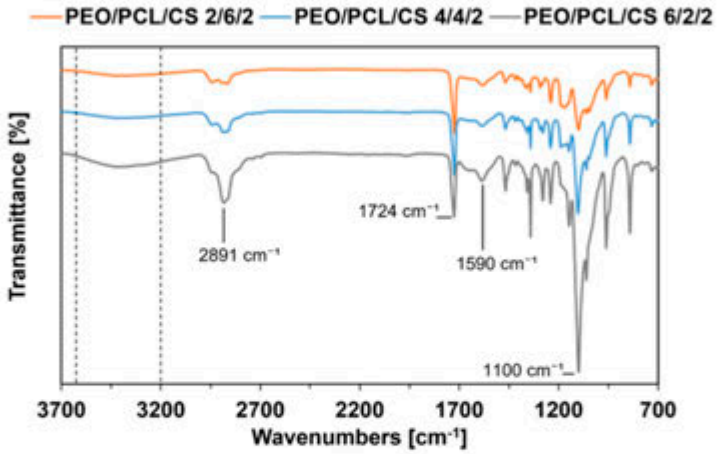

Graph 1. ATR-FTIR spectra of nanofibrous scaffolds composed of PEO/PCL/CS with varying mass ratios (6/2/2, 4/4/2, 2/6/2). The spectra display peaks corresponding to different functional groups present in the scaffolds: 1724 cm^{-1} (confirming the presence of PCL), 1100 cm^{-1} and 2891 cm^{-1} (indicating the presence of PEO), and a broad peak between 3200 and 3600 cm^{-1} along with a sharp peak at 1590 cm^{-1} (confirming the presence of CS).

content. The C–O–C stretching vibrations at 1100 cm^{-1} and C-H stretching at 2891 cm^{-1} verify the presence of PEO, with the intensity of these bands increasing as the PEO mass ratio increased. Additionally, a broad peak between 3200 and 3600 cm^{-1}, along with a sharp peak at 1590 cm^{-1}, attributed to the amino, hydroxyl, and amide II groups in CS, confirmed its successful incorporation. Moreover, the FTIR data suggest potential chemical interactions, particularly hydrogen bonding, between PEO and CS. This is supported by the increasing intensity in the 3200–3600 cm^{-1} range as PEO content increases. Notably, this increase occurs despite a constant CS content across all scaffolds, indicating that the changes in peak intensity are primarily driven by amount of PEO. PCL, being hydrophobic, likely contributes to the scaffold's mechanical strength through physical entanglement rather than direct chemical bonding. Additionally, possible ionic interactions between PEO and CS may further enhance the scaffold's structural integrity.[41,59,97]

Further analysis of the FTIR results revealed notable changes during the solubility study, particularly in the spectrum of PEO/PCL/CS nanofibrous scaffolds after 7 days of hydrolytic degradation in DI water at 37°C. Specifically, a reduction in the characteristic peak associated with PEO (1100 cm^{-1}) was observed, indicating the gradual dissolution of PEO from the scaffold during the soaking period, as shown in Graph 2. This information is crucial for designing scaffolds that retain their integrity and functionality throughout the intended application period, such as in wound healing.

The immobilization of molecules onto nanofibers is highly dependent on the presence of surface-accessible functional groups. Functional groups such as amine, imine, and carboxylic groups are crucial for making the surface active and suitable for molecule immobilization. Among these, primary amine groups, like those found in CS, are particularly favorable for antibiotic conjugation purposes.[86]

The presence of surface-accessible amino groups was confirmed across all nanofibrous scaffolds. As shown in Graph 3., the variation in the mass ratios of PEO/PCL/CS did not significantly affect the presence of these amino groups. This is likely because the mass ratio of CS remained constant in all mixtures. Specifically, the quantification of available

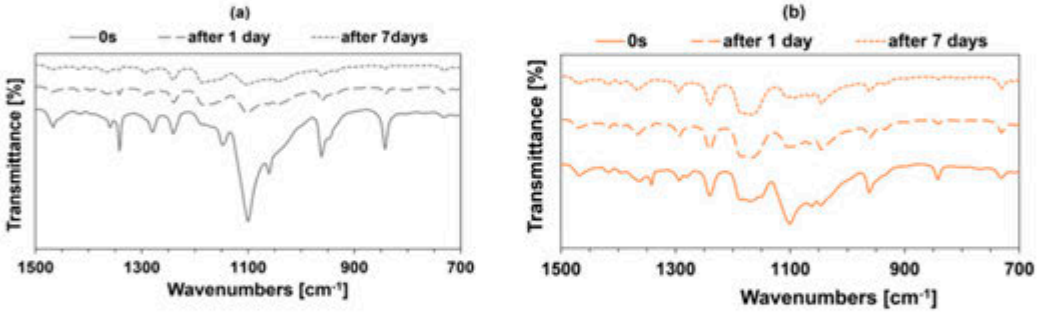

Graph 2. ATR-FTIR spectra of nanofibrous scaffolds made from PEO/PCL/CS with mass ratios of (a) 6/2/2 and (b) 2/6/2, both before and after hydrolytic degradation in DI water for 7 days at 37°C. The spectra highlight a peak attributed to C–O–C stretching, which signifies the presence of PEO.

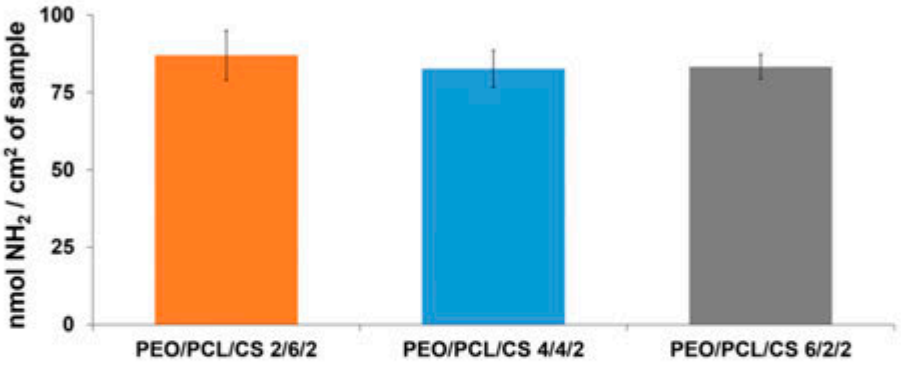

Graph 3. Quantification of available amino groups on PEO/PCL/CS nanofibrous scaffolds with different mass ratios (6/2/2, 4/4/2, 2/6/2). Error bars represent SD. (n = 3).

amino groups on PEO/PCL/CS scaffolds with mass ratios of 2/6/2, 4/4/2, and 6/2/2 were 86.9 ± 8, 82.6 ± 6, and 83.3 ± 4 nmol NH_2/cm^2, respectively. Statistical analysis using the t test revealed no significant differences in the number of amino groups between scaffolds with different mass ratios of PEO/PCL/CS.

Hydrolytic degradation

Hydrolytic degradation is critical for the functionality of wound healing patches, influencing how the scaffold degrades in body fluids. The degradation rate must be carefully controlled: too rapid degradation may fail to provide adequate support for the wound, while too slow degradation can hinder healing or require surgical removal.[87]

Materials like PCL, which degrade slowly, provide extended structural support, whereas PEO, a more hydrophilic and faster-degrading polymer, contributes to rapid hydrolytic degradation.[88] Balancing hydrolytic degradation is essential to ensure scaffolds provide effective support while degrading safely over time.[89]

The hydrolytic degradation study of the nanofibrous scaffolds provided insights into their degradation behavior and weight loss profiles over 7 days in DI water. All scaffolds demonstrated noticeable degradation, as indicated by their weight loss. Specifically, scaffolds with PEO/PCL/CS mass ratios of 6/2/2, 4/4/2, and 2/6/2 experienced weight losses of 73.2 ± 0.8%, 54 ± 1.3%, and 35.8 ± 1%, respectively, within 7 days (see Graph 4). The study revealed a correlation between weight loss and PEO content: higher PEO content resulted in greater weight loss, indicating that PEO concentration directly affects the degradation kinetics of the scaffolds. The degradation did not plateau over the 7-day period, showing a continuous decrease with the most significant degradation observed on the first day of, indicating an initial burst degradation phase (see Graph 4.). Statistical analysis using the t test revealed significant differences in weight loss between scaffolds with varying mass ratios of PEO/PCL/CS.

SEM analysis revealed that the scaffolds maintained a partially porous structure throughout the dissolution period, as shown in Figure 5. Despite prolonged immersion in

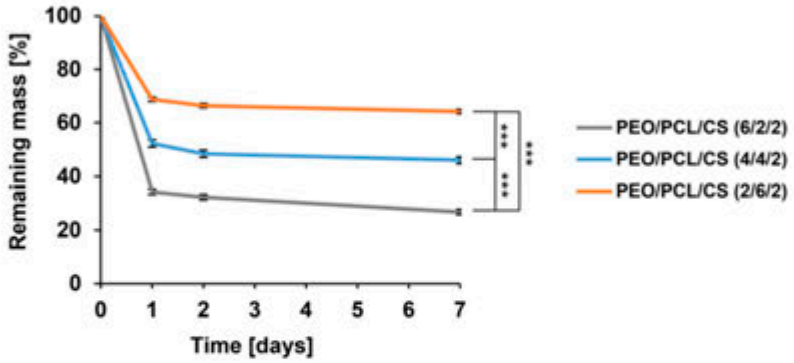

Graph 4. Hydrolytic degradation of nanofibrous scaffolds composed of PEO/PCL/CS with different mass ratios, immersed in DI water at 37°C for 1, 2, and 7 days. Significant statistical differences between the scaffolds with different mass ratios of PEO/PCL/CS were observed using the *t* test, with *** indicating $p \leq 0.001$. Error bars represent SD. ($n = 3$).

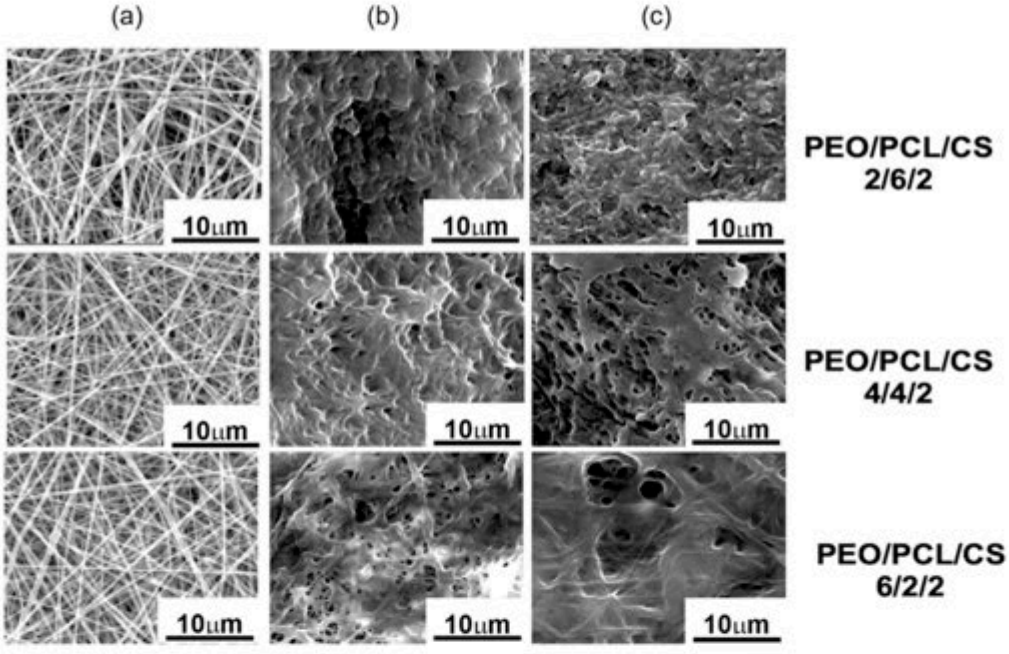

Figure 5. SEM images of thermal stabilized nanofibrous scaffolds with different mass ratios of PEO/PCL/CS immersed into DI water at 37°C for (a) 0 s, (b) 1 day and (c) 7 days.

DI water, the scaffolds did not collapse into a homogeneous film, demonstrating their stability and durability in an aqueous environment.

In a study,[41] a two-component PCL/CS system was electrospun for wound healing applications, resulting in a hydrolytic degradation rate of approximately 90% after 7 days. In contrast, our PEO/PCL/CS scaffolds exhibited lower degradation rates, ranging from

73.2 ± 0.8% to 35.8 ± 1%, depending on the PEO/PCL mass ratio. The ability to tailor degradation rates by adjusting the PEO/PCL ratio enhances the adaptability of our scaffolds to specific wound healing requirements. Furthermore, the stability and durability of our scaffolds in an aqueous environment, achieved without toxic cross-linking agents, underscore their potential for biomedical applications, particularly in scenarios involving prolonged fluid exposure.

Wettability of PEO/PCL/CS nanofibrous scaffolds

The hydrophilicity of materials used for wound healing is a critical parameter that significantly influences their ability to manage wound exudate and maintain a moist environment conducive to proper healing. Assessing the hydrophilic properties of nanofibrous scaffolds is vital for evaluating their suitability in wound care, particularly regarding their capacity to facilitate fluid drainage while retaining optimal moisture levels.[90] Hydrophilic surfaces are generally preferred over hydrophobic ones in wound healing patches, as they promote a moist environment, which accelerates epithelialization and improves overall healing outcomes.[91,92] Furthermore, hydrophilic surfaces adhere more effectively to wet surfaces, enhancing treatment efficacy.[93] Conversely, hydrophobic surfaces can disrupt moisture balance and inhibit cell migration, potentially hindering the healing process.[94]

Contact angle measurements were performed to quantitatively assess the wetting behavior of water droplets on the nanofibrous scaffolds' surfaces. As shown in Figure 6, these measurements provide valuable insights into how variations in scaffold

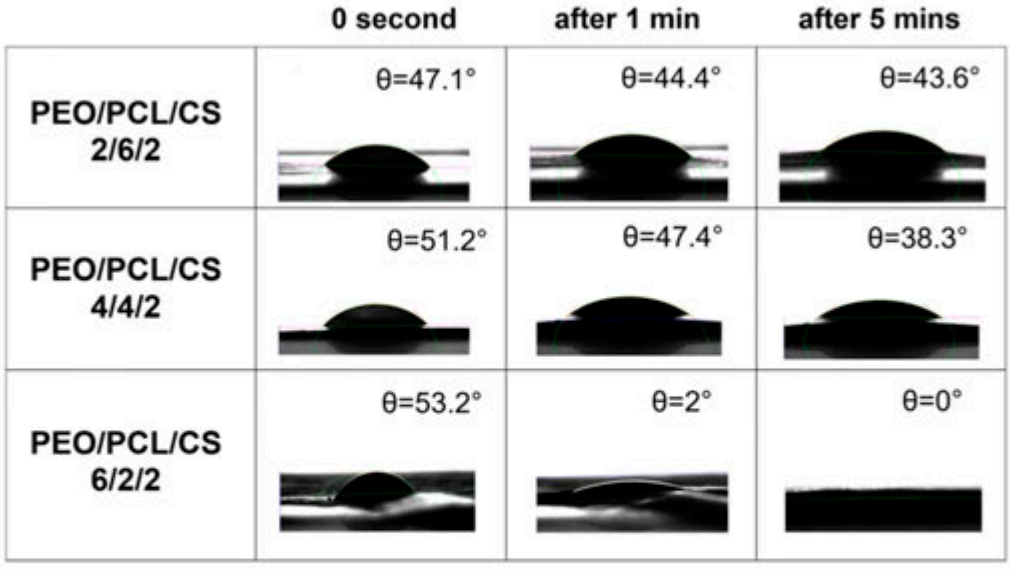

Figure 6. Water contact angle measurement of nanofibrous scaffolds composed of PEO/PCL/CS with mass ratios of 6/2/2, 4/4/2, and 2/6/2, measured at 0 s, 1 min, and 5 min.

composition, particularly changes in the proportions of PCL and PEO, influence their surface properties.

The static contact angle of water droplets on the PEO/PCL/CS scaffolds with mass ratios of 2/6/2 and 4/4/2 was measured at 42.9 ± 3.8° and 37.7 ± 3.3°, respectively, within 5 min of applying DI water, indicating moderate hydrophilicity. In contrast, the scaffold with a 6/2/2 mass ratio achieved a contact angle of 0.7 ± 1.3° within just 60 s, suggesting rapid surface wetting. The difference in contact angles after 5 min between the PEO/PCL/CS scaffolds with mass ratios of 6/2/2 and 2/6/2 was found to be statistically significant using the *t* test. This behavior can be attributed to the different mass ratios of PEO and PCL, as PEO is known for its hydrophilic properties, while PCL is more hydrophobic.

In a previous study,[48] the contact angles for a mesh of PCL nanofibers combined with CS/PEO nanofibers ranged from 55.5° to 107°, indicating a relatively hydrophobic surface. In contrast, our study achieved significantly lower contact angles, ranging from approximately 0 to 43°, depending on the PEO/PCL/CS mass ratio, indicating a more hydrophilic surface. The reduced contact angles and enhanced hydrophilicity of our scaffolds are expected to improve the functionality and therapeutic effectiveness of wound healing patches.[95]

Mechanical properties of PEO/PCL/CS nanofibrous scaffolds

Scaffolds intended for implantation must possess suitable mechanical properties to endure applied stresses while maintaining the flexibility required for diverse wound healing applications.[12] To evaluate these properties, the average ultimate tensile strength (UTS), elongation at fracture (A), and Young's modulus (E) of the scaffolds were measured. Ultimate tensile strength refers to the point at which the scaffold begins to fail under stress, while Young's modulus is determined from the slope of the linear region of the stress-strain curve, prior to reaching the yield stress. The results of these mechanical tests are summarized in Table 2.

The Young's modulus of the PEO/PCL/CS nanofibrous scaffolds with mass ratios of 2/6/2, 4/4/2, and 6/2/2 is 106.7 ± 8.5 MPa, 128.9 ± 7.2 MPa, and 170.7 ± 11.9 MPa, respectively. The decrease in Young's modulus with increasing PCL content is due to PCL's inherent flexibility, which reduces the overall stiffness of the scaffold. Despite this, the ultimate tensile strength increases with higher PCL content, as PCL enhances the scaffold's ability to distribute stress and bear higher loads.[96] Additionally, the elongation at fracture for the PEO/PCL/CS 2/6/2 scaffold is 26 times greater compared to scaffold

Table 2. Mechanical properties of PEO/PCL/CS nanofibrous scaffolds with different mass ratios.

Nanofibrous scaffold	Young's modulus E [MPa]	Ultimate tensile stress UTS [MPa]	Elongation at fracture A [%]
PEO/PCL/CS 2/6/2	106.7 ± 8.5	4.8 ± 0.2	21 ± 2.9
PEO/PCL/CS 4/4/2	128.9 ± 7.2	3.2 ± 0.1	2.1 ± 0.3
PEO/PCL/CS 6/2/2	170.7 ± 11.9	2.3 ± 0.2	0.8 ± 0.1

with higher PEO content. This significant increase in elongation at fracture is attributed to PCL's high ductility and flexibility. As PCL content increases, the scaffold becomes more stretchable and can undergo larger deformations before breaking, resulting in much higher elongation at fracture.[97]

Despite the different mechanical behaviors observed with varying PEO and PCL compositions, the mechanical properties of the scaffolds—such as Young's modulus, ultimate tensile strength, and elongation at fracture—are comparable to those of native human skin. Native skin typically exhibits a Young's modulus in the range of 6-140 MPa, an ultimate tensile strength between 2 and 16 MPa, and significant elongation at break.[98,99] The scaffolds' properties closely align with these values, making them suitable for applications in skin regeneration, where mimicking the natural mechanical behavior of skin is crucial.

Moisture vapor transmission rate of PEO/PCL/CS nanofibrous scaffolds

Maintaining optimal moisture content is crucial for effective wound healing, as a moist environment supports cell proliferation and function.[100] Scaffolds with an MVTR below 1000 g/m^2/day may not effectively manage wound moisture, potentially leading to issues such as exudate buildup and patient discomfort.[101,102] An ideal MVTR, ranging from 1000 to 2000 *g*/m^2/day, strikes a balance between moisture retention and breathability, thereby enhancing the healing process by maintaining optimal moisture levels.[103,104] Conversely, scaffolds with an MVTR above 2000 *g*/m^2/day are suitable for wounds with high exudate levels, ensuring effective moisture management without excess buildup.[105]

The MVTR of PEO/PCL/CS nanofibrous scaffolds was assessed using the standardized Paddington cup method. Graph 5. Depicts the results, where a lower proportion of the original medium corresponds to a higher MVTR. Initially, there was no significant difference between the nanofibrous scaffolds and a commonly used certified polypropylene/viscose-based patch cushion (commercial dressing patch). However, over a period of 7 days, the moisture content of the nanofibrous scaffolds decreased by approximately 55%–63%, compared to the commercial dressing patch, which retained only

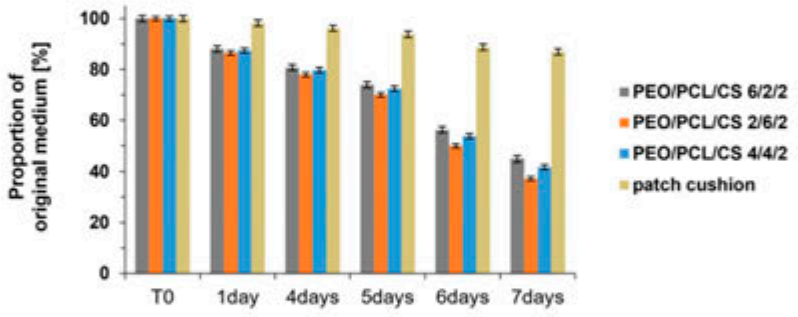

Graph 5. Monitoring of moisture vapor leakage from the Paddington cup system through nanofibrous scaffolds composed of PEO/PCL/CS with different mass ratios, and a commercially available patch cushion, evaluated according to the EN13726-2 standard. Error bars represent SD. (n = 3).

13% of its original moisture. This suggests that the commercial dressing may not effectively release water vapor, potentially hindering the wound healing process by maintaining a consistently wet environment.

Specifically, scaffolds with a higher mass ratio of PEO retained 44.9 ± 1.2% of their original moisture content after 7 days, whereas those with a lower PEO mass ratio retained 37.3 ± 0.8%. Furthermore, no statistically significant differences were observed between the nanofibrous scaffolds with varying mass ratios of PEO/PCL/CS, as shown in Graph 5.

Recalculating the proportion of the original medium to the MVTR using formula[3] yielded values of 1904.3 ± 28.6, 1941.4 ± 35.7, and 2005.7 ± 42.9 g/m^2/day for nanofibrous scaffolds with PEO/PCL/CS mass ratios of 6/2/2, 4/4/2, and 2/6/2, respectively. In contrast, the commercial dressing patch demonstrated less effective moisture management, potentially impeding the healing process. This highlights the superior performance of our scaffolds in maintaining optimal moisture levels for enhanced wound care. Notably, the MVTR values of our scaffolds exceed those reported in the literature,[59] where a two-layer scaffold (PCL nanofibers as the first layer and CS/PEO nanofibers as the second layer) achieved MVTR values of approximately 1252–1452 g/m^2/day. These results indicate that our nanofibrous scaffolds are highly effective in moisture management, making them suitable for exudative wounds, where precise moisture control is crucial.

Cytotoxicity of PEO/PCL/CS nanofibrous scaffolds

Cytotoxicity assessment is a critical step in developing safe and effective wound healing patches. Materials must be non-toxic and biocompatible, ensuring that they support healing without harming cells.[106,107] Common tests, such as MTT assays and direct contact evaluations, measure cell viability by observing how materials interact with cells. Compliance with ISO 10993 standards, particularly ISO 10993-5 for in vitro cytotoxicity testing, is crucial to ensure that materials meet safety and performance requirements, instilling confidence in their clinical use. These assessments are essential for confirming the safety of wound healing patches for patient care.[108,109]

To assess the suitability of the nanofibrous scaffolds for wound healing, a cytotoxicity study was conducted using the MTT assay. This method evaluates cell viability and metabolic activity, offering valuable insights into the biocompatibility of the scaffolds. Mouse fibroblast 3T3 cells were used as a model system due to their relevance in mimicking skin cell behavior in response to biomaterials. Graph 6. Presents the results of the cytotoxicity tests, showing the response of 3T3 fibroblasts when cultured in both direct and indirect contact with the scaffolds. The results are highly promising, indicating minimal cytotoxic effects of the nanofibrous scaffolds on the cultured cells. Viability consistently exceeded the 70% threshold recommended by ISO 10993-5, confirming the biocompatibility of the scaffolds. The MTT assay in direct contact demonstrated high cell viability, affirming that the PEO/PCL/CS nanofibrous scaffolds are suitable for wound healing applications. These findings align with existing literature that emphasizes the importance of direct methods for evaluating the safety of wound healing patches.[110] Statistical analysis using the *t* test revealed no significant differences in cytotoxicity

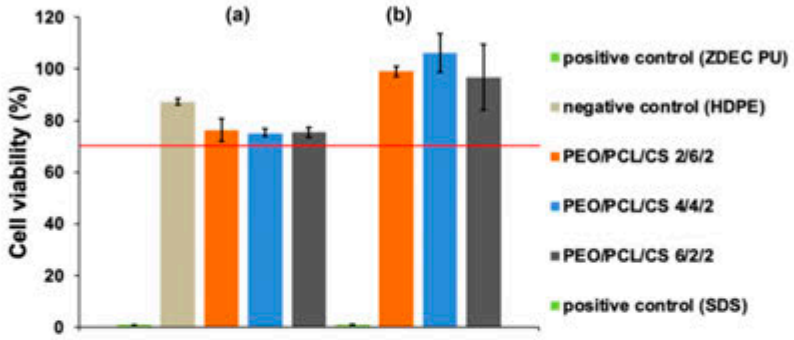

Graph 6. In vitro cytotoxicity assessed by the MTT assay of 3T3 cells seeded in (a) direct and (b) indirect contact with PEO/PCL/CS nanofibrous scaffolds after 1 day of culture. Error bars indicate SD. (n = 3).

between scaffolds with varying PEO/PCL/CS ratios, further demonstrating the consistent biocompatibility and safety of these scaffolds.

Antibacterial efficacy of PEO/PCL/CS nanofibrous scaffolds

Incorporating antibacterial properties into nanofibrous wound healing patches is crucial for preventing infections that could impede the healing process.[111] These patches are designed to combat bacterial contamination on contact, thus reducing inflammation and the risk of systemic infection while supporting tissue regeneration.[112,113] Evaluating their efficacy against common bacterial strains is essential to ensure effective infection prevention and wound healing.[114,115]

To assess the antibacterial efficacy of our nanofibrous scaffolds, we performed microbiological testing using the Kirby-Bauer method on *E. coli* and *S. gallinarum*. The size of the inhibition zone is indicative of antimicrobial activity, with a larger zone reflecting greater potency. The results revealed minimal antibacterial activity for the control scaffold without TET. In contrast, the nanofibrous scaffolds with immobilized TET demonstrated significant antibacterial activity, particularly against *E. coli*, with inhibition zones exceeding 20 mm. The inhibition zone was notably smaller for *S. gallinarum*, indicating antibacterial activity directly under or near the scaffolds, as shown in Figure 7.

Of particular interest was the difference in antibacterial activity between samples AB and B, which differ in their post-TET immobilization treatment (see section Immobilization of tetracycline onto the nanofibrous scaffolds). The distinct immobilization methods were used to assess the antibacterial efficacy of nanofibrous scaffolds with surface-bound TET (sample_B) compared to those where TET was merely adsorbed onto the nanofibers (sample_AB). As shown in Graph 7, the results clearly indicate that despite the removal of TET by washing, some antibacterial activity persisted, albeit at a reduced level. This suggests that TET binding involves more than just simple surface adsorption. Specifically, for the nanofibrous scaffold with a PEO/PCL/CS mass ratio of 6/2/2, the difference in inhibition zones between samples AB and B was 7 mm, while for the PEO/

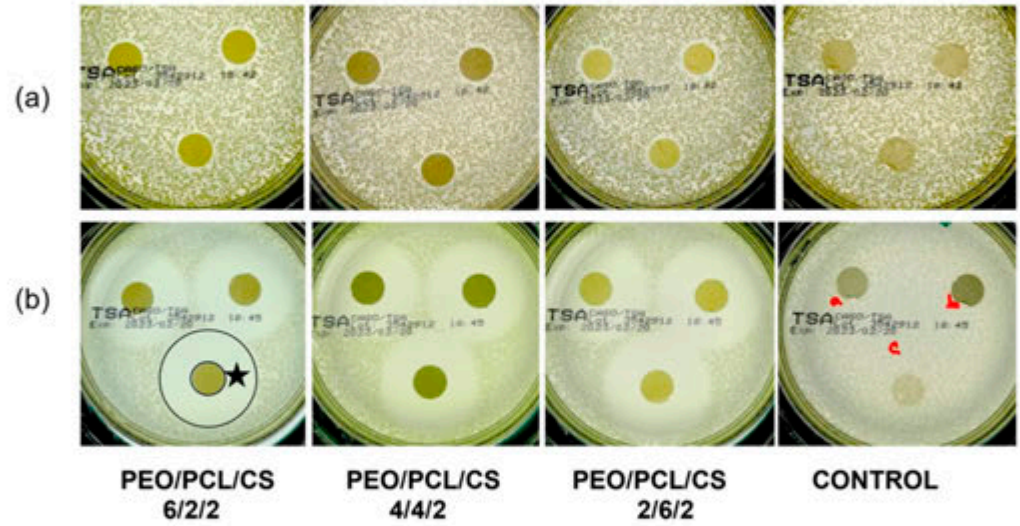

Figure 7. Photographs of inhibition zones (asterisks) around nanofibrous scaffolds with different compositions of PEO/PCL/CS, as determined by the Kirby-Bauer test: (a) *Staphylococcus gallinarum* and (b) *Escherichia coli*.

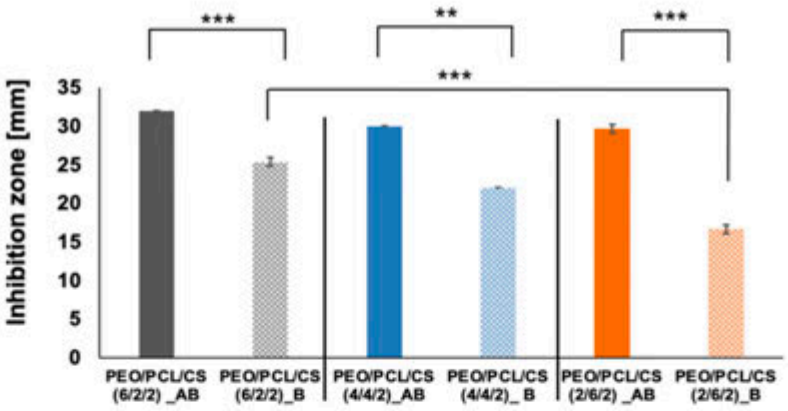

Graph 7. Antibacterial activity of nanofibrous scaffolds with PEO/PCL/CS mass ratios of 6/2/2, 4/4/2, and 2/6/2 against *Escherichia coli* after 24 h, as assessed by the Kirby-Bauer test. Significant statistical differences were observed using the *t* test between nanofiber scaffolds with TET immobilized in different ways (samples_A and AB). Significant differences were also noted between scaffolds with varying mass ratios of PEO/PCL/CS. ** indicates $p \leq 0.01$, and *** indicates $p \leq 0.001$. Error bars represent SD. ($n = 3$).

PCL/CS 2/6/2 scaffold, the difference was 13 mm against *E. coli*. This underscores the effectiveness of the immobilization method in sustaining antibacterial effects, even after washing.

Moreover, statistical analysis using the *t* test revealed significant differences in antibacterial activity between scaffolds with different mass ratios of PEO/PCL/CS. Notably,

Table 3. Detailed comparison of PEO/PCL/CS nanofibrous scaffolds in this study versus previous studies.

Study, material, technology	Advantages	Disadvantages	Comparison to this study
CS-based nanofibers: Needle electrospinning[32]	Good antibacterial properties	Low mechanical strength	Enhanced mechanical strength and sustained antibacterial properties from TET
PCL/CS nanofibers: Needle-less electrospinning[41]	Good hydrolytic stability over 30 days	High hydrophobicity, low Young's modulus (6-23 MPa)	Higher mechanical stability; hydrophilicity
PCL and CS/PEO nanofibers with *A. euchroma* extract: Two-nozzle electrospinning.[48]	Slow degradation rate (10%–28% after 28 days)	Low water vapor permeability; hydrophobic surface	Significantly better hydrophilicity and water vapor permeability; industrial scale productivity by nanospiderTM technology
PCL/ polydioxanone bi-layered nanofibers with TiO2 and TTC: Two-nozzle electrospinning[54]	High mechanical strength and elasticity	Use of toxic solvents; high fibers diameters; low antibacterial efficacy	Better antibacterial efficacy with TET, customization through post-fabrication soaking; industrial scale productivity by nanospiderTM technology
PCL/CS_PEO and PCL/CS_aloe vera_PEO bilayer nanofibers: Needle electrospinning[59]	Moderate moisture vapor transmission rate	Low Young's modulus (22-46 MPa); hydrophobic top layer	Significantly higher Young's modulus; improved hydrophilicity compared to the hydrophobic PCL top layer
PCL or gelatin nanofibers: Needle-less electrospinning[80]	Scalability; low fiber diameters (90-280 nm)	Use of toxic solvents; no antibiotic agents incorporated	Improved structural integrity (higher GSM values) without toxic solvents

scaffolds with higher PEO content exhibited better antibacterial efficacy compared to those with lower PEO content, albeit at the expense of PCL. TET, a multifunctional compound, contains chemical groups capable of interacting with counterparts in PEO, CS, and PCL. The observed differences in antibacterial activity can be attributed to the varying stability and strength of the bonds formed between TET's chemical groups and the hydroxyl groups in PEO or the carbonyl groups inherent in PCL. Additionally, the density of attachment sites plays a crucial role in modulating antibacterial activity.

Discussion

In nanofibrous scaffolds composed of PEO/PCL/CS, the interactions between these polymers are crucial in determining the scaffold's properties. Hydrogen bonding between PEO and CS enhances structural integrity by increasing intermolecular interactions. Additionally, the presence of amino groups in CS may facilitate ionic interactions with PEO, particularly in moist environments, further reinforcing the scaffold's structural framework. While PCL is hydrophobic and does not participate in strong chemical interactions with the other components, its physical entanglement with the flexible chains of PEO significantly enhances the scaffold's mechanical strength and flexibility. The combination of these materials through hydrogen bonding, ionic interactions, and physical entanglements results in a scaffold that effectively balances enhanced mechanical strength, structural stability, and bioactivity, making it highly suitable for wound healing applications.

Our results confirm that adjusting the PEO/PCL mass ratio allows for tailoring scaffold properties to specific wound care applications. Scaffolds with higher PCL content may be better suited for acute wounds or surgical sites requiring long-term support due to their slower hydrolytic degradation, higher hydrophilicity along with elongation at fracture. Conversely, scaffolds with higher PEO content, which exhibit better hydrophilicity, GSM, enhanced hydrolytic degradability and higher Young´s modulus, may be ideal for chronic or highly exudative wounds. These attributes are essential for effective moisture retention, infection control, and wound healing. Compared to previous studies, our scaffolds provide customizable hydrolytic degradation and mechanical properties, superior moisture management, and improved antibacterial properties against *E. coli*. A detailed comparison of the PEO/PCL/CS nanofibrous scaffolds with those reported in previous studies is presented in Table 3. This table highlights both the advantages and limitations of various approaches to wound healing scaffold fabrication, with particular emphasis on scalability, mechanical performance, and moisture management.

Conclusion

In summary, this study introduces a versatile approach to fabricating PEO/PCL/CS nanofibrous scaffolds using needle-less electrospinning (Nanospider™ technology). Our findings demonstrate that combining PEO, PCL, and CS in nanofibrous scaffolds achieves an optimal balance of hydrophilicity, superior moisture vapor transmission rate, and adjustable hydrolytic degradation and mechanical properties. The ability to tailor scaffold properties—such as hydrolytic degradation, mechanical strength, and hydrophilicity—by adjusting the PEO/PCL ratio allows for specific adaptations based on wound type.

Our hypothesis that scaffold properties could be effectively adjusted by manipulating the PEO/PCL ratio was validated, demonstrating significant improvements over existing methods. Compared to other studies, our scaffolds offer enhanced customization capabilities, achieved using needleless electrospinning technique. Post-fabrication soaking in TET solutions further enhances antibacterial performance and allows for tailored adjustments. This approach is more efficient than producing multiple scaffold variants

with different TET concentrations. Instead, scaffolds are immersed in a TET solution just before application, enabling direct adaptation to the patient's wound needs. This method streamlines the customization process, providing on-demand adjustments and significantly improving the practicality and efficiency of wound care solutions.

Future work will focus on in vivo studies and detailed TET release profiles to fully assess the clinical applicability of our scaffolds. The successful transition from laboratory to industrial-scale production represents a significant milestone, with the potential to address challenges associated with chronic wounds and complex skin injuries, paving the way for advanced wound care products in clinical settings.

Acknowledgements

This work was supported by the Ministry of Education, Youth and Sports of the Czech Republic and the European Union - European Structural and Investment Funds in the frames of Operational Programme Research, Development and Education - project Hybrid Materials for Hierarchical> Structures (HyHi, Reg. No. CZ.02.1.01/0.0/0.0/16_019/0000843)

Declaration of conflicting interests

The author(s) declared no potential conflicts of interest with respect to the research, authorship, and/or publication of this article.

Funding

The author(s) disclosed receipt of the following financial support for the research, authorship, and/or publication of this article: This work was supported by the Ministerstvo Skolstvi, Mladeze a Telovychovy; CZ.02.1.01/0.0/0.0/16_019/0000843.

ORCID iD

Daniela Lubasova https://orcid.org/0000-0002-7084-575X

References

1. Gonzalez AC, Costa TF, Andrade ZA, et al. Wound healing - a literature review. *An Bras Dermatol* 2016; 91(5): 614–620.
2. Mahyudin F, Edward M, Basuki MH, et al. Modern and classic wound dressing comparison in wound healing, Comfort and Cost. *J Ners* 2020; 15: 31–36.
3. Liang Y, He J and Guo B. Functional hydrogels as wound dressing to enhance wound healing. *ACS Nano* 2021; 15(8): 12687–12722.
4. Gounden V and Singh M. Hydrogels and wound healing: current and future prospects. *Gels* 2024; 10(1): 43.
5. Dong L, Zhang W, Ren M, et al. Moisture adaptive contractile biopolymer derived fibers for wound healing promotion. *Small* 2023; 19(27): e2300589.
6. Jin S, Newton MAA, Cheng H, et al. Progress of hydrogel dressings with wound monitoring and treatment functions. *Gels* 2023; 9(9): 694.

7. Roy S, Elgharably H, Sinha M, et al. Mixed-species biofilm compromises wound healing by disrupting epidermal barrier function. *J Pathol* 2014; 233(4): 331–343.
8. Khaerotib YP and Wardani R. Modern wound care application: a literature review. *Int J Sci Soc* 2021; 3(1): 1.
9. Krishani M, Shin WY, Suhaimi H, et al. Development of scaffolds from bio-based natural materials for tissue regeneration applications: a review. *Gels* 2023; 9(2): 100.
10. Vigani B, Ianev D, Adami M, et al. Porous functionally graded scaffold prepared by a single-step freeze-drying process. A bioinspired approach for wound care. *Int J Pharm* 2024; 656: 124119.
11. Yayehrad AT, Siraj EA, Matsabisa M, et al. 3D printed drug loaded nanomaterials for wound healing applications. *Regen Ther* 2023; 24: 361–376.
12. Jiang Z, Zheng Z, Yu S, et al. Nanofiber scaffolds as drug delivery systems promoting wound healing. *Pharmaceutics* 2023; 15(7): 1829.
13. Chen S, Liu B, Carlson MA, et al. Recent advances in electrospun nanofibers for wound healing. *Nanomedicine* 2017; 12(11): 1335–1352.
14. Schulte-Werning LV, Murugaiah A, Singh B, et al. Multifunctional nanofibrous dressing with antimicrobial and anti-Inflammatory properties prepared by needle-Free electrospinning. *Pharmaceutics* 2021; 13(9): 1527.
15. Zaarour B, Liu W, Omran W, et al. A mini-review on wrinkled nanofibers: preparation principles via electrospinning and potential applications. *J Ind Text* 2024; 54.
16. He H, Kara Y and Molnár K. In situ viscosity-controlled electrospinning with a low threshold voltage. *Macromol Mater Eng* 2019; 304(11).
17. Wei L, Cheng X, Wang Q, et al. Establishment of a one-dimensional physical model for electrospinning multiple jets of spinnerets. *J Ind Text* 2023; 53.
18. Syrový M, Čapková P, Ryšánek P, et al. Effect of wire and needle spinning on the direct manufacturing PAN/amine nanofibrous membranes for CO2 sorption. *J Ind Text* 2023; 53: 152808372311760.
19. Ganesh S, Anushikaa R, Swetha Victoria VS, et al. Recent advancements in electrospun chitin and chitosan nanofibers for bone tissue engineering applications. *J Funct Biomater* 2023; 14(5): 288.
20. Jiang J, Chen X, Wang H, et al. Response surface methodology to explore the influence fiber diameter in a new multi-needle electrospinning spinneret. *Polymers*. 2024; 16(15): 2222, In this issue.
21. Jirsak O, Sanetrnik F, Lukas D, et al. A method of nanofibres production from a polymer solution using electrostatic spinning and a device for carrying out the method. WO2005024101A1 (Patent) 2003.
22. Omer S, Forgách L, Zelkó R, et al. Scale-up of electrospinning: market overview of products and devices for pharmaceutical and biomedical purposes. *Pharmaceutics* 2021; 13(2): 286.
23. Ajmal G, Yadav N, Rashid Iqba M, et al. Electrospun nanofiber: application in tissue regeneration. *Int J Life Sci Pharm Res* 2022; 13: 127–140.
24. Muthukrishnan L, Rajendran S, Maniam G, et al. Electrospun nanofibers for tissue engineering and regenerative medicine: a review. *J Biomed Sci* 2020; 27: 12.
25. Diller RB and Tabor AJ. The role of the extracellular matrix (ECM) in wound healing: a review. *Biomimetics* 2022; 7(3): 87.

26. Wu J, Yu F, Shao M, et al. Electrospun nanofiber scaffold for skin tissue engineering: a review. *ACS Appl Bio Mater* 2024; 7(6): 3556–3567.
27. Muthukrishnan L. An overview on electrospinning and its advancement toward hard and soft tissue engineering applications. *Colloid Polym Sci* 2022; 300(8): 875–901.
28. Gholipour-Kanani A, Bahrami SH and Rabbani S. Effect of novel blend nanofibrous scaffolds on diabetic wounds healing. *IET Nanobiotechnol* 2016; 10(1): 1–7.
29. Chen R, Liu Z, Cui T, et al. He@PCL/PCE gel-nanofiber dressing with robust self-adhesion toward high wound-healing rate via microfluidic electrospinning technology. *ACS Appl Mater Interfaces* 2023; 15(39): 46322–46332.
30. Zhang X, Wang Y, Gao Z, et al. Advances in wound dressing based on electrospinning nanofibers. *Appl Polym Sci* 2024; 141(1): e54746.
31. Abdollahimajd F, Pourani MR, Mahdavi H, et al. Efficacy and safety of chitosan-based biocompatible dressing versus nanosilver (Acticoat™) dressing in treatment of recalcitrant diabetic wounds: a randomized clinical trial. *Dermatol Ther* 2022; 35(9).
32. Johnson M, Smith AR and Lee K. Advanced wound healing scaffolds: a comprehensive review on structure, composition, and performance. *J Biomed Mater Res, Part A* 2020; 108(5): 1234–1245.
33. Rajinikanth BS, Rajkumar DSR and Vijayaragavan V. Chitosan-based biomaterial in wound healing: a review. *Cureus* 2024; 16(2): e55193.
34. Dai T, Tanaka M, Huang Y, et al. Chitosan preparations for wounds and burns: antimicrobial and wound-healing effects. *Expert Rev Anti Infect Ther* 2011; 9(7): 857–879.
35. Taokaew S and Chuenkaek T. Developments of core/shell chitosan-based nanofibers by electrospinning techniques: a review. *Fibers* 2024; 12(3): 26.
36. Dhandayuthapani B, Krishnan UM and Sethuraman S. Fabrication and characterization of chitosan-gelatin blend nanofibers for skin tissue engineering. *J Biomed Mater Res B Appl Biomater* 2010; 94(1): 264–272.
37. Kang YO, Yoon IS, Lee SY, et al. Chitosan-coated poly(vinyl alcohol) nanofibers for wound dressings. *J Biomed Mater Res B Appl Biomater* 2010; 92(2): 568–576.
38. Jia J, Lin Z, Zhu J, et al. Anti-adhesive and antibacterial chitosan/PEO nanofiber dressings with high breathability for promoting wound healing. *Int J Biol Macromol* 2024; 261(Pt 1): 129668.
39. Levengood SL, Erickson AE, Chang FC, et al. Chitosan-poly(caprolactone) nanofibers for skin repair. *J Mater Chem B* 2017; 5(9): 1822–1833.
40. Bagheri M, Validi M, Gholipour A, et al. Chitosan nanofiber biocomposites for potential wound healing applications: antioxidant activity with synergic antibacterial effect. *Bioeng Transl Med* 2021; 7(1): e10254.
41. Andrade del Olmo J, Mikes P, Asatiani N, et al. Alternating current electrospinning of polycaprolactone/chitosan nanofibers for wound healing applications. *Polymers* 2024; 16: 1333.
42. Cai Z, Mo X, Zhang K, et al. Fabrication of chitosan/silk fibroin composite nanofibers for wound-dressing applications. *Int J Mol Sci* 2010; 11(9): 3529–3539.
43. Golchin A, Hosseinzadeh S, Staji M, et al. Biological behavior of the curcumin incorporated chitosan/poly(vinyl alcohol) nanofibers for biomedical applications. *J Cell Biochem* 2019; 120(9): 15410–15421.

44. Pezhman M, Hossein N, Zahed A, et al. Fabrication and characterization of polycaprolactone/chitosan nanofibers containing antibacterial agents of curcumin and ZnO nanoparticles for use as wound dressing. *Front Bioeng Biotechnol* 2022; 10.
45. Dang Z, Ma X, Yang Z, et al. Electrospun nanofiber scaffolds loaded with metal-based nanoparticles for wound healing. *Polymers* 2023; 16(1): 24.
46. Liu H, Bai Y, Huang C, et al. Recent progress of electrospun herbal medicine nanofibers. *Biomolecules* 2023; 13(1): 184.
47. El-Attar AA, El-Wakil HB, Hassanin AH, et al. Silver/snail mucous PVA nanofibers: electrospun synthesis and antibacterial and wound healing activities. *Membranes* 2022; 12(5): 536.
48. Asghari F, Rabiei Faradonbeh D, Malekshahi ZV, et al. Hybrid PCL/chitosan-PEO nanofibrous scaffolds incorporated with A. euchroma extract for skin tissue engineering application. *Carbohydr Polym* 2022; 278: 118926.
49. Alyamani AA, Al-Musawi MH, Albukhaty S, et al. Electrospun polycaprolactone/chitosan nanofibers containing cordia myxa fruit extract as potential biocompatible antibacterial wound dressings. *Molecules* 2023; 28(6): 2501.
50. Parvinzadeh Gashti M, Dehdast SA, Berenjian A, et al. PDDA/honey antibacterial nanofiber composites for diabetic wound-healing: preparation, characterization, and in vivo studies. *Gels* 2023; 9(3): 173.
51. Alotaibi B, Khan AK, Kharaba Z, et al. Development of poly(vinyl alcohol)–chitosan composite nanofibers for dual drug therapy of wounds. *ACS Omega* 2024; 9(11): 12825–12834.
52. Liu X, Xu H, Zhang M, et al. Electrospun medicated nanofibers for wound healing: review. *Membranes* 2021; 11(10): 770.
53. Wali A, Gorain M, Inamdar S, et al. In vivo wound healing performance of halloysite clay and gentamicin-incorporated cellulose ether-PVA electrospun nanofiber mats. *ACS Appl Bio Mater* 2019; 2(10): 4324–4334.
54. Rezk AI, Lee JY, Son BC, et al. Bi-layered nanofibers membrane loaded with titanium oxide and tetracycline as controlled drug delivery system for wound dressing applications. *Polymers* 2019; 11: 1602.
55. Leyva-Verduzco AA, Quiroz Castillo JM, Chan-Chan LH, et al. Study of electrospun membranes composed of PCL and Tilapia-skin collagen with tetracycline or chloramphenicol in contact with human skin fibroblasts for wound dressing treatment. *ACS Omega* 2024; 9(5): 5361–5370.
56. Zhang H, Chen Y, Zhang L, et al. An overview of recent advances in electrospun nanofibers for tissue engineering. *J Mater Chem B* 2023; 11(15): 3294–3314.
57. Zhang X, Yang Q, Li Y, et al. Electrospun nanofibers for tissue engineering applications: current state and future perspectives. *Mater Sci Eng C* 2023; 148: 115762.
58. Lin M, Liu Y, Gao J, et al. Synergistic effect of co-delivering ciprofloxacin and tetracycline hydrochloride for promoted wound healing by utilizing coaxial PCL/gelatin nanofiber membrane. *Int J Mol Sci* 2022; 23(3): 1895.
59. Miguel SP, Ribeiro MP, Coutinho P, et al. Electrospun polycaprolactone/aloe vera_chitosan nanofibrous asymmetric membranes aimed for wound healing Applications. *Polymers* 2017; 9: 183.

60. Gholipour-Kanani A, Mohsenzadegan M, Fayyazi M, et al. Poly (ε-caprolactone)-chitosan-poly (vinyl alcohol) nanofibrous scaffolds for skin excisional and burn wounds in a canine model. *IET Nanobiotechnol* 2018; 12(5): 619–625.
61. Ninomiya T, Yamamoto M, Takahashi K, et al. Chitosan scaffolds for tissue engineering: a review. *J Mater Sci Mater Med* 2012; 23(5): 1081–1090.
62. Martinová L and Lubasová D. Electrospun chitosan based nanofibers. *Res J Text Apparel* 2008; 12(2): 72–79.
63. Bakhsheshi-Rad HR, Ismail AF, Aziz M, et al. Antibacterial activity and in vivo wound healing evaluation of polycaprolactone-gelatin methacryloyl-cephalexin electrospun nanofibrous. *Mater Lett* 2019; 256: 126618.
64. Ning Y, Shen W and Ao F. Application of blocking and immobilization of electrospun fiber in the biomedical field. *RSC Adv* 2020; 10(61): 37246–37265.
65. Amiri N, Ajami S, Shahroodi A, et al. Teicoplanin-loaded chitosan-PEO nanofibers for local antibiotic delivery and wound healing. *Int J Biol Macromol* 2020; 162: 645–656.
66. Lubasova D and Spanek R. Study of relationships between morphology of polyvinylbutyral nanofibers and solvents properties using a predictive numerical model. *J Comput Theor Nanosci* 2017; 14: 2802–2811.
67. Hartwig A, Mulder M and Smolders CA. Surface amination of poly(acrylonitrile). *Adv Colloid Interface Sci* 1994; 52: 65–78.
68. Castilla-Cortázar I, Más-Estellés J, Meseguer-Dueñas JM, et al. Hydrolytic and enzymatic degradation of a poly(ε-caprolactone) network. *Polym Degrad Stabil* 2012; 97(8): 1241–1248.
69. Lander LM, Siewierski LM, Brittain WJ, et al. A Systematic comparison of contact angle methods. *Langmuir* 1993; 9(8): 2237–2239.
70. British Standards Institute. *BS EN 13726-1:2002. Test methods for primary wound dressings. Part 2: moisture vapour transmission rate of permeable film dressings*. London: BSI, 2002.
71. International Organization for Standardization. *ISO 10993-5: biological evaluation of medical devices. Part 5: test for in vitro cytotoxicity.* Geneva: ISO, 2009.
72. Paaver U, Tamm I, Laidmäe I, et al. Soluplus graft copolymer: potential novel carrier polymer in electrospinning of nanofibrous drug delivery systems for wound therapy. *BioMed Res Int* 2014; 2014: 789765.
73. Tan G, Wang L, Pan W, et al. Polysaccharide electrospun nanofibers for wound healing applications. *Int J Nanomed* 2022; 17: 3913–3931.
74. Fiaschini N, Carnevali F, Van der Esch SA, et al. Innovative multilayer electrospun patches for the slow release of natural oily extracts as dressings to boost wound healing. *Pharmaceutics* 2024; 16(2): 159.
75. White P, Chooprajong S and Pankaew P. A study of sericin-Thunbergia laurifolia electrospun fibre for wound healing applications. *Key Eng Mater* 2019; 798: 53–58.
76. Liu J, Dong W, Mou X, et al. In situ electrospun zein/thyme essential oil-based membranes as an effective antibacterial wound dressing. *ACS Appl Bio Mater* 2019; 3(1): 302–307.
77. Memić A, Abudula T, Mohammed H, et al. Latest progress in electrospun nanofibers for wound healing applications. *ACS Appl Bio Mater* 2019; 2(3): 952–969.

78. Bayati V, Abbaspour M, Dehbashi F, et al. A dermal equivalent developed from adipose-derived stem cells and electrospun polycaprolactone matrix: an in vitro and in vivo study. *Anat Sci Int* 2016; 92(4): 509–520.
79. Hang C, Wei Z, Jieyu X, et al. ZIF-8/curcumin-loaded electrospun nanofiber membrane for wound healing. *ACS Appl Nano Mater* 2023; 6(17): 15620–15631.
80. Dubský M, Kubinová Š, Širc J, et al. Nanofibers prepared by needleless electrospinning technology as scaffolds for wound healing. *J Mater Sci Mater Med* 2012; 23: 931–941.
81. Dalton M, Ebrahimi F, Xu H, et al. The influence of the molecular weight of poly(ethylene oxide) on the hydrolytic degradation and physical properties of polycaprolactone binary blends. *Macromolecules (Washington, DC, U S)* 2023; 3: 431–450.
82. Elzein T, Nasser-Eddine M, Delaite C, et al. FTIR study of polycaprolactone chain organization at interfaces. *J Colloid Interface Sci* 2004; 273(2): 381–387.
83. Bhattarai N, Edmondson D, Veiseh O, et al. Electrospun chitosan-based nanofibers and their cellular compatibility. *Biomaterials* 2005; 26(31): 6176–6184.
84. Sánchez-Machado DI, López-Cervantes J, Escárcega-Galaz AA, et al. Measurement of the degree of deacetylation in chitosan films by FTIR, ^{1}H NMR and UV spectrophotometry. *MethodsX* 2024; 12: 102583.
85. Sun Z, Zussman E, Yarin AL, et al. Compound core–shell polymer nanofibers by co-electrospinning. *Adv Mater* 2003; 15(22): 1929–1932.
86. Guo Y, Zhang L, Cao F, et al. Surface modification of nanofibers for biomedical applications. *Adv Mater Res* 2013; 875: 481–485.
87. Zhu Y, Yang X and Han C. Polyethylene oxide-based biodegradable hydrogels for wound dressings. *J Mater Chem B* 2016; 4(21): 3747–3759.
88. Li X, Wu D, Zeng J, et al. Biodegradable polycaprolactone-based scaffolds for tissue engineering: review and advances. *J Biomed Mater Res, Part A* 2018; 106(1): 63–82.
89. Zhang Y, Yu T and Zhang Z. Controlled degradation of polycaprolactone-based biomaterials for wound healing applications. *Biomater Sci* 2017; 5(7): 1389–1401.
90. Nguyen HM, Ngoc Le TT, Nguyen AT, et al. Biomedical materials for wound dressing: recent advances and applications. *RSC Adv* 2023; 13(8): 5509–5528.
91. Augustine R, Hasan A, Patan N, et al. Titanium nanorods loaded PCL meshes with enhanced blood vessel formation and cell migration for wound dressing applications. *Macromol Biosci* 2019; 19(7): e1900058.
92. Ahearn DJ, Hsu R, Yung A, et al. Hydrophilic dressings for enhanced wound healing: a review of recent developments. *Wound Repair Regen* 2016; 24(1): 18–26.
93. Gul A, Gallus I, Tegginamath A, et al. Electrospun antibacterial nanomaterials for wound dressings applications. *Membranes* 2021; 11(12): 908.
94. Wang Q, Zhang S, Jiang J, et al. Electrospun radially oriented berberine-PHBV nanofiber dressing patches for accelerating diabetic wound healing. *Regen Biomater* 2024; 11: rbae063.
95. Gupta P, Sharma S, Singh A, et al. Evaluation of hydrophilicity in wound healing patches. *J Biomed Mater Res* 2020; 108(6): 1200–1210.
96. Khan Y, Khan MM and Syed SMI. Polycaprolactone (PCL) and its composite properties: a review. *J Mater Sci Technol* 2020; 40: 55–78.
97. Yuan X, Liao MHH and Tseng TY. Mechanical properties of PEO/PCL blends and their potential applications. *Polym Eng Sci* 2008; 48(11): 2115–2123.

98. Burgess DR. Mechanical properties of human skin. *J Biomech* 2001; 34(6): 719–724.
99. Kalra A, Lowe A and Ai Jumaily AM. Mechanical behaviour of skin: a review. *J Mater Sci Eng* 2016; 5: 4.
100. Shi C and Zhang M. Incidence and management of skin lesions and minor wounds in chronic obstructive pulmonary disease patients undergoing advanced bronchodilator therapy. *Int Wound J* 2024; 21(2).
101. Brown K, Smith J, Liu H, et al. MVTR balance in wound dressing technology. *Adv Wound Care* 2021; 10(6): 306–315.
102. Ellis C, Thompson J, Wilson A, et al. MVTR and its optimal range for wound healing. *Adv Mater* 2021; 33(45): 2103657.
103. Harris A, Lee M, Carter R, et al. Ideal MVTR for effective wound dressings. *Clin Innov Wound Care* 2019; 8(1): 22–29.
104. Wilson TL, Anderson R, Patel S, et al. High MVTR in dressings for high exudate wounds. *J Wound Care* 2020; 29(11): 632–641.
105. Patel V, Kumar A, Gupta S, et al. Moisture management and its clinical implications. *Int J Wound Care* 2022; 18(4): 203–212.
106. El-Sherbiny I and Ali I. Eco-friendly electrospun polymeric nanofibers-based nano-composites for wound healing and tissue engineering. *Advanced Functional Nanomaterials*. Berlin: Springer, 2015, pp. 399–431.
107. Pusnik M, Imeri M, Deppierraz G, et al. The agar diffusion scratch assay - a novel method to assess the bioactive and cytotoxic potential of new materials and compounds. *Sci Rep* 2016; 6(1): 20854.
108. Szymański L, Gołaszewska K, Wiatrowska A, et al. ISO 10993 biological evaluation of novel hemostatic powder – 4Seal. *Biomater Res* 2022; 26(1).
109. Sharma A and Luthra G. Significance of ISO 10993 standards in ensuring biocompatibility of medical devices: a review. *J Pharm Res Int* 2023; 35(8): 23–34.
110. Ali I, Khalil I and El-Sherbiny I. Design, development, in-vitro and in-vivo evaluation of polylactic acid-based multifunctional nanofibrous patches for efficient healing of diabetic wounds. *Sci Rep* 2023; 13(1): 3215.
111. GhavamiNejad A, Rajan Unnithan A, Ramachandra Kurup Sasikala A, et al. Mussel-inspired electrospun nanofibers functionalized with size-controlled silver nanoparticles for wound dressing application. *ACS Appl Mater Interfaces* 2015; 7(22): 12176–12183.
112. Yin H, Li H and He Q. Nanomaterials for wound healing and antibacterial applications. *Nanomaterials* 2021; 11(6): 1471.
113. Yao L, Jiang M and Wang L. Antibacterial and wound-healing properties of metal-based nanomaterials. *Nanomedicine* 2021; 36: 102417.
114. Yang L. Evaluation of antibacterial activity in wound healing materials. *J Clin Med* 2024; 13(4): 867.
115. Huang X, Liang R and Zhang Y. Antibacterial performance of nanofibrous scaffolds against wound infection pathogens. *Adv Funct Mater* 2021; 31(14): 2009082.

Appendix 6

LUBASOVA, D. and Martinova, L. Controlled morphology of porous polyvinylbutyral nanofibers. Journal of nanomaterials;2011.

Hindawi Publishing Corporation
Journal of Nanomaterials
Volume 2011, Article ID 292516, 6 pages
doi:10.1155/2011/292516

Research Article

Controlled Morphology of Porous Polyvinyl Butyral Nanofibers

Daniela Lubasova and Lenka Martinova

Department of Nonwovens, Technical University of Liberec, 46117 Liberec, Czech Republic

Correspondence should be addressed to Daniela Lubasova, daniela.lubasova@tul.cz

Received 12 August 2010; Revised 3 December 2010; Accepted 17 January 2011

Academic Editor: Theodore Tsotsis

A simple and effective method for the fabrication of porous nanofibers based on the solvent evaporation methods in one-step electrospinning process from the commercial polyvinyl butyral (PVB) is presented. The obtained nanofibers are prevalently amorphous with diameters ranging from 150 to 4350 nm and specific surface area of approximately 2–20 m^2/g. Pore size with irregular shape of the porous PVB fibers ranged approximately from 50 to 200 nm. The effects of polymer solution concentration, composition of the solvents mixture, and applied voltage on fiber diameter and morphology were investigated. The theoretical approach for the choice of poor and good solvents for PVB was explained by the application Hansen solubility parameter (HSP) and two-dimensional graph. Three basic conditions for the production of porous PVB nanofibers were defined: (i) application of good/poor solvent mixture for spinning solution, (ii) differences of the evaporation rate between good/poor solvent, and (iii) correct ratios of good/poor solvent (v/v). The diameter of prepared porous PVB fibers decreased as the polymer concentration was lowered and with higher applied voltage. These nanofiber sheets with porous PVB fibers could be a good candidate for high-efficiency filter materials in comparison to smooth fibers without pores.

1. Introduction

Many literature references discuss the production of porous nanofibers in the electrospinning process. There are a lot of methods, such as the extraction of a component from bicomponent nanofibers, phase separation during electrospinning, and production of porous nanofibers under specific process conditions (temperature, humidity). These methods are technically difficult and demand two step production or special additional device [1–3].

First idea for producing the porous nanofibers in one step arose after studying works published by Elford [4] and Ferry [5]. One of the earliest methods of making microporous membranes was described there. In the method's simplets form, a polymer is dissolved in a two-component solvent mixture consisting of volatile good solvent and an involatile poor solvent for a polymer. This two-component polymer solution is cast on a glass plate. As the good, volatile solvent evaporates the casting solution is enriched in the poor, non-volatile solvent. The polymer precipitates, forming the porous membrane structure.

An interesting finding is that the use of evaporation of solvents yields polymer fibers with a relatively regular porous structure. The regular phase morphology is induced by rapid phase separation in an electrospinning jet when a highly volatile solvent is used. The solvent-rich regions in the jet result in the pores after its intensive evaporation.

The development of porous fibers by electrospinning was studied by Lubasova and Martinova [6], where porous PCL nanofibers from a nonsolvent/solvent/polymer system were prepared. The same principle is described in the reference of Qi et al. [7], where an alcohol was used as a non-solvent and dichloromethane as a solvent for PLA. It was confirmed that a porous structure of nanofibers could be obtained by varying the ratio of non-solvent/solvent in the ternary system with different values of evaporation rate.

It was proved that porous nanofibers are more efficient for cultivation of different cells and the growth could be influenced by the morphology of the nanofibers in previous work. The cells attach easily to porous nanofibers and show better growth than the cells grown on nonporous nanofibers. Khil et al. [8] prepared a porous polycaprolactone (PCL)

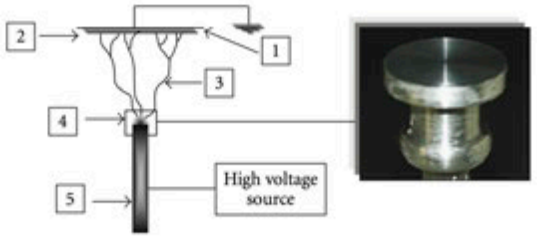

FIGURE 1: Schematic of a simple electrospinning experiment; (1) electrode grounding shield, (2) nanofiber sheet, (3) direction of nanofiber formation, (4) a special flat electrode with polymer solution, and (5) a positive electrode.

filament by an electrospinning process and studied the growth characteristics of cells on these nonwoven fabrics. This work revived the important role of scaffold porosity for proliferation of living animal cells.

2. Materials and Method

PVB (Mowital B60H, dynamic viscosity of 10% solution in ethanol 160–260 mPa·S) was purchased from Kuraray. Several spinning solutions were prepared by dissolving PVB in the different types and quantities of solvents and their mixtures (methanol, ethanol, tetrahydrofuran (THF), dimethylsulfoxide (DMSO)). The total polymer concentration was fixed at 8 and 10 wt.%. PVB solutions in solvent mixtures were prepared by magnetic stirring at room temperature overnight.

A schematic representation of the equipment used in the laboratory for electrospinning is depicted in Figure 1. The electrospinning process of PVB solutions was carried out at a voltage of 30 or 35 kV and the electrode-to-collector distance was fixed at 10 cm.

3. Experimental Results and Discussion

3.1. Theoretical Approach for Choice of Optimal Solvents. HSP was used for the prediction of the solubility of polymers in various solvents or their mixture. The application of a solubility parameter is the practical way of predicting the polymer solubility or quality of the solvent. Hansen [9] derived a practical extension of Hildebrand solubility parameter into three parts: polar force component (δ_p), dispersion force component, (δ_d) and hydrogen bonding component (δ_h):

$$\delta_{\text{total}}^2 = \delta_d^2 + \delta_p^2 + \delta_h^2. \quad (1)$$

HSP for polymers is commonly obtained by an indirect method which involves testing the relevant material in contact with many solvents under conditions relevant to a given problem. When the bond energy of the material is similar to that of a given solvent, it will dissolve, swell, or adsorb onto the material. An accurate prediction of solubility parameter components from the chemical structure is difficult because the interaction of different structural groups

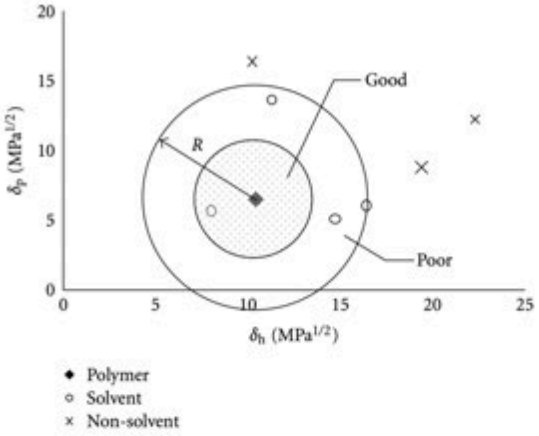

FIGURE 2: The solubility sphere for a polymer.

producing overall polar and hydrogen-bonding properties does not obey simple rules. Despite this, a useful prediction method based on molecular structure has been proposed by Van Krevelen [10]. According to Van Krevelen each parameter can be estimated using (2), where F_d is the dispersion component, F_p the polar component, E_h the contribution of hydrogen bond forces to the cohesive energy, i the contributing group, and V_m the molar volume of the polymer:

$$\delta_d = \frac{\sum F_{di}}{V_m}, \qquad \delta_p = \frac{\sqrt{\sum F_{pi}^2}}{V_m}, \qquad \delta_h = \sqrt{\frac{\sum E_{hi}}{V_m}}. \quad (2)$$

Hansen used a three-dimensional geometrical model to the interpret solubility of a polymer by a graphical method. Hansen's three-dimensional volume can be similarly illustrated in a two-dimensional (2D) graph that uses only two of the three parameters, most commonly δ_p and δ_h, see Figure 2. This model introduces a "solubility sphere" of a polymer as a circle in a 2D system where the axes are represented by the two solubility components (δ_p and δ_h). The centre of the solubility sphere is located at the point ($^P\delta_p$, $^P\delta_h$) with HSP of the polymer. The radius of the solubility sphere is the interaction radius R. Solvent points are represented by HSP of solvents ($^S\delta_p$, $^S\delta_h$). If a solvent point is located at the centre of the solubility sphere, then the polymer can be dissolved by the solvent. On the other hand, if the solvent point is placed outside the solubility sphere, such solvent does not dissolve the polymer.

3.2. Preparation and Spinning of PVB Solutions. Determination of the good and poor solvents for PVB and processing of porous nanofibers was the main goal. The solubility parameter of the polymer PVB was predicted using (2) to calculate δ_d, δ_p, and δ_h which are shown in Table 1. For a more detailed explanation refer to Van Krevelen [10].

The 2D graph was constructed in the first step. This graph uses only two of the three HSP components, particularly δ_p and δ_h; see Figure 3.

Table 1: HSP calculation for PVB using the Hoftyzer-Van Krevelen method.

Structural groups	No. of groups N [–]	$N \cdot F_{di}$ [$J^{1/2} \cdot cm^{3/2} \cdot mol^{-1}$]	$N \cdot F_{pi}^2$ [$J \cdot cm^3 \cdot mol^{-2}$]	$N \cdot E_{hi}$ [$J \cdot mol^{-1}$]
$-CH_2-$	5	1,350	0	0
=CH–	4	800	0	0
–O–	2	200	320,000	6,000
CH3–	1	420	0	0
OH–	1	210	250,000	20,000
	Sum	2,980	570,000	26,000
		δ_d [$MPa^{1/2}$]	δ_p [$MPa^{1/2}$]	δ_h [$MPa^{1/2}$]
PVB		15.5	6.5	10.4

Table 2: Quality of solvents for dissolving PVB.

Polymer/solvents	PVB		Vapor pressure (25°C) [kPa]
	$\Delta\delta_{(S\text{-}P)}$ [$MPa^{1/2}$]	Character of the solvent	
THF	2.5	Good	26.27
DMSO	9.9	Poor	0.08
Ethanol	9.3	Poor	24.60
Methanol	13.2	Poor	32.7

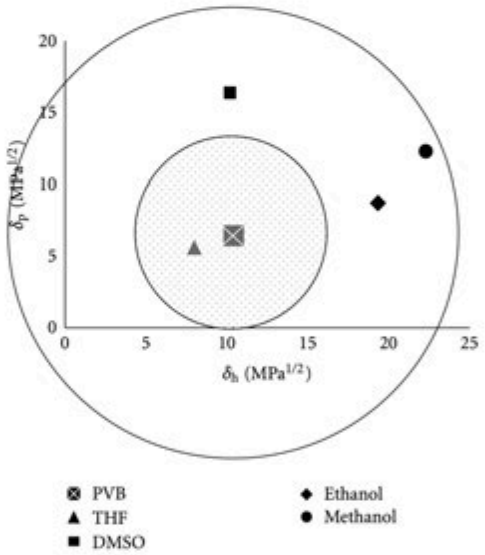

Figure 3: Two-dimensional graph for prediction of good or poor solvent for PVB: grey area implies poor solvent; white area implies good solvent.

Table 3: Solvent mixtures used as PVB solvents for electrospinning.

Solvent mixtures
Ethanol/methanol (9/1, 8/2 and 7/3 v/v)
Ethanol/DMSO (9/1, 8/2 and 7/3 v/v)
THF/DMSO (95/5, 9/1 and 8/2 v/v)

Secondly, a parameter $\Delta\delta_{(S\text{-}P)2D}$ was evaluated, which is given by the distance between the HSP of solvent-point and the centre of the solubility sphere in the 2D graph, see (3). This parameter can be simply used for prediction of the poor or good solvent. It is expected that the low values of this parameter signify good solvent while higher values indicate poor solvent (see Table 2):

$$\Delta\delta_{(S\text{-}P)2D} = \left[\left({}^{S}\delta_p - {}^{P}\delta_p\right)^2 + \left({}^{S}\delta_h - {}^{P}\delta_h\right)^2\right]^{1/2}. \quad (3)$$

Several spinning solutions were prepared by dissolving PVB in a mixture of different good and poor solvent combinations (ethanol/methanol, ethanol/DMSO and THF/DMSO). The volume ratios of good and poor solvents were varied; see Table 3. The concentration of polymer solutions was a constant 10 wt.%.

Table 4: Morphology of PVB fibers.

Solvent mixtures	Morphology of nanofibers
Ethanol/methanol 9/1 (v/v)	nonporous
Ethanol/DMSO 9/1 (v/v)	partly porous
THF/DMSO 95/5 (v/v)	porous
THF/DMSO 9/1 (v/v)	porous

3.3. The Effect of the Mixture of Good/Poor Solvents on Fiber Morphology. The nanofiber sheets were observed by a scanning electron microscope (SEM). It was found that electrospinning of PVB led to porous, nonporous, or partly porous fibers; see Table 4. The electrospinning process was intensive in all cases. Figure 4 shows SEM images of the PVB fibers with the effect of the mixture of good and poor solvents on the fiber morphology.

Examination of the SEM images (Figure 4) indicates that the PVB fibers obtained from the solvent mixture THF/DMSO (9/1 v/v) exhibit a highly porous structure with

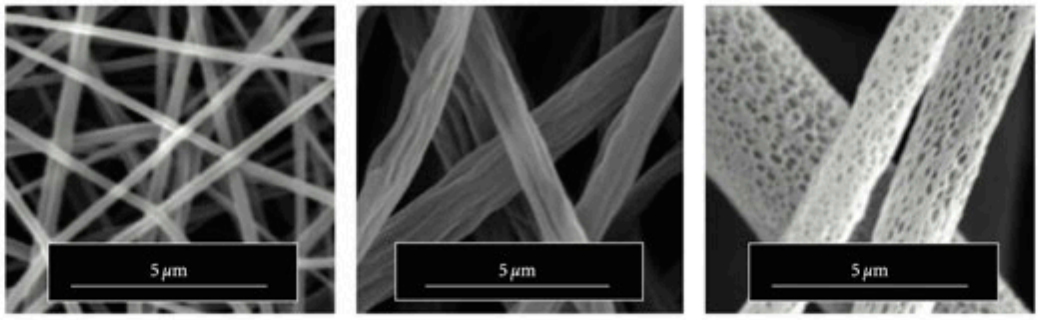

FIGURE 4: SEM images of PVB nanofibers prepared from 10 wt.% polymer solution from the mixtures: (a) ethanol/methanol (9/1 v/v), (b) ethanol/DMSO (9/1 v/v), (c) THF/DMSO (9/1 v/v).

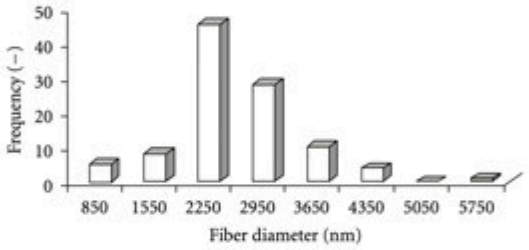

FIGURE 5: Histogram of the fiber diameter for electrospun PVB 10 wt.% solution from the electrode-to-collector distance of 10 cm and applied voltage of 30 kV.

a pore size of approximately 100 nm. The elliptically shaped pores covered the entire surface of the fibers. Electrospinning of PVB from ethanol/DMSO 9/1 (v/v) led to partially porous fibers with smaller fiber diameters. Non-porous nanofibers were prepared from the mixture of the ethanol/methanol 9/1 (v/v). The SEM images shown in Figure 4 imply that the emerging porous structure of fibers is observed only for the mixtures of good and poor solvents with the higher difference in the evaporation rate between good and poor solvents. The results in Table 2 show the smallest value of vapor pressure for DMSO in comparison with other solvents.

A difference in porous and partially porous nanofibers may be attributed to the parameter $\Delta\delta_{(S\text{-}P)2D}$. In the case of partially porous fibers, the values of $\Delta\delta_{(S\text{-}P)2D}$ parameter for ethanol and DMSO are 9.3 and 9.9 $MPa^{1/2}$, respectively. In comparison with porous fibers, the values of parameter $\Delta\delta_{(S\text{-}P)2D}$ for THF and DMSO are 2.5 and 9.9 $MPa^{1/2}$, respectively. These differences play a significant role for the production of porous fibers.

The described method for the preparation of porous fibers was successful although it leads to higher fiber diameters; see Figure 5. Histograms of fiber diameters were obtained from the image analysis LUCIA G. The average fiber diameter of these fibers was 2546 nm. For that reason, decreasing the fiber diameter by the effect of lower concentration or higher applied voltage during process was solved.

3.4. The Effect of PVB Concentration on Fiber Diameter. The electrospinning of 8 wt.% solutions PVB prepared from the mixture of the THF/DMSO and the effect of the ratio of good and poor solvent were investigated. The pore size of electrospun nanofibers formed by the good and poor solvent evaporation method is influenced by many factors. In general, increasing the ratio of the poor solvent or decreasing the polymer concentration changes the porosity. The SEM images confirm that the quantity of the pores on the fibers increases when the ratio of good and poor solvent decreases (Figure 6).

The histogram of the fiber diameters shows the reduction of fiber diameter by decreasing PVB concentration from 10 to 8 wt.%. The average fiber diameter of these fibers was 605 nm (Figure 7).

3.5. The Effect of Applied Voltage on Fiber Diameter. It was found that the small change of voltage from 30 to 35 kV influences both fiber diameter and porosity. Solutions of PVB in the mixture of the THF/DMSO (9/1 v/v) with a concentration of 10 wt.% was electrospun. SEM micrographs (Figure 8) show the result. The jet of the polymer fluid can easily start the phase separation with a lower voltage of 30 kV, and the structure is more porous. Diffusivity of good and poor solvents reduces the difference of the vapor pressure of the components when increasing the voltage. Therefore nanofibers with lower porosity and smaller fiber diameter are obtained. The average fiber diameter of these fibers was 1411 nm; see Figure 9.

4. Conclusion

The results show that the vapor pressure of the solvents plays an important role in fiber diameter and porosity. The dependence of nanofiber morphology on different solvent mixtures (good and poor), volume ratios of good and poor solvent and the concentration of polymer solution were studied. HSP was found as a useful tool for the prediction of suitable solvents for preparation of the porous nanofibers via the electrospinning process. All three defined conditions for

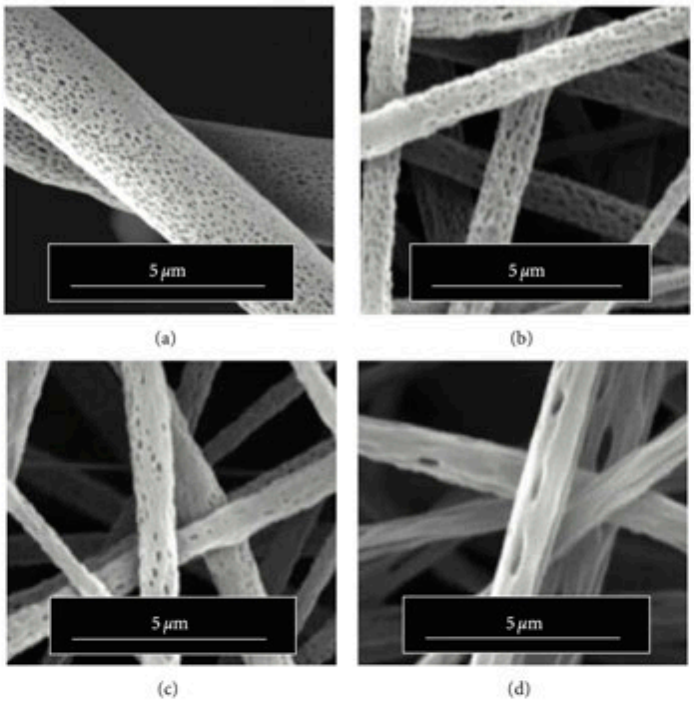

FIGURE 6: SEM images of PVB nanofibers prepared from (a) 10 wt.% THF/DMSO (9/1 v/v), (b) 8 wt.% THF DMSO (95/5 v/v), (c) 8 wt.% THF/DMSO (9/1 v/v), and (d) 8 wt.% (8/2 v/v).

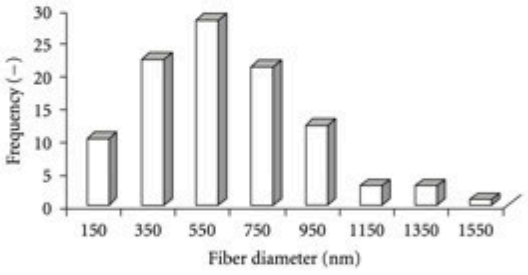

FIGURE 7: Histogram of the fiber diameter for electrospun PVB 8% wt. solution by the electrode-to-collector distance of 10 cm and applied voltage of 30 kV.

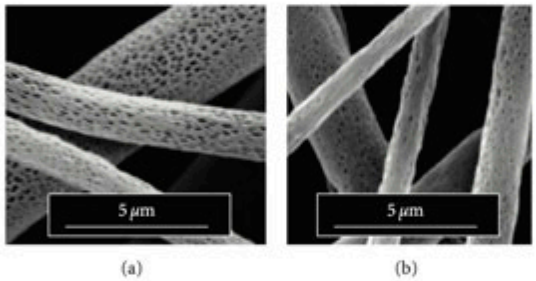

FIGURE 8: SEM images of PVB nanofibers prepared from 10 wt.% THF/DMSO (9/1 v/v): (a) applied voltage of 30 kV (b) applied voltage of 35 kV and an electrode-to-collector distance of 10 cm.

the creation of the porous nanofibers structure must be valid: (i) application of the mixture of good and poor solvents for the spinning solution, (ii) a distinct difference in the evaporation rate between good and poor solvents, and (iii) correct ratios of good and poor solvents (v/v). The above-mentioned conditions were fulfilled for the preparation of porous and nonporous PVB fibers.

In the case of the electrospinning of PVB solutions from ethanol/methanol mixtures, smooth fibers were formed regardless of the composition of solvent mixture. Both solvents act as a poor solvent for ethanol, thus the first condition is not fulfilled. In the case of the ethanol/DMSO (9/1 v/v) mixture, the indication of wrinkled fiber structure was evident. In this case the second condition (the difference in vapor pressure) was fulfilled. Nonporous fibers were formed in the case because both the solvents belong to the group of poor solvents for PVB. The first successful attempts to prepare porous nanofibers were realized by the spinning of the THF/DMSO (9/1 v/v) mixture. This composition of the spinning solution fulfils all three basic conditions (mixture of the good and poor solvents, difference in the vapor pressure of individual solvents, and correct ratio of mixed solvents).

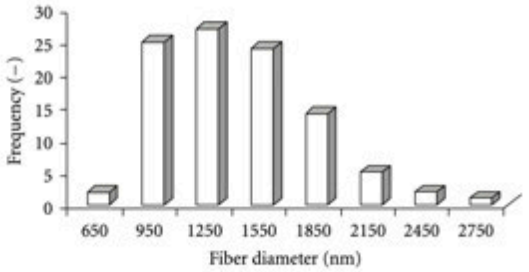

FIGURE 9: Histogram of the fiber diameter for electrospun PVB 10 wt.% solution from the electrode-to-collector distance of 10 cm and applied voltage of 35 kV.

Three qualities of PVB nanofibers were obtained: (i) nonporous, (ii) partially porous, and (iii) porous. The mixture of good and poor solvents applied for preparation of the polymer solution leads to porous or partially porous nanofibers through electrospinning. A qualitative and quantitative difference in porosity of the nanofibers is given by the different value of the evaporation rate of good and poor solvents. The correct ratios of the good and poor solvents have to be exactly defined. In the case of the ratio 9/1 (v/v), the nanofibers were more porous than in the case of the ratio 8/2 (v/v). The smooth and finer nanofibers were obtained from the PVB solution in an ethanol/methanol mixture. Both these solvents are defined as poor for PVB. Experimental results showed that the decrease of the polymer concentration reduced the fiber diameter while the porous structure remained unchanged. In contrast, an increase in the applied voltage reduces the fiber diameter but porosity of the fibers is diminished.

It is expected that the porous fibers could find a utilization in filtration applications, in which the effective surface area of porous fibers is the advantage.

Acknowledgments

This work was supported by Grant no. 1M0554 and GAČR no. 304/07/1129.

References

[1] C. H. Kim, Y. H. Jung, H. Y. Kim, D. R. Lee, N. Dharmaraj, and K. E. Choi, "Effect of collector temperature on the porous structure of electrospun fibers," *Macromolecular Research*, vol. 14, no. 1, pp. 59–65, 2006.

[2] Y. You, J. H. Youk, S. W. Lee, B. M. Min, S. J. Lee, and W. H. Park, "Preparation of porous ultrafine PGA fibers via selective dissolution of electrospun PGA/PLA blend fibers," *Materials Letters*, vol. 60, no. 6, pp. 757–760, 2006.

[3] S. O. Han, W. K. Son, D. Cho, J. H. Youk, and W. H. Park, "Preparation of porous ultra-fine fibres via selective thermal degradation of electrospun polyetherimide/poly(3-hydroxybutyrate-co-3-hydroxyvalerate) fibres," *Polymer Degradation and Stability*, vol. 86, no. 2, pp. 257–262, 2004.

[4] W. J. Elford, "Principles governing the preparation of membranes having graded porosities. The properties of "gradocol" membranes as ultrafilters," *Transactions of the Faraday Society*, vol. 33, pp. 1094–1104, 1937.

[5] J. D. Ferry, "Ultrafilter membranes and ultrafiltration," *Chemical Reviews*, vol. 18, no. 3, pp. 373–455, 1936.

[6] D. Lubasova and L. Martinova, "Formation mechanism of porous polycaprolactone nanofibers prepared by electrospinning," in *Proceedings of the 42nd IUPAC Congress*, Glasgow, Scotland, August 2009.

[7] Z. Qi, H. Yu, Y. Chen, and M. Zhu, "Highly porous fibers prepared by electrospinning a ternary system of nonsolvent/solvent/poly(l-lactic acid)," *Materials Letters*, vol. 63, no. 3-4, pp. 415–418, 2009.

[8] M. S. Khil, S. R. Bhattarai, H. Y. Kim, S. Z. Kim, and K. H. Lee, "Novel fabricated matrix via electrospinning for tissue engineering," *Journal of Biomedical Materials Research Part B*, vol. 72, no. 1, pp. 117–124, 2005.

[9] Ch. Hansen, *Hansen Solubility Parameters: A User's Handbook*, CRC Press/Taylor and Francis, New York, NY, USA, 2007.

[10] D. W. Van Krevelen, *Properties of Polymers: Their Correlation with Chemical Structure; Their Numerical Estimation and Prediction from Additive Group Contributions*, Elsevier, Amsterdam, The Netherlands, 1990.

Appendix 7

Masek, J., LUBASOVA, D., Lukac, R., Turanek-Knotigova, P., Kulich, P., Plockova, J., Maskova, E., Prochazka, L., Koudelka, S., Sasithorn, N., Gombos, J., Bartheldyova, E., Hubatka, F., Raska, M., Miller, A.D., Turanek, J. Multi-layered nanofibrous mucoadhesive films for buccal and sublingual administration of drug-delivery and vaccination nanoparticles - important step towards effective mucosal vaccines. Journal of Controlled Release 2017;249:183-195.

Journal of Controlled Release 249 (2017) 183–195

Contents lists available at ScienceDirect

Journal of Controlled Release

journal homepage: www.elsevier.com/locate/jconrel

Multi-layered nanofibrous mucoadhesive films for buccal and sublingual administration of drug-delivery and vaccination nanoparticles - important step towards effective mucosal vaccines

Josef Mašek [a,*], Daniela Lubasová [b], Róbert Lukáč [a], Pavlína Turánek-Knotigová [a], Pavel Kulich [a], Jana Plocková [a], Eliška Mašková [c], Lubomír Procházka [a], Štěpán Koudelka [a], Nongnut Sasithorn [b], Jozsef Gombos [d], Eliška Bartheldyová [a], František Hubatka [a], Milan Raška [a,e], Andrew D. Miller [f,g], Jaroslav Turánek [a,*]

[a] Department of Pharmacology and Immunotherapy, Veterinary Research Institute, Brno, Czech Republic
[b] Technical University of Liberec, Institute for Nanomaterials, Advanced Technologies and Innovation, Liberec, Czech Republic
[c] Department of Pharmaceutics, Faculty of Pharmacy, University of Veterinary and Pharmaceutical Sciences Brno, Czech Republic
[d] Leica Microsystems, Heerbrugg, Switzerland
[e] Department of Immunology, Palacky University, Olomouc, Czech Republic
[f] Institute of Pharmaceutical Science, King's College London, London, United Kingdom
[g] KP Therapeutics Ltd, 86 Deansgate, Manchester, M3 2ER, United Kingdom

ARTICLE INFO

Article history:
Received 8 April 2016
Received in revised form 22 July 2016
Accepted 23 July 2016
Available online 18 August 2016

Keywords:
drug delivery
sublingual vaccines
mucoadhesive film
nanofibres
mucus penetrating nanoparticles
electrospinning

ABSTRACT

Nanofibre-based mucoadhesive films were invented for oromucosal administration of nanocarriers used for delivery of drugs and vaccines. The mucoadhesive film consists of an electrospun nanofibrous reservoir layer, a mucoadhesive film layer and a protective backing layer. The mucoadhesive layer is responsible for tight adhesion of the whole system to the oral mucosa after application. The electrospun nanofibrous reservoir layer is intended to act as a reservoir for polymeric and lipid-based nanoparticles, liposomes, virosomes, virus-like particles, dendrimers and the like, plus macromolecular drugs, antigens and/or allergens. The extremely large surface area of nanofibrous reservoir layers allows high levels of nanoparticle loading. Nanoparticles can either be reversibly adsorbed to the surface of nanofibres or they can be deposited in the pores between the nanofibres. After mucosal application, nanofibrous reservoir layers are intended to promote prolonged release of nanoparticles into the submucosal tissue. Reversible adsorption of model nanoparticles as well as sufficient mucoadhesive properties were demonstrated. This novel system appears appropriate for the use in oral mucosa, especially for sublingual and buccal tissues. To prove this concept, trans-/intramucosal and lymph-node delivery of PLGA-PEG nanoparticles was demonstrated in a porcine model. This system can mainly be used for sublingual immunization and the development of "printed vaccine technology".

1. Introduction

The oromucosal route of administration is an alternative route for drug-delivery and vaccine delivery. This has been used successfully for local and systemic delivery of low-molecular-weight substances with a rapid onset of pharmacological effects, and also for drugs formulated into controlled-release systems (i.e. Onsolis®, fentanyl comprising mucoadhesive film for buccal administration). Sublingual immunotherapy that makes use of allergens and antigens for the treatment of allergies and sublingual vaccination strategies, have also been explored. In addition, mucosal, especially sublingual delivery of macromolecular drug and antigen-delivery nanoparticles has become an important topic of recent research as well [1]. In general, high permeability, a lack of enzymatic barriers, mild pH values, easy access for self-administration, and opportunities to bypass first-pass metabolism, all make the non-keratinized oral regions attractive sites for the administration of drugs and/or vaccines [2]. Oral mucosae, especially its sublingual region, are densely populated with specialized dendritic cells. The adjacent submucosal tissue is drained with lymphatic vessels, through which free antigen as well as antigen-loaded dendritic cells move to reach regional lymph nodes. Thus, oral cavity and especially sublingual region is a potentially favourable site for inducing a specific immune response or tolerance towards given antigens and allergens. The sublingual mucosa, in particular, has been recognized as a suitable immunoinductive area giving the opportunity for safe and efficient mucosal vaccination and immunomodulation [3].

* Corresponding authors.
E-mail addresses: masek@vri.cz (J. Mašek), turanek@vri.cz (J. Turánek).

http://dx.doi.org/10.1016/j.jconrel.2016.07.036
0168-3659/

However, although mucosal surfaces are the main route of pathogen entry, yet the induction of effective mucosal immunity is still a challenge for researchers in the field of vaccinology [4]. In order to induce an effective immune response not only is the vaccine system itself important but so too is the method of application [5]. Factors that limit successful administration and delivery of nano-based therapeutic systems include the mucus layer itself on the surface of oral mucosa, continuous saliva production, and epithelial absorption barriers [6]. Typically, administered drugs/antigens are efficiently removed by mucus clearance mechanisms and systemic absorption, precluding a prolonged local drug presence [7]. New approaches and formulations that utilize mucoadhesives, mucus penetrating particles, or absorption enhancers can enable effective transmucosal delivery of macromolecular therapeutics [8] and nanoparticle-based delivery systems [6]. In addition, a variety of dosage forms have been developed to face these obstacles for oral mucosal delivery – including mucoadhesive tablets, mucoadhesive oral films, fast dissolving films as well as liquid formulations and sprays. Many nanoparticle-based delivery systems including polymeric and lipid-based nanoparticles have also been tested as mucosal drug-delivery and vaccination nanoparticle systems, especially for protein, peptide, and nucleic acid delivery [9].

Successful delivery of drug-delivery or vaccination nanoparticles through mucosal tissues represents a multidisciplinary problem that embraces aspects of mucosal physiology and mucosal barrier properties, nanotechnology and nanoparticle surface chemistries. This problem also embraces pharmaceutical sciences with particular reference to appropriate pharmaceutical formulations, dose regimens, drug-delivery devices, and proper elucidation of therapeutic approach [10]. For the first time, here we describe the combination of electrospun nanofibrous reservoir layers prepared by electrospinning, with mucoadhesive layers that together appear to represent an important new dosage platform for effective administration of drug-delivery and vaccination nanoparticles into the sublingual and buccal mucosa.

Electrospinning is a simple and efficient technique to produce nanofibers [11]. It utilizes a high electrostatic field to generate nanofibers from a fluid. Electrospun nanofibers often show large surface-to-weight (volume) ratio, high porosity, and excellent pore interconnectivity [12]. These unique features allow electrospun nanofibers have extensive applications in diverse areas including filtration, wound healing, cosmetic, drug delivery systems, and medicine [13,14].

Our nanofibrous mucoadhesive films are shown to avoid fast clearance of nanoparticles from sites of application, maintain a long-term concentration gradient of nanoparticles at the mucosal surface, and ensure unidirectional diffusion of nanoparticles towards mucosal surfaces by means of an impermeable surface layer(s) that faces the oral cavity.

2. Materials and Methods

2.1. Preparation of nanofibrous mucoadhesive films

Each three-layered film prepared consisted of 1) a mucoadhesive layer, 2) a backing layer and 3) an electrospun nanofibrous reservoir layer. In the first step, the upper surface of a prepared mucoadhesive layer was coated with polymer to form a backing layer. In the second step the bottom side of each mucoadhesive layer was wetted with a vapour stream and a corresponding nanofibrous layer immediately pressed against this mucoadhesive layer.

Mucoadhesive layers were prepared as follows: initially Carbopol 934P (Lubrizol Advanced Materials, Cleveland, USA) and hydroxypropyl methylcelulose K4M (HPMC) (Colorcon Limited, UK) were combined in a 2:1 (w/w) ratio in water giving a viscous opaque solution that was supplemented with glycerol at 15% (w/w). The combination mixture was then treated by sonication to remove air bubbles and required volumes were poured out into plastic Petri dishes. Excess water was removed by evaporation at room temperature for 48 h leading to the formation of the desired mucoadhesive layers.

Non-adhesive backing layers were formed by the spraying of a 2% ethanolic solution of Eudragit® L 100-55 (soluble) directly onto the surface of a given mucoadhesive layer. During the spraying, each Petri dish with a given mucoadhesive layer was heated to 50°C to accelerate the evaporation of the solvent. The thickness of backing layer was measured using SEM pictures of cross-sectioned nanofibrous mucoadhesive films.

2.2. Nanofibrous reservoir layer

All nanofibrous reservoir layers were prepared using a roller electrospinning device (**see schema in Supporting information, section A**). The device contains a rotating cylinder, 145 mm in length and 20 mm in diameter, partially immersed in a blended polymer solution reservoir attached to a positive electrode. Blended polymer solutions were electrospun at a high voltage of 50 kV with the cylinder rotating at ~ 15 rpm in order to become rapidly coated with polymer solution followed by the electrospinning process itself and the creation of new materials. By this method each electrospun nanofibrous reservoir layer was collected on backing material (PEGATEX S 30 g/m^2) that was moving along a negative collector electrode at a velocity of 30 mm/min. Electrospinning was carried out at a distance of 100 mm; air temperature 21°C, and air humidity 60 ± 2%.

2.3. Silk fibroin nanofibrous reservoir layer

Raw silk cocoons were degummed twice with 0.1 M of sodium carbonate and 0.5% of standard reference detergent at 100°C for 30 min, rinsed with warm water to remove the sericin from the surface of the fibre and then dried at room temperature. Silk fibroin solution (SF) was prepared by dissolving the degummed silk fibres in formic acid (98%). The formic acid solution used in the process contains 3 wt% calcium chloride. The SF concentration was fixed at 12 wt%. The SF solution was magnetically stirred at room temperature overnight, then electrospun at conditions described above.

The SF nanofibrous reservoir layers were immersed in ethanol for 30 min to induce crystallization of SF and reduce the water solubility of the nanofibrous reservoir layers. After drying at room temperature, the treated nanofibrous reservoir layers were immersed in distilled water overnight, which was followed by rinsing in distilled water to remove residual salts. Afterwards, the nanofibrous reservoir layers were air-dried.

2.4. Chitosan-PEO nanofibrous reservoir layer

Chitosan (viscosity 10 cP, 5 wt% in 1% acetic acid and a degree of deacetylation of 0.8) was purchased from Wako Pure Chemical Industries, polyethylene-oxide (PEO, average Mw ~ 400.000 g/mol by gel permeation chromatography) was obtained from Sigma-Aldrich and used as received. Deionized water with sodium chloride was used to prepare PEO polymer solution. Sodium chloride was added to an aqueous solution of 4 wt% PEO at 0.24 mol/L. Chitosan was then dissolved in 10 wt% citric acid to achieve a polymer concentration of 8 wt%. Chitosan and PEO solutions were afterwards blended and stirred at room temperature overnight at a volume ratio of 8/2 (chitosan-PEO). This blended chitosan-PEO polymer solution was electrospun at conditions described above.

2.5. Polycaprolactone nanofibrous reservoir layer

Polycaprolactone (PCL, Mw 80 000 g/mol, Sigma Aldrich) solution was prepared by dissolving PCL pellets in the solvent mixture acetone/ethanol (7/3 v/v) by means of overnight stirring at room temperature. The total polymer concentration was fixed at 16 wt%. Thereafter, the blended PCL polymer solution was electrospun at conditions described above.

3. Preparation of nanoparticles

3.1. Liposomes

Liposomes were prepared by the lipid film hydration method. The composition of liposomes was 10% DSPE-PEG, 89.5% EPC (egg phosphatidylcholine) (Avanti Polar Lipids, USA) and 0.5 molar % 1,2-dioleoyl-*sn*-glycero-3-phosphoethanolamine-N-(lissamine rhodamine B sulfonyl) (Avanti Polar Lipids, USA). After hydration by PBS, liposomes were extruded using a 200 nm polycarbonate filter (Millipore, USA).

Metallochelating nanoliposomes were prepared by the lipid film hydration method and were extruded using a 200 nm polycarbonate filter. The composition of liposomes was 5% DOGS-NTA-Ni-1,2-dioleoyl-*sn*-glycero-3-[(N-(5-amino-1-carboxypentyl)iminodiacetic acid)succinyl] (nickel salt) (Avanti Polar Lipids, USA), 71% EPC, 19% POPG (1-palmitoyl-2-oleoyl-*sn*-glycero-3-phospho-(1'-*rac*-glycerol) (sodium salt) (Avanti Polar Lipids, USA). Prepared liposomes were mixed with His-tagged green fluorescent protein (GFP) (20ug GFP per 1mg of lipid). The preparation is described in detail in Masek et al [30].

3.2. PLGA-PEG nanoparticles

PLGA particles were prepared by the emulsifying method. Briefly, Poly(ethylene glycol) methyl ether-block-poly(lactide-co-glycolide), Mw 55.000Da, PEG average 5.000Da (PLGA-PEG), Poly(D,L-lactide-co-glycolide) (lactide:glycolide (5:5), mol wt 30.000-60.000) (PLGA) (Sigma) and 1,2-dioleoyl-*sn*-glycero-3-phosphoethanolamine-N-(lissamine rhodamine B sulfonyl) (Avantilipids) were dissolved in 1ml chloroform and emulsified in 5 ml of 1% sodium deoxycholate solution using the ultrasound device SONOPULS HD 3100 (Bandelin, Germany). The particles were formed by evaporation from chloroform using a rotary evaporator. The excess of sodium deoxycholate was removed and PLGA-PEG particles were concentrated in one step using MikroKros hollow fibre modules (50 kDa) (Spectrum, USA).

3.3. Profilometry and macroscopic morphology analysis of nanofibrous mucoadhesive film

Scanning electron microscope (SEM) (Hitachi8010, Hitachi, Japan) was used to investigate the macroscopic morphology of nanofibrous mucoadhesive films, the surface texture of nanofibrous layers as well as nanoparticles adsorbed to the surfaces of fibres. A cross-section of a nanofibrous mucoadhesive film was prepared at -130°C. The sample was coated with Pt-Pd and observed by cryo-SEM at -130°C. Adsorption of fluorescent-labelled nanoparticles to nanofibres was observed by confocal microscopy (Leica SP2, Germany) and the adsorption of liposomes was observed by TEM (Philips Morgagni). Detailed measurements of the thicknesses of nanofibrous reservoir layers, texture analyses of these layers and of backing layers were performed using an optical surface metrology system (Leica DCM8, Germany) under confocal mode (50X objective).

3.4. Analysis of the diameter of nanofibrous reservoir layers

Nanofibrous reservoir layers were observed under a SEM Vega 3 (Tescan, Czech Republic) at an accelerated voltage of 20 kV. Prior to measurements, all the samples were sputter-coated (Q150R ES, Quorum Technologies Ltd., England) with gold at a thickness of 7 nm. The SEM images were analysed with NIS-Elements AR software. The average fibre diameter and its distribution were determined from 150 random fibres.

3.5. Measurement of water contact angle

The hydrophilicity of the nanofibrous reservoir layers was evaluated by water contact angle measurements using a See System E instrument (Advex Instruments, s. r. o., Czech Republic). A distilled water droplet of the size of 10 μL was placed carefully onto the surface of the nanofibres at room temperature. After a period of 20 s, the contact angle was recorded. The mean value and standard deviation (SD) were also calculated through testing at ten different positions on the same sample.

3.6. Determination of in-vitro release of nanoparticles from nanofibrous reservoir layer

PLGA-PEG or liposomal nanoparticles (20 mg/ml) were allowed to infiltrate nanofibrous reservoir layers (surface area of 1 cm^2) that were dipped into appropriate suspensions for 2 mins. Immediately after adsorption of particles, nanofibrous reservoir layers were cleansed of excess fluids and placed into PBS buffer (1 ml) for 30 mins. The final PBS solution of PLGA nanoparticles was diluted and the concentrations of released nanoparticles were calculated using a NanoSight 500 instrument (Malvern Instruments, UK). As an alternative method, the final PBS solution of fluorescence-labelled nanoparticles was diluted and the ratios of bound to released nanoparticles were calculated from differential fluorescence intensities measured at the emission wavelength of 560 nm using a spectrofluorimeter LS55B (Perkin Elmer).

3.7. Determination of ex-vivo release of nanoparticles from nanofibrous reservoir layer

The ability of the electrospun nanofibrous reservoir layer to release associated nanoparticles in real conditions (moistened mucosal tissue surfaces with limited water volumes, typical of viscous mucus layers etc.) was confirmed by 2 h incubation of nanofibrous mucoadhesive films with cryo-altered mucosa having reduced barrier functions at 37°C [45]. The release of nanoparticles from nanofibrous reservoir layers was demonstrated by observation of fluorescence signals on cross-sections of adjacent tissues by confocal microscopy. The surface of each mucosa was moistened (flow rate 0.1 ml/min) with PBS during experiments using a linear pump and tubing.

3.8. Ex-vivo study of penetration of nanoparticles into tissues

Ex-vivo penetration of nanoparticles into adjacent mucosa was tested on freshly excised porcine sublingual or buccal tissues. Nanofibrous mucoadhesive films with fluorescently labelled nanoparticles were applied to mucosa and incubated for 2 h at 37°C. The surface of each mucosa was wetted as described above during the experiment.

Sublingual and buccal tissues were removed using surgical instruments immediately after slaughter of the animal. The excised tissues were transferred immediately to the laboratory in PBS buffer and were cut into cube-shaped pieces used for testing. The interval between slaughter of the animal and start of experiment did not exceed 20 mins.

3.9. In-vivo study of penetration of nanoparticles to adjacent mucosa and lymph node delivery

The experiments on animals were approved by the Ethics Committee of the Veterinary Research Institute, Brno and by the Ethics Committee of the Ministry of Agriculture, Czech Republic.

Piglets (15 kg) were anesthetized with the short-term anaesthetic Zoletil (Virbac, France). Multi-layered mucoadhesive film loaded with fluorescently labelled PLGA-PEG nanoparticles in 2% sodium deoxycholate was applied to the porcine sublingual mucosa. After 2 h of incubation, animals were anesthetised and sacrificed by an *i.v.*-application of T61. Sublingual mucosa samples with nanofibrous mucoadhesive films attached and regional draining lymph nodes were excised, frozen and stored at -80°C. The tissues were sectioned using Leica Cryocut 1800 Cryostat (Leica, Germany). All sections were stained and observed by confocal microscope (Leica SP2). Nuclei were stained with SytoxBlue (Molecular Probes), Actin was stained with Alexa

Fluor® 633 Phalloidin, phagocytic cells were stained with SLA Class II DR Antibody | 2E9/13 (Serotec) and goat anti-mouse secondary Alexa Fluor® 488 conjugate (Abcam). Nanoparticles were stained with lissamine-rhodamine phosphatidylethanolamine (Avanti Polar Lipids, USA).

3.10. Cryo-SEM of adhesion of nanofibrous layer onto mucosal surface

2 h post application of mucoadhesive films to piglets, cube-shaped samples of mucosal tissue with adhered mucoadhesive films were removed and cross-sectioned with Cryocut (Cryocut 1800, Leica, Austria) at -20°C. Subsequently, the samples were transferred under nitrogen atmosphere into the SEM (Hitachi SU8010, Hitachi Ltd., Japan). The tightness of adherence of the mucoadhesive layer to mucosa and the structure of nanofibrous mucoadhesive films were observed under cryo-mode by SEM at -130°C.

3.11. Cryo-alteration of porcine mucosa

Freshly excised porcine mucosa was rinsed twice with PBS buffer at room temperature. Subsequently, the rinsed sublingual mucosa samples were freeze-thawed in two cycles to -20°C. The sublingual mucosa samples were stored at -20°C until use. Cryo-altered mucosa was used as a positive control to confirm the in-situ release of nanoparticles from nanofibres.

3.12. Physicochemical analyses of nanoparticles

Nanoparticle sizes and zeta potentials were measured by dynamic light scattering (DLS) (ZetaSizer Nano ZS, Malvern, UK) at the wavelength of 633 nm. The sizes of nanoparticles and the rate of release of PLGA-PEG nanoparticles were measured using a Nanoparticle Tracking Analysis (NTA) (Nanosight 500, Malvern, UK). The samples were diluted appropriately prior to the measurement. During the NTA measurements, the camera level was set to 7. Captured videos were analysed with a detection threshold set to the value of 10. The morphology of nanoparticles was characterised using TEM. Specimens for TEM analysis were prepared by drop-casting particles on carbon coated copper grids stained with phosphomolybdenic acid solution (2%) and dried at room temperature before observation. Bright field imaging was performed using TEM (Phillips 208 S, FEI, Czech Republic) operating at 80 kV.

4. Results and Discussion

4.1. Nanofibrous mucoadhesive film

The main task for any mucoadhesive system used for mucosal delivery of drug-delivery or vaccination nanoparticles is maintaining effective nanoparticle concentrations at the given site of application for a sufficient time span to enable functional nanoparticle-mediated delivery to take place. This task can be accomplished by multi-layered nanofibrous mucoadhesive films for the controlled release and delivery of nanoparticles/macromolecules into the oral mucosa in a unidirectional fashion while avoiding nanoparticle losses from the site of the application due to wash-out by saliva (Fig. 1).

In our case, this objective was achieved by designing nanofibrous mucoadhesive films with three different layers (see Fig. 2): a nanofibrous reservoir layer (1), a mucoadhesive layer (2), and a backing layer (3). Alternatively, an interlayer (4) could be added in between layers 2 and 3 (Fig. 2A). The three-layered film is pictured in (Fig. 2B) and the SEM image is shown in (Fig. 2C). The nanofibrous layer serves as reservoir for nanoparticles attached to the surface of nanofibres or embedded into the pores between nanofibres. The mucoadhesive layer was introduced to keep the whole platform affixed at the site of its application for a prolonged time span adjusted by the degree of adhesiveness of the material used for the preparation of the mucoadhesive film layer. The backing layer was added to prevent diffusion of nanoparticles out of the site of application and to protect both the mucoadhesive layer and the nanofibrous reservoir layer from the effect of saliva and flow of mucosal fluid. Moreover, the backing layer facilitates the self-administration of the film to the oral mucosa by protecting the surface from sticky properties of the mucoadhesive film itself.

Mucoadhesive film layer was prepared by a casting/solvent evaporation technique as described elsewhere [15] adapted for deposition of a backing layer onto the surface of a preformed mucoadhesive layer by spray-drying. In our case, we selected an oro-dissolving backing layer

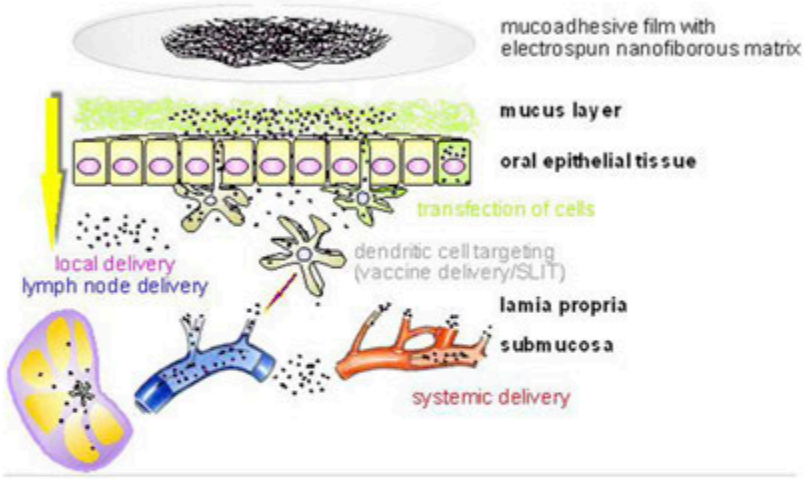

Fig. 1. Schematic presentation of the principle for improving delivery of drug-delivery and vaccination nanoparticles by means of a nanofibrous mucoadhesive film High adsorption loading capacity of nanofibrous material ensures a high concentration of nanoparticles to be reached after the rapid release from reservoir layer to the limited volume of the fluids at the application site. Protective backing layer prevents removal of nanoparticles from the site of administration by flow of mucosal secretions and saliva. A concentration gradient is formed, which then exerts a "pressure" on the mucosal layer, thus rapidly enabling the formation of a nanoparticle diffusion potential across the mucosal surface into the submucosa. The different fate of nanoparticles (local/systemic delivery) is based on their physicochemical properties and presence of targeting moieties. Dendritic cells (DCs) present in the submucosa are then free to capture vaccination nanoparticles for delivery to the local lymph nodes that drain the submucosal zone of application. Vaccination nanoparticles not captured by DCs, are otherwise free to diffuse through the submucosa reaching lymphatic capillaries by means of which they drift to the local lymph nodes for capture by professional antigen-presenting cells.

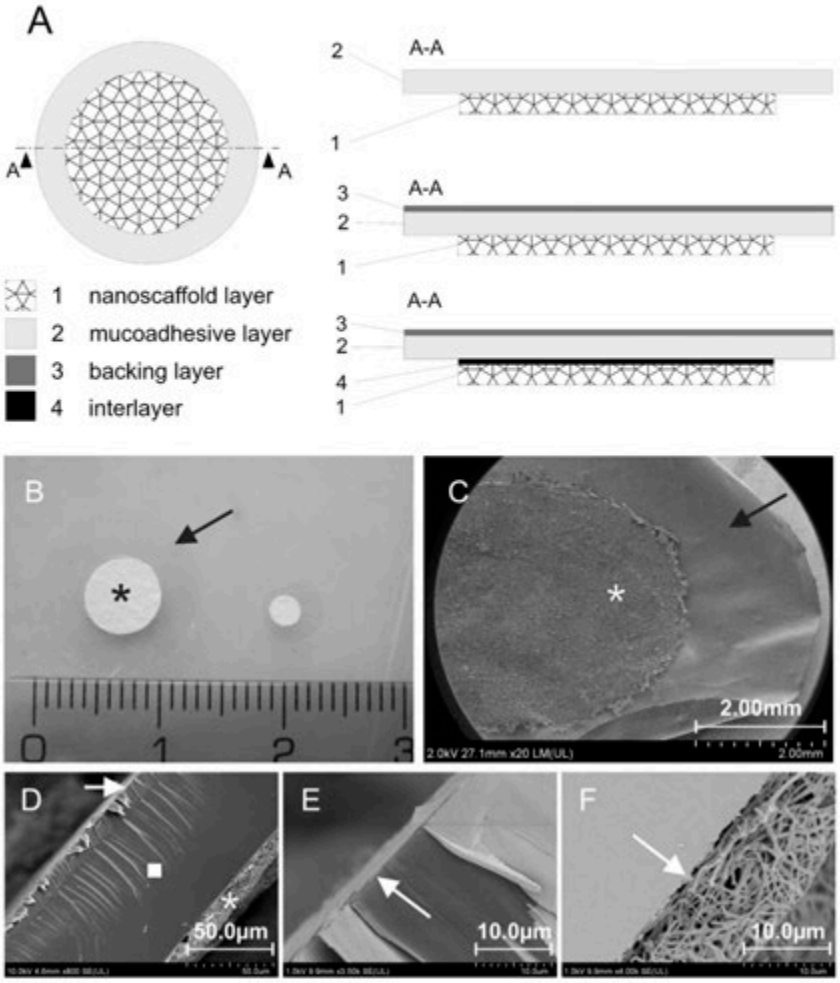

Fig. 2. Schematic structure and real appearance of nanofibrous mucoadhesive film A: The scheme shows the bottom view (left) and cross-section (right) of possible variants for construction of nanofibrous mucoadhesive film; B: Photograph of nanofibrous mucoadhesive film, left – design for large animal experiments (pig), and right – design for small animal experiments (mice) (centimetre scale). Nanofibrous reservoir layer (asterisk), mucoadhesive layer (arrow); C: Scanning electron microscopy (SEM) picture showing individual layers of a three-layered nanofibrous mucoadhesive film. The mucoadhesive layer creates a peripheral adhesive ring surrounding the central part on which the electrospun nanofibrous reservoir layer is fixed. Nanofibrous reservoir layer (asterisk), mucoadhesive layer (arrow); D: Cross-section of mucoadhesive layer observed in its native state after freezing (cryo-SEM). Nanofibrous reservoir layer (asterisk), mucoadhesive layer (square) and backing layer (arrow); E: Detail of cross-section of nanofibrous mucoadhesive film, arrow indicates the Eudragit® L 100-55 backing layer (arrow); F: Detail of cross-section of nanofibrous mucoadhesive film, arrow indicates the connection of the mucoadhesive layer and the nanofibrous reservoir layer.

composed of Eudragit® L 100-55 that dissolves at pH 5.5 or higher (see Supporting information for dissolution kinetics of the backing layer). The oro-dissolving backing layer was introduced for better patient comfort since nanofibrous mucoadhesive films can dissolve or undergo erosion with time without the need for removal. By tuning the oro-dissolving properties of the backing layer, the time of adhesion of a given nanofibrous mucoadhesive film to the oral mucosa can be adjusted. Controlled thickness of 240 ± 86 nanometres can be achieved (Fig. 2D). In contrast, using a common solvent-casting method, the backing layer of several microns in depth is usually obtained [16–18].

The selected mucoadhesive layer was prepared with a specific composition for low swellability and a strong mucoadhesive strength, thereby ensuring sufficient mucoadhesive properties [19]. The thicknesses of our prepared mucoadhesive layers were observed to be approx. 80 µm, as measured by SEM in the cryo-mode (Fig. 2D). Nanofibrous reservoir layers were then affixed onto these backing layer coated, pre-formed mucoadhesive layers. As observed by SEM in the cryo-mode, the structure of a given mucoadhesive layer remained essentially unchanged after coating with a backing layer by spray drying (see the arrow in Fig. 2E), and also after attachment of a nanofibrous reservoir layer by means of a sticking procedure (see the arrow in Fig. 2F). Profilometry was used for visualization of features of particular layers of the prepared nanofibrous mucoadhesive film (see supporting info, section B)

4.2. Electrospun nanofibrous reservoir layer

The internal features of electrospun nanofibrous reservoir layers are considered ideal for adsorption of nanoparticles and macromolecules due to their extremely high surface area and porosity, enabling a high nanoparticle to mass ratio in comparison with reservoir layers constructed from other materials [20]. For example, Jung et al. prepared a chitosan nanoparticle/polycaprone composite for sustained drug delivery intended as wound dressing material [21]. In general, well known

flexibility of thin electrospun nanofibrous reservoir layers is also important for intimate contact to be established between nanofibrous mucoadhesive films and mucosal surfaces. Otherwise, adjusting the physical properties of electrospun nanofibrous reservoir layers is extremely important to achieve efficient adsorption of drug-delivery and/or vaccination nanoparticles, and their rapid/controlled release when required. Hydrophobic and ionic interactions are the dominant forces that influence binding and controlled release. Hence, we prepared nanofibrous reservoir layers with three different materials, PCL, chitosan/ PEO and SF (Table 1, **Supporting information, section C**). In addition, various treatment procedures were employed to change the surface properties of nanofibers. For example, mild sodium hydroxide or deoxycholate surfactant pre-treatment of PCL nanofibrous reservoir layers were both found to increase layer hydrophilicity (i.e. reduce the contact angle) that might otherwise be relatively hydrophobic in character (Table 1).

4.3. Application of nanofibrous mucoadhesive film to porcine mucosa

The nanofibrous mucoadhesive films used were able to adhere for at least 2 h to the sublingual region (Fig. 3A,B). Neither adverse reactions such as local irritation observed in the course of testing, including the post-treatment period.

4.4. Tight adhesion of nanofibrous reservoir layer to oral mucosa

Our nanofibrous mucoadhesive films were also shown to adhere tightly to porcine sublingual mucosa (Fig. 3C-I). The tight adherence of a nanofibrous mucoadhesive film to the porcine oral sublingual mucosa after 2 h incubation was confirmed by cryo-SEM on cube-shaped cross-section samples (Fig. 3C). Mucoadhesive film is flexible enough to copy the surface of the sublingual mucosa (Fig. 3D) and adhere firmly to it (Fig. 3E). The benefits of such visible tight adhesion are that drug-delivery and/or vaccination nanoparticles located within the nanofibrous reservoir layer of nanofibrous mucoadhesive films are maintained in close contact with the surface of the mucosa and avoid being subject to mucosal self-cleaning effects caused by a continuous flow of saliva. Particular layers are clearly visible in (Fig. 3F), (Fig. 3G) showing mucoadhesive layer and SF nanofibrous reservoir layer. The layers can be well identified at the edges of the sample specimen where they were detached from the mucosal surface owing to cutting procedure during preparation of the sample. The upper layer of mucus is detached from mucosal tissue (detail in Fig. 3G). Detailed structure of the SF nanofibrous reservoir layer adhered to the mucosal surface is shown at (Fig. 3H). The mesh of mucin fibers is visible in the bottom part. PLGA-PEG (poly(lactic-co-glycolic acid)-polyethylene glycol) nanoparticles are found adsorbed on the surface of nanofibers as well as permeating the mesh of mucin fibers. Fig. 3I (detail from Fig. 3E) represents a general view of SF nanofibrous mucoadhesive film and adjacent mucosa after 2 h incubation. Gel mucoadhesive layer can be seen below the nanofibrous layer. A mucin mesh is clearly distinguished on the surface of the mucosa in the middle part of the image. At the bottom of the image, particular epithelial cells are visible.

Table 1
Physical properties of nanofibres.

Material	Weight/m^2 (g)	Contact angle (°)	Nanofibre diameter (nm)
PCL	5	118.77 ± 3.62	114.13 ± 17.87
SF	5	43.56 ± 5.07	670.22 ± 123.73
Chitosan-PEO	5	11.69 ± 3.18	169.3 ± 43.3
PCL pre-treated NaOH	5	54.04 ± 5.61	N/A*
PCL pre-treated sodium deoxycholate	5	15.1 ± 2.92	N/A*

* refers to diameter of untreated PCL nanofibres.

4.5. Mucus penetration by drug-delivery or vaccination nanoparticles

Polymeric nanoparticles that possess a dense low-molecular weight polyethylene glycol (PEG) coating and are known as mucus penetrating particles (MPPs) with an enhanced ability to diffuse through mucus layers [22]. MPPs penetrate through mucus by a mechanism of passive diffusion driven by concentration gradients. The dense, hydrophilic PEG coating prevents interactions of the hydrophobic nanoparticle core with mucin mesh and therefore minimises mucoadhesive interactions [23–25]. The inclusion of a PEG layer at the liposome surface also ensures mucus-penetrating properties [26]. PLGA-PEG nanoparticles and PEG containing liposomes were prepared for testing in this study. The morphology of both nanoparticles was studied using TEM. Both types of particles exhibited a regular spherical shape and were prepared as essentially monodisperse. The electron micrographs of model PLGA-PEG nanoparticles and liposomes are presented. The observed sizes of both nanoparticle types were in good agreement with DLS data as well as NTA data. Both liposomes and PLGA-PEG nanoparticles also demonstrated similar size distributions and zeta-potentials (electroneutral) (**see Supporting information, section D**).

4.6. Loading the nanofibrous reservoir layer with nanoparticles

SF nanofibrous reservoir layers were loaded with nanoparticle dispersions (liposomal or PLGA-PEG nanoparticles). Nanoparticle dispersion was applied directly to the surface of a given nanofibrous layer and were absorbed immediately and uniformly into the whole volumes of the given nanofibrous reservoir layers due to the capillary action. The process of loading affected neither physical nor morphological properties of the adjoining mucoadhesive film layer (Fig. 4A). Strikingly, we observed a dense and homogenous covering of nanofibre surfaces by nanoparticles (PLGA-PEG or liposomes) as demonstrated by electron microscopy and confocal microscopy (Fig. 4B-F). Furthermore, using GFP-proteoliposomes, a model for proteoliposomal vaccination nanoparticles [27–29], we were unable to observe any signs of nanoparticle aggregation, nor apparent disruption of GFP metallochelation binding to liposome surfaces [30], thereby suggesting that nanofibre adsorption is neither physically or chemically disruptive for lipid-based nanoparticle systems (Fig. 4D).

4.7. The release of nanoparticles from nanofibrous reservoir layer

The ability of nanofibrous reservoir layer to release adsorbed nanoparticles from nanofibrous reservoir layers into the surrounding milieu was demonstrated using different types of nanofibres. The tested nanofibrous layers were prepared with all three main biocompatible materials of interest, namely with PCL, chitosan-PEO, and SF polymers. In addition, PCL nanofibrous reservoir layers were treated with 3M sodium hydroxide for 5 mins, or with sodium deoxycholate to improve the wettability of nanofibre surfaces. These procedures significantly improved wettability as reflected in a decrease in the contact angle (see Table 1). The extent of nanoparticle release from a given type of nanofibrous reservoir layer was determined by calculation of nanoparticle concentrations (measured by the NTA technique) after incubation of nanoparticle-loaded nanofibrous reservoir layers with PBS buffer (Fig. 5A). Alternatively, *in-vitro* release was determined by monitoring changes in fluorescence intensity of lissamine rhodamine-labelled nanoparticles (PLGA-PEG or liposomes) after the incubation of nanoparticle-loaded nanofibrous layer in PBS buffer (see Fig. 5). The NTA assay was found to be in good agreement with the fluorescence release assay data for both types of nanoparticles (data not shown). Moreover, cholate salts are widely used as penetration enhancers (see next paragraph), also sodium deoxycholate can perform dual role.

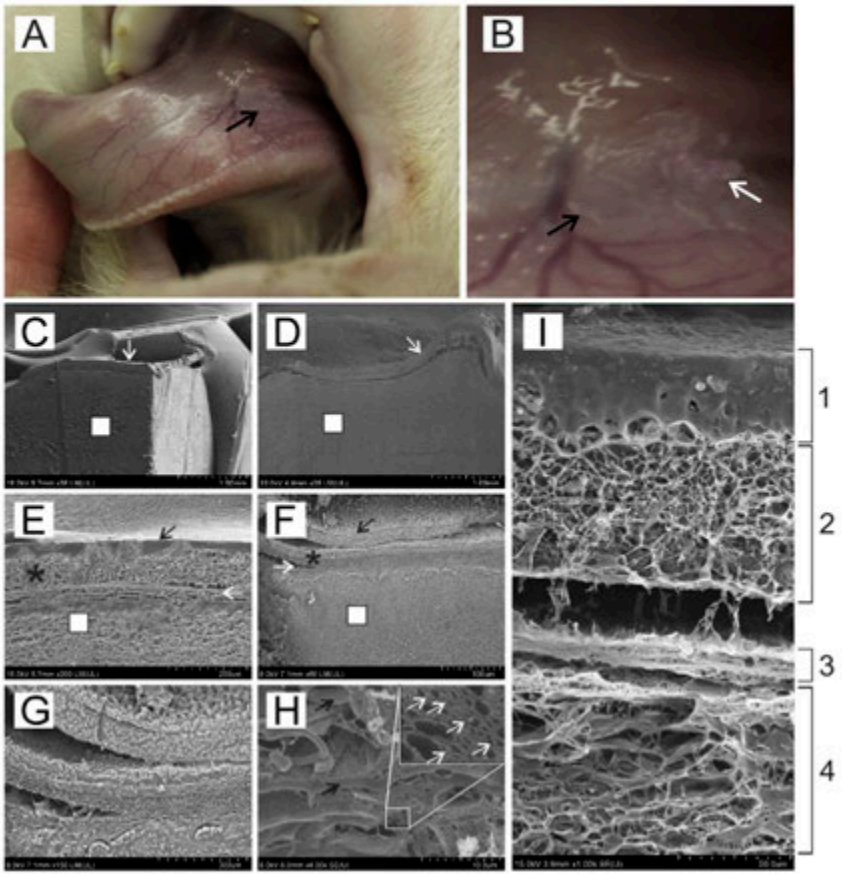

Fig. 3. Scanning electron microscopy representation of tight adhesion of nanofibrous mucoadhesive film to the sublingual mucosa A: Application of nanofibrous mucoadhesive film with SF nanofibrous reservoir layer to porcine sublingual mucosa. Black arrow indicates mucoadhesive layer 2h after the administration. B: Detail of mucoadhesive film. Black arrow indicates mucoadhesive layer, white arrow indicates PLGA-PEG loaded nanofibrous reservoir layer. C-I: Adhered film after 2 h of contact incubation with porcine sublingual mucosa as observed by Cryo-SEM. C: A cube-like sample of sublingual tissue with a nanofibrous mucoadhesive film in a cryo-SEM chamber at -130°C; D: tight adhesion of a nanofibrous reservoir layer to sublingual mucosa; E: A detailed picture of tight adhesion; F & G; Illustrative pictures with clearly visible mucoadhesive layer (upper) and SF nanofibrous reservoir layer (lower) detached from the mucosal surface during the sample preparation; H: detailed picture of SF nanofibrous reservoir layer adhered to the mucosal surface (nanofibres marked by black arrows). The mesh of mucin fibres is visible in the bottom part. PLGA-PEG (poly(lactic-co-glycolic acid)-polyethylene glycol) nanoparticles are found adsorbed on the surface of nanofibres as well as permeating the mesh of mucin fibres (white arrows in the detailed inset); I: A general picture of SF nanofibrous mucoadhesive film and adjacent mucosa after 2 h incubation. A residue of mucoadhesive gel layer is seen above the nanofibrous layer. The gap between the nanofibrous reservoir layer and the mucosa is an artefact generated during sample preparation. A mucin mesh is clearly distinguished on the surface of the mucosa in the middle part of the image. At the bottom of the image, particular epithelial cells are visible. 1) Residue of removed backing and mucoadhesive layers; 2) nanofibre reservoir layer; 3) layer of mucin; 4) surface layer of mucosal epithelium tissue.

The extent of nanoparticle release was observed to be nanofibre dependent. Essentially quantitative release of nanoparticles was observed with both SF and chitosan-PEO nanofibers after 30 mins. On the other hand, when standard PCL nanofibers were used, then significantly lower levels of nanoparticle release were observed (approx. 50%). Thereafter, when PCL nanofibers were pre-treated with 3M sodium hydroxide solution or with 2% (w/v) sodium deoxycholate, then the levels of PLGA-PEG nanoparticle release were also near 100%. These data are in a good accordance with the reduction of a contact angle value caused by both pre-treatment procedures used (Table 1). The increase in hydrophilicity of the nanofiber surface (decrease of contact angle) results in weakening of hydrophobic interaction between relatively hydrophobic nanoparticles like PLGA-based nanoparticles. Therefore, such particles are deadhered more easily from the nanofiber surface and are released into the inter-fibre space and diffuse towards the mucosa. The almost complete release of PLGA-PEG nanoparticles from SF nanofibers *in-vitro* was confirmed by observation of nanoparticle-loaded nanofibers before and after the dissolution test using SEM (Fig. 5C, D). In general, nanofibres with hydrophilic surfaces (chitosan-PEO, SF and PCL treated with NaOH) were all competent to release almost all adsorbed nanoparticles into the surrounding medium. By contrast, non-treated PCL nanofibers with rather more hydrophobic surface properties were not able to affect the quantitative release of PLGA-PEG nanoparticles or liposomes within the given incubation time (see Fig. 5A, B).

However, the conditions occurring during an *in vitro* release test differ significantly from those occurring after the application of the nanofibrous film onto the mucosal surface *in vivo*. Therefore, the established cryo-altered mucosa test is used as an ideal model giving much less false negative results with regard to the assessment of the potential of mucosal delivery system to release the nanoparticles directly onto the site of application. Cryo-altered mucosa has limited barrier functions while maintaining its general physical properties and anatomical structure [31]. This model was used to confirm the data from *in vitro* release experiments and for testing the release of PLGA-PEG nanoparticles from electrospun nanofibrous reservoir (SF) adhered on cryo-altered mucosa *ex vivo*. The *ex-vivo* release test using cryo-

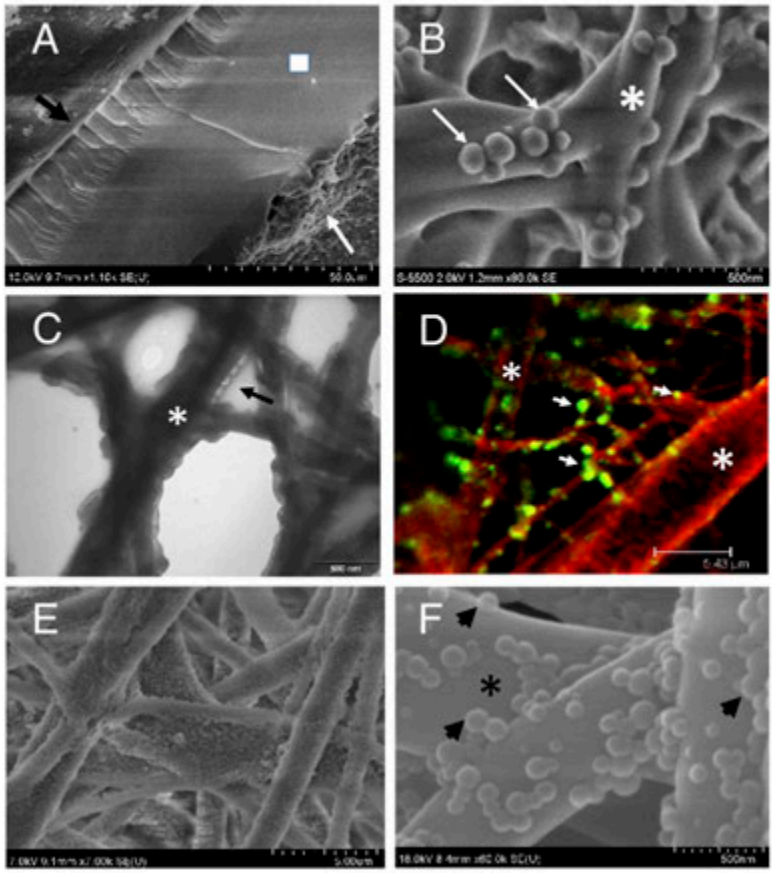

Fig. 4. Liposomes and PLGA-PEG nanoparticles adsorbed to nanofibrous reservoir layer observed by cryo-SEM, SEM, TEM and Confocal Laser Scanning Microscopy A: Cross-section of an SF nanofibrous mucoadhesive film with liposome-loaded reservoir layer (cryo-SEM). Backing layer (black arrow), mucoadhesive layer (white square) and the nanofibrous reservoir layer (white arrow); B: Detail of SF nanofibrous reservoir layer loaded with liposomes (SEM, deceleration mode). Liposomes (white arrow), nanofiber (asterisk). Note the spherical shape of liposomes adsorbed on nanofibres and the fact that their aqueous internal cavities are intact in spite of being in vacuum for 10 min or more; C: Detail of liposomes adsorbed to the PCL nanofibrous reservoir layer (TEM). Liposomes (white arrow) nanofiber (asterisk). Note the appearance of liposomes as hollow spheres demonstrating their preserved vesicular structure. The shell-like structures of liposomes with aqueous interiors are clearly visible; D: GFP-proteoliposomes (green) adsorbed to PCL nanofibrous layer (red) (nanofibres were counterstained with fluorescent lipid lissamine rhodamine-PE). Liposomes (white arrow), nanofiber (asterisk); E: SF nanofibrous reservoir layer with adsorbed PLGA-PEG nanoparticles (SEM); F: Detailed picture of PLGA-PEG nanoparticles adsorbed onto the surface of the SF nanofibrous reservoir layer (SEM). PLGA-PEG nanoparticles (black arrowheads) and nanofiber (black asterisk).

altered porcine oral mucosa testified to the ability of released nanoparticles to reach the mucosal surface and penetrate into deep mucosal tissue (Fig. 5E, F).

The penetration of fluorescently labelled PLGA-PEG nanoparticles into the epithelium of cryo-altered mucosa was investigated. Whereas the fluorescence signal comes predominantly from the upper part of the epithelial tissue in case of PLGA-PEG particles without sodium deoxycholate, incubation of cryo-altered mucosa with sodium deoxycholate makes the fluorescence signal from nanoparticles more uniform within the tissue (see Fig. 5E, F). This observation is in good accordance with the fact that a barrier of extracellular lipids is located in the upper third of epithelium [32]. It is important to note that the mechanism of action of cholate salts lies in solubilisation of the extracellular lipids. So, this type of pharmaceutical excipient acts only if its local concentration is maintained above the critical micellar concentration [33]. This implies that the dosage form should release the nanoparticles as well as excipients in unidirectional manner, it should be in the intimate contact with oral mucosa for a prolonged period of time, and it should prevent dilution of the substances by saliva.

For subsequent *ex vivo* and *in vivo* experiments, our preference was to use SF nanofibrous mucoadhesive films.

4.8. Mucus penetration of nanoparticles and interactions with mucosal tissue – ex vivo and in vivo models

Dramatic anatomical differences are observed in buccal and sublingual mucosa among species. In general, large animals possess a non-keratinized stratified buccal mucosa, which is more similar to the anatomy of the human mucosa. In terms of availability, thickness, and permeation properties, the porcine buccal mucosa appears to be the most appropriate animal model due to the highest similarity to human mucosa [34]. By contrast, rodents possess keratinised mucosa in the sublingual region. In spite of this fact, many studies evaluating biological effects *in vivo*, including sublingual vaccination nanoparticle formulations, are performed on more accessible small animal models (mice, rat) having poorly permeable, keratinised oral mucosa [35]. In our studies we used both pig and mouse models with our nanofibrous mucoadhesive films applied to buccal and sublingual mucosa. In our case, nanofibrous mucoadhesive films were also designed to have properties appropriate for application to the oral region of mice, piglets, and even man.

Due to availability and simplicity, the evaluation of the effectiveness of transmucosal delivery of nanoparticles is often tested on *ex-vivo* tissues. As discussed above, crucial consideration for the permeation test

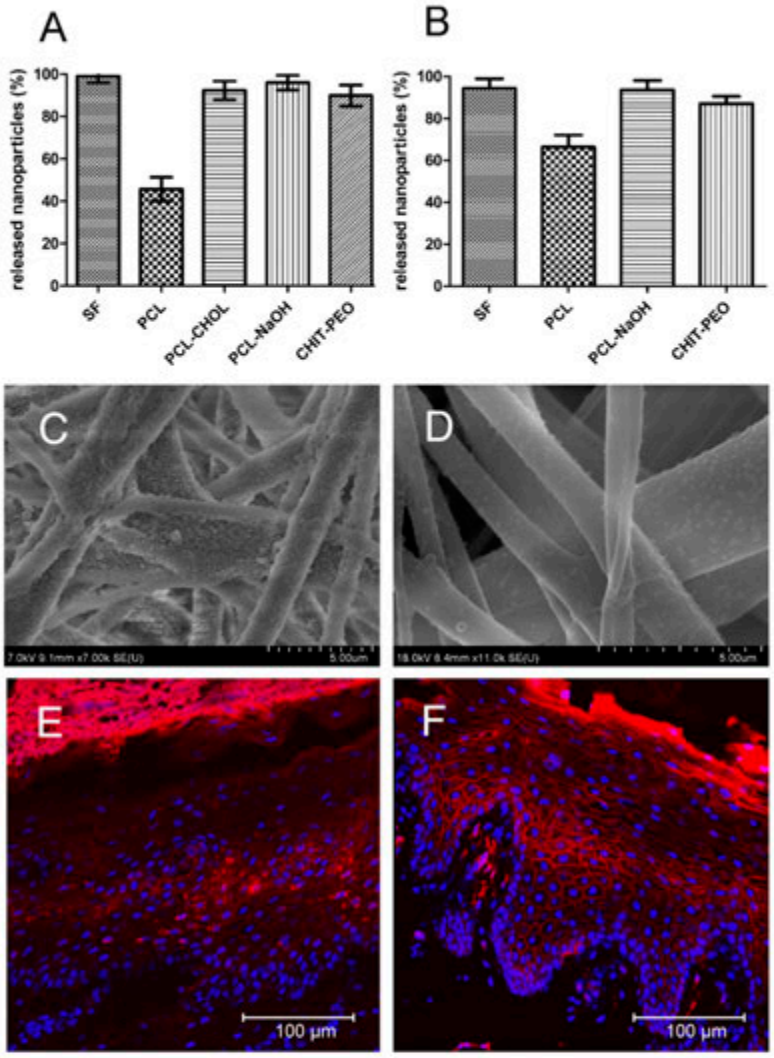

Fig. 5. Determination of the quantity of released nanoparticles from reservoir nanofibrous layer *in-vitro*/*ex-vivo* A: Extent of liposome release from different types of nanofibrous reservoir layer determined by means of the modified dissolution test; B: Extent of PLGA-PEG nanoparticle release from different types of nanofibrous reservoir layer by modified dissolution test; C: Representative picture of PLGA-PEG loaded onto an SF nanofibrous reservoir layer as observed by SEM before the dissolution test; D: Representative image of SF nanofibrous layer after the dissolution test; E: Cross-section of cryo-altered porcine sublingual mucosa with PLGA-PEG nanoparticles (red) penetrated into mucosal tissue after 2 h incubation with a nanofibrous mucoadhesive film; F: Cross-section of cryo-altered sublingual mucosa penetrated with PLGA-PEG nanoparticles (red) with 2% sodium deoxycholate after 2 h exposition.

must be adequate tissue storage and isolation before the experiment [31]. Freshly excised mucosal tissues were used for all *ex-vivo* penetration tests. The penetration tests were started approximately 30 min after excision and were conducted under physiological conditions in terms of temperature and with continuous moistening of the surface as described in the section Materials and Methods.

4.9. Ex-vivo study of penetration of nanoparticles to porcine oral mucosa

Ex-vivo penetration of nanoparticles to oral mucosa was tested on freshly excised porcine sublingual and buccal tissues (**see the schema in Supporting information, section E**). A given nanofibrous mucoadhesive film with pre-loaded nanoparticles was applied to excised mucosa and incubated for 2 h at 37°C. During the whole experiment, the surface of the mucosa was moistened with PBS buffer to simulate conditions in the oral mucosa. For control purposes, free nanoparticles were applied to excised mucosa. The difference between both routes of application was clearly distinguishable by means of the intensity of pink colouration at the site of application. Whereas nanofibrous mucoadhesive films maintained their fluorescent nanoparticles in the middle of a mucoadhesive ring during the incubation period, free nanoparticles were wash out from mucosal surface after a short time of the test and did not penetrate into mucosa at all (**Supporting information, section E**).

The penetration of nanoparticles into oral mucosa was confirmed by cross-sectioning of adjacent mucosa and observation with confocal microscopy (see Fig. 6). Freshly excised sublingual and buccal oral mucosa with model PLGA-PEG nanoparticles and DSPE-PEG (distearoyl phosphatidylethanolamine-polyethylene glycol) liposomes were tested. The penetration to the epithelium of the oral mucosa was observed in all tested samples. The intensity of fluorescence reflects the concentration gradient of nanoparticles diffusing deeper into submucosal

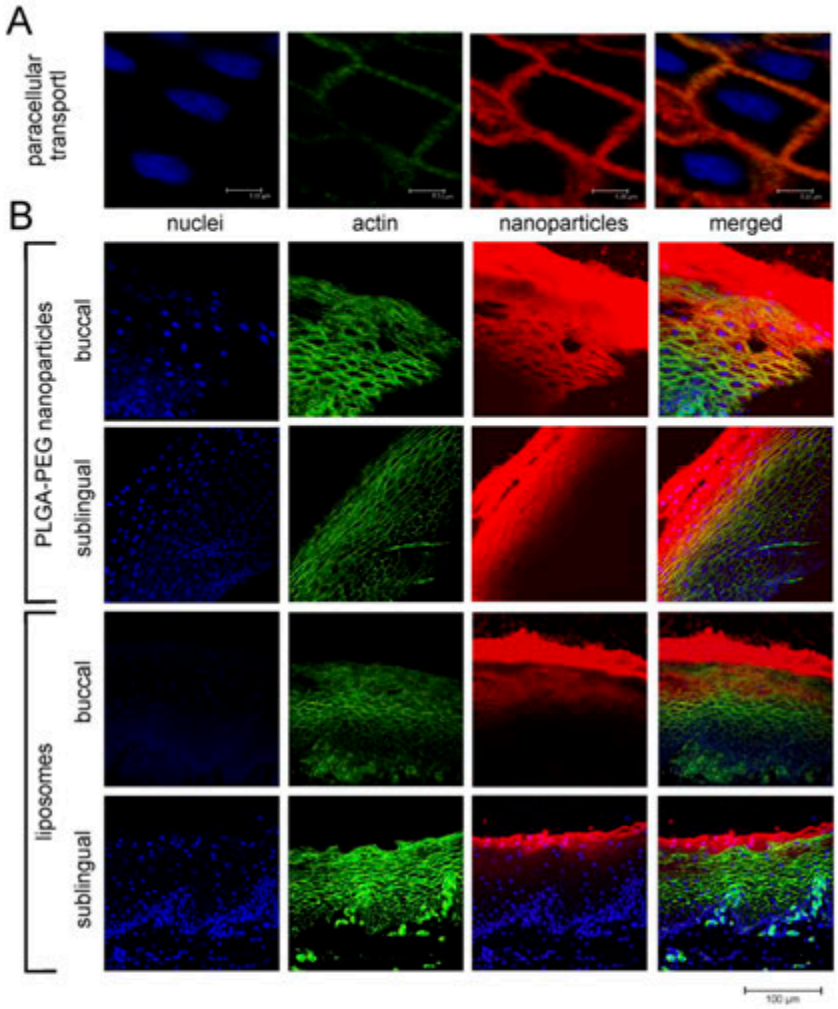

Fig. 6. Oral mucosa after 2 h *ex-vivo* incubation at 37°C with nanofibrous mucoadhesive films containing rhodamine labelled nanoparticles; A: Images demonstrating the paracellular pathway of nanoparticle penetration through porcine sublingual epithelium (PLGA-PEG nanoparticles were used throughout); B. Penetration of PLGA-PEG nanoparticles and liposomes into porcine oral mucosa tissue after release from nanofibrous mucoadhesive films.

tissue. The transport of model nanoparticles in epithelium undergoes the paracellular pathway as clearly demonstrated by confocal microscopy in tissue slices. Fig. 6A shows the paracellular transport of nanoparticles in detail.

However, cleaning of mucosal surface by continuous production of saliva, presence of viscous mucus layer and the existence of epithelial barriers are main factors limiting the extrapolating of the results from *in vitro* dissolution test and *ex-vivo* tests to real in vivo conditions. Therefore, *in vivo* study of penetration of nanoparticles into adjacent mucosa was carried out using mouse and pig models.

4.10. In-vivo study of penetration of nanoparticles into adjacent mucosa in mouse model

In the case of the mouse model, administration of nanoparticles by means of a given nanofibrous mucoadhesive film resulted only rarely in specific cell-associated delivery even if a high concentration of nanoparticles was maintained on the surface of sublingual mucosa for a 2 h period without washing out by saliva (Fig. 7B, C). This is in good agreement with the fact that rodent sublingual mucosa is highly keratinised and thus the permeability for nanoparticles is low. The presence of high concentration of specific immune cells (determined as MHC II positive cells) in this area is clearly visible in Fig. 7A. Accordingly, the porcine model is more appropriate for sublingual delivery experiments given the lower levels of keratinisation and the greater anatomical similarity of porcine sublingual to the human equivalent mucosa [34]. Cells responsible for the transport of nanoparticles and antigens across mouse sublingual mucosa, have been defined by Nagai and coworkers [36].

4.11. Mucosal and transmucosal transport of nanoparticles to regional lymph nodes in piglets

Owing to strong keratinisation of sublingual mucosa in mice, the pig model is more appropriate for sublingual delivery experiments because of similarity with the anatomy of human sublingual mucosa [34]. We believe that the described system is especially suitable for sublingual immunotherapy and vaccine applications. Thus, finally, the piglet model was used to evaluate the delivery of PLGA-PEG nanoparticles into lymph nodes. Sodium deoxycholate was tested in this experiment

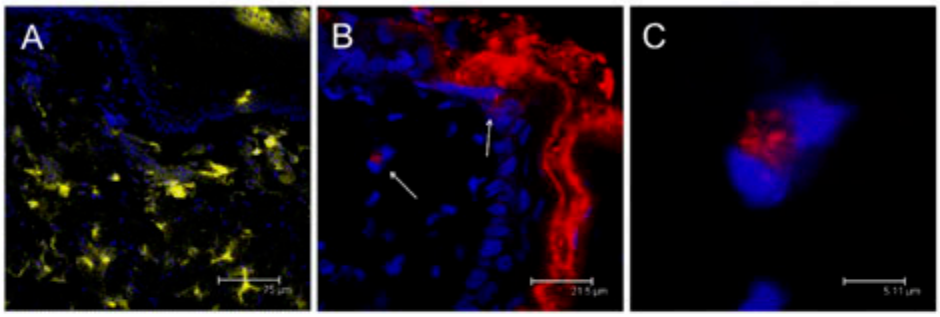

Fig. 7. *In-vivo* delivery of PLGA-PEG nanoparticles to mouse sublingual mucosa; A: MHC II positive cells (yellow-green stained cells) in sublingual region of mice. Note a dense population of sublingual mucosa by APC (bar 75μm); B: The deposit of nanoparticles (red) on the surface of sublingual mucosa after 2 h. The arrows indicate nanoparticles internalised in specialised APC cells. No free diffusion of nanoparticles across the keratinised sublingual mucosa in mice was observed (bar 21.5μm); C: Detail of internalised nanoparticles (bar 5.11μm).

as a penetration enhancer. Endocytosis of fluorescent NPs by antigen presenting cells (APC) was demonstrated by histochemical staining of tissue sections and their observation by confocal microscopy.

Cross-sectioned slices from histological samples excised 2 h after the application of nanoparticles demonstrated penetration of nanoparticles into mucosa (Fig. 8A) as well as into regional lymph nodes (Fig. 8B, C). Some portion was recognised and endocytosed by Swine Leucocyte Antigens (SLA) type II positive cells (porcine antigen presenting cells, pAPC) and detected in draining regional lymph nodes (Fig. 8D, E). Also pAPC cells with fluorescent nanoparticles were found in both B and T-cell area in lymph nodes (Fig. 8D, E). This observation is well confirmed by a detail picture of pAPC with endocytosed fluorescent nanoparticles (Fig. 8F). The interaction of human DCs with PLGA-PEG or liposome nanopaticles was studied *in vitro* to demonstrate their ability to endocytose them and to see their subcellular distribution. Accumulation of fluorescent nanoparticles in the cytoplasm of human DCs was found to be similar to that in porcine DCs (**see Supporting information, section F**).

In general, successful delivery by the oromucosal route of administration is opposed by mucus and mucosal secretions (diffusion barrier) [37]. The mucosal epithelium also represents another main barrier for transport of nanoparticles and macromolecules into the submucosa (absorption barrier) [2,37]. Several strategies were introduced for prolonged or enhanced oromucosal delivery of pharmaceutical substances: mucoadhesive formulations, mucus penetrating particle formulations, fast dissolving films and co-application of penetration enhancers.

Thus far, PLGA-PEG nanoparticles are the most frequently used polymer nanoparticle options used for transmucosal delivery. The density of PEG coating is crucial for its mucus penetrating properties [38]. Nevertheless, MMPs have been widely used for mucosal delivery of a broad range of macromolecules, for example peptides, proteins, and nucleic acids [26]. The presence of PEG also appears to enhance the lymph node delivery of nanoparticles [23]. Such nanoparticles appear useful as vaccination nanoparticles since they can promote the transport of an encapsulated molecular adjuvant and antigen to the draining

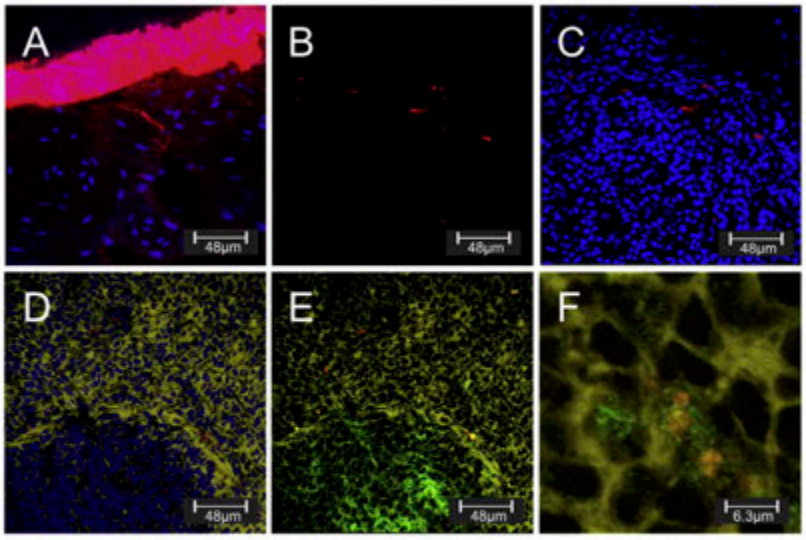

Fig. 8. Lymph node delivery of PLGA-PEG nanoparticle applied onto sublingual mucosa via nanofibrous mucoadhesive films; A: Cross-section of porcine sublingual mucosa after 2 h incubation *in-vivo*. PLGA-PEG loaded nanofibrous mucoadhesive film (red layer), PLGA-PEG nanoparticles (red dots) penetrating through sublingual tissue, nuclei of epithelial cell (blue); B: Regional lymph node. PLGA-PEG nanoparticles (red) on the cross-section of a regional lymph node (cortex); C: PLGA-PEG nanoparticles (red) on the cross-section of a regional lymph node (cortex), cell nuclei were counterstained by Sytox Blue; D: Regional lymph node. PLGA-PEG particles (red) in the cortex (T-cell area) of a regional lymph node. In the bottom part of the picture, a primary lymph nodule (folliculi lymphatici corticales) is clearly distinguished. Yellow-actin, blue-nuclei; E: Regional lymph node. PLGA-PEG particles (red) in the cortex of a regional lymph node. A high number of SLA II-positive B-cells is typical of a primary lymph nodule. pAPC in cortex containing fluorescent nanoparticles (red); F: Detailed picture of pAPC (green) transporting endocytosed fluorescent PLGA-PEG nanoparticles (red) into T-cell region in a lymph node. pAPC was stained by monoclonal antibody against SLA. Stromal cells (yellow-green) in the cortex are stained by antibodies against actin.

lymph nodes. Nanoparticle-mediated accumulation of molecular adjuvants to lymph nodes should enable a significant decrease in dose of molecular adjuvants. This approach has been reported with a number of toll-like receptor (TLR) agonists, including monophosphoryl lipid A (MPLA), CpG DNA, poly (I:C), and small-molecule TLR7/8 compounds [39]. However, while PEGylation may promote tissue penetration of nanoparticles, functional delivery of molecular adjuvants and antigens to APCs can be impaired suggesting the need for nanoparticle triggerability [40] and/or targetability. In general, ideal nanoparticle for mucosal delivery of vaccines/immunotherapeutics may comprise a paradigm known as ABCD nanoparticle structure as described by A.D. Miller: antigen/immunomodulator/API payload of nanoparticle (A-component) surrounded by associated lipidic/polymeric material (B-component) forming the AB-core. The AB-core requires shielding coatings protecting from interactions of nanoparticle with mucus (C-component) and, finally, targeting layer (D-components—specific ligands e.g. mannan, anti-DEC 205, TLR agonists, etc.) might be added to target/activate specific immune dendritic cells [41].

The above mentioned paradigm is perfectly suited for liposomes, the first nanoparticles which received FDA (Food and Drug Administration) approval for human application and have appeared as marketed products, also represent versatile biocompatible systems composed of biological lipids. Besides albumin-based nanoparticles and monoclonal antibodies (also included in nanoparticles), liposomes remain only drug nanocarriers approved by FDA for human applications. Factors such as the size, the surface charge, and surface modification, lamellarity, presence of targeting moieties etc. influence particles biodistribution and their fate in an organism. Liposomes are unique concerning to their ability to co-encapsulate drugs and antigens of various physical-chemical properties (e.g., molecular weight, hydrophobicity, charge and shape) in one self-assembly system. The inclusion of a PEG layer in the liposome surface also ensures mucus-penetrating properties [26]. Effective delivery of nanoparticles across the epithelium is a great challenge, too, and in fact the transfer of nanoparticles across the epithelium requires paracellular pathways involving the penetration through extracellular matrix. This process limits the velocity of diffusion across the epithelium. A frequent strategy to overcome the epithelium barrier is co-administration of nanoparticles with absorption enhancers [33,42]. Cholate salts are examples of the most commonly used enhancers [43]. Accordingly, we tested the mucosal penetration of PLGA-PEG nanoparticles after loading into our nanofibrous mucoadhesive films containing a mixture of 2% deoxycholate sodium. Subsequent data demonstrated unidirectional penetration of nanoparticles into porcine submucosa *in vivo* and their internalisation into immune cells (see Figs. 6, 7, 8).

Nanofibrous mucoadhesive films seem to be an ideal dosage form for nanoparticle-based vaccine delivery systems. As reviewed by Dukhin and Labib, the pathway of antigens and nanoparticles to a lymph node can be divided into particular steps. The transport across mucus layer (1), across epithelium and its barriers (2), transport through the interstitial fluids of submucosa (3), and transport through lymphatic capillaries to a lymph node (4). As the first three steps are driven by passive diffusion, the transport through lymphatic ways is driven by convective diffusion. This explains why nanoparticles were observed in the lymph nodes after only a few hours post mucosal administration [32]. With respect to vaccines, the endocytosis of nanoparticles by APCs and their active translocation to draining lymph nodes also represents another important mechanism involved in the penetration of nanoparticles through mucosal tissue. Accordingly, this high adsorption loading capacity ensures high concentration of nanoparticles to be reached after the rapid release from reservoir layer to the limited volume of the fluids at the application site. This concentration gradient then exerts a "pressure" on the mucosal layer so rapidly enabling the formation of a nanoparticle diffusion potential across the mucosal surface into the submucosa (Figs. 1, 8A, **supporting information, section E**).

Dendritic cells present in the submucosa are then free to capture nanoparticles for delivery to the local lymphatic nodes that drain the submucosal zone of application [44]. Nanoparticles not captured by DCs, are otherwise free to diffuse through the submucosa reaching lymphatic capillaries by means of which they drift to the local lymph nodes for capture by professional APCs [32].

The surface adhesive properties of the nanofibres in our nanofibrous reservoir layers can be modified by virtue of the very materials used to prepare nanofibrous reservoir layers or by down-stream treatment [20,21] (Fig. 5). Such variations of surface properties, either inherent or chemically induced, ensure that the nanoparticle binding and release characteristics of nanofibrous reservoir layers can in principle be tailor-made or adapted according to the requirements of the corresponding nanoparticle delivery system being used for high concentration binding and chemical potential driven release into the submucosa.

Taking the nanofibrous mucoadhesive film as a whole, if a nanofibrous reservoir layer is central to nanoparticle binding and release, then the properties of the other components should also be optimal. Thus the swelling properties of the neighbouring mucoadhesive film layer should have no direct effect on the binding and release of nanoparticles directed to the mucosal surface. In contrast to our own observations, others have reported that nanoparticles can be incorporated into mucoadhesive film layer and experience a delay in release through the mucosa caused by gradual swelling of the mucoadhesive film and diffusion-limitations [18]. Otherwise, the mucoadhesive film layer needs to be prepared to resist movements of the tongue and the extensive production of saliva by sublingual glands. Furthermore, motional stress is more pronounced in the sublingual region as compared to the buccal mucosal region. Thus, nanofibrous mucoadhesive films need to be particularly flexible and thin with sufficient mucoadhesive properties to maintain adherence. The protective backing layer can be modified in the mean of solubility according to specific demands without any influence on the release rate of nanoparticles, too. The shape, composition, surface area and thickness of mucoadhesive layers all need to be optimized to achieve the desired mucoadhesive properties and time span of adhesion. As demonstrated in our study, mechanical and physical-chemical properties of nanofibrous materials predetermine their application for development and production of mucosal drug delivery systems. Especially, nanoparticle drug delivery systems and vaccines are applications of great potential with respect to non-invasive mucosal applications. Such systems can be superior to gel materials with respect to compatibility with a broad range of material intended for incorporation, technology of production and storage conditions.

5. Conclusion

Overcoming the barriers to successful carriage of drug-delivery and vaccination nanoparticles into submucosal tissues and draining lymphatic nodes is a prerequisite for many new drug and vaccination opportunities. Here we demonstrate on an *ex vivo* and *in vivo* pig model how electrospun nanofibrous mucoadhesive films can serve as protective nanoparticle reservoirs for the controlled and sustained delivery of nanoparticles into submucosal tissue and draining lymphatic node sites.

Furthermore, our electrospun nanofibrous mucoadhesive films can in principle be variously prepared from different polymeric materials and surface functionalised for use with many different types of nanoparticles. Liposomes, viruses and virus-like particles, polymeric and lipid-based nanoparticles, biopolymers (e.g. protein and peptide antigens, plasmid DNA, polysaccharides), molecular adjuvants and pharmaceutical excipients (e.g. enhancers of penetration, mucolytics and cryoprotectants) can be combined with nanofibrous materials to develop appropriate product for non-invasive mucosal application.

Owing to the potential versatility of our presented systems, we anticipate future applications in the development of non-invasive

sublingual vaccines and immunotherapeutics as well as in enabling the use of therapeutic drug-delivery nanoparticles in the oromucosal environment. The development of industrial-scale production of our nanofibrous mucoadhesive films is now in progress. We propose to describe this technology going forward as "printed vaccines technology" and testing of this system with some vaccine formulations like influenza and papilloma virus are being in progress.

Acknowledgements

This work was supported by the following grants: the Czech Science Foundation GAP503/12/G147 (JT), the Ministry of Education, Youth and Sports CZ.1.07/2.3.00/20.0164 (JT, MR); DL would like to thank to the Ministry of Education, Youth and Sports in the framework of National Program for Sustainability I, the OPR and DI project LO1201, Centre for Nanomaterials, Advanced Technologies and Innovation (CZ.1.05/2.1.00/01.0005); the Ministry of Health CZ AZV-ČR 15-32198A (MR and JT); the project MZE0002716202 RO0516 of the Czech Ministry of Agriculture (JT). Special thanks to the project AdmireVet (CZ.1.05/2.1.00/01.0006 - ED0006/01/01 from the Czech Ministry of Education) for permit the access to the scanning electron microscope. The team headed by Jaroslav Turánek, Andrew D. Miller, and Milan Raška is obligated to the Ministry of Education, Youth and Sports for supporting the project "FIT" (Pharmacology, Immunotherapy, nanoToxicology).

Appendix A. Appendix A Supplementary data

Supplementary data to this article can be found online at http://dx.doi.org/10.1016/j.jconrel.2016.07.036.

References

[1] E. Cario, Nanotechnology-Based Drug Delivery in Mucosal Immune Diseases: Hype or Hope? Mucosal Immunol. 5 (2012) 2–3.
[2] N.V.S. Madhav, A.K. Shakya, P. Shakya, K. Singh, Orotransmucosal Drug Delivery Systems: A Review, J. Control. Release 140 (2009) 2–11.
[3] A.H. Hovav, Dendritic Cells of the Oral Mucosa, Mucosal Immunol. 7 (2014) 27–37.
[4] L.B. Lawson, E.B. Norton, J.D. Clements, Defending the Mucosa: Adjuvant and Carrier Formulations for Mucosal Immunity, Curr. Opin. Immunol. 23 (2011) 414–420.
[5] H. Kraan, H. Vrieling, C. Czerkinsky, W. Jiskoot, G. Kersten, J.P. Amorij, Buccal and Sublingual Vaccine Delivery, J. Control. Release 190 (2014) 580–592.
[6] R.J. Mrsny, Lessons from Nature: "Pathogen-Mimetic" Systems for Mucosal Nano-Medicines, Adv. Drug Deliv. Rev. 61 (2009) 172–192.
[7] B.C. Tang, M. Dawson, S.K. Lai, Y.Y. Wang, J.S. Suk, M. Yang, P. Zeitlin, M.P. Boyle, J. Fu, J. Hanes, Biodegradable Polymer Nanoparticles That Rapidly Penetrate the Human Mucus Barrier, PNAS 106 (2009) 19268–19273.
[8] V.F. Patel, F. Liu, M.B. Brown, Advances in Oral Transmucosal Drug Delivery, J. Control. Release 153 (2011) 106–116.
[9] M. de la Fuente, N. Csaba, M. García-Fuentes, M.J. Alonso, Nanoparticles as Protein and Gene Carriers to Mucosal Surfaces, Nanomed. (Lond. U. K.) 3 (2008) 845–857.
[10] W. Shan, X. Zhu, M. Liu, L. Li, J. Zhong, W. Sun, Z. Zhang, Y. Huang, Overcoming the Diffusion Barrier of Mucus and Absorption Barrier of Epithelium by Self-Assembled Nanoparticles for Oral Delivery of Insulin, ACS Nano 9 (2015) 2345–2356.
[11] N. Bhardwaj, S.C. Kundu, Electrospinning: A Fascinating Fiber Fabrication Technique, Biotechnol. Adv. 28 (2010) 325–347.
[12] X. Lu, C. Wang, Y. Wei, One-Dimensional Composite Nanomaterials: Synthesis by Electrospinning and Their Applications, Small 5 (2009) 2349–2370.
[13] Nanofibers - Production, Properties and Functional Applications; Lin, T., Ed.; In Tech, 2011.
[14] L. Malinová, M. Stolínová, D. Lubasová, L. Martinová, J. Brožek, Electrospinning of Polyesteramides Based on ε-Caprolactam and ε-Caprolactone from Solution, Eur. Polym. J. 49 (2013) 3135–3143.
[15] J.O. Morales, J.T. McConville, Manufacture and Characterization of Mucoadhesive Buccal Films, Eur. J. Pharm. Biopharm. 77 (2011) 187–199.
[16] C. Remuñán-López, A. Portero, J.L. Vila-Jato, M.J. Alonso, Design and Evaluation of Chitosan/ethylcellulose Mucoadhesive Bilayered Devices for Buccal Drug Delivery, J. Control. Release 55 (1998) 143–152.
[17] Z. Cui, R.J. Mumper, Bilayer Films for Mucosal (genetic) Immunization via the Buccal Route in Rabbits, Pharm. Res. 19 (2002) 947–953.
[18] H. Chunbai, C. Fuying, Y. Lichen, Q. Feng, T. Cui, Y. Chunhua, A Polymeric Composite Carrier for Oral Delivery of Peptide Drugs: Bilaminated Hydrogel Film Loaded with Nanoparticles, Eur. Polym. J. 45 (2009) 368–376.
[19] F. Cilurzo, P. Minghetti, F. Selmin, A. Casiraghi, L. Montanari, Polymethacrylate Salts as New Low-Swellable Mucoadhesive Materials, J. Control. Release 88 (2003) 43–53.
[20] H.S. Yoo, T.G. Kim, T.G. Park, Surface-Functionalized Electrospun Nanofibers for Tissue Engineering and Drug Delivery, Adv. Drug Deliv. Rev. 61 (2009) 1033–1042.
[21] S.M. Jung, G.H. Yoon, H.C. Lee, H.S. Shin, Chitosan nanoparticle/PCL Nanofiber Composite for Wound Dressing and Drug Delivery, J. Biomater. Sci. Polym. Ed. 26 (2015) 252–263.
[22] S.K. Lai, J. Suk, A. Pace, Y.Y. Wang, M. Yang, O. Mert, J. Chen, J. Kim, J. Hanes, J. Drug carrier nanoparticles that penetrate human chronic rhinosinusitis mucus, Biomaterials 32 (2011) 6285–6290.
[23] Y.Y. Wang, S.K. Lai, J.S. Suk, A. Pace, R. Cone, J. Hanes, Addressing the PEG Mucoadhesivity Paradox to Engineer Nanoparticles That "Slip" through the Human Mucus Barrier, Angew. Chem. Int. Ed. Eng. 47 (2008) 9726–9729.
[24] A. Vila, H. Gill, O. McCallion, M.J. Alonso, Transport of PLA-PEG Particles across the Nasal Mucosa: Effect of Particle Size and PEG Coating Density, J. Control. Release 98 (2004) 231–244.
[25] L.M. Ensign, C. Schneider, J.S. Suk, R. Cone, J. Hanes, Mucus Penetrating Nanoparticles: Biophysical Tool and Method of Drug and Gene Delivery, Adv. Mater. 24 (2012) 3887–3894.
[26] S.K. Lai, Y.Y. Wang, J. Hanes, Mucus-Penetrating Nanoparticles for Drug and Gene Delivery to Mucosal Tissues, Adv. Drug Deliv. Rev. 61 (2009) 158–171.
[27] J. Mašek, E. Bartheldyová, P. Turánek-Knotigová, M. Skrabalová, Z. Korvasová, J. Plocková, S. Koudelka, P. Skodová, P. Kulich, M. Křupka, et al., Metallochelating Liposomes with Associated Lipophilised norAbuMDP as Biocompatible Platform for Construction of Vaccines with Recombinant His-Tagged Antigens: Preparation, Structural Study and Immune Response towards rHsp90, J. Control. Release 151 (2011) 193–201.
[28] M. Křupka, J. Mašek, E. Bartheldyová, P. Turánek Knötigová, J. Plocková, Z. Korvasová, M. Škrabalová, Š. Koudelka, P. Kulich, K. Zachová, et al., Enhancement of Immune Response towards Non-Lipidized Borrelia Burgdorferi Recombinant OspC Antigen by Binding onto the Surface of Metallochelating Nanoliposomes with Entrapped Lipophilic Derivatives of norAbuMDP, J. Control. Release 160 (2012) 374–381.
[29] P.T. Knotigová, D. Zyka, J. Mašek, A. Kovalová, M. Křupka, E. Bartheldyová, P. Kulich, Š. Koudelka, R. Lukáč, Z. Kauerová, et al., Molecular Adjuvants Based on Nonpyrogenic Lipophilic Derivatives of norAbuMDP/GMDP Formulated in Nanoliposomes: Stimulation of Innate and Adaptive Immunity, Pharm. Res. 32 (2015) 1186–1199.
[30] J. Mašek, E. Bartheldyová, Z. Korvasová, M. Skrabalová, S. Koudelka, P. Kulich, I. Kratochvílová, A.D. Miller, M. Ledvina, M. Raška, et al., Immobilization of Histidine-Tagged Proteins on Monodisperse Metallochelation Liposomes: Preparation and Study of Their Structure, Anal. Biochem. 408 (2011) 95–104.
[31] V. Hearnden, V. Sankar, K. Hull, D.V. Juras, M. Greenberg, A.R. Kerr, P.B. Lockhart, L.L. Patton, S. Porter, M.H. Thornhill, New Developments and Opportunities in Oral Mucosal Drug Delivery for Local and Systemic Disease, Adv. Drug Deliv. Rev. 64 (2012) 16–28.
[32] S.S. Dukhin, M.E. Labib, Convective Diffusion of Nanoparticles from the Epithelial Barrier toward Regional Lymph Nodes, Adv. Colloid Interf. Sci. 199-200 (2013) 23–43.
[33] J.A. Nicolazzo, B.L. Reed, B.C. Finnin, Buccal Penetration Enhancers–How Do They Really Work? J. Control. Release 105 (2005) 1–15.
[34] C. Thirion-Delalande, C. Fisch, R. Forster, B. Palate, Comparative Histology of Mouth Mucosae (sublingual Region), Toxicol. Lett. 238 (2015) 271–272.
[35] F. Salari, A.R. Varasteh, F. Vahedi, M. Hashemi, M. Sankian, Down-Regulation of Th2 Immune Responses by Sublingual Administration of Poly (lactic-Co-Glycolic) Acid (PLGA)-Encapsulated Allergen in BALB/c Mice, Int. Immunopharmacol. 29 (2015) 672–678.
[36] Y. Nagai, D. Shiraishi, Y. Tanaka, Y. Nagasawa, S. Ohwada, H. Shimauchi, H. Aso, Y. Endo, S. Sugawara, Transportation of Sublingual Antigens across Sublingual Ductal Epithelial Cells to the Ductal Antigen-Presenting Cells in Mice, Clin. Exp. Allergy 45 (2015) 677–686.
[37] R.A. Cone, Barrier Properties of Mucus, Adv. Drug Deliv. Rev. 61 (2009) 75–85.
[38] Q. Xu, L.M. Ensign, N.J. Boylan, A. Schön, X. Gong, J.C. Yang, N.W. Lamb, S. Cai, T. Yu, E. Freire, et al., Impact of Surface Polyethylene Glycol (PEG) Density on Biodegradable Nanoparticle Transport in Mucus Ex Vivo and Distribution in Vivo, ACS Nano 9 (2015) 9217–9227.
[39] M.C. Hanson, M.P. Crespo, W. Abraham, K.D. Moynihan, G.L. Szeto, S.H. Chen, M.B. Melo, S. Mueller, D.J. Irvine, Nanoparticulate STING Agonists Are Potent Lymph Node–targeted Vaccine Adjuvants, J. Clin. Invest. 125 (2015) 2532–2546.
[40] A.D. Miller, Delivery of RNAi Therapeutics: Work in Progress, Expert Rev. Med. Devices 10 (2013) 781–811.
[41] K. Kostarelos, A.D. Miller, Synthetic, Self-Assembly ABCD Nanoparticles; a Structural Paradigm for Viable Synthetic Non-Viral Vectors, Chem. Soc. Rev. 34 (2005) 970–994.
[42] B.J. Aungst, Absorption Enhancers: Applications and Advances, AAPS J. 14 (2011) 10–18.
[43] S. Şenel, Y. Çapan, M.F. Sargon, G. İkinci, D. Şolpan, O. Güven, H.E. Boddé, A.A. Hincal, Enhancement of transbuccal permeation of morphine sulfate by sodium glycodeoxycholate in vitro, J. Control. Release 45 (1997) 153–162.
[44] C. Hervouet, C. Luci, S. Bekri, T. Juhel, F. Bihl, V.M. Braud, C. Czerkinsky, F. Anjuère, Antigen-Bearing Dendritic Cells from the Sublingual Mucosa Recirculate to Distant Systemic Lymphoid Organs to Prime Mucosal CD8 T Cells, Mucosal Immunol. 7 (2014) 280–291.
[45] U. Kulkarni, R. Mahalingam, I. Pather, X. Li, B. Jasti, Porcine Buccal Mucosa as in Vitro Model: Effect of Biological and Experimental Variables, J. Pharm. Sci. 99 (2010) 1265–1277.

Appendix 8

LUBASOVA, D., Safont, M.M., and McCormack, E. Localized paclitaxel delivery using a novel hyaluronic acid-coated fibrous carrier produced via needle-less electrospinning. Journal of Industrial Textiles 2025;55.

Original Research Article

Journal of Industrial Textiles

Volume 55: 1–27

DOI: 10.1177/15280837251322712
journals.sagepub.com/home/jit
Sage

Localized paclitaxel delivery using a novel hyaluronic acid-coated fibrous carrier produced via needle-less electrospinning

Daniela Lubasova[1], Mireia Mayoral Safont[2,3] and Emmet McCormack[2,3,4,5]

Abstract

Pancreatic cancer remains one of the most challenging malignancies to treat due to its dense stromal microenvironment and resistance to conventional therapies. This study introduces a novel localized drug delivery system design to target residual cancer cells following surgery. Electrospun fibrous carriers were fabricated using needle-less electrospinning from polycaprolactone (PCL), silk fibroin (SF), and their blend. Among these, PCL carriers (average fiber diameter: 141 ± 28 nm) exhibited the highest and most sustained paclitaxel (PTX) release *in vitro*. Coating the PCL carrier with hyaluronic acid (HA) increased the fiber diameter to 535 ± 116 nm and modulated PTX release, shifting from an initial rapid release phase in uncoated carrier to a more gradual and sustained release over 120 hours. PTX-loaded HA-coated electrospun PCL carriers significantly reduced MiaPaCa cell viability, with only 13% viability at 96 hours compared to 22% for

[1]Faculty of Textile Engineering, Technical University of Liberec, Liberec, Czech Republic
[2]Precision Oncology Research Group, University of Bergen, Norway
[3]Department of Clinical Science, University of Bergen, Norway
[4]Department of Hematology, Haukeland University Hospital, Begen, Norway
[5]Centre for Pharmacy, Department of Clinical Science, University of Bergen, Bergen, Norway

Corresponding author:
Daniela Lubasova, Faculty of Textile Engineering, Technical University of Liberec, Studentska 1402, Liberec 461 17, Czech Republic.
Email: daniela.lubasova@tul.cz

the non-coated carrier. This HA-coated electrospun PCL carrier offers a scalable and efficient solution for localized PTX delivery, providing sustained drug release, prolonged cytotoxic efficacy, and reduced off-target effects. Its industrial scaleability, combined with its potential for post-surgical pancreatic cancer management, presents an innovative approach to minimizing reliance on systemic chemotherapy and its associated toxicities. The use of needle-less Nanospider™ electrospinning technology further emphasizes its clinical potential, with future *in vivo* studies needed to confirm carrier's safety, pharmacokinetics, and therapeutic benefits.

Keywords
Electrospun fibrous carrier, polycaprolactone, hyaluronic acid, paclitaxel, cancer therapy, pancreatic cancer

Introduction

Pancreatic cancer remains one of the most lethal malignancies, characterized by poor prognosis and limited treatment options. The 5-year survival rate for patients diagnosed with distant metastases is alarmingly low, ranging from 3% to 10%, depending on the stage at diagnosis.[1] Current treatment modalities include surgery, chemotherapy, radiation therapy, and palliative care. Surgical resection remains the gold standard for localized disease.[2] For patients with locally advanced or metastatic disease, chemotherapy is the cornerstone of treatment. Common regimens, such as gemcitabine with paclitaxel (PTX) and FOLFIRINOX, have shown some success in extending survival.[3] However, chemotherapy presents significant drawbacks, including systemic side effects, technical limitations, and cancer recurrence due to incomplete tumor removal during treatment.[4]

Drug delivery systems have the potential to lower these limitations during pancreatic cancer treatment. They offer a significant advantage by releasing drugs efficiently at the target site, reducing systemic side effects and lowering the likelihood of tumor recurrence.[5] Drug delivery systems can be classified as either systemic (e.g., nanoparticles) or localized (e.g., nanofibers, films, hydrogels) based on their application.[6] Systemic drug delivery, such as nanoparticles, are beneficial due to their small size, specificity, and non-invasive nature. These features allow nanoparticles to travel through smaller vessels and target specific receptors without invasive procedures.[7,8] However, nanoparticles may lose specificity or face functionalization challenges due to the complexities of the delivery mechanism.[9] For example, hyaluronic acid (HA) nanoparticles have gained attention for targeting cancer cells, particularly those expressing the CD44 receptor, a common marker in pancreatic cancer. This receptor-targeting improves the delivery of chemotherapeutic agents like PTX, increasing therapeutic efficacy while reducing toxicity.[10] HA's biocompatibility reduces immune responses, enhancing its potential as a drug delivery system.[11] Additionally, HA can modify the tumor microenvironment, potentially

improving drug penetration in dense tumors.[12] However, challenges such as rapid degradation in biological environments may limit sustained drug release.[13] Developing stable and effective HA nanoparticles remains complex and requires further optimization.[14]

Localized drug delivery systems offer an alternative by releasing drugs directly at the target site through diffusion or degradation.[15] Examples include foams, hydrogels, and nanofibers.[16–18] While hydrogels and foams rely primarily on rapid diffusion, which limits sustained therapy, electrospun fibrous materials have shown superior potential for controlled, long-term drug release.[19] Additionally, localized systems can complement surgical tumor removal, reducing recurrence risk.[20] Electrospun fibrous materials have gained attention due to their high surface area, porosity, and ability to deliver drugs in a controlled and sustained manner. These materials are biocompatible and biodegradable, minimizing immune responses while offering customization in composition and drug release properties.[21] Recent advances have explored electrospun fibrous materials for targeting pancreatic cancer cells. These materials, engineered to deliver antibodies, have demonstrated significant potential in minimizing off-target effects and enhancing treatment efficacy.[22] Nanofibrous carriers loaded with chemotherapeutics, such as irinotecan, have also been investigated for post-surgical adjuvant therapy.[23] Moreover, co-delivery systems that combine microRNA-21 antisense oligonucleotides with gemcitabine have demonstrated synergistic effects in inhibiting cancer metastasis.[24] These studies highlight electrospun fibrous drug delivery systems as a promising strategy for enhancing therapeutic efficacy in pancreatic cancer.

Electrospinning is a widely used technique for producing electrospun fibrous carriers. It involves applying an electric force to draw charged polymer solutions into nanofibers. While needle-based electrospinning allows for precise control of fibers, it has limitations like needle clogging and scalability issues.[25] Needle-less electrospinning technique, such as free-liquid electrospinning, addresses these limitations by offering higher production rates and more uniform fiber diameters.[26] Nanospider™ technology, a needle-less electrospinning method, enables high-quality nanofiber production with minimal solvent use. This makes it suitable for industrial-scale applications.[27,28] The use of polycaprolactone (PCL) and silk fibroin (SF) electrospun fibrous materials in pancreatic cancer treatment is a promising area of research due to their unique properties. These polymers enhance drug delivery even though direct studies targeting pancreatic cancer with PCL or SF nanofibers are limited. Several papers suggest their potential in related biomedical applications, which could be extrapolated to pancreatic cancer treatment.[29] PCL is a biodegradable polymer known for its mechanical properties and biocompatibility, making it suitable for drug delivery systems. Its slow degradation rate enables sustained drug release, which is crucial for aggressive cancers like pancreatic cancer, where prolonged therapeutic exposure enhances efficacy.[30] For instance, study has shown that PCL-based nanofibers could effectively deliver quercetin, an anticancer agent, with a controlled release profile suitable for cancer treatment.[31] In another study, nanofibers incorporating tamoxifen citrate for use in the treatment of breast tumors, highlighted their potential as an alternative for local chronic tamoxifen citrate use for breast cancer treatment.[32] SF, derived from silkworms, has favorable mechanical properties,

biocompatibility, and the ability to form nanofibers that mimic the extracellular matrix, facilitating cell adhesion, proliferation, and differentiation. Study has reported that SF electrospun materials could be engineered with tunable mechanical properties, critical for supporting tumor cells or healthy tissue during treatment. Additionally, the high β-sheet content in SF electrospun materials contributes to their stability and controlled drug release capabilities.[33] The combination of PCL and SF offers a synergistic effect that could enhances their application in pancreatic cancer treatment. For example, PCL/SF hybrid nanofibers have been shown to improve cell viability compared to PCL alone, suggesting enhanced biological performance.[34] Furthermore, PCL/SF core-sheath nanofibers have demonstrated the ability to encapsulate drugs effectively, offering a controlled release profile suitable for cancer therapies.[35]

Building on the recognized potential of electrospun PCL and SF fibrous materials for localized drug delivery systems, this study investigated the PTX release profiles from these carriers, targeting applications in pancreatic cancer treatment. To facilitate potential industrial-scale production, electrospun fibrous carriers were fabricated using needle-less Nanospider™ technology and surface-loaded with PTX, a chemotherapeutic agent renowned for its efficacy against pancreatic cancer. The fibrous carriers—consisting of PCL, HA-coated PCL, SF, and SF/PCL blends—were systematically evaluated to determine their PTX release kinetics and suitability for localized drug delivery. Additionally, *in vitro* cytotoxicity assays were conducted to evaluate the therapeutic potential of HA-coated electrospun PCL fibrous carrier loaded with PTX against pancreatic cancer cell line MiaPaCa. This novel approach integrates electrospun PCL fibrous material with HA to create a localized drug delivery system aimed at targeting residual cancer cells post-surgery. Unlike systemic chemotherapy, which often results in off-target effects, localized delivery through fibrous materials offers controlled and sustained drug release, enhancing therapeutic efficacy. The proposed system serves as a complementary approach to systemic therapies, particularly for localized treatment, with the potential to minimize systemic side effects, optimize drug delivery at the target site, and ultimately improve patient outcomes when used alongside conventional treatments. This research stands out by introducing a distinctive combination of materials—PCL, HA, and PTX—processed via Nanospider™ technology, a method that has not been previously explored for localized pancreatic cancer treatment.

Materials and methods

Materials

PCL (Mw 80,000 g/mol) and HA (sodium salt, Mw ~ 1 MDa) were obtained from Sigma-Aldrich, USA. Acetone, sodium hydroxide (NaOH), and ethanol were sourced from Penta, Czech Republic. Thai silk cocoons of Bombyx mori Linn. silkworms (Nang-Noi Srisakate 1) were collected from Amphoe Mueang Chan, Si Sa Ket Province, Thailand. ECE phosphate reference detergent (FBA free, Union TSL Co., Ltd, Thailand) was used as a soaping agent during the degumming process. The chemicals used for the preparation of SF spinning solutions included calcium chloride (Fluka AG, Switzerland) and 98%

formic acid (Penta, Czech Republic). PTX injection solution (Hospira, 6 mg/mL) was purchased from Pfizer, USA. MiaPaCa pancreatic cancer cells, along with cell culture medium (Dulbecco's Modified Eagle's Medium, DMEM), phosphate-buffered saline (PBS), trypsin, and the tetrasodium salt WST-1 assay reagent, were all supplied by Sigma-Aldrich, USA. All materials and reagents used in this study were of analytical grade.

Preparation of electrospun fibrous carriers

All fibrous layers were electrospun from polymer solutions using the Nanospider™ NS-Lab 1WS500U electrospinning system (Elmarco, Czech Republic). This system combines industrial production capabilities with the precision of a high-end laboratory instrument. The Nanospider™ technology utilizes a spinning electrode, shaped as a thin wire, with a head that applies the polymer solution along the entire length of the wire. When exposed to a strong electric field, fibrous materials are generated from the thin polymer layer deposited on the wire electrode, see Figure 1.

The polymer solutions (listed below) were sequentially transferred into a 500 mL head with a polymer solution connected to the electrospinning apparatus. To achieve the production of defect-free fibrous layers with consistent morphology and high productivity using Nanospider™ technology, it was imperative to optimize both the polymer solution preparation and the electrospinning parameters. The electrospinning parameters were systematically optimized through a series of trials to achieve defect-free electrospunPCL, SF, and SF/PCL fibrous materials with high throughput efficiency. The optimization process involved adjusting key parameters such as voltage, collector distance, environmental conditions, as discussed in our previous study.[36] These refinements ensured consistent and reproducible results, which are crucial for the needle-less electrospinning of fibrous materials. A voltage of 50 kV was applied between the wire and the collector, with the two positioned 100 mm apart. Environmental conditions were maintained at 21°C and 60 ± 2% relative humidity using an AC system to optimize the electrospinning process.

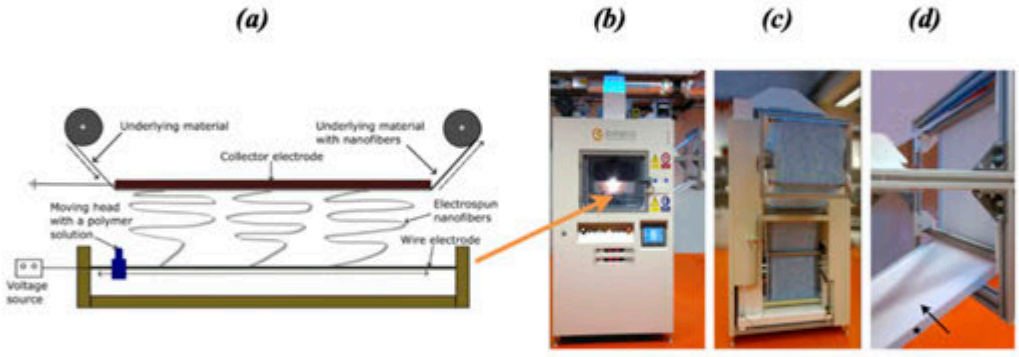

Figure 1. Needle-less electrospinning system and resulting fibrous material. (a) Schematics of the needle-less electrospinning process. The photography of NS-Lab 1WS500U: (b) front view of the electrospinning system. (c) Side view of the electrospinning system, (d) detail of the resulting fibrous material (arrow), deposited onto a spun-bond substrate (asterisk).

The fibrous materials were deposited onto a moving baking paper advancing at 30 mm/min along a negatively charged collector electrode, resulting in a 500 × 600 cm fibrous sheet. After electrospinning, the fibrous material was stabilized, and removed from the baking paper before PTX loading onto the carriers, as detailed in the following sections.

Polycaprolactone fibrous carrier. The solvent mixture composition and PCL solution concentration were thoroughly optimized through numerous trials to achieve defect-free fibrous material. This process involved adjusting the solvent ratios to ensure complete polymer dissolution and fine-tuning the polymer concentration to balance viscosity and needle-less spinnability. These parameters were selected based on our findings to ensure consistent fiber morphology and high production efficiency. Further details on this optimization process can be found in our previous work.[36] The solvent mixture, consisting of acetone and ethanol in a volume ratio of 7:3 (v/v), was used to dissolve solid PCL polymer. The polymer solution was stirred at a rotational speed of 200 RPM at room temperature for 24 hours using a magnetic stirrer, resulting in an optimal polymer concentration of 16 wt%. Electrospinning of the PCL solution was performed under the conditions described above. For comparison, half of the electrospun PCL fibrous sheets were pretreated with 3M NaOH for 5 minutes to enhance the wettability of the fiber surfaces.

Silk fibroin fibrous carrier. The optimization of the degumming process and SF solution parameters was achieved through systematic trials, ensuring the production of high-quality, defect-free fibers. These parameters were carefully selected to control both the degumming and electrospinning conditions, which are essential for enhancing the properties of the final fibrous structure. This approach is consistent with our practices in SF needle-less processing, as outlined in our previous work.[36] The degumming process of raw silk cocoons was conducted twice, utilizing a 0.1 M sodium carbonate solution and a 0.5% standard reference detergent at 100°C for 30 minutes each. This process effectively removed sericin from the fiber surface, after which the fibers were rinsed with warm water and allowed to dry at room temperature. Subsequently, SF solution was prepared by dissolving degummed silk fibers in 98% formic acid, supplemented with 3 wt% calcium chloride, resulting in a polymer solution with a concentration of 12 wt%. This solution was subjected to magnetic stirring at room temperature for 24 hours to ensure homogeneity before electrospinning under the specified conditions described above. The electrospun SF fibrous carrier underwent crystallization by immersion in ethanol for 30 minutes, which contributed to a reduction in water solubility. After drying at room temperature, the treated fibrous carrier was immersed in distilled water overnight to facilitate the removal of residual salts, followed by rinsing with distilled water and air drying.

Silk fibroin/polycaprolactone fibrous carrier. The preparation of SF solution was following the protocol outlined in previous section. The PCL solution was prepared by dissolving PCL in formic acid to achieve a concentration of 20 wt%, followed by magnetic stirring to ensure complete dissolution. For the production of the SF/PCL blend fibrous carrier,

electrospinning was conducted using a mixture of the SF and PCL solutions in an 8:2 (v/v) volume ratio. This ratio was selected based on findings from our previous research, which indicated that the proportion of PCL in the blend significantly influences the properties of the resulting electrospun fibrous material. Specifically, increasing the PCL content in the spinning solution has been shown to reduce fiber diameter and enhance electrospinning performance while simultaneously decreasing the brittleness of the fibrous carriers. Furthermore, the incorporation of PCL contributes to improved hydrophobicity of the fibers, making this blend particularly suitable for applications where such properties are desired. To examine the effects of the hydrophobic and hydrophilic characteristics of the fibers on the loading of PTX, we opted to investigate this specific 8:2 SF to PCL volume ratio. The electrospinning process for the SF/PCL blended solution was carried out under the conditions described above.

Loading of PTX onto the electrospun fibrous carriers

The electrospun fibrous carriers were cut into 1 cm^2 pieces and immersed in a 0.6 wt% PTX solution for 48 hours to ensure uniform drug adhesion and absorption throughout the entire volume of the fibrous carriers. Following this loading process, the fibrous carriers were dried at 37°C for 2 hours. Importantly, this method did not alter the physical or morphological properties of the fibrous layers. For comparative analysis, an additional set of electrospun fibrous carriers was prepared by first soaking them in the PTX solution, followed by immersion in the HA (1 wt% in 0.1 M NaOH) for 1 minute. These HA coated carriers were then dried in oven at 30°C for 24 hours (refer to Figure 2 for a schematic representation and photograph of electrospun carrier loaded with PTX and coated by HA). Three batches of these carriers were prepared.

Methods

Morphological characterization. The surface morphology of the electrospun fibrous carriers was characterized using a Vega TS 5130 scanning electron microscope (SEM, Tescan, Czech Republic). SEM images were obtained with an accelerating voltage of 30 kV. Prior to imaging, each fibrous carrier was sputter-coated with gold (Q150R ES, Quorum

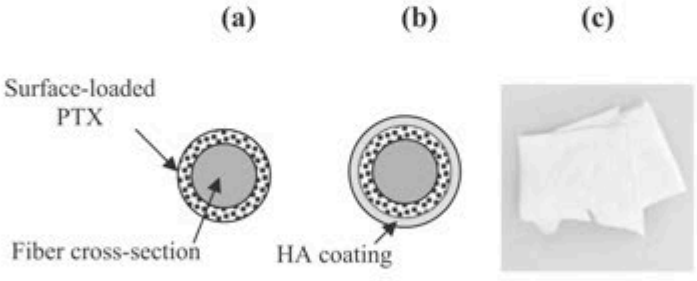

Figure 2. Schematic representation and photograph of electrospun fibrous carrier. (a) Cross-section of electrospun fiber loaded with PTX, (b) cross-section of electrospun fiber loaded with PTX and coated by HA, and (c) photograph of the actual electrospun fibrous carrier.

Technologies Ltd, England) to a thickness of 7 nm. The SEM images were analyzed using NIS-Elements AR software. The average fiber diameter and its distribution were determined by measuring 100 randomly selected fibers from the PCL, SF, SF/PCL, and HA-coated PCL fibrous carriers. This approach ensured a comprehensive assessment of fiber morphology and consistency across all tested materials.

The gram per square meter (GSM) of the electrospun fibrous carriers was measured according to the ISO 3801:1977 standard.

Contact angle measurement. Optical tensiometry, commonly referred to as contact angle goniometry, is a widely employed technique for determining the contact angle of a liquid droplet on a solid surface, thereby characterizing its surface properties.[37] To evaluate the hydrophilicity of the electrospun fibrous carriers, contact angle measurements were performed at three distinct positions on the carrier per material using a Kruss Drop Shape Analyzer DS4 at room temperature. A 2 μL droplet of deionized water was carefully placed on the surface of the dry carrier, and the average contact angle values were calculated from these measurements.

In vitro *PTX release test.* The *in vitro* release test for PTX was performed by immersing 1 cm^2 electrospun fibrous carriers into 1 mL of PBS buffer (pH 7.4, 0.15 M ionic strength) in 4 mL glass vials. The PBS buffer was chosen because it closely mimics the physiological conditions of the human body, maintaining a pH of 7.4, which is optimal for both the stability of PTX and the biological relevance of the system. Additionally, PBS has an ionic strength similar to that of bodily fluids, making it suitable for simulating the extracellular environment where the drug release would occur. The vials were incubated at 37°C and agitated at 100 rpm using an Innova 4000 incubator shaker (New Brunswick Scientific, NJ, USA). At predetermined time intervals (0, 1, 2, 4, 6, 24, 48, 96, and 120 hours), 300 μL of the release medium was collected for UV-vis analysis, and an equal volume of fresh PBS buffer was added to the incubation solution to maintain a constant volume and ensure that the drug release process was not disrupted by changes in the volume or composition of the medium. The UV-vis absorbance of the collected release medium was measured at 290 nm using a SpectraMax Plus 384 UV-vis spectrophotometer (Molecular Devices, CA, USA). A linear correlation (R^2 = 0.9982) was established between absorption intensity and PTX concentration for standard samples ranging from 0 to 50 μg/mL. All measurements were conducted in triplicate to ensure accuracy and reproducibility of the results.

Drug release modelling. The release profile of PTX from the electrospun carriers was evaluated using two established mathematical models to characterize the underlying drug release mechanisms. These models provide insight into the relative contribution of different processes, such as diffusion, erosion, and degradation, in the release behavior. The experimental data on cumulative drug release at different time points was used to fit the following models. Higuchi model is based on Fickian diffusion and assumes that the drug is released from the matrix via diffusion through the medium.

The model relates the cumulative drug release to the square root of time. The mathematical expression is given by:

$$\frac{M_t}{M_\infty} = k \cdot t^{1/2} \quad (1)$$

Where Mt is the cumulative drug release at time t, M_∞ is the total drug amount, and k is the diffusion constant.[38] Hixson-Crowell model is particularly useful for systems where the drug release is governed by the erosion or disintegration of the matrix. This model assumes that the decrease in surface area available for release controls the process. The equation is:

$$M_\infty^{1/3} - M_t^{1/3} = k_{HC} \cdot t \quad (2)$$

Where Mt is the cumulative drug release at time t, M_∞ is the total drug amount, and kHC represents the rate constant for matrix erosion.[39] For each of these models, the parameters were fitted using a linear regression approach, and the goodness of fit was assessed using the R^2 value. A higher R^2 value suggests a better fit of the data to the model, indicating that the model can accurately describe the release kinetics. The drug release data were plotted, and the models were fitted to assess the release rate constants and the dominant release mechanism (diffusion, erosion, or a combination of both). The analysis of the release kinetics allows for a deeper understanding of the processes controlling the release of PTX from the HA coated carriers, which is important for optimizing sustained release formulations.

In vitro *cytotoxicity evaluation.* *In vitro* cytotoxicity of the electrospun fibrous carriers was evaluated in accordance with ISO 10993-5.[40] Prior to testing, the fibrous carriers were sterilised using short-wavelength UV light for 10 minutes to ensure sterility without compromising the structural or chemical properties of the carriers. For the cytotoxicity assay, MiaPaCa pancreatic cancer cells were cultured in DMEM growth medium supplemented with 10% fetal bovine serum (Sigma-Aldrich, Cat# F7524), 1% L-glutamine (Sigma-Aldrich, Cat# G7513) and 1% Penicillin-Streptomycin (Sigma -Aldrich, Cat# P0781). Cells were kept at 37°C in an incubator with an atmosphere containing 5% CO2. When the cells reached 70% confluence, they were trypsinized with 1x trypsin (Sigma-Aldrich, Cat# T3924). Subsequently, MiaPaCa pancreatic cancer cells were seeded in 24-well plates at a confluence of 1×10^5 cells per well and cultured for 24 hours at 37°C to form monolayers of tumor cells covering the 1.9 cm^2 growth area of each well. After confirming cell layer consistency, the supplemented DMEM was removed, and the fibrous carriers loaded with PTX (0.5 cm^2) were placed in each well. The electrospun carriers along with MiaPaCa pancreatic cells were incubated in 1 mL of fresh-added DMEM medium at 37°C for 24, 48, and 96 hours. At the end of each time period, the fibrous carriers were removed, and cell viability was determined using the WST-1 assay. This assay is based on the reduction of tetrazolium salt WST-1 to soluble formazan by electron transport across the plasma membrane of dividing cells. The level of WST-1 reduction into formazan reflects cell metabolism. The sample aliquots (10 per each time point) of

100 µL were transferred to a 96-well plate, and the absorbances were measured using a SpectraMax Plus 384 UV-vis spectrophotometer at a wavelength of 450 nm. For reference, MiaPaCa cells were seeded in DMEM fresh culture medium under the same seeding conditions.

Cytotoxicity of electrospun fibrous carriers was calculated based on the absorbance values obtained from wells containing cells incubated with the carrier/eluate (A_{SAMPLE}), the mean absorbance of wells containing only DMEM (A_{DMEM}), and the absorbance of wells containing non-affected cells (incubated with no material) (A_{CELLS}):

$$Viability(\%) = \left(\frac{A_{SAMPLE} - A_{DMEM}}{A_{CELLS} - A_{DMEM}}\right) * 100 \quad (3)$$

Statistical analysis. All experiments were performed in triplicate (at a minimum) to ensure accuracy and reproducibility. Results are expressed as the mean ± standard deviation (SD). Statistical analysis was conducted using one-way or two-way ANOVA test to compare data between carriers. Significance levels are indicated: $p < 0.001$ (***) and $p < 0.0001$ (****).

Results and discussions

Morphological analysis of electrospun carriers

The primary goal of any drug delivery system, particularly in cancer treatment, is to ensure the targeted release of drugs at the tumor site, maximizing therapeutic efficacy while minimizing side effects. Electrospun fibers are particularly advantageous for delivering high local drug concentrations required in cancer therapies due to their ability to absorb significant amounts of therapeutic agents. The drug release profile is influenced by various factors, including fiber diameter, polymer composition, and the nature of the drug. Moreover, fiber uniformity plays a critical role in ensuring consistent release profiles. Smaller fibers, with their higher surface area, typically release drugs more rapidly, while larger fibers provide a more sustained release, helping to maintain therapeutic drug levels over extended periods.[41,42] Achieving a balance between electrospun fiber size and uniformity is essential for optimizing drug delivery performance. One challenge in needle-less electrospinning is ensuring uniformity and consistent fiber morphology at scale. Variations in the electrospinning environment, such as humidity and temperature, can affect fiber deposition. To address this, we optimized solution parameters and controlled process conditions (voltage, spinneret distance, temperature and humidity) to maintain carriers uniformity. In this study, Nanospider™ technology was utilized to enable the continuous and stable production of electrospun fibrous materials with high uniformity. Additionally, the AC chamber in the Nanospider™ system, which we utilized in this study, helps stabilize the electrostatic field, minimizing variations and improving fiber uniformity for large-scale production.

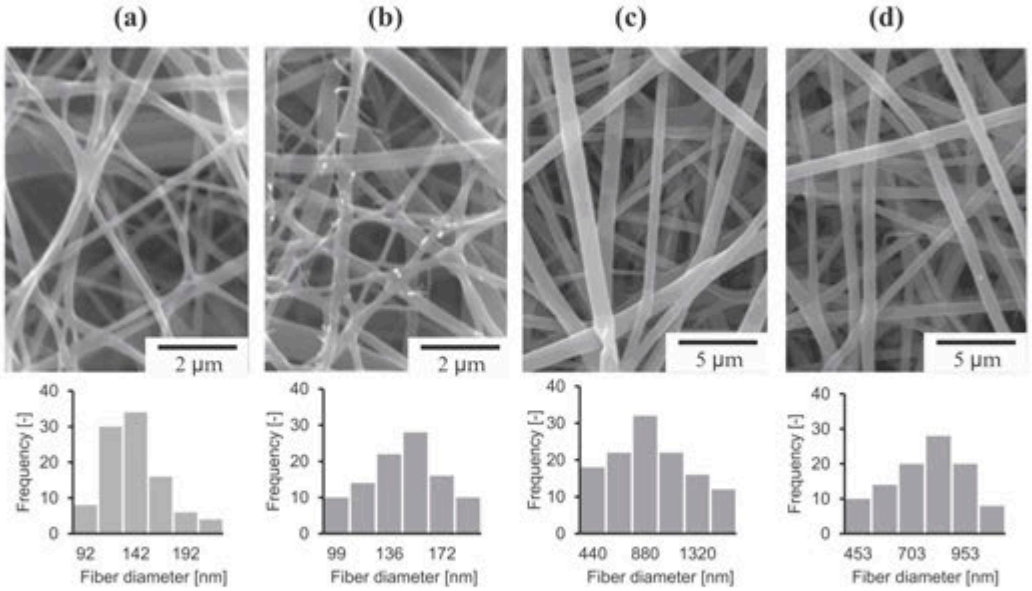

Figure 3. SEM images of electrospun fibrous carriers. (a) PCL carrier, (b) PCL carrier treated with 3M NaOH, (c) SF carrier, and (d) SF/PCL carrier. The images illustrate the fiber diameter and surface texture for each carrier type. Corresponding histograms of fiber diameter distributions are provided, with measurements taken from the carrier for each material (n = 100 fibers).

In this study, PCL, SF, and SF/PCL fibrous carriers were successfully needle-less electrospun, exhibiting no beads or structural defects. The fibers demonstrated a narrow diameter distribution and a smooth, round morphology, as illustrated in Figure 3. The average fiber diameters for the PCL, SF, and SF/PCL carriers were determined using SEM. For each material, a total of 100 fibers were measured from the carrier to ensure reliable data representation. The average diameters of the fibers for the PCL, SF, and SF/PCL carriers were found to be 141 ± 28 nm, 903 ± 331 nm, and 772 ± 187 nm, respectively. Notably, NaOH-treated PCL fibers maintained their original diameter of 150 ± 31 nm while exhibiting significant alterations in surface morphology. Specifically, the treated fibers presented a disturbed surface characterized by protruding fluff, indicating that NaOH treatment effectively modifies surface characteristics without impacting the fiber diameter.

The results demonstrated that the electrospun SF fibrous carrier exhibited the largest fiber diameter, while the PCL fibers displayed the smallest diameter. The SF/PCL blend fibers had a diameter slightly smaller than that of pure SF, likely due to the incorporation of PCL, which tends to facilitate the formation of finer fibers. Generally, smaller fiber diameters correlate with a higher surface area-to-volume ratio, thereby enhancing drug absorption. As a result, PCL fibers, characterized by their smaller diameters, provide a larger surface area, thereby should improve drug loading capacity. To compare PTX release from the electrospun fibrous materials, we produced carriers with the same GSM value, specifically 6.5 ± 0.2 g/m^2. By maintaining this consistent GSM, we ensured that the amount of material and fiber density remained the same across samples, allowing for a

more accurate comparison of the release profiles of PTX between the different fiber compositions. This approach helps isolate the influence of the material properties (such as PCL and SF) on the drug release rate, ensuring that any observed differences are not due to variations in carrier mass or thickness.

Wettability of electrospun carriers

The surface hydrophobicity or hydrophilicity of electrospun fibrous carriers, as indicated by the contact angle, plays a critical role in determining the interaction between loaded drugs and the fibrous surface, significantly influencing drug release behavior. Contact angle measurements serve as essential parameter for assessing the wettability of fibrous materials, directly correlating with their hydrophilic or hydrophobic nature. Specifically, fibrous materials with a contact angle greater than 90° are classified as hydrophobic, while those with a contact angle below 90° are deemed hydrophilic.[43] This distinction is crucial for drug delivery systems, particularly for chemotherapeutics like PTX, where the interaction between the drug and the electrospun fibrous carrier can significantly affect the efficiency of drug delivery to tumor sites.[44]

In this study, the electrospun PCL fibrous carrier demonstrated hydrophobic characteristics, exhibiting an average contact angle of 119 ± 4°. Conversely, the SF and SF/PCL fibrous carriers displayed hydrophilic properties, with an average contact angles measuring 44 ± 5° and 63 ± 6°, respectively. The incorporation of PCL into the SF matrix contributed to an increased contact angle, thereby enhancing the hydrophobic nature of the resultant fibrous carrier, as illustrated in Table 1. Notably, treating the PCL fibrous carrier with 3M NaOH significantly enhanced its wettability, reducing the contact angle to 54 ± 6°. This treatment effectively improved the surface hydrophilicity of the PCL carrier, a critical factor in modulating drug release profiles.

The observed variations in contact angle and corresponding wettability can substantially affect both the loading capacity and release kinetics of PTX, a hydrophobic drug. The release dynamics of PTX are closely linked to the surface characteristics of the drug carrier, such as its hydrophobicity or hydrophilicity. Additionally, factors such as carrier porosity, surface charge, and environmental conditions (e.g., pH or biological fluids) also play a significant role in modulating the drug-carrier interactions. Understanding of these variables is essential for the development of advanced drug delivery systems aimed at maximizing the therapeutic efficacy of PTX.

In vitro *PTX release from electrospun carriers*

As mentioned above, the hydrophobicity or hydrophilicity of fibrous carriers significantly influences the release profile of PTX, a hydrophobic chemotherapeutic widely used in pancreatic cancer treatment. Hydrophobic fibers, such as those made of PCL, strongly interact with PTX due to their compatibility with hydrophobic environments, resulting in a slower diffusion rate and sustained release. This controlled release is crucial for maintaining therapeutic drug levels over prolonged periods, enhancing cancer cell eradication while minimizing systemic exposure.[45] In contrast, increasing the

Table 1. Wettability characteristics of electrospun PCL, PCL (NaOH treated), SF, and SF/PCL carriers. The table include images of water droplets on each fibrous carrier.

Fibrous carrier	PCL	PCL (NaOH treated)	SF	SF/PCL
Wettability				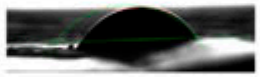

hydrophilicity of fibers—through modifications like surfactant application or sodium hydroxide treatment— enhances water penetration and accelerates drug dissolution and diffusion, often leading to an initial rapid release phase. While beneficial for rapid drug action, this may reduce long-term therapeutic effects.[46] Optimizing these properties is key to designing drug delivery systems that balance immediate and prolonged release based on the specific demands of cancer treatment. Understanding this interplay helps create fibrous materials tailored for effective cancer therapies while minimizing adverse effects.[47]

In this study, 0.6 wt% PTX injectable solution was used which is prepared using PTX, polyoxyl 35 castor oil, and dehydrated alcohol. These components facilitate the dissolution of the castor oil and stabilize the formulation, resulting in a solution where PTX exhibits a markedly hydrophobic character. As discussed in Section 3.2, the electrospun fibrous carriers utilized in this study demonstrated varying degrees of hydrophobicity and hydrophilicity, which significantly may influence the interaction between the fibrous materials and PTX, ultimately affecting the drug release profile. The release behavior of PTX from four types of electrospun fibrous carriers—PCL, NaOH-treated PCL, SF, and SF/PCL blend—was evaluated in triplicates, and the data were analyzed using a one-way ANOVA test to assess statistical differences between the groups. The results, illustrated in the accompanying Graph 1, revealed distinct differences in PTX release behavior among the electrospun fibrous carriers types.

The electrospun PCL fibrous carrier, characterized by its hydrophobic nature and fine fiber structure, exhibited the highest and most sustained PTX release. The sustained release curve indicates a controlled and gradual release over time, with a delayed onset. This sustained release is attributed to strong hydrophobic-hydrophobic interactions, driven by van der Waals forces, which enable PTX molecules to adhere tightly to the electrospun PCL fibrous carrier, thus facilitating prolonged drug delivery. In contrast, SF

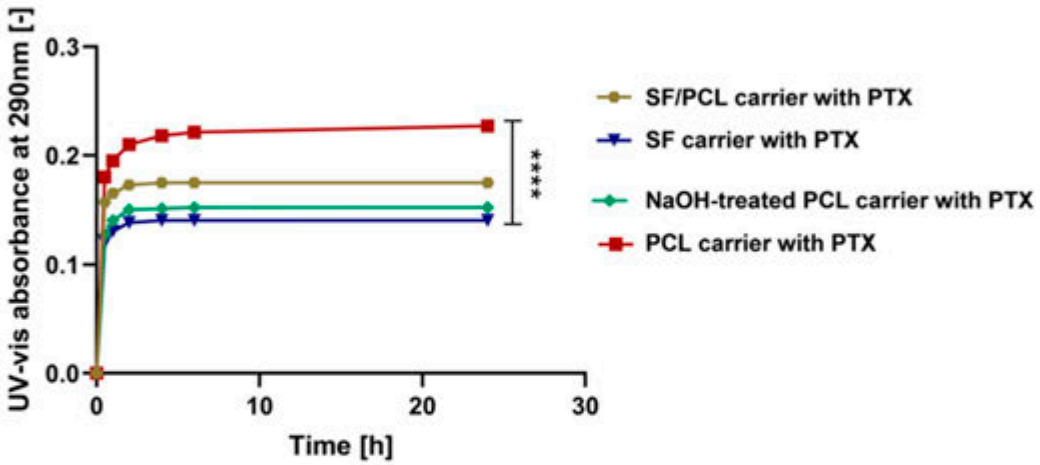

Graph 1. PTX release from electrospun fibrous carriers. The release behavior of PTX from four types of electrospun fibrous carriers—PCL, NaOH treated PCL, SF, and SF/PCL blend—was evaluated. Statistical analysis using a one-way ANOVA test revealed significant differences in the release profiles among the carriers ($p < 0.0001$, $n = 3$).

fibrous carrier, being more hydrophilic, exhibit a weaker affinity for PTX due to hydrophobic-hydrophilic interactions, resulting in an initial rapid release phase curve that shows a rapid increase in drug release early on. While this rapid release can be beneficial for achieving quick therapeutic action, it is less suited for applications requiring sustained drug release. The SF/PCL blend demonstrated intermediate release characteristics. Notably, the highest UV-vis absorbance 0.23 was recorded for PCL fibrous carrier, indicating a greater absorption of PTX compared to SF carrier, which exhibited the lowest absorbance 0.14. This observation aligns well with the contact angle measurements, highlighting the relationship between the hydrophobicity of the PCL fibrous carrier and its ability to absorb and release PTX. Statistical analysis using a one-way ANOVA test revealed significant differences in the release profiles among the carriers. In summary, the contact angle measurements and corresponding PTX release profiles clearly demonstrate the pivotal role that surface hydrophobicity or hydrophilicity plays in controlling drug release kinetics. Hydrophobic electrospun PCL fibrous carrier offers a more sustained release of PTX, ideal for applications requiring prolonged therapeutic effects. This is particularly relevant for conditions like pancreatic cancer, where long-term drug exposure is crucial for effective treatment. In contrast, hydrophilic fibrous carrier, such as SF, facilitate an initial rapid release phase of PTX, making them suitable for scenarios requiring immediate therapeutic action. The findings highlight that selecting fibrous materials tailored to the desired release kinetics is essential for optimizing drug delivery systems for cancer treatment. Given the sustained release profile of PTX, PCL fibrous carrier has been identified as the most suitable candidate for further investigation.

Morphology and in vitro *release of PTX from electrospun carrier coated by HA*

Biopolymer coatings such as alginate and polyethylene glycol (PEG) have been widely explored for drug delivery applications due to their biocompatibility and ability to control drug release. Alginate, a naturally derived polysaccharide from brown seaweed, is frequently used in drug delivery due to its gel-forming ability and structural similarity to the extracellular matrix. Alginate-based hydrogels can encapsulate drugs, providing a protective barrier and enabling sustained release. However, alginate lacks intrinsic bioactivity, limiting its interaction with specific cellular receptors, which may be a drawback for targeted therapies.[48] Similarly, PEG, a synthetic polymer, is known for its hydrophilicity and non-immunogenic properties, making it an excellent material for reducing protein adsorption and prolonging circulation time in drug delivery systems. PEG-based hydrogels offer tunable degradation rates and mechanical properties, allowing for controlled drug release. However, PEG lacks specific cellular interactions, which can limit its bioactive potential.[49] In contrast, HA presents unique advantages in drug delivery due to its intrinsic bioactivity. The incorporation of HA as a surface coating on fibrous carriers may significantly enhanced the release profile and therapeutic efficacy of PTX. HA, a naturally occurring polysaccharide, is renowned for its biocompatibility and capacity to create a hydrophilic environment, which is particularly beneficial for maintaining therapeutic drug levels over extended periods.[10] This characteristic helps reduce dosing frequency and minimize associated side effects.[50] The mechanism through

which HA improves PTX's release profile is multifaceted. Firstly, HA enhances the solubility and stability of PTX, addressing the drug's inherent hydrophobicity. Additionally, the molecular weight of HA is critical in modulating the release kinetics of PTX; higher molecular weight HA can create a more viscous barrier, potentially slowing drug diffusion, while lower molecular weight HA may facilitate a faster release profile.[51] This balance is essential for optimizing therapeutic outcomes, allowing for tailored drug release rates according to specific treatment requirements.

Coating the PTX-loaded PCL fibrous carrier with HA resulted in significant changes in both morphology and release profiles, as shown in Figure 4 and Graph 2. The HA coating formed a continuous film on the surface of individual fibers. Fiber diameters were measured across three batches of HA-coated electrospun PCL carriers, with a total of 100 fibers analyzed to ensure batch-to-batch consistency, as illustrated in the SEM images in Figure 4(a)–(c). Variability in fiber diameter was observed, with Batch 1 averaging 549 ± 120 nm, Batch 2 averaging 544 ± 124 nm, and Batch 3 averaging 512 ± 121 nm. Despite these differences, the overall average fiber diameter across all batches was 535 ± 115 nm, indicating relatively consistent fiber morphology. The observed variation in fiber diameters is attributed to the HA coating process rather than the electrospinning. Before

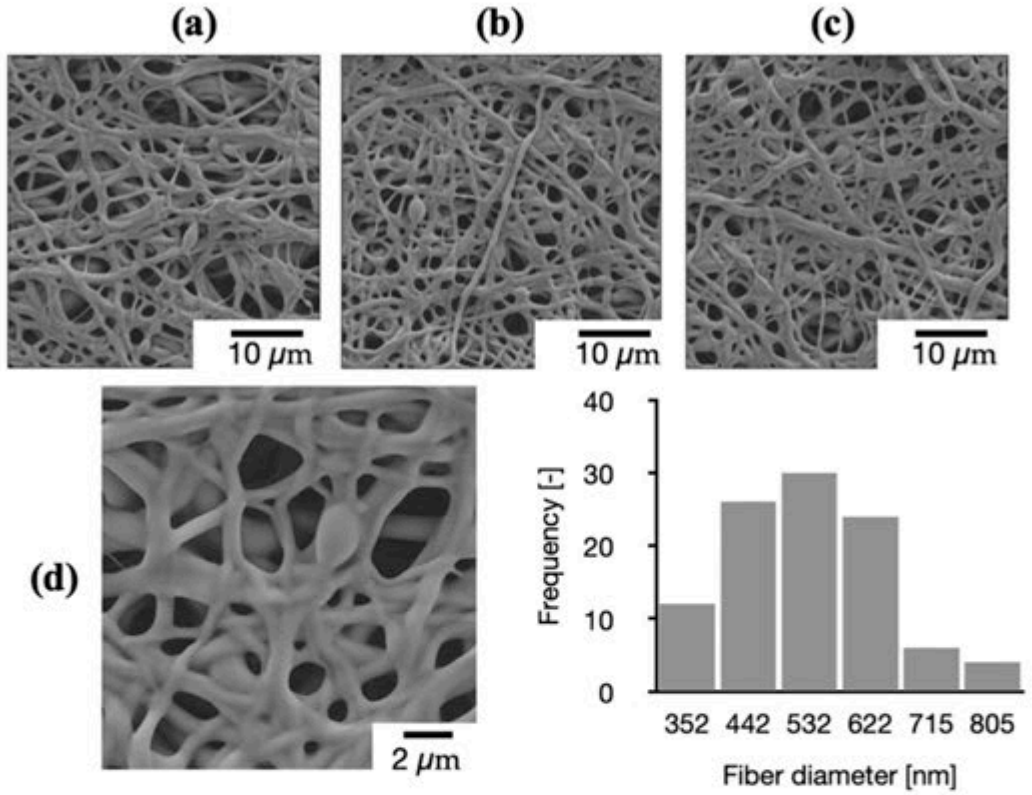

Figure 4. SEM image of electrospun PCL fibrous carrier loaded with PTX and coated with HA. (a–c) SEM images of three different batches, confirming reproducibility. (d) Detailed SEM image of the fiber structure. The accompanying histogram presents the fiber diameter distribution, with measurements taken from three batches of HA-coated carriers (n = 100 fibers in total).

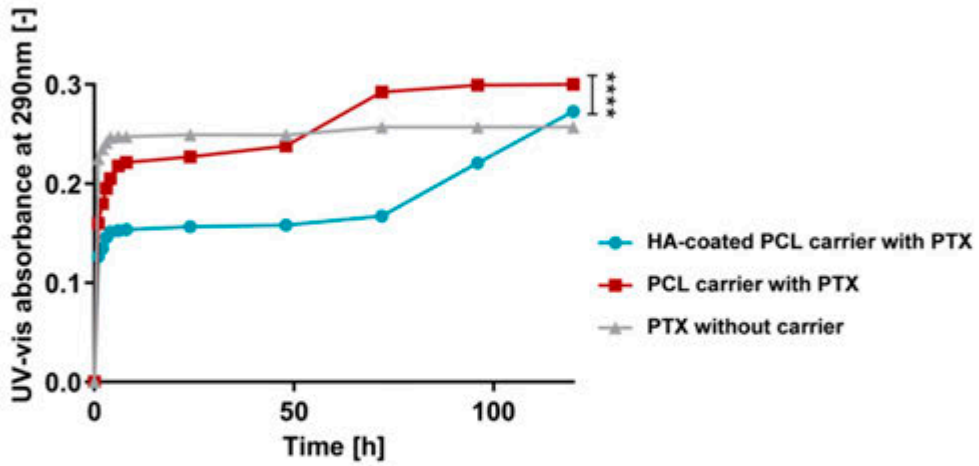

Graph 2. Release kinetics of PTX from electrospun PCL fibrous carrier coated with HA. The graph demonstrates a gradual release of PTX over time, highlighting the effect of HA coating on PTX delivery dynamics. Statistical analysis using a one-way ANOVA test revealed significant differences in the release profiles among the carriers ($p < 0.0001$, $n = 3$).

HA coating, the standard deviation of fiber diameters was 28 nm, indicating tightly distributed morphology, whereas after HA coating, it increased to 115 nm, reflecting typical variability from surface modification. Despite this, the consistency across batches confirms the reproducibility of the HA coating process, demonstrating that both electrospinning and coating techniques are reliable for scalable production. The porous fibrous structure indicates that the HA primarily coated the fiber surfaces, increasing their diameter without compromising the carrier's integrity. This ensures maintained functional properties, enhanced drug absorption, and improved controlled release capabilities.

To comprehensively evaluate the carrier's performance, the PTX loading efficiency (DLE) and loading capacity were determined. The DLE, calculated as the ratio of the total amount of PTX released to the initial amount applied, was 97.5% for the non-coated electrospun PCL carrier and 90.9% for the HA-coated PCL carrier. Additionally, the PTX loading capacity was found to be 533 mg PTX per 1 g of carrier, demonstrating the carrier's high drug absorption efficiency. Since the electrospun carriers were immersed in the PTX solution, drug loading predominantly occurred on the fiber surface rather than within the fiber matrix. In an ideal scenario without degradation or irreversible binding, the theoretical DLE would approach 100%. However, slight deviations from this value were observed, likely due to PTX adsorption onto fiber surfaces or partial entrapment within the fibrous structure, as reflected in the measured DLE values.

Moreover, statistical analysis using a one-way ANOVA test revealed significant differences in the release profiles between PCL carriers with and without HA coating, as illustrated in Graph 2. For the electrospun PCL carrier without HA, UV-Vis absorbance measurements indicated a steady release during the first 2 days, followed by a rapid increase after 48 hours. This suggests that the release from the uncoated fibers was primarily diffusion-controlled, with a faster initial release and a slight variation after 48 hours. In contrast, the HA-coated PTX-loaded electrospun PCL carrier exhibited a

more controlled and gradual increase in release over time. The release rate remained stable for the first 3 days, followed by a significant increase in PTX release after 72 hours, continuing until 120 hours. The HA-coated carrier achieved a substantially prolonged drug release compared to the uncoated PCL carrier, supporting the hypothesis that HA enhances drug retention and modulates release characteristics. As a control, PTX alone (without the electrospun carrier) was tested and exhibited a nearly constant release profile throughout the test period. This underscores the superior efficacy of the HA-coated electrospun PCL carrier in providing a more favorable drug release environment, promoting regulated PTX release over time.

Additionally, the release profile of PTX from HA-coated electrospun PCL carrier was analyzed using the Hixson-Crowell and Higuchi models to gain insight into the mechanisms governing drug release. The Hixson-Crowell model, which describes drug release through matrix erosion, demonstrated a good fit with an R^2 value of 0.85. This indicates that HA disintegration is one of the key mechanisms for PTX release, with the HA coating degrading over time and gradually increasing the exposed surface area of the drug-loaded carrier. The derived rate constant ($k = 0.001$) reflects the rate of HA coating degradation, facilitating sustained drug release as the coating progressively breaks down. The Higuchi model, commonly used to describe diffusion-driven release, showed an R^2 value of 0.74. This suggests that diffusion also plays a role, particularly in the later stages of the release process as the HA coating continues to degrade. The rate constant ($k = 2.9$) indicates that as the HA coating degrades, diffusion becomes more dominant, contributing to the sustained release of PTX. By applying these two models, it is evident that the release of PTX from HA-coated electrospun PCL carrier occurs in multiple stages, initially driven by HA degradation and later governed by diffusion. Early in the release process, a rapid PTX release is observed as the HA coating degrades. Over time, as the HA coating continues to break down, diffusion becomes the primary release mechanism, resulting in a prolonged release phase that sustains the therapeutic effect of PTX. These findings are consistent with existing literature on HA-based electrospun fibrous drug delivery systems, which have consistently demonstrated comparable sustained release profiles. For example, HA/gelatin coaxial nanofibers loaded with arginine effectively controlled the release of cationic biomolecules, highlighting the potential of HA-based electrospun fibers in drug delivery applications.[52] Similarly, studies have reported an initial rapid release phase followed by sustained release over extended periods, further confirming HA's efficacy in modulating drug release kinetics.[53] Building on these observations, biocompatible electrospun polyvinyl alcohol/chitosan/HA fibrous materials were evaluated for the sustained release of human growth hormone, showing an initial rapid release phase of 11% within 2 hours, followed by sustained release reaching 64% over 48 hours.[54] Furthermore, electrospun HA/polyvinyl alcohol/2-hydroxypropyl-β-cyclodextrin fibrous materials demonstrated sustained naproxen release over 48 hours, attributed to the structural stability of the carriers.[55] These examples collectively emphasize the ability of electrospun HA-based fibrous carriers to provide controlled release of therapeutic agents through structural and material composition.

The degradation behavior of HA-coated PCL carrier, while tested *in vitro* in PBS, is expected to differ significantly *in vivo*, where enzymatic process mediates HA

breakdown. Under physiological conditions, HA is primarily degraded by hyaluronidases, which cleave glycosidic bonds between disaccharide units. The degradation rate of HA is influenced by the presence and concentration of these enzymes, often upregulated in tumor environments.[56] Additionally, non-enzymatic processes, such as hydrolysis, also contribute to HA degradation. Physiological conditions, including pH, temperature, and the ionic environment, may further modulate the rate of degradation, either accelerating or slowing the process.[57] In contrast, PCL degrades much more slowly in physiological conditions, with *in vivo* studies showing only partial degradation over 90 days, ensuring sustained drug release.[58] The combination of HA and PCL creates a dual-release system—an initial rapid release from HA, driven by rapid enzymatic degradation, followed by a sustained release from the slowly degrading PCL matrix. This approach optimizes drug retention at the target site while maintaining prolonged therapeutic effects, making it particularly valuable for controlled drug delivery in pancreatic cancer therapy. This intricate balance between enzymatic and non-enzymatic degradation is crucial for ensuring a controlled and sustained release of the therapeutic agent, a key factor in the localized treatment of pancreatic cancer. Understanding these processes is important to fine-tuning the release profile for optimal therapeutic efficacy. Future studies focusing on the precise degradation kinetics of HA under physiological conditions and the specific influence of the tumor microenvironment will be critical. Such investigations will aid in optimizing the drug delivery system, enhancing its potential for clinical applications.

Cytotoxicity of electrospun PCL fibrous carrier loaded by PTX against pancreatic cell line

The utilisation of HA to coat electrospun PCL carrier loaded with PTX represents a strategic approach to enhancing targeted delivery against pancreatic cancer. This strategy is particularly relevant given the unique characteristics of pancreatic tumors, which often feature a dense stromal environment that complicates effective drug delivery. HA's ability to specifically bind to CD44 receptors, frequently overexpressed on pancreatic cancer cells, facilitates the selective delivery of PTX directly to the tumor site while minimizing off-target effects.[11] CD44 is a transmembrane glycoprotein that serves as the principal cell surface receptor for HA. The binding occurs via the link domain of CD44, which recognizes and attaches to specific sequences within the HA polymer. This interaction follows a catch-bond mechanism, where the bond between HA and CD44 strengthens under mechanical stress, enhancing cell adhesion under dynamic conditions.[59] The HA-CD44 interaction is pivotal in cancer progression, particularly in tumors where CD44 is overexpressed. By exploiting this binding specificity, HA-coated nanocarriers can target CD44-expressing tumor cells, facilitating preferential tumor accumulation and increased cellular uptake of chemotherapeutic drugs. This targeted delivery mechanism is crucial for navigating the dense stroma of pancreatic tumors, as it can impede the effective penetration and distribution of therapeutic agents. By enhancing the interaction between the drug-loaded fibrous carrier and cancer cells, HA improves drug localization, promoting better therapeutic outcomes. Moreover, the incorporation of HA for targeting reduces systemic exposure to PTX, thereby decreasing potential side effects and improving patient

safety—a significant consideration in cancer therapy.[60] The HA-CD44 axis plays a pivotal role in cancer biology, as CD44 is closely linked to cancer stem cell properties, metastasis, and resistance to therapy. Leveraging this interaction enables the development of targeted therapeutic strategies. For instance, HA-decorated nanocarriers can preferentially accumulate in CD44-overexpressing tumors, enhancing the delivery and efficacy of chemotherapeutic agents.[61] Furthermore, disrupting the HA-CD44 interaction has been explored as a therapeutic approach. Soluble CD44 or peptides that block HA binding can inhibit tumor growth and metastasis by preventing CD44-mediated signaling pathways.[62] In summary, the molecular interaction between HA and CD44 is a critical mediator of cellular functions and presents a valuable target for therapeutic interventions, particularly in oncology. Importantly, applying the HA-coated PCL fibrous carrier directly onto the surgical site after tumor removal may offer a dual benefit: inhibit the regrowth of residual cancer cells and directly deliver PTX to the affected area. This aligns with the principles of precision medicine, where therapies are tailored to the specific characteristics of the tumor and patient needs. This combined approach may represent a promising adjunctive therapeutic strategy that addresses the challenges of drug delivery in pancreatic cancer while prioritizing improved patient safety.

The results demonstrate that MiaPaCa cell viability remained relatively constant when treated with free PTX, ranging from 58% to 40% over 96 hours. This limited efficacy is like due to PTX's poor solubility and rapid systemic clearance. In contrast, PTX-loaded electrospun PCL carriers exhibited a significant decrease in cell viability after 48 hours, attributed to the sustained release profile of PTX from the hydrophobic PCL carrier. Notably, HA-coated PTX-loaded electrospun PCL carriers demonstrated a more pronounced cytotoxic effect, reducing cell viability from 44% at 72 hours to 13% at 96 hours. This effect was significantly greater than that observed with non-HA-coated carriers,

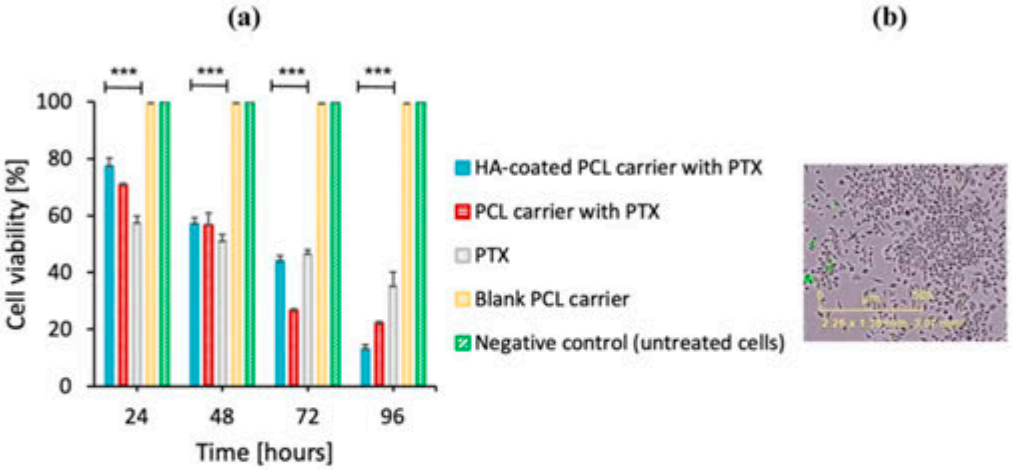

Graph 3. Cytotoxicity of PTX-loaded PCL fibrous carriers against MiaPaCa pancreatic cancer cell monolayers. (a) Cell viability at varying exposure times, showing significant differences ($p < 0.001$, $n = 3$) between HA-coated and uncoated PTX-loaded carriers, as well as in comparison to free PTX, as determined by two-way ANOVA. (b) Representative optical microscope image of the MiaPaCa cell monolayer.

which exhibited a modest reduction from 27% at 72 hours to 22% at 96 hours, as illustrated in Graph 3. This enhanced cytotoxicity in HA-coated electrospun PCL carrier can be attributed to two key mechanisms: (i) HA's ability to selectively bind to CD44 receptors, which are overexpressed on pancreatic cancer cells, thereby improving drug localization and uptake, and (ii) the HA coating's role in modulating PTX release, mitigating the initial rapid release and promoting a more sustained therapeutic effect. Statistical analysis using a two-way ANOVA test confirmed significant differences in cell viability between HA-coated and uncoated PTX-loaded carriers, as well as in comparison to free PTX ($p < 0.001$, $n = 3$).

The distinct PTX release profiles of HA-coated and uncoated carriers further highlight the impact of HA on drug delivery kinetics. Uncoated PCL fibrous carriers exhibited a rapid PTX release within the first 48 hours, correlating with the observed reduction in cell viability at 72 hours (27%). While this immediate drug release provides an initial therapeutic response, the rapid clearance from the tumor site may limit long-term efficacy. In contrast, HA-coated fibrous carriers exhibited a slower, sustained release profile, with a significant increase in PTX release at 72 hours, corresponding to a more gradual but ultimately greater reduction in cell viability (13% at 96 hours). This prolonged exposure likely enhances PTX accumulation within the tumor microenvironment, ensuring more effective targeting of cancer cells over time.[63] Although this study does not directly investigate the HA-CD44 interaction via blocking assays, prior researches supports HA's role in improving CD44-mediated drug delivery. This interaction facilitates internalization and intracellular drug activation, making HA-conjugated nanocarriers and HA-functionalized drug delivery systems highly effective. For instance, HA-decorated nanoparticles loaded with gemcitabine (GEM) or quercetin have successfully overcome chemoresistance with minimal systemic cytotoxicity.[64,65] Similarly, HA-functionalized carbon nano-onion particles have shown enhanced encapsulation and delivery of GEM-derived prodrugs, improving treatment outcomes against chemoresistant pancreatic tumors.[66] These findings align with the current study, reinforcing the role of HA in facilitating targeted drug delivery and sustained therapeutic effects. However, nanoparticles dispersed in liquid form face challenges in achieving controlled and localized delivery to specific tumor sites.

Localized drug delivery systems, such as electrospun carriers, address this limitation by enabling sustained anticancer drugs release directly at the tumor site, minimizing systemic toxicity. While electrospun carriers have been investigated for various cancers, relatively few studies have focused on pancreatic cancer treatment. For instance, GEM-loaded core–shell electrospun fibers fabricated via emulsion electrospinning with HA hydrosol demonstrated sustained drug release for up to 3 weeks. By optimizing GEM load and hydrosol thickness, these fibers effectively inhibited pancreatic cancer cell proliferation and promoted apoptosis in both *in vitro* and *in vivo* models. Notably, GEM-loaded electrospun fibers outperformed systemic GEM administration by enhancing apoptosis rates and reducing liver toxicity.[67] Electrospun fibrous materials also show promise for delivering complex chemotherapies. Coaxial electrospinning has been employed to encapsulate 5-Fluorouracil and methotrexate within PCL fibers, achieving effective drug integration. However, due to PCL's slow degradation, drug release was limited to 20%

over 4 days. Despite this limitation, coaxial electrospinning remains a promising strategy for delivering combination therapies like FOLFIRINOX, commonly used in pancreatic cancer treatment.[68] In contrast, our HA-coated PCL carriers offer a more balanced degradation profile and sustained PTX release. Unlike previous studies, where slow-degrading PCL matrices resulted in limited drug release, our carrier ensures a more consistent and prolonged PTX release, improving therapeutic efficacy. Furthermore, while needle-based electrospinning has been widely used, it presents scalability and reproducibility challenges. Our approach, utilizing needle-less electrospinning technology, simplifies production, enhances adaptability, and improves scalability for potential industrial production. By integrating HA coating with electrospun PCL carriers for PTX delivery, our system provides a more efficient, scalable, and localized therapeutic strategy for pancreatic cancer treatment. Compared to other drug delivery approaches, such as GEM-loaded fibers or coaxial electrospun PCL fibers, our method addresses both drug release kinetics and industrial-scale production challenges.

Discussion

This study demonstrates the potential of HA-coated electrospun PCL carrier as a novel, scalable platform for localized PTX delivery in pancreatic cancer treatment. The integration of HA into the electrospun carrier allows for controlled, and more sustained drug release, addressing the rapid clearance challenges typically encountered with hydrophobic fibrous materials. The findings indicate improved drug delivery efficiency and prolonged cytotoxic effects, as evidenced by sustained reductions in MiaPaCa cell viability. The PTX release profile from the HA-coated PCL carriers revealed a dual-release mechanism. Initial rapid release, governed by matrix erosion, was characterized by the Hixson-Crowell model ($R^2 = 0.85$, $k = 0.001$), reflecting degradation of the HA coating. Following the initial rapid release, a sustained diffusion-driven release occurred, characterized by the Higuchi model ($R^2 = 0.74$, $k = 2.9$), ensuring prolonged drug availability. This dual-release profile may help ensure prolonged therapeutic concentration at the tumor site. However, the initial rapid release phase suggests potential areas for optimization, particularly to mitigate premature drug loss and enhance therapeutic precision. In comparison to conventional HA-based nanoparticle systems, which are often limited by short residence times in the target tissue, the HA-coated electrospun PCL carriers provide a stable and efficient platform for localized chemotherapy. These carriers offer several key advantages, including a high surface area for drug loading, control over drug release kinetics, and the ability to function as localized patches that stay in close contact with the target tissue. Unlike injectable HA-based nanoparticles, which depend on circulation and are often cleared rapidly, our carriers can be directly applied to surgical sites, ensuring prolonged local drug retention and minimizing systemic exposure. This localized drug delivery system could also optimize drug diffusion, maintain a consistent concentration gradient, and help address critical challenges such as preventing local recurrence. Additionally, the needle-less electrospinning technology Nanospider™ used in this study offers significant advantages for industrial scalability and clinical translation. Unlike traditional needle-based methods, this system enables efficient production of

uniform fibers on a larger scale, addressing bottlenecks in fiber morphology and coating uniformity. Optimization of process parameters, such as solution viscosity and voltage, further ensures production consistency and quality. Our carrier also holds promise for further optimization through nanoparticle loading, as demonstrated in our previous study, which combined PCL, SF/PCL and SF electrospun carriers with nanoparticles, enhancing vaccine penetration and localized delivery.[36] This approach could further improve therapeutic efficacy by leveraging the synergistic effects of nanoparticles and electrospun carriers to enhance drug delivery and overcome the tumor microenvironment's challenges. Looking ahead, we plan to conduct comprehensive *in vivo* studies to further evaluate the pharmacokinetics, tumor penetration, and therapeutic efficacy of the HA-coated electrospun PCL carriers. These studies will help validate the carrier's safety and effectiveness, particularly in real-time tumor growth inhibition and recurrence prevention. Advanced imaging techniques will be employed to monitor the distribution of the carriers and assess their ability to maintain consistent drug concentrations at the target site. These studies will bridge preclinical and clinical translation, reinforcing the feasibility of our scalable approach for pancreatic cancer therapy.

Conclusion

This study presents a scalable and innovative approach for localized PTX delivery in pancreatic cancer treatment using HA-coated electrospun PCL carriers. By addressing challenges such as rapid drug clearance and scalability, this system enhances drug delivery efficiency and cytotoxic efficacy, as evidenced by significant and sustained reductions in MiaPaCa cell viability. Compared to conventional HA-based nanoparticle systems, HA-coated PCL carriers enables stable, localized chemotherapy with prolonged tissue contact and minimized off-target effects. The integration of needle-less Nanospider™ technology underscores the industrial scalability and clinical potential of this platform, overcoming the productivity limitations of traditional needle-based electrospinning methods. This HA-coated electrospun carrier offers a promising complementary approach to systemic chemotherapy, potentially improving therapeutic outcomes while reducing adverse effects. Future *in vivo* studies will be crucial to validating its safety, pharmacokinetics, and therapeutic potential, paving the way for clinical application in pancreatic cancer treatment.

Declaration of conflicting interests

The author(s) declared no potential conflicts of interest with respect to the research, authorship, and/or publication of this article.

Funding

The author(s) disclosed receipt of the following financial support for the research, authorship, and/or publication of this article: this work was supported by the Ministry of Education, Youth and Sports of the Czech Republic and the European Union - European Structural and Investment Funds in the

frames of Operational Programme Research, Development and Education - project Hybrid Materials for Hierarchical> Structures (HyHi, Reg. No. CZ.02.1.01/0.0/0.0/16_019/0000843).

ORCID iD

Daniela Lubasova https://orcid.org/0000-0002-7084-575X

References

1. Deng Z. Different therapies in pancreatic cancer treatment. *Theoretical and Natural Science* 2023; 17(1): 262–266.
2. Hernández-Blanquisett A, Quintero-Carreño V, Martínez-Ávila MC, et al. Metastatic pancreatic cancer: where are we? *Onco Rev* 2024; 17: 11364.
3. Wang M, Zhu P, Chen Z, et al. Conversion therapy, palliative chemotherapy and surgery, which of these is the best treatment for locally advanced and advanced pancreatic cancer? *Anti Cancer Drugs* 2021; 33(1): e686–e691.
4. García-Sampedro A, Gaggia G, Ney A, et al. The state-of-the-art of phase ii/iii clinical trials for targeted pancreatic cancer therapies. *J Clin Med* 2021; 10(4): 566.
5. Cassano R and Trombino S. Drug delivery systems: smart polymeric materials. In: Puoci F (ed) *Advanced Polymers in Medicine*. Cham, Switzerland: Springer, 2015.
6. Torres-Martinez EJ, Cornejo Bravo JM, Serrano Medina A, et al. A summary of electrospun nanofibers as drug delivery system: drugs loaded and biopolymers used as matrices. *Curr Drug Deliv* 2018; 15: 1360–1374.
7. Yang J, Wang S, Liu P, et al. Platelet-inspired medicine for tumor therapy. *Oncotarget* 2017; 8: 115748–115753.
8. Gong J, Chen M, Zheng Y, et al. Polymeric micelles drug delivery system in oncology. *J Contr Release* 2012; 159: 312–323.
9. Rafei H, Mehta RS and Rezvani K. Editorial: cellular therapies in cancer. *Front Immunol* 2019; 10: 2788.
10. Kesharwani P, Chadar R, Sheikh A, et al. CD44-Targeted nanocarrier for cancer therapy. *Front Pharmacol* 2022; 12: 800481.
11. Ravar F, Saadat E, Gholami M, et al. Hyaluronic acid-coated liposomes for targeted delivery of paclitaxel, in-vitro characterization and in-vivo evaluation. *J Contr Release* 2016; 229(229): 10–22.
12. Puluhulawa LE, Joni IM, Elamin KM, et al. Chitosan–hyaluronic acid nanoparticles for active targeting in cancer therapy. *Polymers* 2022; 14(16): 3410.
13. Hu K, Zhou H, Liu Y, et al. Hyaluronic acid functional amphipathic and redox-responsive polymer particles for the co-delivery of doxorubicin and cyclopamine to eradicate breast cancer cells and cancer stem cells. *Nanoscale* 2015; 7(18): 8607–8618.
14. Wei W, Dong X and Liu C. *In vitro* investigation of self-assembled nanoparticles based on hyaluronic acid-deoxycholic acid conjugates for controlled release doxorubicin: effect of degree of substitution of deoxycholic acid. *Int J Mol Sci* 2015; 16(4): 7195–7209.
15. Borandeh S, van Bochove B, Teotia A, et al. Polymeric drug delivery systems by additive manufacturing. *Adv Drug Deliv Rev* 2021; 173: 349–373.

16. Hoc D and Haznar-Garbacz D. Foams as unique drug delivery systems. *Eur J Pharm Biopharm* 2021; 167: 73–82.
17. Ezike TC, Okpala US, Onoja UL, et al. Advances in drug delivery systems, challenges and future directions. *Heliyon* 2023; 9(6): e17488.
18. Liu B and Chen K. Advances in hydrogel-based drug delivery systems. *Gels* 2024; 10(4): 262.
19. Jiang Z, Zheng Z, Yu S, et al. Nanofiber scaffolds as drug delivery systems promoting wound healing. *Pharmaceutics* 2023; 15(7): 1829.
20. Ung T, Malone H, Canoll P, et al. Convection-enhanced delivery for glioblastoma: targeted delivery of antitumor therapeutics. *CNS Oncol* 2015; 4(4): 225–234.
21. Cui W, Zhou Y and Chang J. Electrospun nanofibrous materials for tissue engineering and drug delivery. *Sci Technol Adv Mater* 2010; 11(1): 014108.
22. Soares JC, Iwaki LEO, Soares AC, et al. Immunosensor for pancreatic cancer based on electrospun nanofibers coated with carbon nanotubes or gold nanoparticles. *ACS Omega* 2017; 2(10): 6975–6983.
23. Cepeda-Franco C, Mitxelena-Iribarren O, Calero-Castro FJ, et al. Tartessus: a customized electrospun drug delivery system loaded with irinotecan for local and sustained chemotherapy release in pancreatic cancer. *Bioengineering* 2023; 10(2): 183.
24. Li Y, Chen Y, Li J, et al. Co-delivery of microrna-21 antisense oligonucleotides and gemcitabine using nanomedicine for pancreatic cancer therapy. *Cancer Sci* 2017; 108(7): 1493–1503.
25. Wei L, Cheng X, Wang Q, et al. Establishment of a one-dimensional physical model for electrospinning multiple jets of spinnerets. *J Ind Textil*. 2023; 53.
26. Lukas D, Sarkar A, Martinova L, et al. Physical principles of electrospinning (electrospinning as a nano-scale technology of the twenty-first century). *Textil Prog* 2009; 41(2): 59–140.
27. Jirsak O, Sanetrnik F, Lukas D, et al. A method of nanofibres production from a polymer solution using electrostatic spinning and a device for carrying out the method. *Czech Republic*. 2005; US7585437: B2.
28. Omer S, Forgách L, Zelkó R, et al. Scale-up of electrospinning: market overview of products and devices for pharmaceutical and biomedical purposes. *Pharmaceutics* 2021; 13(2): 286.
29. Khan MQ, Alvi MA, Nawaz HH, et al. Cancer treatment using nanofibers: a review. *Nanomaterials* 2024; 14(15): 1305.
30. Azari A, Golchin A, Mahmoodinia Maymand M, et al. Electrospun polycaprolactone nanofibers: current research and applications in biomedical application. *Adv Pharmaceut Bull* 2022; 12(4): 658–672.
31. Vashisth P, Singh R and Pruthi V. A controlled release system for quercetin from biodegradable poly(lactide-co-glycolide)–polycaprolactone nanofibers and its *in vitro* antitumor activity. *J Bioact Compat Polym* 2015; 31(3): 260–272.
32. Pinzón-García AD, Sinisterra R, Cortes M, et al. Polycaprolactone nanofibers as an adjuvant strategy for Tamoxifen release and their cytotoxicity on breast cancer cells. *PeerJ* 2021; 9: e12124.
33. Bai S, Han H, Huang X, et al. Silk scaffolds with tunable mechanical capability for cell differentiation. *Acta Biomater* 2015; 20: 22–31.
34. Sheikh FA, Ju HW, Moon BM, et al. A comparative mechanical and biocompatibility study of poly(ε-caprolactone), hybrid poly(ε-caprolactone)–silk, and silk nanofibers by colloidal

electrospinning technique for tissue engineering. *J Bioact Compat Polym* 2014; 29(5): 500–514.
35. Lim J, Ki CS, Kim JW, et al. Fabrication and evaluation of poly(epsilon-caprolactone)/silk fibroin blend nanofibrous scaffold. *Biopolymers* 2011; 97(5): 265–275.
36. Masek J, Lubasova D, Lukac R, et al. Multi-layered nanofibrous mucoadhesive films for buccal and sublingual administration of drug-delivery and vaccination nanoparticles - important step towards effective mucosal vaccines. *J Contr Release* 2017; 249: 183–195.
37. Lander LM, Siewierski LM, Brittain WJ, et al. A systematic comparison of contact angle methods. *Langmuir* 1993; 9(8): 2237–2239.
38. Siepmann J and Peppas NA. Higuchi equation: derivation, applications, use and misuse. *Int J Pharm* 2011; 418(1): 6–12.
39. Wu IY, Bala S, Skalko-Basnet N, et al. Interpreting non-linear drug diffusion data: utilizing Korsmeyer-Peppas model to study drug release from liposomes. *Eur J Pharm Sci* 2019; 138: 105026.
40. International Organization for Standardization. *ISO 10993-5: biological evaluation of medical devices. Part 5: test for in vitro cytotoxicity.* Geneva, Switzerland: ISO, 2009.
41. Luraghi A, Peri F and Moroni L. Electrospinning for drug delivery applications: a review. *J Contr Release* 2021; 334: 463–484.
42. Jiffrin R, Razak SIA, Jamaludin MI, et al. Electrospun nanofiber composites for drug delivery: a review on current progresses. *Polymers (Basel)* 2022; 14(18): 3725.
43. Szewczyk PK, Ura DP, Metwally S, et al. Roughness and fiber fraction dominated wetting of electrospun fiber-based porous meshes. *Polymers (Basel)* 2018; 11(1): 34.
44. Unnithan AR, Gnanasekaran G, Sathishkumar Y, et al. Electrospun antibacterial polyurethane-cellulose acetate-zein composite mats for wound dressing. *Carbohydr Polym* 2014; 102: 884–892.
45. Cai Z, Zhuang H, Li X, et al. Sustained release system of paclitaxel based on composite nanofibers for inhibiting renal clear cell carcinoma. *J Mater Sci* 2022; 57(45): 21192–21205.
46. Zupancic S, Sinha-Ray S, Sinha-Ray S, et al. Long-term sustained ciprofloxacin release from pmma and hydrophilic polymer blended nanofibers. *Mol Pharm* 2015; 13(1): 295–305.
47. Gaydhane MK, Sharma CS and Majumdar S. Electrospun nanofibres in drug delivery: advances in controlled release strategies. *RSC Adv* 2023; 13(11): 7312–7328.
48. Abourehab MAS, Rajendran RR, Singh A, et al. Alginate as a promising biopolymer in drug delivery and wound healing: a review of the state-of-the-art. *Int J Mol Sci* 2022; 23(16): 9035.
49. Cao H, Duan L, Zhang Y, et al. Current hydrogel advances in physicochemical and biological response-driven biomedical application diversity. *Signal Transduct Targeted Ther* 2021; 6: 426.
50. Mittapalli RK, Liu X, Adkins CE, et al. Paclitaxel–hyaluronic nanoconjugates prolong overall survival in a preclinical brain metastases of breast cancer model. *Mol Cancer Therapeut* 2013; 12(11): 2389–2399.
51. Deng B, Xia M, Qian J, et al. Calcium phosphate-reinforced reduction-sensitive hyaluronic acid micelles for delivering paclitaxel in cancer therapy. *Mol Pharm* 2017; 14(6): 1938–1949.
52. Koohzad F and Asoodeh A. Hyaluronic acid/gelatin coaxial nanofibers incorporated with berberine–arginine for wound healing. *ACS Appl Nano Mater* 2024; 7(12): 14641–14653.

53. Khan S, Ullah S, Ullah A, et al. Hyaluronic acid-based nanofibers: electrospun synthesis and their medical applications; recent developments and future perspective. *Front Chem* 2022; 10: 1092123.
54. Hosseini H, Shahraky MK, Amani A, et al. Electrospinning of polyvinyl alcohol/chitosan/hyaluronic acid nanofiber containing growth hormone and its release investigations. *Polym Adv Technol* 2021; 32(2): 574–581.
55. Séon-Lutz M, Couffin A-C, Vignoud S, et al. Electrospinning in water and in situ crosslinking of hyaluronic acid / cyclodextrin nanofibers: towards wound dressing with controlled drug release. *Carbohydr Polym* 2019; 207: 276–287.
56. Payan E, Jouzeau JY, Lapicque F, et al. Hyaluronidase degradation of hyaluronic acid from different sources: influence of the hydrolysis conditions on the production and the relative proportions of tetra- and hexasaccharide produced. *Int J Biochem* 1993; 25(3): 325–329.
57. Patterson J, Siew R, Herring SW, et al. Hyaluronic acid hydrogels with controlled degradation properties for oriented bone regeneration. *Biomaterials* 2010; 31(26): 6772–6781.
58. Dias JR, Sousa A, Augusto A, et al. Electrospun polycaprolactone (PCL) degradation: an *in vitro* and in vivo study. *Polymers (Basel)* 2022; 14(16): 3397.
59. Guan X, Bian Y, Guo Z, et al. Bidirectional allostery mechanism in catch-bond formation of CD44 mediated cell adhesion. *J Phys Chem Lett* 2024; 15(43): 10786–10794.
60. Machado V, Morais M and Medeiros R. Hyaluronic acid-based nanomaterials applied to cancer: where are we now? *Pharmaceutics* 2022; 14(10): 2092.
61. Kesharwani P, Chadar R, Sheikh A, et al. CD44-targeted nanocarrier for cancer therapy. *Front Pharmacol* 2022; 12: 800481.
62. Misra S, Heldin P, Hascall VC, et al. Hyaluronan-CD44 interactions as potential targets for cancer therapy. *FEBS J* 2011; 278(9): 1429–1443.
63. Li Y, Chen N, Palmisano M, et al. Pharmacologic sensitivity of paclitaxel to its delivery vehicles drives distinct clinical outcomes of paclitaxel formulations. *Mol Pharm* 2015; 12(4): 1308–1317.
64. Serri C, Quagliariello V, Iaffaioli RV, et al. Combination therapy for the treatment of pancreatic cancer through hyaluronic acid-decorated nanoparticles loaded with quercetin and gemcitabine: a preliminary *in vitro* study. *J Cell Physiol* 2019; 234: 4959–4969.
65. Tarannum M and Vivero-Escoto JL. Nanoparticle-based therapeutic strategies targeting major clinical challenges in pancreatic cancer treatment. *Adv Drug Deliv Rev* 2022; 187: 114357.
66. Bartkowski M, Bincoletto V, Salaroglio IC, et al. Enhancing pancreatic ductal adenocarcinoma (PDAC) therapy with targeted carbon nano-onion (CNO)-mediated delivery of gemcitabine (GEM)-derived prodrugs. *J Colloid Interface Sci* 2024; 659: 339–354.
67. Xia G, Zhang H, Cheng R, et al. Localized controlled delivery of gemcitabine via microsol electrospun fibers to prevent pancreatic cancer recurrence. *Adv Healthcare Mater* 2018; 7(18): e1800593.
68. Mitxelena-Iribarren O, Riera-Pons M, Pereira S, et al. Drug-loaded PCL electrospun nanofibers as anti-pancreatic cancer drug delivery systems. *Polym Bull* 2023; 80: 7763–7778.

Appendix 9

Yalcinkaya, F., Komarek, M., LUBASOVA, D., Sanetrnik, F. and Maryska, J. Preparation of antibacterial nanofibre/nanoparticle covered composite yarns,.Journal of nanomaterials;2016.

Hindawi Publishing Corporation
Journal of Nanomaterials
Volume 2016, Article ID 7565972, 7 pages
http://dx.doi.org/10.1155/2016/7565972

Hindawi

Research Article

Preparation of Antibacterial Nanofibre/Nanoparticle Covered Composite Yarns

Fatma Yalcinkaya,[1] Michal Komarek,[1] Daniela Lubasova,[1] Filip Sanetrnik,[1,2] and Jiri Maryska[1]

[1] *Department of Nanotechnology and Informatic, Institute for Nanomaterials, Advanced Technologies and Innovation, Technical University of Liberec, 46117 Liberec, Czech Republic*
[2] *Department of Nonwoven and Nanofibrous Materials, Faculty of Textile Engineering, Technical University of Liberec, 46117 Liberec, Czech Republic*

Correspondence should be addressed to Fatma Yalcinkaya; yenertex@hotmail.com

Received 16 November 2015; Revised 6 January 2016; Accepted 12 January 2016

Academic Editor: Tamer Uyar

The antibacterial efficiency of nanofibre composite yarns with an immobilized antibacterial agent was tested. This novel type of nanofibrous composite material combines the good mechanical properties of the core yarn with the high specific surface of the nanofibre shell to gain specific targeted qualities. The main advantages of nanofibre covered composite yarns over the standard planar nanofibre membranes include high tensile strength, a high production rate, and their ability to be processed by standard textile techniques. The presented paper describes a study of the immobilization of an antibacterial agent and its interaction with two types of bacterial colonies. The aim of the study is to assess the applicability of the new composite nanomaterial in antibacterial filtration. During the experimental tests copper(II) oxide particles were immobilized in the polyurethane and polyvinyl butyral nanofibre components of a composite yarn. The antibacterial efficiency was evaluated by using both Gram-negative *Escherichia coli* and Gram-positive *Staphylococcus gallinarum* bacteria. The results showed that the composite yarn with polyvinyl butyral nanofibres incorporating copper(II) oxide nanoparticles exhibited better antibacterial efficiency compared to the yarn containing the polyurethane nanofibres. The nanofibre/nanoparticle covered composite yarns displayed good antibacterial activity against a number of bacteria.

1. Introduction

Nanofibrous materials have attracted a huge amount of interest during the last few decades mainly in the framework of research and innovation studies. Their high surface area, high porosity, small pore size, and compatibility with functionalizing additives mean that they are promising for various applications including filtration, membranes, medical applications, sensors, catalysts, and enzyme carriers [1–10]. Many scientists focus on evaluating the activity and application of nanofibres and nanoparticles [3, 11–13]. However, most of their work is done on a laboratory scale and future developments in technology are anticipated.

In addition to the laboratory scale, there are several companies which produce nanofibres on an industrial scale using various production methods. The most commonly used methods include melt blowing, centrifugal spinning, island-in-the-sea splitting, and needleless electrospinning [14–16]. Each technology has its own advantages and disadvantages. For instance, melt blowing is an environmentally friendly technology with a high production rate; however, the fibre diameter is usually high and the diameter distribution is very wide. This method has an additional problem with die clogging. Island-in-the-sea bicomponent fibre splitting is another technology suitable for the production of nanofibres with relatively high productivity; however, the resultant fibres

are tangled and it is difficult to separate them from each other. In the case of centrifugal spinning, production rate is high but with a wide fibre diameter distribution.

In this work, the needleless electrospinning process was used to eliminate the disadvantages of productivity and wide fibre diameter distribution. Specifically, the needleless roller electrospinning method developed by Jirsak et al. was used [17]. The disadvantage of the RES is the fact that not all polymer solutions can be spun into nanofibres. The reason for this has been explained in previous studies [18, 19]. On the other hand, the RES system was found to be suitable for many polymer-solvent systems [18–21].

A modified RES system for the production of nanofibre/nanoparticle covered yarn was recently developed by Jirsak et al. [22]. In this system, instead of using a flat sheet collecting material, a textile yarn was used. The principle of the roller electrospinning system has been explained in more detail in previous works [20, 21]. This method was used to cover the core yarn with nanofibres. Afterwards, a supporting yarn was covered around the composite yarn to improve the abrasion resistance of the nanofibre cover during further processing, for example, weaving.

Due to the intended use of the material in antimicrobial filters, the suitable antibacterial agent had to be immobilized in the nanofibre component of the composite yarn. There are many antibacterial agents available on the market but copper(II) oxide was chosen due to its long life and low cost. Two types of polymers, polyvinyl butyral (PVB) [20, 21] and polyurethane (PU) [23, 24], were tested in this study to form the nanofibre component of the system.

Compared to the antibacterial test where both PU and PVB were used, the PVB polymer solution was selected for the next step of the experiment. In the next step, the effects of the amounts of copper(II) oxide (CuO) on the antibacterial efficiency were determined by changing its amount in the solution and changing the linear weight of nanofibres on the produced yarn.

For this paper it was important to produce the lowest possible efficient amount of nanofibres with an antibacterial agent at a high nanofibre composite yarn production speed, which is promising for industrial application.

2. Materials and Methods

PVB was purchased from Kuraray America Inc. (Mowital B 60 H, 60,000 g/mol). PU Larithane LS 1086 (Novotex, Italy), which is an aliphatic elastomer composed of 2,000 g/mol linear polycarbonate diol and isophorone diisocyanate and extended by isophorone diamine, was selected as the second polymer.

DMF (Fluka, Switzerland) was used as the solvent for the PU, whereas acetic acid (Penta, Czech Republic) was used as the solvent for the PVB. CuO nanoparticles were purchased from Penta (Czech Republic). The surfactant Triton X-100, obtained from Sigma Aldrich, was used to provide a uniform distribution of the CuO nanoparticles in the PVB and PU polymer solutions.

The principle of a modified RES system based on a rotating roller electrode was used. The electrode roller is immersed in a polymer solution tank and connected to a high voltage source. As mentioned above, the modified RES system was used to cover the base yarn (Figure 1).

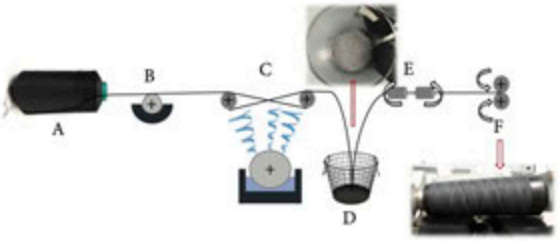

FIGURE 1: Schematic diagram of a continuous production device. A: black core yarn, B: application of a conductive solution, C: roller electrospinning system, D: collector, E: application of protective yarn(s), and F: take-up mechanism.

The morphology of the nanofibre covered yarns with CuO particles was evaluated using a Tescan Vega3 SB scanning electron microscope (SEM). The zero-shear viscosity of the polymer solutions was measured using a HAAKE Roto Visco rheometer at 25°C. The antibacterial efficiency of the CuO agent immobilized in the composite yarns against Gram-positive *Staphylococcus gallinarum* (*S. gallinarum*) and Gram-negative *Escherichia coli* (*E. coli*) was tested by the modified AATCC test method 100-2004.

3. Experimental

3.1. Fabrication of Composite Nanofibrous Yarns

3.1.1. Preparation of the Polymer Solutions. Two polymers, PVB and PU, were tested for the production of nanofibre composite yarns in order to compare their antibacterial effect. PVB was selected because of its low cost, good mechanical properties, and nontoxicity of the solvent. PVB was dissolved in concentrated acetic acid to form an 11% wt. solution. A total of 10% wt. CuO was added to the PVB solution. PU was selected because of its high elasticity and the relatively good abrasion resistance of the nanofibre part of the composite. PU was dissolved in DMF to form a 15% wt. of solution and stirred overnight and then 10% wt. of CuO was added to the PU solution and dispersed using an ultrasonic disperser for 5 minutes. Finally, 1% wt. of Triton X-100 surfactant was added to minimize the aggregation of the CuO nanoparticles. The bulk viscosity of the polymer solutions was measured to characterize the flow behaviour.

3.1.2. Electrostatic Spinning. A textured polyester base yarn (dtex 167f 36 × 1 × 3) was transported to the roller electrospinning system and used as a collector. After being covered by the nanofibres, the yarn was transported into the collector. Stable electrospinning conditions were used for both solution systems (Table 1).

To compare the antibacterial efficiency of the two solution systems, the speed of the yarn was set to 134 m/min.

Table 1: Process parameters of the electrostatic spinning.

Applied voltage (kV)	Distance between electrodes (mm)	Speed of yarn on the collector (m/min)	Humidity (% RH)	Temperature (°C)	Width of roller (mm)
60	170	80-120-134-160-200	18 ± 1	24 ± 1	470

Table 2: Viscosity of PVB polymer solutions with 0, 5, and 10% wt. of CuO nanoparticles.

Sample and abbreviations	Viscosity (Pa·s)
(P0) Content: 11% wt. PVB60H in 4% wt. H_2O and 85% wt. acetic acid mixture	0.30
(P5) Content: 11% wt. PVB60H in 4% wt. H_2O, 1% wt. surfactant, 5% wt. CuO, and 79% wt. acetic acid mixture	1.59
(P10) Content: 11% wt. PVB60H in 4% wt. H_2O, 1% wt. surfactant, 10% wt. CuO, and 74% wt. acetic acid mixture	2.47

To optimize the concentration of CuO, 11% wt. of the PVB polymer solution with 0, 5, and 10% wt. of CuO was used during fabrication of the nanofibres covered yarns, and 1% wt. of surfactant was used to prevent aggregation. The viscosity of the solutions was measured and is included in Table 2.

The descriptions of the samples are listed in Table 3. The symbol "P" is the abbreviation for PVB, the number next to P is the amount of CuO particles (% wt.) in the polymer solution, and the last number indicates the speed of composite yarn production.

3.1.3. Characterization of Amounts of Nanofibres in the Product. The amounts of PVB/CuO nanofibres for different production speeds were evaluated by dissolving the specific nanofibre material in ethanol. Ethanol is a good solvent for PVB [25]. The 1 m samples were cut, weighed, and immersed in ethanol overnight. After dissolution of the nanofibrous component, the samples were washed with distilled water, dried, and weighed again. The results were calculated according to the following equation:

$$\text{Amount of nanofibres (\%)} = \frac{(W_0 - W_1)}{W_0} * 100, \quad (1)$$

where W_0 is the weight of composite yarn before nanofibre dissolution and W_1 is the weight of the yarn without nanofibres.

3.2. Antibacterial Test. *Escherichia coli* (*E. coli*) and *Staphylococcus gallinarum* (*S. gallinarum*) bacteria were purchased from the Czech Collection of Microorganisms, Masaryk University. Incubation of the bacteria was performed on a sterile agar with a broth agar medium from Oxoid Ceska Republika.

The antibacterial activities of the fabric systems were evaluated quantitatively in accordance with ASTM E 2149-01 and AATCC test method 100 (standard test method for determining the antibacterial activity of immobilized antibacterial agents under dynamic contact conditions).

The samples were sterilized in an oven at 80°C for 60 min before conducting the test. A blank sample was prepared without any antibacterial agent (CuO). The antibacterial test against Gram-negative (*E. coli*) and Gram-positive (*S. gallinarum*) was performed as the first step. The microorganisms were cultivated in a sterilized LB broth medium and then incubated overnight at 37°C in a shaking incubator. The bacterial suspensions employed for this test contained between 10^2 and 10^3 colony forming units (CFU).

Sterilized samples of nanofibre covered yarns were individually placed into a sterilized test tube and inoculated with 30 mL of *E. coli* or *S. gallinarum* bacterial suspension. At "0" contact time and after 1, 2, 3, 4, and 24 hours, 600 μL of bacterial suspension was extracted and quickly spread on tryptic soy agar plates. The number of viable *E. coli* or *S. gallinarum* was determined by plating the extracted solution onto the Tryptic Soy agar plates and counting the colonies after 24 hours of incubation at 37°C.

Three selected yarns P0-200, P5-200, and P10-200 (each around 1 ± 0.01 g) were used for the disinfection test. The disinfection test was performed on the selected samples against Gram-negative (*E. coli*) and Gram-positive (*S. gallinarum*) bacteria. The bacterial suspensions contained 10^6 colony forming units (CFU).

The percentage reduction of test microorganisms in the test tubes with the nanofibre membranes was calculated using the following equation:

$$\text{Reduction \%} = \frac{(A_0 - A_1)}{A_0} * 100, \quad (2)$$

where R is the percentage reduction of test microorganism; A_1 is the number of bacteria recovered from the inoculated nanofibre membrane with the nanoparticles in the test tube after specified contact time, and A_0 is the number of bacteria recovered from the inoculated nanofibre membrane with the nanoparticles in the test tube at "0" contact time.

4. Results and Discussion

4.1. Morphology Characterization. A polyester base yarn was covered with nanofibres/NPs and then a polyamide filament was used to protect against mechanical abrasion. The SEM images of the nanofibre/NP covered yarns made of 15% wt. PU with 10% wt. CuO and 11% wt. PVB with 10% wt. CuO are shown in Figure 2.

Figure 2 shows the nanofibres/NPs on the surface of the core yarn. Beads are present on the surface of the nanofibres. The number of beads on the PVB/CuO yarns is higher than the number on the PU/CuO yarns. These beads can be caused by aggregation of 10% wt. CuO or the low concentration of the PVB polymer solution compared to the PU solution.

Table 3: Abbreviations of the second group of samples.

Abbreviation	Content solution (% wt.)	Speed of yarn (m/min)
P0-80	11% wt. PVB60H in 4% wt. H_2O and 85% wt. acetic acid mixture	80
P0-120	11% wt. PVB60H in 4% wt. H_2O and 85% wt. acetic acid mixture	120
P0-160	11% wt. PVB60H in 4% wt. H_2O and 85% wt. acetic acid mixture	160
P0-200	11% wt. PVB60H in 4% wt. H_2O and 85% wt. acetic acid mixture	200
P5-80	11% wt. PVB60H in 4% wt. H_2O, 1% wt. surfactant, 5% wt. CuO, and 79% wt. acetic acid mixture	80
P5-120	11% wt. PVB60H in 4% wt. H_2O, 1% wt. surfactant, 5% wt. CuO, and 79% wt. acetic acid mixture	120
P5-160	11% wt. PVB60H in 4% wt. H_2O, 1% wt. surfactant, 5% wt. CuO, and 79% wt. acetic acid mixture	160
P5-200	11% wt. PVB60H in 4% wt. H_2O, 1% wt. surfactant, 5% wt. CuO, and 79% wt. acetic acid mixture	200
P10-80	11% wt. PVB60H in 4% wt. H_2O, 1% wt. surfactant, 10% wt. CuO, and 74% wt. acetic acid mixture	80
P10-120	11% wt. PVB60H in 4% wt. H_2O, 1% wt. surfactant, 10% wt. CuO, and 74% wt. acetic acid mixture	120
P10-160	11% wt. PVB60H in 4% wt. H_2O, 1% wt. surfactant, 10% wt. CuO, and 74% wt. acetic acid mixture	160
P10-200	11% wt. PVB60H in 4% wt. H_2O, 1% wt. surfactant, 10% wt. CuO, and 74% wt. acetic acid mixture	200

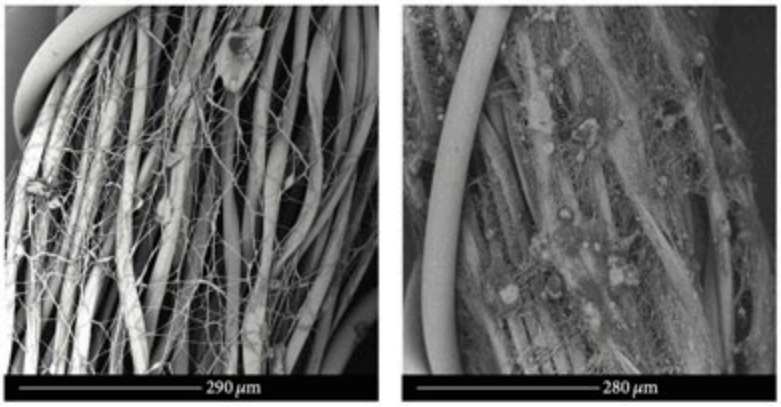

(a) (b)

Figure 2: SEM images of (a) PU/CuO, (b) PVB/CuO.

4.2. Antibacterial Efficiency

4.2.1. Dependence of the Antibacterial Efficiency on the Type of Nanofibre Polymer. The inhibition efficiency (% reduction of bacteria colony) was calculated according to (2) and the results are shown in Figure 3. The results show that, even after 1 minute of contact of the bacteria with the PVB/CuO, the antibacterial efficiency is over 90%. For each polymer, a blank sample without CuO was tested and a comparison showed that the bacterial colonies started to die after two hours.

This experiment shows that the antibacterial efficiency of nanofibre/NP covered yarns made from PVB/CuO is much higher than nanofibre/NPs covered yarns made from PU/CuO. This could be explained by the formation of cupric acetate, which distributes the Cu^{2+} ions more homogenously than in the case of the nanoparticles. Acetic acid reacts with copper oxide to form cupric acetate. The reaction between CuO and acetic acid is shown in the following equation:

$$2CH_3COOH + CuO \longrightarrow (CH_3COO)_2\,Cu + H_2O \quad (3)$$

4.2.2. Dependence of the Antibacterial Efficiency on the Amount of Nanofibres in the Product. Three polymer solutions, listed in Table 3 as P0-200, P5-200, and P10-200, were prepared with a constant PVB polymer concentration. From the previous experiment it was determined that the PVB dissolved in acetic acid with the CuO particles evinced an enormous antibacterial efficiency. It was determined that more than 90% of the bacteria died at "0" contact time of the nanofibre/NP covered yarns with the tested microorganism. This excellent antibacterial effect was observed after 1 hour. For that reason, the concentration of CuO was optimized (decreased) and various yarn speeds were used to improve productivity. To prevent aggregation of CuO particles, 1% wt. of nonionic Triton X-100 surfactant was used. PVB with 10% wt. of CuO has a very high bulk viscosity compared to the other samples. The viscosity results are shown in Table 2. High viscosity restricts the ability of the polymer solution to be electrospun into submicron fibres. As a result, a lower amount of nanofibres is collected on the yarn. SEM images show that the amount of nanofibres is lower but the amount

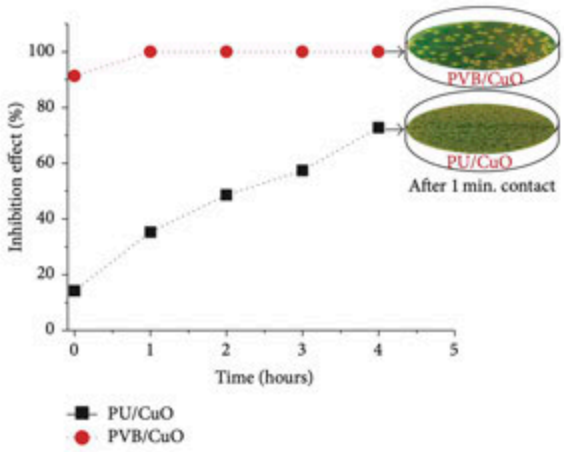

FIGURE 3: Reduction of bacteria (*E. coli*) overtime.

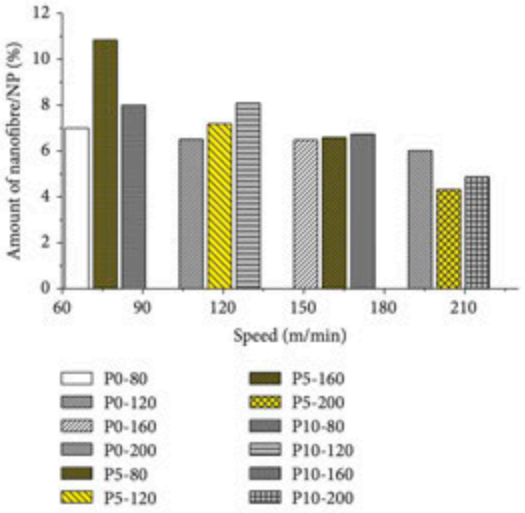

FIGURE 4: Amount of PVB/CuO nanofibres versus production speed of yarn. The amount of nanofibres on the yarn slightly decreased with an increase in speed due to a lower nanofibre collecting time.

of immobilized particles is higher in the case of 10% wt. of CuO.

The percentage amounts of nanofibre covered base yarn were calculated according to (1) and are shown in Figure 4.

Figure 4 indicates that the change in the amount of nanofibre/NPs depends on the speed of production. P0 indicates that no CuO is immobilized in the nanofibre component, while P5 has 5% wt. and P10 has 10% wt. of nanoparticles, respectively. When the speed of yarn production increases, the amount of nanofibres/NPs decreases on the surface of the composite yarn.

The aim of the experiment was to determine the lowest possible efficient amount of nanofibres and antibacterial agent. The results of the antibacterial efficiencies are shown in Figure 5. It was determined that PVB with CuO exhibits good antibacterial efficiency against *E. coli* and *S. gallinarum*. The amount of 5% wt. of CuO immobilized in PVB nanofibres showed an antibacterial efficiency of 99.99% at a production rate of 200 m/min. At "0" contact time more than 50% of *E. coli* and *S. gallinarum* bacteria were dead. CuO has a better antibacterial efficiency against *E. coli* at "0" contact time. On the other hand, after one hour contact time, no bacteria remained alive.

It can be seen that, even at high speeds and low amounts of nanofibres/NPs, CuO showed remarkable antibacterial properties against *E. coli* and *S. gallinarum*. It is possible to conclude that the production rate of the equipment can be increased with the same amount of CuO or the concentration of CuO can be decreased at a low yarn production speed. Both methods will show good results. For mass production, a higher yarn speed is more desirable.

Because the inhibition effect was found to be excellent even for nanofibre covered yarn with a lower concentration of CuO, a higher (10^6 CFU/mL) bacteria inoculum was prepared as explained in Section 2. Three yarns, P0-200, P5-200, and P10-200, were selected for subsequent testing. These samples were produced at the highest production rate, which means that the amount of nanofibres or nanofibre/NPs is the lowest compared to the others. The antibacterial test was performed against Gram-positive and Gram-negative microorganisms and the results are shown in Figure 6.

The results of the experiment show that more than 50% of *S. gallinarum* bacteria are killed by the immobilized agent at "0" contact time. In one hour, PVB with immobilized CuO has a disinfection effect in accordance with the high concentration of the tested bacteria inoculum (10^6 CFU).

The results in Figure 6 show that the initial antibacterial efficiency of CuO against *S. gallinarum* is higher than that against *E. coli* at "0" contact time. CuO nanoparticles are more effective against Gram-positive microorganisms. After 1 hour contact time, it was observed that both Gram-positive and Gram-negative bacteria were successfully disinfected. It can be concluded that the CuO agent in PVB nanofibre composite yarn exhibits a 99.99% disinfection efficiency against *E. coli* and *S. gallinarum* bacteria even at high CFU.

5. Conclusion

In this work, composite yarns with a nanofibre cover were prepared by a modified needleless electrospinning method. The testing comprised two types of polymers (PU and PVB). The process properties affecting the quality of the nanofibre compound, for example, the solution concentration, viscosity, spinning distance, voltage, and air humidity, were empirically optimized. The effect of the production rate on the linear weight of the nanofibre cover was evaluated. An inversely proportional effect of the production speed on the linear weight of the nanofibre cover was confirmed.

In accordance with the intended use of the composite yarn in antimicrobial filtration cartilages, the antibacterial agent CuO was incorporated into the nanofibrous layers and the antibacterial performance of the materials was studied.

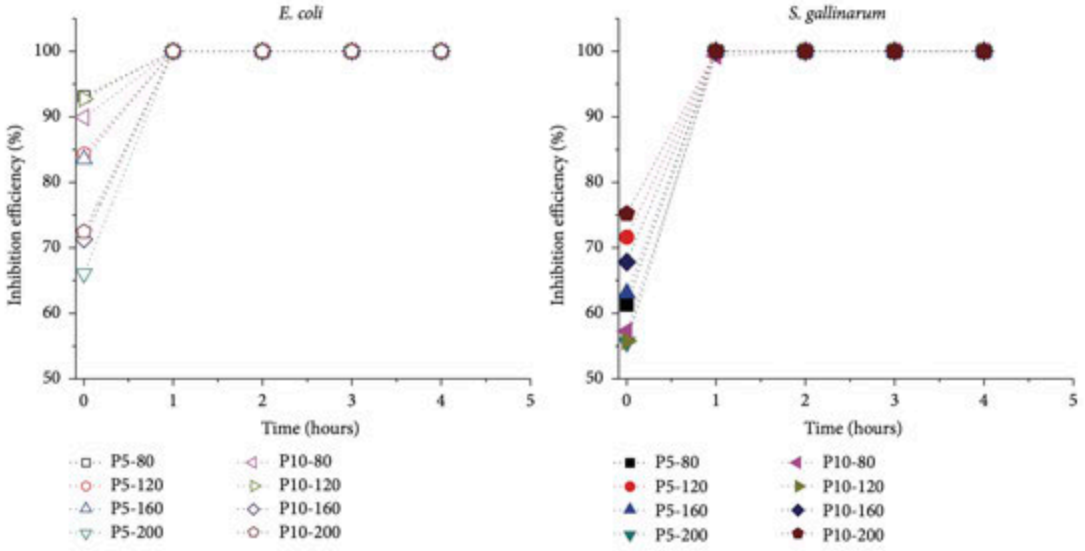

FIGURE 5: Antibacterial efficiency of nanofibre covered yarn with different concentrations of CuO agent.

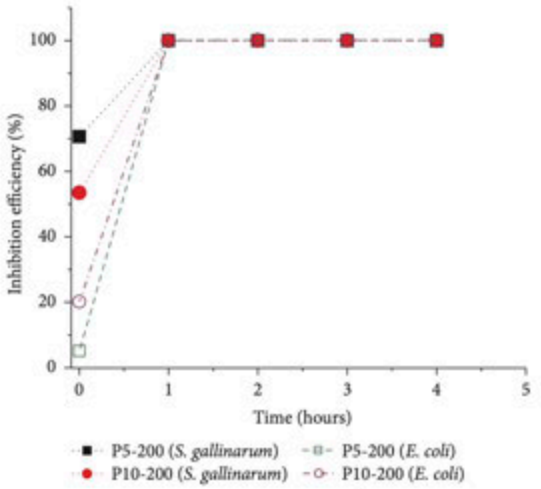

FIGURE 6: Antibacterial efficiency against 10^6 CFU bacterial concentrations.

The effect of the CuO concentration in the solution and the linear weight of the nanofibre cover on the antibacterial performance were measured.

Testing procedures comprised studies of the interaction of the prepared material with two bacterial types, that is, *E. coli* and *S. gallinarum* (Gram-positive and Gram-negative).

It was concluded through an evaluation of the sets of results that materials prepared by covering the core yarn with PVB/nanofibres with a CuO antibacterial agent generally show significantly higher antibacterial efficiency compared to yarns covered with PU nanofibres. This can be attributed to the better uniformity of the antibacterial agent distribution caused by the reaction of CuO with acetic acid creating copper acetate. Copper acetate then dissociates in the abundant acetic acid which helps to distribute the Cu^{2+} ions in the nanofibre mass. Better distribution of the Cu^{2+} ions enhances the probability of the contact between the antibacterial agent and the bacteria improving the overall antibacterial efficiency. The results showed that an antibacterial efficiency of 99.99% is achieved at 5% wt. of CuO additive and a production rate of 200 m/min. One hour contact is sufficient to disinfection all of the bacterial colonies.

The experimental work showed that the new type of composite nanofibrous yarns with immobilized antibacterial agents can be utilized to design antibacterial filtration cartridges for air and water purification.

Conflict of Interests

The authors declare that there is no conflict of interests regarding the publication of this paper.

Acknowledgment

The results of this project LO1201 were obtained through the financial support of the Ministry of Education, Youth and Sports in the framework of the targeted support of the "National Programme for Sustainability I."

References

[1] J. J. Ahire and L. M. T. Dicks, "2,3-Dihydroxybenzoic acid-containing nanofiber wound dressings inhibit biofilm formation by Pseudomonas aeruginosa," *Antimicrobial Agents and Chemotherapy*, vol. 58, no. 4, pp. 2098–2104, 2014.

[2] A. Fathi-Azarbayjani, L. Qun, Y. W. Chan, and S. Y. Chan, "Novel vitamin and gold-loaded nanofiber facial mask for topical delivery," *AAPS PharmSciTech*, vol. 11, no. 3, pp. 1164–1170, 2010.

[3] B.-H. Jang, O. Landau, S.-J. Choi, J. Shin, A. Rothschild, and I.-D. Kim, "Selectivity enhancement of SnO_2 nanofiber gas sensors by functionalization with Pt nanocatalysts and manipulation of the operation temperature," *Sensors and Actuators B: Chemical*, vol. 188, pp. 156–168, 2013.

[4] S. Lee and S. K. Obendorf, "Use of electrospun nanofiber web for protective textile materials as barriers to liquid penetration," *Textile Research Journal*, vol. 77, no. 9, pp. 696–702, 2007.

[5] W. Sambaer, M. Zatloukal, and D. Kimmer, "3D modeling of filtration process via polyurethane nanofiber based nonwoven filters prepared by electrospinning process," *Chemical Engineering Science*, vol. 66, no. 4, pp. 613–623, 2011.

[6] R. Vasita and D. S. Katti, "Nanofibers and their applications in tissue engineering," *International Journal of Nanomedicine*, vol. 1, no. 1, pp. 15–30, 2006.

[7] A. Zajicova, E. Javorkova, P. Trosan, M. Krulova, and V. Holan, "Drug-loaded nanofiber scaffolds for a simultaneous delivery of stem cells and immunosuppressive drugs in cell-based therapy and regenerative medicine," *Journal of Tissue Engineering and Regenerative Medicine*, vol. 8, pp. 277–278, 2014.

[8] D. Lubasova, A. Netravali, J. Parker, and B. Ingel, "Bacterial filtration efficiency of green soy protein based nanofiber air filter," *Journal of Nanoscience and Nanotechnology*, vol. 14, no. 7, pp. 4891–4898, 2014.

[9] L. Malinová, M. Stolínová, D. Lubasová, L. Martinová, and J. Brožek, "Electrospinning of polyesteramides based on epsilon-caprolactam and epsilon-caprolactone from solution," *European Polymer Journal*, vol. 49, no. 10, pp. 3135–3143, 2013.

[10] H. Kolya, S. Pal, A. Pandey, and T. Tripathy, "Preparation of gold nanoparticles by a novel biodegradable graft copolymer sodium alginate-g-poly (N,N-dimethylacrylamide-co-acrylic acid) with anti micro bacterial application," *European Polymer Journal*, vol. 66, pp. 139–148, 2015.

[11] C. D. Saquing, J. L. Manasco, and S. A. Khan, "Electrospun nanoparticle-nanofiber composites via a one-step synthesis," *Small*, vol. 5, no. 8, pp. 944–951, 2009.

[12] R. J. Tseng, J. Huang, J. Ouyang, R. B. Kaner, and Y. Yang, "Polyaniline nanofiber/gold nanoparticle nonvolatile memory," *Nano Letters*, vol. 5, no. 6, pp. 1077–1080, 2005.

[13] H. Wang, T. Wang, Y.-X. Ye et al., "Construction of an electrochemical cytosensor based on polyaniline nanofiber/gold nanoparticle interface and application to detection of cancer cells," *Chinese Journal of Analytical Chemistry*, vol. 40, no. 2, pp. 184–190, 2012.

[14] J. Harding, J. Keller, and R. Buntin, "Melt-blowing die for producing nonwoven mats," USA, Patent US 3825380 A, 1974.

[15] K. Sarkar, C. Gomez, S. Zambrano et al., "Electrospinning to Forcespinning," *Materials Today*, vol. 13, no. 11, pp. 12–14, 2010.

[16] R. Liu, N. Cai, W. Yang, W. Chen, and H. Liu, "Sea-island polyurethane/polycarbonate composite nanofiber fabricated through electrospinning," *Journal of Applied Polymer Science*, vol. 116, no. 3, pp. 1313–1321, 2010.

[17] O. Jirsak, F. Sanetrnik, D. Lukas, V. Kotek, L. Martinova, and J. Chaloupek, "A method of nanofibres production from a polymer solution using electrostatic spinning and a device for carrying out the method, Czech Republic," Article ID S7585437, US7585437 B2, 2005.

[18] F. Yener, B. Yalcinkaya, and O. Jirsak, "On the measured current in needle- and needleless electrospinning," *Journal of Nanoscience and Nanotechnology*, vol. 13, no. 7, pp. 4672–4679, 2013.

[19] B. Yalcinkaya, F. Yener, O. Jirsak, and F. Cengiz-Callioglu, "On the nature of electric current in the electrospinning process," *Journal of Nanomaterials*, vol. 2013, Article ID 538179, 10 pages, 2013.

[20] F. Yener and O. Jirsak, "Comparison between the needle and roller electrospinning of polyvinylbutyral," *Journal of Nanomaterials*, vol. 2012, Article ID 839317, 6 pages, 2012.

[21] F. Yener and O. Jirsak, "Improving performance of polyvinyl butyral electrospinning," in *Proceedings of the 4th International Nanocon Conference*, pp. 356–361, Brno, Czech Republic, 2011.

[22] O. Jirsak, F. Sanetrink, and J. Chaloupek, "Nanofiber-covered yarns," *Chemical Fibers International*, vol. 62, pp. 84–85, 2011.

[23] F. Yalcinkaya, B. Yalcinkaya, and O. Jirsak, "Influence of salts on electrospinning of aqueous and nonaqueous polymer solutions," *Journal of Nanomaterials*, vol. 2015, Article ID 134251, 12 pages, 2015.

[24] B. K. Kim, J. W. Seo, and H. M. Jeong, "Morphology and properties of waterborne polyurethane/clay nanocomposites," *European Polymer Journal*, vol. 39, no. 1, pp. 85–91, 2003.

[25] F. Yener, O. Jirsak, and R. Gemci, "Using a range of PVB spinning solution to acquire diverse morphology for electrospun nanofibres," *Iranian Journal of Chemistry and Chemical Engineering*, vol. 31, no. 4, pp. 49–58, 2012.